



Waves in the Structured Media

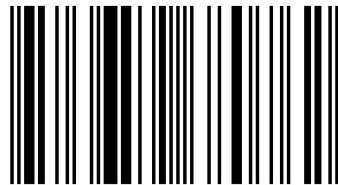
Object for study is multicomponent media with the internal exchanged processes. Intrinsic inhomogeneities give rise to the remarkable/unusual nonlinear behaviors demonstrated by these media at quasistatic and dynamic mechanical loads. The purpose of this book is to describe the dynamic behaviors of these media in terms of physically motivated models. New method of structure diagnostics by means of the nonlinear waves is suggested. The research of nonlinear evolution equations is carried out. The special attention is focused on development of models for describing both stress-strain properties of sandstone under quasistatic loading and vibration resonance in sedimentary rocks. The important result is theoretical prediction of a dynamic effect analogous to the known quasistatic effect of hysteresis with discrete memory. The models describe the experimental results and can be applied for future research. The reader may find some suggestions for future research herein, and open up questions that may be especially useful for young scientists. I hope that the reader will receive a more or less objective picture of the current state of the art of the wave dynamic of the structured media.

Vyacheslav O. Vakhnenko

Wave Dynamics of the Structured Media with Relaxation



Vyacheslav O. Vakhnenko, Chief Scientist at the Subbotin Institute of Geophysics, NAS Ukraine, graduated Moscow Physical Technical Institute, received his Ph.D from the Institute of Chemical Physics, Moscow, and D.Sc. from Odessa State University. One of the nonlinear evolution equations is known as the Vakhnenko equation.



978-3-659-68076-2

Vakhnenko



Vyacheslav O. Vakhnenko

Wave Dynamics of the Structured Media with Relaxation

Vyacheslav O. Vakhnenko

**Wave Dynamics of the Structured
Media with Relaxation**

LAP LAMBERT Academic Publishing

Impressum / Imprint

Bibliografische Information der Deutschen Nationalbibliothek: Die Deutsche Nationalbibliothek verzeichnet diese Publikation in der Deutschen Nationalbibliografie; detaillierte bibliografische Daten sind im Internet über <http://dnb.d-nb.de> abrufbar.

Alle in diesem Buch genannten Marken und Produktnamen unterliegen warenzeichen-, marken- oder patentrechtlichem Schutz bzw. sind Warenzeichen oder eingetragene Warenzeichen der jeweiligen Inhaber. Die Wiedergabe von Marken, Produktnamen, Gebrauchsnamen, Handelsnamen, Warenbezeichnungen u.s.w. in diesem Werk berechtigt auch ohne besondere Kennzeichnung nicht zu der Annahme, dass solche Namen im Sinne der Warenzeichen- und Markenschutzgesetzgebung als frei zu betrachten wären und daher von jedermann benutzt werden dürften.

Bibliographic information published by the Deutsche Nationalbibliothek: The Deutsche Nationalbibliothek lists this publication in the Deutsche Nationalbibliografie; detailed bibliographic data are available in the Internet at <http://dnb.d-nb.de>.

Any brand names and product names mentioned in this book are subject to trademark, brand or patent protection and are trademarks or registered trademarks of their respective holders. The use of brand names, product names, common names, trade names, product descriptions etc. even without a particular marking in this work is in no way to be construed to mean that such names may be regarded as unrestricted in respect of trademark and brand protection legislation and could thus be used by anyone.

Coverbild / Cover image: www.ingimage.com

Verlag / Publisher:

LAP LAMBERT Academic Publishing

ist ein Imprint der / is a trademark of

OmniScriptum GmbH & Co. KG

Heinrich-Böcking-Str. 6-8, 66121 Saarbrücken, Deutschland / Germany

Email: info@lap-publishing.com

Herstellung: siehe letzte Seite /

Printed at: see last page

ISBN: 978-3-659-68076-2

Copyright © 2015 OmniScriptum GmbH & Co. KG

Alle Rechte vorbehalten. / All rights reserved. Saarbrücken 2015

Wave Dynamics of the Structured Media with Relaxation

Vyacheslav O. Vakhnenko ¹,

January 2015

¹E-mail: vakhnenko@ukr.net, Subbotin Institute of Geophysics, Kyiv, Ukraine

Contents

1	Introduction	1
2	Asymptotic averaged model for structured medium	7
2.1	Background and initial equations	8
2.1.1	Motion equations for individual component	8
2.1.2	Dynamic state equation	9
2.2	Asymptotic averaged system of equations	10
2.3	System of equations in Eulerian coordinates	13
2.4	Analysis of the averaged system of equations	14
2.4.1	Acoustic waves	14
2.4.2	Nonlinear waves	15
2.4.3	Analytical–numerical calculation method	17
2.5	Lyakhov model as special case of an asymptotic averaged model	20
2.6	Conclusions	24
3	Solitons in homogeneous relaxing medium	25
3.1	Low-frequency and high-frequency perturbations in relaxing medium	26
3.2	Evolution equation for high-frequency perturbations	31
3.2.1	The connection with the Whitham equation	32
3.2.2	Loop-like traveling wave solutions	33
3.3	Interaction of solitons	36
3.3.1	The Vakhnenko-Parkes equation	36
3.3.2	Hirota method	39
3.3.3	The one and two loop soliton solutions	40
3.4	Ambiguous solutions	43
4	Waves in relaxing two-component medium	47
4.1	Asymptotic averaged model for mixture with thermal relaxation	48
4.2	Dynamic state equation for mixture with thermal relaxation	49
4.3	Similarity in motions of gas and two-phase medium with incompressible component	51
4.3.1	System of equations in the Lagrangian coordinates	52
4.3.2	Similarity of stationary flows	53
4.3.3	Self-similar motions with shock waves	55
4.3.4	Shock front parameters	59

5	Blast waves in medium with structure	61
5.1	System of equations for describing the strong explosion	62
5.2	Calculation of shock waves	66
5.3	Blast waves in foam	72
5.3.1	Experimental study	73
5.3.2	The comparison of the calculation with experiment	75
5.4	Estimation of fracture area in rock under blast	79
5.4.1	Model of wave disturbance attenuation	80
5.4.2	Energy criterion of crack formation	82
5.4.3	Geometric similarity of the explosive fracture area	84
5.4.4	Estimation of region of crack formation	84
5.4.5	Comparison with the experiment	85
6	Diagnostics of medium by long nonlinear waves	89
6.1	The increase of nonlinearity in medium with structure	89
6.2	Fundamentals of new diagnostic method	92
6.3	The governing wave parameters for diagnostic method	95
6.4	Approximation of diagnosed medium by layer medium	97
7	State equation for Berea sandstone under slow loading	103
7.1	Analysis of experimental data	104
7.2	Mechanisms for quasistatic loading	105
7.2.1	Standard solid relaxation mechanism	106
7.2.2	Sticky-spring mechanism	109
7.2.3	Permanent plastic deformation mechanism	112
7.3	Simulation of stress-strain relations	113
7.4	Dissipation of energy in rock under cyclic loading	115
7.4.1	The slopes of main and inner hysteretic loops	116
7.4.2	Energy dissipation	118
7.5	Conclusions	120
8	Dynamics of a sandstone bar under resonance loading	123
8.1	Analysis of experimental data	124
8.2	Model of sandstone dynamics at resonance	128
8.2.1	Physical notions on resonance bar dynamics	129
8.2.2	Kinetics of ruptured cohesive bonds	131
8.2.3	Motion equations. Problem on bar resonance	135
8.3	Soft-ratchet kinetics under harmonic drive	137
8.4	Modeling of resonant nonlinear effects	142
8.4.1	Water saturation	148
8.5	Simulation of slow dynamics	149
8.6	Dynamical realization of end-point memory	150
9	References	155

Preface

Object for study is multicomponent media characterized by the internal exchanged processes. Intrinsic inhomogeneities give rise to the remarkable/unusual nonlinear behaviors demonstrated by these media at quasistatic and dynamic mechanical loads. The purpose of this book is to describe the dynamic behaviors of multicomponent media in terms of physically motivated models. Traditionally it is believed that under long-wave (both linear and nonlinear) perturbations, such media can be modeled as homogeneous ones. In some sense it is so. However, the suggested approach enables us to separate the influence of medium structure on nonlinear waves. The information contained in evolutionary nonlinear wave turns out to be sufficient to reproduce the medium structure with certain accuracy and to obtain the concentration of individual components. The theoretical principles for new method of structure diagnostics by means of the long nonlinear waves and for the control of wave action in the multicomponent media are suggested. The research of nonlinear evolution equations as applied to the evolution of wave fields is carried out. The special attention is focused on development of models for describing both complex stress-strain properties of a sandstone sample under quasistatic loading and longitudinal vibration resonance in bar-shaped sedimentary rocks. The models reproduce the main experimental effects. The important result is theoretical prediction of a dynamic effect analogous to the widely known quasistatic effect of hysteresis with discrete (end-point) memory. Following the theoretical prediction, our colleagues TenCate and Shankland at Los Alamos National Laboratory have performed experimental measurements and verified this prediction. These exclusive experimental results stimulate us to carry out additional simulation, where resonance curves for sandstone were reproduced by using the previously suggested model of the resonance response. Thus, the models we developed can adequately describe the experimental results and can be applied for future research.

Acknowledgements

It is our pleasure to thank and acknowledge our colleagues and co-authors of joint researches B.I. Palamarchuk, V.A. Danylenko, V.M. Kudinov, S.G. Lebed, A.V. Cherkashin, A.T. Malakhov and V.V. Kulich for creative work, exchange by ideas and discussion of the results. We wish to acknowledge the contributions to this work (Chapters 7, 8) by our colleagues at Los Alamos National Laboratory T.J. Shankland and J.A. TenCate. We are also most grateful to P.A. Johnson for helpful discussions and stimulating support. Special thanks go to E.J. Parkes for collaboration in research of the nonlinear evolution equations and my brother Oleksiy O. Vakhnenko for investigations of the dynamics of sandstone under mechanical loading.

Chapter 1

Introduction

Natural media, in the general case, should not be treated as structureless. The experiments have shown that the intrinsic structure of a medium influences the wave motions [17, 22, 55, 67, 70, 106, 115, 126, 130, 131]. Existing inhomogeneities complicate the problem and, at the same time, are fully manifested under the propagation of nonlinear waves. Fast high-gradient processes, such as earthquakes, explosions, etc., lead to irreversible processes [130, 131]. The principal part of the problem is associated with the phenomena caused by the nonlinear behavior of natural media such as (a) soliton-like properties of P-waves [46], and (b) larger increase of nonlinear effects in structured media compared to homogeneous ones [17, 22, 55, 67, 70, 115].

The wave processes in heterogeneous media are usually described in terms of more or less complicated models. Under the conditions of local equilibrium, the media are traditionally modeled irrespective of their structure. In the framework of continuum mechanics, the known idealization of a real medium as a homogeneous one has been fairly successive in the description of wave processes (see, for instance, [4, 8, 151]). The continuum models are commonly applied to the mixtures whose dispersive dissipative properties are treated with regard for the interactions between the components [18, 86, 92, 121, 122]. On this level the media are modeled in the framework of a homogeneous elastic, viscous elastic, and elastic plastic media [86, 110]. In this case the features of the medium structure are taken into account indirectly through the kinetic parameters (relaxation time, viscous coefficients etc.) [8, 18, 67, 70, 86, 92, 110, 106, 121, 122].

The model of multivelocitly interpenetratable continua was developed in terms of classical continuum mechanics [108] and statistical physics [138] in order to describe the dynamical behavior of multi-component media. A fundamental assumption in the theory of mixtures [122] reproduces the assumption in the model of multivelocitly interpenetratable continua [108]; namely, that each micro-volume dv is occupied by a particle of each constituent. The equations of motion for each component involve the terms describing the mass, force and energy interactions between the components. The problem is complicated by the necessity to employ, in the general case, the experimental data for establishing theoretical relations between the macroparameters at the component interaction level. Moreover, if the component interaction is determined, then these models would be indispensable in the theory of multi-component media.

In all the models mentioned, the formalism of continuum mechanics is based on the principle of local action as well as on the generalization of the mechanics laws relating

the point mass to the continuum [151].

When going from the integral equations to differential balance equations, the existence of a differentially small microvolume dv is assumed. On the one hand, this volume is so small that the mechanics laws of the point can be extended to the whole microvolume. On the other hand, the volume contains so many structural elements of the medium that, in this sense, it can be regarded as macroscopic one in spite of its smallness as compared to the entire volume occupied by the medium. So, the passage to the differential balance equations is based on the assumption that microstructural scales ε are small as compared to the characteristic macroscopic scale of the λ , and the passage should be made to the limiting case $\varepsilon/\lambda \rightarrow 0$. Contraction of the volume dv to the point is in the general case correct for continuous functions [122, 151]. This means that all points within the differentially small volume are equivalent. Hence, for the case of a mixture, the equivalence of the points implies that field characteristics should be averaged over dv . Hence, it is assumed that the equations of motion can be written in terms of average density, mass velocity, and pressure of each individual component. We note that these models do not contain explicit sizes of components.

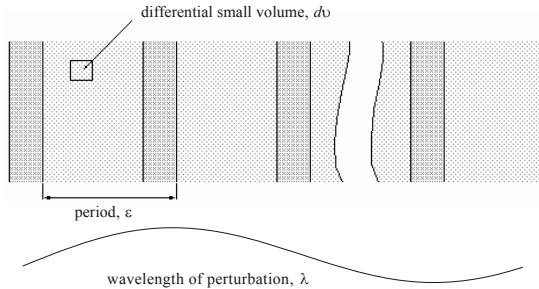


Figure 1.1: Model of the layered medium with two homogeneous components in period.

The application of the models of a homogeneous medium to the description of the dynamical wave processes in a structured natural medium is associated with certain fundamental difficulties [55, 67, 110, 106, 130, 131]. In what follows we treat the medium structure at the macrolevel. We abandon the assumption that the differentially small volume dv contains all the components of the medium, nevertheless we consider the longwave approach with the wavelength λ much greater than the characteristic length of the medium structure ε . We consider a structured medium (Fig. 1.1) in which separated components are considered as a homogeneous medium (the differentially small volume dv is much smaller than the characteristic size of a particular component ε).

We describe the wave processes in non-equilibrium heterogeneous media in terms of an asymptotic averaged model [168, 169, 170, 164, 171, 172]. In this case the obtained integral differential system of equations cannot be reduced to the average terms (pressure, mass velocity, specific volume) and contains the terms with characteristic sizes of individual components.

On the microstructure level of the medium, the dynamical behavior is governed only by the laws of thermodynamics. On the macrolevel, the motion of the medium can be

described by the wave-dynamical laws for the averaged variables with the integrodifferential equation of state containing the characteristics of the medium microstructure. A rigorous mathematical proof is given to show that on the acoustic level, the propagation of long waves can be properly described only in terms of dispersive dissipative properties of the medium, and in this case, the dynamical behavior of the medium can be modeled by a homogeneous relaxing medium. However, finite-amplitude long waves respond to the structure of the medium in such a way that the homogeneous medium model is insufficient for the description of the behavior of the structured medium. An important result that follows from this model is that, for a finite-amplitude wave, the medium structure (in particular, existence of microcracks) produces nonlinear effects even if the individual components of the medium are described by a linear law. It turns out that the known Lyakhov model for the natural multi-component media [92, 150] is an actual case of the asymptotic averaged model, i.e., it is inherently asymptotic.

We have considered averaged systems of hydrodynamical equations in both Lagrangian and Eulerian coordinates. These systems are not expressed in the average hydrodynamical terms, hence the dynamical behavior of the medium cannot be modeled by a homogeneous medium even for long waves, if they are nonlinear. The structure of the medium influences the nonlinear wave propagation. The heterogeneity of the medium structure always introduces additional nonlinearity that does not arise in a homogeneous medium. This effect makes it possible to formulate the theoretical grounds of a new diagnostic method that determines the characteristics of a heterogeneous medium with the use of finite-amplitude long waves (inverse problem). This diagnostic method can also be employed to find the mass contents of individual components.

Natural physical phenomena possess, in general, complicated nonlinear features. Recent advances in nonlinear science have been rather considerable. Starting from the general idea of relaxing phenomena in real media via hydrodynamical approach, we will derive a nonlinear evolution equation for the high-frequency waves. At the same time we will show how to obtain an equation by modeling the propagation of high-frequency waves in a relaxing medium. Historically, the suggested equation has been called the Vakhnenko equation (VE) and we shall follow this name. Periodic and solitary traveling wave solutions are found by direct integration. Some of these solutions are loop-like in nature. The VE can be written in an alternative form, now known as the Vakhnenko–Parkes equation (VPE), by changing the independent variables. The VPE can also be written in Hirota bilinear form. Then it is possible to determine the interaction of two solitons. In contrast to the Korteweg-de Vries (KdV) equation, the VE contains different kinds of phaseshifts. From the mathematical point of view, the ambiguous solution does not introduce difficulties, while the physical interpretation of the ambiguity always introduces some difficulties. We suggest the physical interpretation of an ambiguous solutions. A number of states with their thermodynamical parameters can occupy one microvolume. In this sense the nonequilibrium state of the suggested model is assumed to describe several states with different hydrodynamic parameters.

We suggest a transformation that enables one to reduce, with certain accuracy (the transformation is exact for planar symmetry as well as for stationary flows), the known solutions of gas-dynamic problems to the two-phase media with arbitrary volume portion of incompressible components. It is proved that there is a similarity in motions

of gas and two-phase medium with incompressible component. This transformation is very important from the viewpoint of the study of multi-component media. Indeed, this transformation enables one to obtain the solution of many problems for multi-component media with incompressible phases, provided the solution of a similar problem for a homogeneous compressible medium is known. In this case it is not necessary to solve directly the problem for the medium with incompressible component, and it is sufficient just to transform the known solution of the similar problem for a homogeneous medium. Thus, the solutions of many hydrodynamical problems for multi-component media with incompressible phases can be obtained without solving the initial system of equations. The scope for the suggested transformation is demonstrated by the reference to the strong explosion state in a two-phase medium.

The features of the dynamical behavior of two-component media with interphase interaction will be considered by solving a problem associated with the strong explosion stage. This problem attracts interest also in view of the practical possibility to estimate the efficiency of medium as localizer of shock wave action. The attenuation of shock waves in gas-liquid foam generated by condensed explosive charges will be described in terms of a relaxed transfer of heat from the gas phase to the condensed phase. The problem is how to describe/find the dependence of the flow behind the shock front on the thermophysical properties of the medium and the completeness of relaxation processes. We will analyze the dependence of the shock damping parameters on the thermal relaxation time in order to provide a deeper understanding of the damping of shock waves in such media and to determine their effectiveness as localizing media. Besides, it is of interest to define the dependence of shock wave attenuation on the shock loading, especially on the explosion energy.

An important object for investigation is earth materials. Sedimentary rocks, particularly sandstones, possess grain structure. The peculiarities of grain and pore structures give rise to a variety of remarkable nonlinear mechanical properties demonstrated by rocks, under both quasistatic and alternating dynamical loading.

A phenomenological model describing complex stress-strain properties of a sandstone sample under slow loading is presented. In order to treat the elastic and nonlinear behavior observed in stress cycling experiments, we consider a combination of three mechanisms. The mechanisms of the interior equilibration processes in a sandstone are: the standard solid relaxation mechanism, the sticky-spring mechanism, and the permanent plastic deformation mechanism. With a small number of parameters, the overall model displays both qualitatively and quantitatively the principal experimental observations of the stress-strain trajectories for the Berea sandstone, in particular, the details of the end-point memory under the quasistatic loading.

We have developed and thoroughly examined a model of longitudinal vibration resonance in bar-shaped sedimentary rocks. These materials exhibit memory that originates from an essential asymmetry of rupture and recovery of the intergrain and interlamina cohesive bonds. The theory relies on an appropriate isolation and adequate formalization of two mutually dependent subsystems, namely, a subsystem of ruptured bonds and a subsystem of internal longitudinal displacements. The subsystem of ruptured bonds is shown to be of a soft-ratchet type, so that its response to an alternating internal stress is characterized by broken symmetry and appears as nonzero long-term temporal and spatial changes in the concentration of ruptured bonds. The

internal stress is generated by an alternating external drive acting both directly through the subsystem of longitudinal displacements and indirectly through temporal and spatial modifications of the Young modulus due to the changes in the concentration of ruptured bonds. The scheme reproduces the main experimental effects by using the simplest linear form of attenuation in an elastic subsystem and realistic assumptions of the stress-strain relation. In particular, it correctly describes: hysteretic behavior of the resonance curve on both its upward and downward slopes; linear softening of the resonance frequency under the increase of the driving level; gradual (almost logarithmic) recovery (increase) of the resonance frequency under low dynamical strains that follow the high-strain conditioning of the sample; and temporal relaxation of the response acceleration amplitude for fixed frequency. These are the most interesting observations typical of forced longitudinal oscillations of sandstone bars in the nonlinear regime. Moreover, we can trace how water saturation enhances the hysteresis and simultaneously decreases the quality factor due to the increase in the equilibrium concentration of ruptured cohesive bonds. We also predict theoretically a dynamical effect analogous to the widely known quasistatic effect of hysteresis with discrete (end-point) memory. Following the theoretical prediction, our colleagues TenCate and Shankland from Los Alamos National Laboratory have performed experimental measurements in order to verify this prediction.

These exclusive experimental results obtained at Los Alamos National Laboratory stimulate us to carry out additional simulation. The experimental resonance curves for the Fontainebleau sandstone were reproduced by using the suggested model of the resonance response for the sandstone. The models we developed can adequately reproduce the experimental results and can be applied for future research.

Chapter 2

Asymptotic averaged model for structured medium

The current status of experimental researches demands to develop the models of dynamical behavior of media with account of their inner structure. The real media are not structureless. For example, the geophysical medium has a complicated hierarchical structure. It turns out that the ratio of typical sizes between the neighboring hierarchical levels is a constant value [124, 126, 130]. The inner structure of a medium affects the propagation of waves, which appear as a result of high-gradient fast processes (explosion, earthquake) [125, 130].

Within continuum mechanics [88] the known idealization of a real medium as homogeneous has a wide application to model their dynamic behavior. In these models the effect of heterogeneity is taken into account indirectly throughout the kinetic parameters such as a viscous coefficient and relaxation time. The inner processes in this case are manifested through dispersive dissipative properties of a medium. Traditionally, it was considered that in heterogeneous media with wavelength appreciably exceeding the size of the structural heterogeneities, the perturbations propagate in the same way as in homogeneous media [4, 8, 122]. However, this statement should be proved, and we shall show that this approximation is not universally true. In general case, the wave propagation can not be described in terms of the average characteristics (continuum model).

The properties of a medium deviate from the equilibrium state under the propagation of intensive waves. Moreover, an unperturbed medium can be in one of unstable stationary states. So, a geophysical medium, within a current physical concept, is an open thermodynamic system, which essentially influences on the exchanges of energy and mass. Thus, a description of open systems should take into account the peculiarities of their inner structure, dynamical processes occurring on the level of structural elements. What is more, the state of media under the action of high-frequency wave perturbations departs from equilibrium, and, thus, the behavior of media can not be described in the framework of equilibrium thermodynamics. Consequently, there is necessity to develop the new mathematical models in order to take into account the nonlinear wave perturbations and irreversible inner exchange processes.

2.1 Background and initial equations

The simplest heterogeneous media for which the effect of the structure can be analyzed are media with a regular structure. Features of the propagation of long wave perturbations will be investigated by using as an example, a periodic medium under conditions of an equality of stresses and mass velocities on the boundaries of neighboring components. It is supposed that the microstructure elements of medium dv (see Fig. 1.1) are large enough that it is possible to submit to the laws of classical continuum mechanics for each individual component. At the same time the inner processes in each component will be considered within a relaxation approach. The notions based on the relaxation nature of a phenomenon are regarded to be promising and fruitful. We consider that the properties of the medium, such as density, sound velocity and relaxation time vary in a periodic manner (although this assumption is unessential in the final result).

2.1.1 Motion equations for individual component

The analysis of wave motions is based on the hydrodynamic approach. This restriction can be imposed for the modeling of nonlinear waves in watersaturated soils, bubble media, aerosols, etc. [86, 92]. The set of acceptable media could be extended to solid media where the powerful loads are studied in the condition that the strength and plasticity of the material can be neglected [89]. In the hydrodynamic approach we have considered the media without tangential stresses while there are equalities of the stresses as well as of mass velocities on boundaries of neighboring components. Also, we assume that the medium is barotropic. The individual components of the medium are considered to be described by the classical equations of hydrodynamics. In the Lagrangian coordinate system (l, t) the equations of one-dimensional motion for each individual component have the form

$$\begin{aligned} \frac{\partial r^\nu}{\partial l^\nu} &= \frac{V}{V_0}, \quad u = \frac{\partial r}{\partial t}, \\ \frac{\partial u}{\partial t} + V_0 \left(\frac{r}{l}\right)^{\nu-1} \frac{\partial p}{\partial l} &= 0. \end{aligned} \tag{2.1.1}$$

The equation of continuity can also be used in the alternative form

$$\frac{\partial V}{\partial t} - \nu V_0 \frac{\partial r^{\nu-1} u}{\partial l^\nu} = 0. \tag{2.1.2}$$

Here $V = \rho^{-1}$ is the specific volume, ν is a parameter of symmetry, where $\nu = 1$ is planar symmetry, $\nu = 2$ is cylindrical one, $\nu = 3$ is spherical one; the index 0 relates to the initial state. The other notations are those that are generally accepted.

Conditions for matching are the equality of mass velocities and pressures on the boundaries of the components

$$[u] = 0, \quad [p] = 0. \tag{2.1.3}$$

2.1.2 Dynamic state equation

Considering the models of a relaxing medium as more general than the equilibrium models for describing the evolution of high-gradient waves, we will take into account the relaxing processes for each component. Thermodynamic equilibrium is disturbed owing to the propagation of fast perturbations in a medium. There are processes of the interaction that tend to return the equilibrium. The parameters characterizing this interaction are referred to as the inner variables unlike the macroparameters such as the pressure p , mass velocity u , and density ρ . In essence, the change of macroparameters caused by the changes of inner parameters is a relaxation process. From the nonequilibrium thermodynamics standpoint, the models of a relaxing medium are more general than the equilibrium models for describing the wave propagation.

An equilibrium state equation of a barotropic medium is an one-parameter equation. As a result of relaxation, an additional variable ξ (inner parameter) appears in the state equation. It defines the completeness of the relaxation process

$$p = p(\rho, \xi). \quad (2.1.4)$$

There are two limiting cases:

- (i) the lack of the relaxation (inner interaction processes are frozen) $\xi = 1$,

$$p = p(\rho, 1) = p_f(\rho), \quad (2.1.5)$$

- (ii) the relaxation complete (there is the local thermodynamic equilibrium) $\xi = 0$,

$$p = p(\rho, 0) = p_e(\rho). \quad (2.1.6)$$

The equations of state (2.1.5) and (2.1.6) are considered to be known. These relationships enable us to introduce the sound velocities for fast processes

$$c_f^2 = dp_f/d\rho \quad (2.1.7)$$

and for slow processes

$$c_e^2 = dp_e/d\rho. \quad (2.1.8)$$

The slow and fast processes are compared by means of the relaxation time τ_p . The dynamic state equation is written down in the form of the differential first-order equation

$$\tau_p \left(\frac{d\rho}{dt} - c_f^{-2} \frac{dp}{dt} \right) + (\rho - \rho_e) = 0. \quad (2.1.9)$$

The equilibrium equations of state are considered to be known

$$\rho_e - \rho_0 = \int_{p_0}^p c_e^{-2} dp. \quad (2.1.10)$$

Clearly, for the fast processes ($\omega\tau_p \gg 1$) we have the relation (2.1.5), and for the slow ones ($\omega\tau_p \ll 1$) we obtain (2.1.6).

The substantiation of Eq. (2.1.9) within the framework of the thermodynamics of irreversible processes has been given in [30, 35, 88, 209]. As far as we know the first work in this field was the article by Mandelshtam and Leontovich [96] (see also Section 81 in [88]). We note that the mechanisms of the exchange processes are not defined concretely when deriving Eq. (2.1.9), and the thermodynamic and kinetic parameters appear only in this equation. These characteristics can be found experimentally.

The phenomenological approach for describing the relaxation processes in hydrodynamics has been developed in many publications [86, 88, 92, 209]. The dynamic equation of state was used (a) for describing the propagation of sound waves in a relaxing medium [88], (b) for taking into account the exchange processes within media (gas-solid particles) [209], (c) for studying wave fields in gas-liquid media [86] and in soil [92]. In most works, the equation of state has been derived from the concept of concrete mechanism for the inner process. Within the context of mixture theory, Biot [18] attempted to account for the non-equilibrium in velocities between components directly in the equations of motion in the form of dissipative terms.

We assume that the relaxation time and sound velocities do not depend on time, but they are functions of pressure and the individual properties of the components. This means that in the process of a relaxation interaction we can take into account the exchange of moment and heat but not that of mass. Peculiarities of the intrastructure interaction are determined by the dynamic equation of state for each component.

The equations of motion (2.1.1) have been written in the Lagrangian coordinate system. The necessity of such a description stems from the fact that the dynamic equation of state (2.1.9) has been written to the mass element of a medium. Besides, the use of the Lagrangian coordinates is important for the application of the method of asymptotic averaging, since in these coordinates the structure is independent of a wave process.

2.2 Asymptotic averaged system of equations

A regularity of structure and a nonlinearity of long-wave processes investigated here specify the choice of mathematical methods. One way of studying this heterogeneous medium is based on a method of asymptotic averaging of equations with high-oscillating coefficients [11, 12, 16, 132, 164]. The essence of this method consists in the application of a multiscale method in combination with a space averaging. In accordance with this method, the mass space coordinate $m = l^\nu/V_0$ is divided into two independent coordinates: slow coordinate s and fast one ξ , wherein

$$m = s + \varepsilon\xi, \quad \frac{\partial}{\partial m} = \frac{\partial}{\partial s} + \varepsilon^{-1} \frac{\partial}{\partial \xi}. \quad (2.2.1)$$

The slow coordinate s corresponds to a global change of the wave field and s is a constant value during a period, while the fast coordinate ξ traces the variations of a field in the structure period. The dependent functions are presented as a degree series

over the structure period ε

$$\begin{aligned}
 V(m, t) &= V^{(0)}(s, t, \xi) + \varepsilon V^{(1)}(s, t, \xi) + \varepsilon^2 V^{(2)}(s, t, \xi) + \dots \\
 p(m, t) &= p^{(0)}(s, t, \xi) + \varepsilon p^{(1)}(s, t, \xi) + \varepsilon^2 p^{(2)}(s, t, \xi) + \dots \\
 u(m, t) &= u^{(0)}(s, t, \xi) + \varepsilon u^{(1)}(s, t, \xi) + \varepsilon^2 u^{(2)}(s, t, \xi) + \dots \\
 r^\nu(m, t) &= (r^\nu)^{(0)}(s, t, \xi) + \varepsilon (r^\nu)^{(1)}(s, t, \xi) + \varepsilon^2 (r^\nu)^{(2)}(s, t, \xi) + \dots
 \end{aligned} \tag{2.2.2}$$

where $p^{(i)}$, $u^{(i)}$, $V^{(i)}$, $r^{(i)}$ are defined as the one-period functions of ξ . In the Lagrangian mass coordinates the period is a constant which allows the averaging procedure to be performed.

We now will prove that $p^{(0)} = p^{(0)}(s, t)$, $p^{(1)} = p^{(1)}(s, t)$, $u^{(0)} = u^{(0)}(s, t)$, $(r^\nu)^{(0)} = (r^\nu)^{(0)}(s, t)$ are independent of the fast variable ξ . Indeed, after substitution of Eqs. (2.2.1) and (2.2.2) into the initial equations of motion, we obtain

$$\begin{aligned}
 -\varepsilon^{-1} \frac{\partial (r^\nu)^{(0)}}{\partial \xi} + \varepsilon^0 \left(\frac{\partial (r^\nu)^{(0)}}{\partial s} - \frac{\partial (r^\nu)^{(1)}}{\partial \xi} - V^{(0)} \right) + \dots &= 0, \\
 \varepsilon^0 \left(u^{(0)} - \frac{\partial r^{(0)}}{\partial t} \right) + \dots &= 0, \\
 -\varepsilon^{-1} \nu (r^{\nu-1})^{(0)} \frac{\partial p^{(0)}}{\partial \xi} + \varepsilon^0 \left(\frac{\partial u^{(0)}}{\partial t} + \nu (r^{\nu-1})^{(0)} \frac{\partial p^{(0)}}{\partial s} \right. \\
 \left. + \nu (r^{\nu-1})^{(1)} \frac{\partial p^{(0)}}{\partial \xi} + \nu (r^{\nu-1})^{(0)} \frac{\partial p^{(1)}}{\partial \xi} \right) + \dots &= 0, \\
 -\varepsilon^{-1} \nu \frac{\partial (r^{\nu-1})^{(0)} u^{(0)}}{\partial \xi} + \varepsilon^0 \left(\frac{\partial V^{(0)}}{\partial t} + \nu \frac{\partial (r^{\nu-1})^{(0)} u^{(0)}}{\partial s} \right. \\
 \left. - \nu \frac{\partial (r^{\nu-1})^{(1)} u^{(0)}}{\partial \xi} - \nu \frac{\partial (r^{\nu-1})^{(0)} u^{(1)}}{\partial \xi} \right) + \dots &= 0,
 \end{aligned}$$

According to the general theory of the asymptotic method, the terms of equal powers of ε should vanish independently of each other. Thus, $\partial p^{(0)}/\partial \xi = 0$, $\partial u^{(0)}/\partial \xi = 0$, $\partial (r^{\nu-1})^{(0)}/\partial \xi = 0$, i.e. $p^{(0)} = p^{(0)}(s, t)$, $u^{(0)} = u^{(0)}(s, t)$, $r^{(0)} = r^{(0)}(s, t)$ are independent of ξ . Furthermore

$$\begin{aligned}
 \frac{\partial (r^\nu)^{(0)}}{\partial s} + \frac{\partial (r^\nu)^{(1)}}{\partial \xi} &= V^{(0)}, \\
 u^{(0)} &= \frac{\partial r^{(0)}}{\partial t}, \\
 \frac{\partial u^{(0)}}{\partial t} + \nu (r^{\nu-1})^{(0)} \frac{\partial p^{(0)}}{\partial s} + \nu (r^{\nu-1})^{(0)} \frac{\partial p^{(1)}}{\partial \xi} &= 0, \\
 \frac{\partial V^{(0)}}{\partial t} - \nu \frac{\partial (r^{\nu-1})^{(0)} u^{(0)}}{\partial s} - \nu \frac{\partial (r^{\nu-1})^{(1)} u^{(0)}}{\partial \xi} - \nu \frac{\partial (r^{\nu-1})^{(0)} u^{(1)}}{\partial \xi} &= 0.
 \end{aligned} \tag{2.2.3}$$

Thus, we can average the equations during the period ξ . We define $\langle \cdot \rangle = \int_0^1 (\cdot) d\xi$, and perform the normalization $\int_0^1 d\xi = 1$. Since $p^{(1)}$, $u^{(1)}$ and $r^{(1)}$ are periodic, the

integrals can be calculated as $\langle \partial p^{(1)} / \partial \xi \rangle = 0$, $\langle \partial u^{(1)} / \partial \xi \rangle = 0$, $\langle \partial r^{(1)} / \partial \xi \rangle = 0$. Moreover, as $\langle u^{(0)} \rangle = u^{(0)}$, $\langle p^{(0)} \rangle = p^{(0)}$ than $\partial p^{(1)} / \partial \xi = 0$. This means that $p^{(1)}$ does not also depend on ξ . After integrating over the structure period the equations containing the value of zero order of ε , we obtain the averaged system

$$\begin{aligned} \frac{\partial (r^\nu)^{(0)}}{\partial s} &= \langle V^{(0)} \rangle, \\ u^{(0)} &= \frac{\partial r^{(0)}}{\partial t}, \\ \frac{\partial u^{(0)}}{\partial t} + \nu (r^{\nu-1})^{(0)} \frac{\partial p^{(0)}}{\partial s} &= 0, \\ \frac{\partial \langle V^{(0)} \rangle}{\partial t} - \nu \frac{\partial (r^{\nu-1})^{(0)} u^{(0)}}{\partial s} &= 0 \end{aligned} \tag{2.2.4}$$

with the averaged equation of state

$$d \langle V^{(0)} \rangle = - \left\langle \frac{(V^{(0)})^2}{c_f^2} \right\rangle dp - \left\langle \frac{V^{(0)}}{\tau_p V_e(p^{(0)})} (V^{(0)} - V_e(p^{(0)})) \right\rangle dt. \tag{2.2.5}$$

Unlike the values $u^{(0)}$, $p^{(0)}$, $p^{(1)}$ and $r^{(0)}$, the specific volume $V^{(0)}$ is a function of ξ . Hereafter, we will consider only the zero approximation of the equations and, therefore, the upper index 0 is omitted. Choosing the wavelength λ to be large enough we can always reduce the effect to zero from other approximation terms.

The averaged system of equations (2.2.4), (2.2.5) is an integro-differential one and, in the general case, is not reduced to the averaged variables p , u and $\langle V^{(0)} \rangle$. The derivation of equations (2.2.4), (2.2.5) relates to a rigorous periodic medium. However, it may be shown that equations (2.2.4), (2.2.5) are also relevant to media with a quasi-periodic structure. Indeed, the pressure p and the mass velocity u are independent of the fast variable ξ . Hence on a microscale ξ , the action is statically uniform (waveless) over the whole period of the medium structure, while on the slow scale s , the action of perturbation is manifested by the wave motion of the medium. On a microlevel the behavior of medium adheres only to the thermodynamic laws. There is a mechanical equilibrium. On a macrolevel, the motion of medium is described by the wave dynamics laws for averaged variables. Mathematically, in the zero-order case of ε , the size of the period is infinitesimal ($\varepsilon \rightarrow 0$). This signifies that the location of particular components in the period is irrelevant. The equations (2.2.4), (2.2.5) do not change their form if the components are broken and/or change their location in an elementary cell. This means that equations (2.2.4), (2.2.5) describe the motion of any quasi-periodic (statistical heterogeneous) medium which has a constant mass content of components on the microlevel, and the location of these components within the cell is not important.

In the case of nonlinear wave propagation, the individual components suffer different compressions. The structure of medium is changed, with the result that the averaged specific volume $\langle V \rangle$ is changed. This change differs from the change of the specific volume for homogeneous medium under the same loading. Thus, the structure of medium is manifested in the wave motion, despite the fact that the equations of motion (2.2.4) (but not the equation of state) are written down for the averaged values u , p , $\langle V \rangle$ only.

2.3 System of equations in Eulerian coordinates

In certain cases of theoretical analysis it is more convenient to use the Eulerian coordinate system. The immediate employment of the averaging asymptotic method in Eulerian variables is impossible because of the variability of the microstructure sizes. However, from the zero approximation in the equations of motion (2.2.1), which are presented by the averaged values p , u , $\langle V \rangle$, the equations can be rewritten in the Eulerian system of coordinates (r, t_E) by means of a transformation from the Lagrangian system (s, t) [164, 168, 169, 170, 171, 172]

$$r = r(s, t), \quad t_E = t. \quad (2.3.1)$$

There is an important presumption that the velocity of the particle in the zero approximation is constant over a period of the structure and, consequently, we can describe an averaged trajectory for the particle

$$\left(\frac{\partial r(s, t)}{\partial t} \right)_s = u(s, t). \quad (2.3.2)$$

From the physical point of view, it is clear that the position of the particle is unambiguously defined by its coordinate and time

$$dr^\nu = A ds + \nu r^{\nu-1} u dt, \quad t_E = t. \quad (2.3.3)$$

From the mathematical point of view this means that in the transformation (2.3.3) the value dr^ν is a total differential. Therefore, we must have

$$\frac{\partial A}{\partial t} = \frac{\partial \nu r^{\nu-1} u}{\partial s}.$$

This condition is satisfied if $A = \langle V \rangle$, because the equation converts into the continuity equation (2.2.4). We obtain the following transformation between Lagrangian and Eulerian systems of coordinates:

$$dr^\nu = \langle V \rangle ds + \nu r^{\nu-1} u dt, \quad t_E = t. \quad (2.3.4)$$

It is reasonable to define the slow Lagrangian coordinate (non-mass one) as

$$R^\nu = s \langle V \rangle. \quad (2.3.5)$$

Equations (2.2.4) in the Eulerian system of coordinates then take the form

$$\begin{aligned} \frac{\partial \langle V \rangle^{-1}}{\partial t_E} + \frac{\partial r^{\nu-1} u \langle V \rangle^{-1}}{\partial r} &= 0, \\ \frac{\partial u}{\partial t_E} + u \frac{\partial u}{\partial r} + \langle V \rangle \frac{\partial p}{\partial r} &= 0. \end{aligned} \quad (2.3.6)$$

It is convenient to determine the fast Eulerian coordinate ζ as

$$\left(\frac{\partial \zeta}{\partial \xi} \right)_t = \frac{\tilde{\rho}}{\rho(\xi)}. \quad (2.3.7)$$

It should be noted that the average density $\bar{\rho}$ in the Eulerian coordinates is a value usually used for density. A chain of identities

$$\langle V \rangle = \int_0^1 V(\xi) d\xi = \int_0^1 V \frac{\rho}{\bar{\rho}} d\xi = \bar{\rho}^{-1} \quad (2.3.8)$$

proves that $\langle V \rangle^{-1}$ is the average density of the medium in the Eulerian coordinates. Note that $\bar{\rho} \neq \langle \rho \rangle$. The value $\bar{\rho}$ is a real density. The value $\langle V \rangle$ is the specific volume averaged in units of mass over the period and it is expressed as the ratio of the volume to the mass inside this volume. This value can be determined experimentally. At the same time the averaged values p and u coincide in both Lagrangian and Eulerian systems of coordinates. Now the equations of motion (2.3.6) can be written in the usual form of the averaged density $\bar{\rho}$.

The notation of the equations of motion in the averaged values enables us to suggest the method of the computer solution for the system of equations, where the integration step is restricted by the perturbation wavelength and not by the period of the structure [171, 172] (see point 2.4.3) Then the main computational problem associated with the smallness of the integration step can be avoided, and the equations of motion can be solved at large distance of wave propagation within a reasonable time.

2.4 Analysis of the averaged system of equations

In this section we will study some general properties of the averaged system of equations, and will obtain a rigorous mathematical proof that for the acoustic level the long wave dynamic behavior of the medium with a microstructure can be modeled within the framework of a homogeneous relaxing medium. At the same time the description of nonlinear waves can not be reduced to the average characteristics of wave field [164].

2.4.1 Acoustic waves

Let us consider an acoustic wave ($p' = p - p_0$, $p' \ll p_0$). We shall prove that the propagation of the acoustic waves in a periodic medium with a calculable number of relaxation components is similar to that in a homogeneous medium with the same number of independent relaxation processes.

Now we shall show it for a two-layer periodic medium with one process of relaxation in each structure element. The averaged equation of state (2.2.5)

$$d\langle V \rangle = - \left\langle \frac{V^2}{c_f^2} \right\rangle dp - \left\langle \frac{V}{\tau V_e(p)} (V - V_e(p)) \right\rangle dt$$

for small perturbations in this medium can be represented as

$$- \langle V' \rangle = \langle V^2 / c_f^2 \rangle p' + \varkappa \frac{V_1^2 (c_{1e}^{-2} - c_{1f}^{-2})}{1 + \tau_{1\text{per}} \frac{d}{dt}} p' + (1 - \varkappa) \frac{V_2^2 (c_{2e}^{-2} - c_{2f}^{-2})}{1 + \tau_{2\text{per}} \frac{d}{dt}} p', \quad (2.4.1)$$

$$\langle V^2 / c_e^2 \rangle = \varkappa V_1^2 / c_{1e}^2 + (1 - \varkappa) V_2^2 / c_{2e}^2,$$

where index 1 relates to the first component, and index 2 — to the second component. Here \varkappa is a coordinate of the boundary between the components in the elementary cell. Note that the values \varkappa and $1 - \varkappa$ are equal to the mass concentration of the first and the second component, respectively.

For comparison we take the homogeneous medium with two independent relaxation processes. The state equation of this medium for small perturbations has a form [88]

$$-V' = \frac{V^2}{c_f^2} p' + \frac{V^2(c_{e1}^{-2} - c_{f1}^{-2})}{1 + \tau_{1\text{hom}} \frac{d}{dt}} p' + \frac{V^2(c_{e2}^{-2} - c_{f2}^{-2})}{1 + \tau_{2\text{hom}} \frac{d}{dt}} p', \quad (2.4.2)$$

$$c_f^{-2} = \sum_i c_{fi}^{-2}.$$

It should be noted that the alphanumeric indices for the homogeneous medium and for the periodic one have a reverse succession. Here, index 1 relates to the first relaxation process, and index 2 — to the second process.

Now we can write six relationships

$$\begin{aligned} \varkappa_i V_i^2 (c_{ie}^{-2} - c_{if}^{-2})_{\text{per}} &= V^2 (c_{ei}^{-2} - c_{fi}^{-2})_{\text{hom}}, \\ \langle V^2 / c_e^2 \rangle &= V^2 \sum_i c_{ei}^{-2}, \quad \langle V^2 / c_f^2 \rangle = (V^2 / c_f^2)_{\text{hom}}, \\ \tau_{i\text{per}} &= \tau_{i\text{hom}}, \quad \varkappa_1 = \varkappa, \quad \varkappa_2 = 1 - \varkappa, \quad i = 1, 2. \end{aligned} \quad (2.4.3)$$

These equations show that for any two-component medium with the two relaxation components ($\tau_{i\text{per}}, c_{ie}, c_{if}$) (see Eq. (2.4.1)) we can pick up the homogeneous medium with two relaxation processes ($\tau_{i\text{hom}}, c_{ei}, c_{fi}$) (see Eq. (2.4.2)). In such media the perturbations $\langle V \rangle, p, u$ move in a similar way. Regarding the density $\langle \rho \rangle$ this statement is incorrect. The result can be easily expanded on the media with a calculable number of the relaxation components. This result proves the statement that in the studies of acoustic wave propagation in a periodic medium with N relaxation components, this medium can be substituted by a homogeneous medium in which there are N independent relaxation processes.

The similarity of the propagation of small perturbation in periodic and homogeneous media has been verified numerically. As it was expected, we obtained the traditional result. An inner structure of the medium manifests itself only by means of the dispersive dissipative properties. For the acoustic level the long wave dynamic behavior of the medium with a microstructure can be modeled within the homogeneous relaxing medium. In the past such a statement was accepted *a priori*. In our case we have obtained a rigorous mathematical proof of this statement on the basis of a account, in details, of the structure of medium.

2.4.2 Nonlinear waves

We will analyze the propagation of nonlinear waves in a structured medium. To make the results more clear, we will restrict our consideration to a nonrelaxation media ($c = c_f = c_e$). The averaged equation of state in this case is simplified to the form

$$d\langle V \rangle = - \left\langle \frac{V^2}{c^2} \right\rangle dp, \quad (2.4.4)$$

and we can introduce an effective sound velocity by the formula

$$c_{\text{eff}} = \sqrt{\langle V \rangle^2} / \left\langle \frac{V^2}{c^2} \right\rangle. \quad (2.4.5)$$

We obtain a traditional representation of the system of equations (2.2.4), (2.2.5) and (2.4.4).

The system of the equations is concerned in the hyperbolic type of a system. Now we restrict ourselves to the plane symmetry ($\nu = 1$). Substituting the equation of state (2.4.4) into the equation of the continuity (2.1.1), we get

$$\left\langle \frac{V^2}{c^2} \right\rangle \frac{\partial p}{\partial t} + \frac{\partial u}{\partial s} = 0. \quad (2.4.6)$$

The combination of this equation with the last equation (2.1.1) ($\nu = 1$) leads to the relationships

$$\left(\frac{\partial u}{\partial t} \pm \left\langle \frac{V^2}{c^2} \right\rangle^{1/2} \frac{\partial p}{\partial t} \right) \pm \left\langle \frac{V^2}{c^2} \right\rangle^{-1/2} \left(\frac{\partial u}{\partial s} \pm \left\langle \frac{V^2}{c^2} \right\rangle^{1/2} \frac{\partial p}{\partial s} \right) = 0. \quad (2.4.7)$$

From this relationship it is seen that the averaged system of the equations pertains to the hyperbolic system. The equations for the characteristic in Lagrangian coordinates (mass space coordinate) have the forms

$$\frac{ds}{dt} = \pm \left\langle \frac{V^2}{c^2} \right\rangle^{-1/2}. \quad (2.4.8)$$

In characteristic the relations are the following

$$I_{\pm} = u \pm \int \left\langle \frac{V^2}{c^2} \right\rangle^{1/2} dp. \quad (2.4.9)$$

Analogously to the homogeneous medium we call these relations as the Riemann invariants. The value (2.4.8) has the physical meaning, namely, it is the averaged velocity of the wave propagation in the Lagrangian coordinates. This velocity depends on a pressure and integrally on a structure. Note the special case. It is known that in vacuum the wave does not propagate. This result also follows formally from Eq. (2.4.8). The hyperbolicity of a system points up that this system can describe the shock wave. The equations for the characteristic (2.4.8) and the Riemann invariants (2.4.9) are the integro-differential equations, since they retain the variable $\langle V^2/c^2 \rangle$, which depends on the properties of the structure elements in medium.

Normalization on the averaged specific volume $\langle V \rangle$ and the initial sound velocity c_{eff} allows us to compare the results for various media. For convenience we have chosen that the acoustic waves in these media propagate in a similar way (see Eq. (2.4.3)).

It should be noted that c_{eff} is not an averaged value, i.e. $c_{\text{eff}}^2 \neq \langle c^2 \rangle$. Evidently, the structure of the medium introduces a certain contribution to the nonlinearity. In fact, even if $c_f \neq f(p)$, then in the general case the value of c_{eff} is a function of pressure.

The system of equations (2.2.4) is hyperbolic ones, and this specifies the breaking solutions which are shock waves. For the analysis of such solutions, it is necessary to present Eq. (2.2.4) in the form of integral conservation laws

$$\oint [\langle V \rangle ds + u dt] = 0, \quad \oint [uds - p dt] = 0. \quad (2.4.10)$$

Now we can easily formulate the conditions on the shock front, when there is conservation of the fluxes of mass and of impulse through the shock front

$$(\langle V_1 \rangle - \langle V_0 \rangle) D + u_1 - u_0 = 0, \quad (u_1 - u_0) D - p_1 + p_0 = 0, \quad (2.4.11)$$

where indexes 0 and 1 relate to the parameters of the flow before and after the front, respectively. Hence, the formula for the averaged velocity of the shock front in terms of the Lagrangian variable D (dimension $[D]$ is kg/s) and the mass velocity u follow from the following relations:

$$D = \sqrt{(p_1 - p_0) / (\langle V_0 \rangle - \langle V_1 \rangle)}, \quad (2.4.12)$$

$$u_1 - u_0 = \sqrt{(p_1 - p_0) (\langle V_0 \rangle - \langle V_1 \rangle)}.$$

2.4.3 Analytical–numerical calculation method

Simultaneously with the analytical methods for theoretical investigation, we have carried out the purposeful numerical experiments that are universal to solve the problems considered here. The calculation has been focused both to confirm the analytical results and obtain the features of the studied wave propagation.

The equations of motion (2.2.4)

$$\frac{\partial r^\nu}{\partial s} = \langle V \rangle, \quad u = \frac{\partial r}{\partial t},$$

$$\frac{\partial u}{\partial t} + \nu r^{\nu-1} \frac{\partial p}{\partial s} = 0,$$

are to be written in the averaged variables p , u , $\langle V \rangle$, r depending only on slow space coordinate s and time t . The equation of state (2.2.5)

$$d\langle V \rangle = - \left\langle \frac{V^2}{c_f^2} \right\rangle dp - \left\langle \frac{V}{\tau_p V_e(p)} (V - V_e(p)) \right\rangle dt$$

is integro-differential one with two independent variables — slow coordinate s and fast coordinate ξ . The method for finding of the solutions for the equation system (2.2.4)–(2.2.5) is not obvious.

Let us describe the conceivable approaches in order to reduce the equation of state to the form where the desired variables are to be dependent on slow variable s and time t only [165, 167, 170, 171, 172]. A number of possible ways can be suggested to obtain such form of the equation of state. Now we write two of them. First, there is an universal way with the application of the Fourier transformation [165, 170, 171, 172]. Second, in special case for the layered media we suggest to use the orthogonal basis

which consists of segmentwise permanent functions. This approach allows to carry on the required calculation with suitable computational resource.

At first we consider the universal way. All functions depending on ξ are presented in a form of the Fourier series on interval associated with structure period of a medium. It is convenient to apply a relationship

$$\rho V = 1, \quad (2.4.13)$$

which is also valid for zero-approximation $\rho^{(0)}V^{(0)} = 1$.

In equations (2.2.5), (2.4.13) the values ρ , c_f^{-2} , c_e^{-2} , V , τ_p^{-1} depending on ξ are written as Fourier series on interval $\xi \in [0, 1]$, for example, for $V(\xi)$

$$V(\xi) = V'_0 + \sum_{n=1}^{\infty} (V'_n \cos(2\pi\xi n) + V''_n \sin(2\pi\xi n)). \quad (2.4.14)$$

The series expansion coefficients can be defined from the known formulas [85]. We now rewrite the relationship (2.4.13) in the Fourier transform. Equation (2.4.13) should be multiplied by the factor $\cos(2\pi\xi n)$ ($k = 0, 1, 2, \dots$), and then after the integration over ξ , we obtain for $k = 0$

$$1 = \rho'_0 V'_0 + \frac{1}{2} \sum_{n=1}^{\infty} (\rho'_n V'_n + \rho''_n V''_n) \equiv \psi(\rho, V), \quad (2.4.15)$$

and for $k = 1, 2, 3, \dots$

$$\begin{aligned} 0 &= \rho'_0 V'_k + \rho'_k V'_0 + \frac{1}{2} \sum_{n=1}^{\infty} (\rho'_n V'_{n+k} + \rho'_{n+k} V'_n + \rho''_n V''_{n+k} + \rho''_{n+k} V''_n) \\ &+ \frac{1}{2} \sum_{n=1}^{k-1} (\rho'_n V'_{k-n} - \rho''_n V''_{k-n}) \equiv \psi_k(\rho, V). \end{aligned} \quad (2.4.16)$$

Similar to this procedure the equation (2.4.13) can be multiplied by the factors $\sin(2\pi\xi n)$ with $k = 1, 2, 3, \dots$, then we have

$$\begin{aligned} 0 &= \rho'_0 V''_k + \rho''_k V'_0 + \frac{1}{2} \sum_{n=1}^{\infty} (\rho'_n V''_{n+k} - \rho'_{n+k} V''_n + \rho''_{n+k} V'_n - \rho''_n V'_{n+k}) \\ &+ \frac{1}{2} \sum_{n=1}^{k-1} (\rho'_{k-n} V''_n - \rho''_n V'_{k-n}) \equiv \varphi_k(\rho, V). \end{aligned} \quad (2.4.17)$$

For the sake of convenience we introduce the function $\psi_k(\rho, V)$ and $\varphi_k(\rho, V)$.

Now we rewrite the equation of state (2.2.5) in an appropriate form in order to present it in Fourier transform

$$\left(\frac{d\rho}{dt} - c_f^{-2} \frac{dp}{dt} \right) + c_f^{-2} \tau_p^{-1} (p - p_0) + \tau_p^{-1} (\rho - \rho_0) = 0. \quad (2.4.18)$$

The equation (2.4.18) reveals the product of no more than two functions depending on ξ , namely, $c_f^{-2} \tau_p^{-1}$, $\tau_p^{-1} (\rho - \rho_0)$. The existence of terms with product of two functions only depending on ξ allows one to simplify the finding of the solutions.

In the Fourier transform from the equation of state we obtain $2k + 1$ equations. Indeed, multiplying by factor $\cos(2\pi\xi n)$ or $\sin(2\pi\xi n)$ for each $k = 0, 1, 2, \dots$ and integrating over period $\xi \in [0, 1]$, we obtain

$$\begin{aligned} \frac{d\rho'_0}{dt} - (c_f^{-2})'_0 \frac{dp}{dt} - \psi(c_f^{-2}, \tau_p^{-1})(p - p_0) + \psi(\tau_p^{-1}, \rho - \rho_0) &= 0. \\ \frac{d\rho'_k}{dt} - (c_f^{-2})'_k \frac{dp}{dt} - \psi_k(c_f^{-2}, \tau_p^{-1})(p - p_0) + \psi_k(\tau_p^{-1}, \rho - \rho_0) &= 0. \\ \frac{d\rho''_k}{dt} - (c_f^{-2})''_k \frac{dp}{dt} - \varphi_k(c_f^{-2}, \tau_p^{-1})(p - p_0) + \varphi_k(\tau_p^{-1}, \rho - \rho_0) &= 0. \end{aligned} \quad (2.4.19)$$

As a result, we have the infinite system of equations (2.4.14)–(2.4.19) in which the variables p, u, ρ_k, V_k are the functions of s and t only. The density and the specific volume as functions of a slow variable s can be found from the sums of the Fourier series. In numerical calculations we can restrict ourselves by the partial sums of the finite Fourier series, whereas in this case the equation system is the closed system. The accuracy in the describing wave processes is defined by the accuracy of the finite Fourier series to reproduce the structure of a medium.

The described method is universal for finding the solutions of integral differential system of the equations. However, if the components differ widely in sizes, then a calculation throughout finite Fourier series becomes cumbersome. For overcoming of this restriction we suggest to use the orthonormalized basis which could be appropriate for studying a model period medium. For a layered medium, the components can be described by the segmentwise permanent functions while the sizes of components are constant in the Lagrangian system of coordinates. It is clear that the segmentwise permanent basis is to be more appropriate for describing these segmentwise permanent functions. Then the sought variables in this basis can be expanded in the finite series.

Let us consider the layered medium consisting of the N -components. Let \varkappa_i be the coordinate of the boundary of i component in the fast variable ξ within one structure period. It is important that the boundaries in the Lagrangian coordinates are independent of wave process, i.e. $\varkappa_i = \text{const}$. The segmentwise permanent orthogonal basis is, by definition, as follows

$$\begin{aligned} g_0 &= 1, \quad \varkappa_0; \\ g_i(\xi) &= \begin{cases} 0, & 0 \leq \xi < \varkappa_{i-1}; \\ k_i^{-1}(1 - \varkappa_i), & \varkappa_{i-1} \leq \xi < \varkappa_i; \\ k_i^{-1}(\varkappa_{i-1} - \varkappa_i), & \varkappa_i \leq \xi < 1; \end{cases} \quad i = 1, 2, \dots, N-1, \end{aligned} \quad (2.4.20)$$

where $k_i^2 = (1 - \varkappa_{i-1})(1 - \varkappa_i)(\varkappa_i - \varkappa_{i-1})$. The graphical illustration of the basic functions is presented in Fig. 2.1. It is early to verify that $g_i(\xi)$ are orthogonal, since $\int_0^1 g_i g_j d\xi = \delta_{ij}$. The reduce of the equation system to the form depending only on slow coordinate can be carried out in manner that is similar to the procedure when the Fourier series were applied. The functions depending on ξ are rewritten in form, for example, for specific volume

$$V(\xi) = \sum_{i=0}^{N-1} g_i V_i. \quad (2.4.21)$$

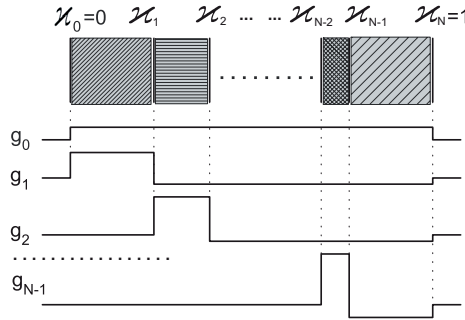


Figure 2.1: One period of the layered medium (upper). The basic functions g_i (lower).

The coefficients V_i are independent of the fast variable ξ . Let us expand the equations (2.4.13) in basis (2.4.20). Multiplying this equation by g_i and integrating over structure period, we obtain

$$1 = \sum_{i=0}^{N-1} \rho_i V_i \equiv \mu_0(\rho, V), \quad (2.4.22)$$

$$0 = \rho_0 V_k + \rho_k V_0 + a_k \rho_k V_k \equiv \mu_k(\rho, V), \quad k = 1, 2, \dots, N-1.$$

The coefficients a_i are found from relationships

$$a_i = \frac{1 - 2\mathcal{X}_k + \mathcal{X}_{k-1}}{\mathcal{X}_k}.$$

The same procedure for state equation (2.4.18) gives

$$\dot{p}(c_f^{-2})_k + \dot{\rho}_k + \mu_k(\tau_p^{-1}, c_e^{-2})(p - p_0) - \mu_k(\rho - \rho_0, \tau_p^{-1}) = 0. \quad (2.4.23)$$

As a result, we have the system of $2N+2$ equations (2.2.4), (2.4.13), (2.4.22), (2.4.23), where the functions depend only on slow space variable s and time t . In this case, the structure of the layered medium is reproduced exactly by finite series in contrast when the Fourier series are used. It allows to carry out the calculations for model media, while their components differ in sizes.

Consequently, we have overcome the principal difficulty, namely, now the equation system consists of the functions depending only on s and t but not on ξ . The numerical algorithm for finding of wave fields can be realized without account of component sizes but with account of wavelength of a perturbation. Thus, this approach enables one to describe the wave fields for long distances.

2.5 Lyakhov model as special case of an asymptotic averaged model

The derivation of the averaged equations of motion (2.2.4) and (2.2.5) gives the rigorous mathematical foundation for the use of one-velocity continuous models for a heterogeneous medium, and these models are of asymptotic origin. One of these models is a

well-known Lyakhov model. Over several years this last model has been successfully applied to describe explosions and nonlinear waves in soil [91, 92, 150]. Now we will prove that the Lyakhov model is particular case of the asymptotic averaged model.

The experiments which have been conducted over a number of years on the action of explosive and shock loading on the soft soil (see Ref. [204]) show an effect of time lag of the strain with respect to the stress (relaxation effect) and large deformations of the soil. The Lyakhov model enables us to take into account all these effects and describe the propagation of nonlinear waves (explosion, shock waves) in soil and also in a bubble media [91, 92]. In this approach the multicomponent medium is considered as a homogeneous continuum with a special equation of state. The macrovolume includes all the components that compose the medium. The average values: pressure p_L , specific volume V_L , mass velocity u_L are defined in the standard way. The equations of motion have the following form in the Lagrangian coordinate system [92]:

$$\begin{aligned} \frac{\partial V_L}{\partial t} - \nu V_{L0} \frac{\partial r_L^{\nu-1} u_L}{\partial R^\nu} &= 0, & u_L &= \frac{\partial r_L}{\partial t}, \\ \frac{\partial u_L}{\partial t} + V_{L0} \left(\frac{r}{R}\right)^{\nu-1} \frac{\partial p_L}{\partial R} &= 0. \end{aligned} \quad (2.5.1)$$

There is a direct connection between Lyakhov model and the averaged equations (2.2.4) and (2.2.5). First we will show that the variable V_L introduced by Lyakhov is nothing more than the averaged value of the specific volume in the mass Lagrangian coordinate $\langle V \rangle$. In order to do it we will start by making the following transformation. The value of a specific volume V_L is expressed through the initial volume content of the i -th component α_i by the formula (see p. 56 in Ref. [92]) $V_L = V_{L0} \sum_{i=1}^3 \alpha_i V_i / V_{i0}$. It is easily seen that

$$\frac{V_L}{V_{L0}} = \sum_{i=1}^3 \alpha_i \frac{\rho_{i0}}{\rho_i} = \sum_{i=1}^3 \frac{\tilde{\rho}_0}{\rho_{i0}} \beta_i \frac{\rho_{i0}}{\rho_i} = \tilde{\rho}_0 \sum_{i=1}^3 \beta_i V_i = \langle V_0 \rangle^{-1} \langle V \rangle. \quad (2.5.2)$$

where we used the connection between the parameter α_i and the size of i -th component β_i (in mass Lagrangian coordinates)

$$\alpha_i = \beta_i \frac{\tilde{\rho}_0}{\rho_{i0}}. \quad (2.5.3)$$

The value β_i is the mass content of the i -th component. Obviously, β_i is constant and independent of the wave motion.

As shown earlier in the asymptotic averaging method for zero order, the pressure and mass velocity are independent of the fast coordinate ξ . At the same time in Lyakhov model it is suggested, *a priori*, that the pressure in all components is equal, and these components move with equal velocities. Comparing the equations of motion (2.2.4) and (2.2.5), we can see that there are connections between the values of pressure $p_L = p^{(0)}$, the values of mass velocities $u_L = u^{(0)}$, and the values of Eulerian space coordinates $r_L = r^{(0)}$. Hereafter, the index L on p , u and r is omitted.

The microstructure is taken into account by means of the dynamic equation of state in Lyakhov model [92]

$$\frac{\dot{V}_L}{V_{L0}} = \varphi(p_L) \dot{p}_L - \frac{\alpha_1}{\eta} \psi(p_L, V_L), \quad (2.5.4)$$

$$\begin{aligned}
\varphi(p_L) &= - \sum_{i=2}^3 \frac{\alpha_i}{\rho_{i0} c_{i0}^2} \left[\frac{\gamma_i(p_L - p_0)}{\rho_{i0} c_{i0}^2} + 1 \right]^{-(1+\gamma_i)/\gamma_i}, \\
\psi(p_L, V_L) &= p_L - p_0 - \frac{\rho_{10} c_{10}^2}{\gamma_1} \\
&\quad \times \left\{ \left[\frac{V_L}{V_{0L}} - \sum_{i=2}^3 \alpha_i \left(\frac{\gamma_i(p_L - p_0)}{\rho_{i0} c_{i0}^2} + 1 \right)^{-1/\gamma_i} \right]^{-\gamma_1} \alpha_1^{\gamma_1} - 1 \right\}.
\end{aligned} \tag{2.5.5}$$

Here the index number 0 relates to the initial nonperturbed state; 1 corresponds to the parameters of air; 2 — to the parameters water; 3 — to the solid substance; α_i is the initial volume content of the i -th phase in soil; $\sum_{i=1}^3 \alpha_i = 1$; and γ_i is the exponent in the Tait equations of state. The coefficient of the volume viscosity η plays an important role in Lyakhov equations of state. Whereas, in the general case it depends on the pressure and the specific volume $\eta = \eta(p, V_L)$.

At $\dot{p} = 0$ and $\dot{V}_L = 0$ we obtain the following equation of the equilibrium compressibility medium:

$$\frac{V_L}{V_{0L}} = \sum_{i=1}^3 \alpha_i \left(\frac{\gamma_i(p_L - p_0)}{\rho_{i0} c_{i0}^2} + 1 \right)^{-1/\gamma_i}. \tag{2.5.6}$$

The sound velocity in such a process can be found by the formula [92]

$$c_L = \frac{\sum_{i=1}^3 \alpha_i \left(\frac{\gamma_i(p_L - p_0)}{\rho_{i0} c_{i0}^2} + 1 \right)^{-1/\gamma_i}}{\left\{ V_{L0}^{-1} \sum_{i=1}^3 \frac{\alpha_i}{\rho_{i0} c_{i0}^2} \left[\frac{\gamma_i(p_L - p_0)}{\rho_{i0} c_{i0}^2} + 1 \right]^{-(1+\gamma_i)/\gamma_i} \right\}^{1/2}}. \tag{2.5.7}$$

Let us now compare the equations of state (2.2.5) and (2.5.4). We shall prove that the equation of state (2.5.4) in Lyakhov model implies that the medium cannot be considered as homogeneous one and this equation of state is an averaged equation.

At first we shall consider the nonrelaxation medium. In this case the equation of state (2.5.4) takes the form of equation (2.5.6). It can be shown that expressions (2.5.6) and (2.4.4) coincide if in equation (2.2.5) the dependence of the sound velocity on the pressure is concretely defined by Tait relationship as in equation (2.5.6). Therefore, we must check the case $p \rightarrow p_0$. The substitution of expression (2.5.3) into equation (2.5.7) gives

$$\begin{aligned}
c_{L0} &= \left(V_{L0}^{-1} \sum_{i=1}^3 \frac{\alpha_i}{\rho_i^2 c_{i0}^2} \right)^{-1/2} = V_{L0} \left(\sum_{i=1}^3 \beta_i \frac{V_{i0}^2}{c_{i0}^2} \right)^{-1/2} \\
&= \langle V_0 \rangle \left\langle \frac{V_0^2}{c_0^2} \right\rangle^{-1/2} = (c_{\text{eff}})_0.
\end{aligned}$$

Hence, we have proved that the sound velocity c_{L0} is an effective averaged sound velocity for the periodic medium $c_{\text{eff}0}$ (2.4.5). Thus the expression (2.5.7) changes to the

equation (2.4.4). Let us take into account the processes of relaxation and consider the dynamic equation of state in Lyakhov model (2.5.4), (2.5.5). For weak perturbations we have

$$\begin{aligned}\psi(p, V_L) &= \Delta p - \frac{\rho_{10}c_{10}^2}{\gamma_1} \left[\left\{ \frac{V_L}{V_{L0}} - \sum_{i=2}^3 \alpha_i \left(\frac{\gamma_i \Delta p}{\rho_{i0}c_{i0}^2} + 1 \right)^{-1/\gamma_i} \right\}^{-\gamma_1} \alpha_1^{\gamma_1} - 1 \right] \\ &= \Delta p - \frac{\rho_{10}c_{10}^2}{\gamma_1} \left[\left\{ \frac{V_L - (V_L)_e}{V_{L0}} + \alpha_i \left(\frac{\gamma_i \Delta p}{\rho_{i0}c_{i0}^2} + 1 \right)^{-1/\gamma_i} \right\}^{-\gamma_1} - 1 \right] \\ &= \Delta p - \frac{\rho_{10}c_{10}^2}{\gamma_1} \left(-\gamma_1 \frac{V_L - (V_L)_e}{\alpha_1 V_{L0}} + \frac{\gamma_1 \Delta p}{\rho_{i0}c_{i0}^2} \right) = \rho_{10}c_{10}^2 \frac{V_L - (V_L)_e}{\alpha_1 V_{L0}},\end{aligned}$$

where $(V_L)_e$ is defined by Eq. (2.5.6). The equation of state takes the form

$$\frac{\dot{V}_L}{V_{L0}} = \varphi(p_L) \dot{p}_L - \frac{\rho_{10}c_{10}^2}{\eta} \frac{V_L - (V_L)_e}{\alpha_1 V_{L0}}. \quad (2.5.8)$$

We will now consider the value of φ in equation (2.5.5). The sum is calculated for the solid components ($i = 2, 3$) and this signifies that the high-frequency sound velocity of a multicomponent medium is determined by the sound velocity in the solid components. The gas phase is considered as incompressible one for these perturbations [92] ($c_{1f} \rightarrow \infty$). We will now restore this term and take the high-frequency sound velocity c_{1f} equal to the sound velocity in the solid component, and under the condition $p \rightarrow p_0$ we can obtain

$$\varphi(p) = - \sum_{i=2}^3 \frac{\alpha_i}{\rho_{i0}c_{i0}^2} = - \sum_{i=1}^3 \frac{\alpha_i}{\rho_{i0}c_{if}^2} = - \langle V_0 \rangle^{-1} \left\langle \frac{V^2}{c_f^2} \right\rangle. \quad (2.5.9)$$

Finally, when we use the notation of the model of asymptotic averaging $v_L = \langle V \rangle$ together with Eq. (2.5.9) then the Lyakhov equation of state (2.5.8) takes the following form:

$$\langle \dot{V} \rangle = - \left\langle \frac{V^2}{c_f^2} \right\rangle \dot{p} - \frac{\langle V \rangle - \langle V_e \rangle}{\tau}. \quad (2.5.10)$$

where $\tau = \eta V_{10}/c_{e1}^2$. Thus, we see that expression (2.5.10) is the averaged equation of state. It does not reduced to the averaged variables $p, u, \langle V \rangle, \tau$ because of the term $\langle V^2/c_f^2 \rangle$.

Let us compare expression (2.5.10) with the dynamic equation of state for a periodic medium (2.2.5). In a periodic medium the relaxation processes are considered to occur in each component. Eq. (2.2.5) becomes the expression (2.5.10) only when one component is a relaxing component, whereas in Lyakhov model the dependence of sound velocity on pressure is concretely defined.

Thus, a rigorous mathematical analysis has shown that for both models the equations of motion are written in terms of averaged values $p, u, \langle V \rangle$, while the properties of separate components are contained in the equations of state. It is shown that the equations of motion coincide completely. The dynamic equations of state of the averaged

description for these models also coincide in the sense that only one relaxation process is considered in the Lyakhov model. However, in Lyakhov model the dependence of sound velocity on the pressure is defined concretely, and the gas phase is considered incompressible for high-frequency perturbations. Our approach explains these details in a rigorous manner. Therefore, using an asymptotic method Lyakhov model has been directly verified. Thus, it is proved that Lyakhov model is of asymptotic origin.

2.6 Conclusions

Thus, in this chapter we present an asymptotic averaged model to explain the propagation of long nonlinear waves in a nonequilibrium medium with a regular structure. In the general case, the averaged system of equations is integrodifferential and does not reduce to the averaged variables $p, u, \langle V \rangle$. On a microstructure level of the medium the dynamic behavior adheres only to the thermodynamic laws. On a macrolevel the motion of the medium can be described by wave dynamic laws for averaged variables with an integrodifferential equation of state containing the characteristics of microstructure in medium. The suggested model justifies the one-velocity continuous model. A comparison of this model was carried out with Lyakhov model for the natural multicomponent media. We have shown that the Lyakhov model is of asymptotic origin. A rigorous mathematical proof is provided for the statement that on an acoustic level for long waves the inner structure of the medium manifests itself only by means of the dispersive dissipative properties, and the dynamic behavior of the medium can be modeled in the framework of a homogeneous relaxing medium. However, the long wave with a finite amplitude responds to the structure of the medium so that the behavior of the structured medium cannot be modeled by a homogeneous medium.

An important result (which will be proved in Sec. 6.1) foretold by this model is that the medium structure always increases the nonlinear effects on the long waves, and a nonlinearity takes place even if the individual components are described by a linear law. In chapter 6 we will prove that this effect provides the basis for a new method of diagnostics to define the properties of multicomponent media using the evolution of long nonlinear waves.

Chapter 3

Solitons in homogeneous relaxing medium

The physical phenomena and processes that take place in nature generally have complicated nonlinear features. This leads to nonlinear mathematical models for the real processes. The modern physicist should be aware of aspects of nonlinear wave theory developed over the past few years. There is much interest in the practical issues involved, as well as the development of methods to investigate the associated nonlinear mathematical problems including nonlinear wave propagation. An early example of the latter was the development of the inverse scattering method for the Korteweg-de Vries (KdV) equation [47] and the subsequent interest in soliton theory.

Starting from a general idea of relaxing phenomena in real media via a hydrodynamic approach, we will derive a nonlinear evolution equation for describing high-frequency waves. To develop physical models for wave propagation through media with complicated inner kinetics, notions based on the relaxational nature of a phenomenon are regarded to be promising. From the nonequilibrium thermodynamics standpoint, models of a relaxing medium are more general than equilibrium models.

We will show how the KdV equation arises in modeling the propagation of low-frequency waves in a relaxing medium. In high-frequency case the waves in a relaxing medium are described by an equation called now in scientific literature as the Vakhnenko equation (VE). The VE is related to a particular form of the Whitham equation. Periodic and solitary traveling wave solutions are found by direct integration. Some of these solutions are loop-like in nature. The VE can be written in an alternative form, now known as the Vakhnenko-Parkes equation (VPE), by a change of independent variables. The VPE can be written in Hirota bilinear form. It is then possible to show that the VPE has the N -soliton solution. This solution is found by using a blend of the Hirota method and ideas originally proposed by Moloney and Hodnett [101]. This solution is discussed in detail, including the derivation of phase shifts due to the interaction between solitons. Hence, the suggested equation has ambiguous loop-like solutions. It is established that a dissipative term, with a dissipation parameter less than some limit value, does not destroy these loop-like solutions.

3.1 Low-frequency and high-frequency perturbations in relaxing medium

To analyze the wave motion in relaxing medium, we shall use the hydrodynamic equations in planar symmetry ($\nu = 1$): the mass conservation law (2.1.2)

$$\frac{\partial V}{\partial t} + \frac{\partial u}{\rho_0 \partial x} = 0 \quad (3.1.1)$$

and the momentum conservation law (2.1.1)

$$\frac{\partial u}{\partial t} - \frac{\partial u}{\rho_0 \partial x} = 0. \quad (3.1.2)$$

The closed system of equations consists of two motion equations (3.1.1), (3.1.2) and the dynamic state equation (2.1.9)

$$\tau_\rho \left(\frac{dp_e}{dt} - c_f^2 \frac{d\rho}{dt} \right) + (p - p_e(\rho)) = 0$$

that is applied to account for the relaxation effects.

Let us consider a small perturbation $p' \ll p_0$. The equations of state for fast (2.1.4) and slow (2.1.5) processes are considered to be known. They can be expanded as the power series with accuracy $O(p'^2)$

$$\begin{aligned} V_f(p_0 + p') &= V_0 - V_0^2 c_f^{-2} p' + \frac{1}{2} \left. \frac{d^2 V_f}{dp^2} \right|_{p=p_0} p'^2 + \dots, \\ V_e(p_0 + p') &= V_0 - V_0^2 c_e^{-2} p' + \frac{1}{2} \left. \frac{d^2 V_e}{dp^2} \right|_{p=p_0} p'^2 + \dots. \end{aligned} \quad (3.1.3)$$

Hereafter, the velocities c_e , c_f are related to the initial pressure p_0 . Combining these two relationships with the equations of motion (3.1.1) and (3.1.2), we obtain the equation in one unknown quantity (the dash in p' is omitted) [153, 158]:

$$\begin{aligned} \tau_p \frac{\partial}{\partial t} \left(\frac{\partial^2 p}{\partial x^2} - c_f^{-1} \frac{\partial^2 p}{\partial t^2} + \frac{1}{2V_0^2} \left. \frac{d^2 V_f}{dp^2} \right|_{p=p_0} \frac{\partial^2 p^2}{\partial t^2} \right) \\ + \left(\frac{\partial^2 p}{\partial x^2} - c_e^{-1} \frac{\partial^2 p}{\partial t^2} + \frac{1}{2V_0^2} \left. \frac{d^2 V_e}{dp^2} \right|_{p=p_0} \frac{\partial^2 p^2}{\partial t^2} \right) = 0. \end{aligned} \quad (3.1.4)$$

A similar equation has been obtained in Ref. [30], but without nonlinear terms.

The hydrodynamic nonlinearity $p \partial p / \partial x$ and the complicated dispersive law are inherent in medium which is described by the evolution equation (3.1.4). Now we consider the dispersive relation which follows from equation (3.1.4) after a substitution of the slow perturbation in a form $p' \sim \exp[i(kx - \omega t)]$,

$$-i\omega \tau_p \frac{c_e^2}{c_f^2} (\omega^2 - c_f^2 k^2) + (\omega^2 - c_e^2 k^2) = 0. \quad (3.1.5)$$

From this relationship we obtain the functional dependence $k = k(\omega)$

$$k^2 = \frac{\omega^2}{c_f^2} \cdot \frac{\tau_p^2 \omega^2}{1 + \tau_p^2 \omega^2} \cdot \left(1 + \frac{i}{\tau_p \omega} \cdot \frac{c_f^2 - c_e^2}{c_e^2} + \frac{1}{\tau_p^2 \omega^2} \cdot \frac{c_e^2}{c_f^2} \right). \quad (3.1.6)$$

Taking the roots we write the result in a form $k = k' + ik''$. It is clear that k'' is associated with the speed of wave attenuation as a function of the distance [88], while a value $c = \omega/k'$ can be considered as the velocity of the perturbation propagation. The expressions for k' and k'' take the form

$$k' = a_1 \sqrt{\sqrt{a_2^2 + a_3^2} + a_2}, \quad k'' = a_1 \sqrt{\sqrt{a_2^2 + a_3^2} - a_2},$$

$$a_1 = \frac{\tau_p^2 \omega^2}{\sqrt{2} c_f \sqrt{1 + \tau_p^2 \omega^2}}, \quad a_2 = 1 + \frac{c_f^2}{\tau_p^2 \omega^2 c_e^2}, \quad a_3 = \frac{c_f^2 - c_e^2}{\tau_p \omega c_e^2}.$$

In Fig. 3.1, for example, we show the dependencies c and k'' on $\tau_p \omega$ for water-saturation soil with concentration of air 0.1. For this medium $c_f = 1620$ m/s and $c_e = 260$ m/s [92]. The velocity c increases monotonically from c_e to c_f at bottom-up sweep $\tau_p \omega$. The dependence $k'' = k''(\omega)$ points that at $\omega \rightarrow 0$ the dispersion is absent,

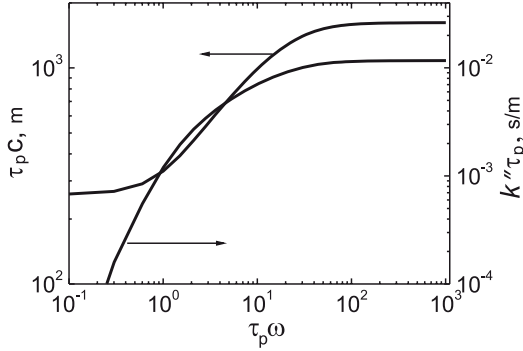


Figure 3.1: The dependencies of the velocity c and the attenuation factor k'' on frequency $\tau_p \omega$.

while at high frequency the variable k'' becomes a constant and does not depend on ω (see Fig. 3.1) with the limit value

$$\tau_p k'' = \frac{c_f^2 - c_e^2}{2c_f^2 c_e^2}.$$

Hence, the energy in high-frequency wave dissipates always. For this wave the pressure attenuation is the same as at fixed distance and does not depend on frequency ω .

The equation of state in the form (2.1.9) enables us to describe the effects associated with bulk viscosity of a medium. Let us show that for slow processes (since for these processes the notion of viscosity coefficient is defined, i.e. for processes in which a small deviation from equilibrium is taken into account in linear approximation) a bulk viscosity coefficient relates to the relaxation time $\tau_p = \tau_p c_e^2 / c_p^2$ [30, 88, 96]

$$\zeta = \tau_p \rho (c_f^2 - c_e^2). \quad (3.1.7)$$

Let us rewrite (2.1.9) in a form of the power series p in $\tau_p d/dt$. To do it, we differentiate equation (2.1.9) with respect to time t and substitute the result into the same equation (2.1.9). Repeating several times this procedure, we obtain with required accuracy the expression

$$dp = c_e^2 d\rho + \tau_p (c_f^2 - c_e^2) d\dot{\rho} - \tau_p^2 (c_f^2 - c_e^2) d\ddot{\rho} + \dots \quad (3.1.8)$$

Let us consider two terms only in this relation. The value $c_e^2 d\rho$ associates with increase of a pressure dp_e in infinitely slow process, i.e. $dp_e = c_e^2 d\rho$. It is noted that the value p acquires more general sense than merely a pressure. With accuracy of a sign the value $(-p)$ is nothing other than a stress π_{ii} . By definition, in the low-frequency approximation the stress is written through the bulk viscosity coefficient [88]

$$\pi_{ii} = -p_e + \zeta \frac{\partial u}{\partial x}.$$

Then it is easily to obtain the expression for the bulk viscosity coefficient in the form (3.1.7).

Now we shall show that for low-frequency perturbations the equation (3.1.4) is reduced to the Korteweg-de Vries-Burgers (KdVB) equation, while for high-frequency waves we shall obtain the equation with hydrodynamic nonlinearity and term that appeared in the Klein-Gordon equation. To analyze the equation (3.1.4) let us apply the multiscale method [99, 105]. The value $\varepsilon \equiv \tau_p \omega$ is chosen to be small (large) parameter where the quantity ω is the characteristic frequency of wave perturbation. For the sake of convenience we rewrite the equation (3.1.4) as follows:

$$\begin{aligned} \tau_p \omega \frac{\partial}{\partial t\omega} \left(\frac{\partial^2 p}{\partial (x\omega)^2} - c_f^{-2} \frac{\partial^2 p}{\partial (t\omega)^2} + \alpha_f \frac{\partial^2 p^2}{\partial (t\omega)^2} \right) + \\ + \left(\frac{\partial^2 p}{\partial (x\omega)^2} - c_e^{-2} \frac{\partial^2 p}{\partial (t\omega)^2} + \alpha_e \frac{\partial^2 p^2}{\partial (t\omega)^2} \right) = 0, \end{aligned} \quad (3.1.9)$$

$$\alpha_f = \frac{1}{2V_0^2} \left. \frac{d^2 V_f}{dp^2} \right|_{p=p_0}, \quad \alpha_e = \frac{1}{2V_0^2} \left. \frac{d^2 V_e}{dp^2} \right|_{p=p_0},$$

and introduce the new independent variables

$$T_0 = t\omega, \quad X_0 = x\omega, \quad T_{-2} = t\omega/\varepsilon^2, \quad X_{-2} = x\omega/\varepsilon^2. \quad (3.1.10)$$

The dependent variable p is a function of T_0, X_0, T_{-2}, X_{-2} , i.e. $p = p(T_0, X_0, T_{-2}, X_{-2})$.

The existing derivatives in (3.1.9) are to be rewritten in the new independent variables

$$\begin{aligned}
\frac{\partial}{\partial x\omega} &= \frac{\partial}{\partial X_0} + \varepsilon^{-2} \frac{\partial}{\partial X_{-2}}, \\
\frac{\partial}{\partial t\omega} &= \frac{\partial}{\partial T_0} + \varepsilon^{-2} \frac{\partial}{\partial T_{-2}}, \\
\frac{\partial^2}{\partial (x\omega)^2} &= \frac{\partial^2}{\partial X_0^2} + 2\varepsilon^{-2} \frac{\partial^2}{\partial X_0 \partial X_{-2}} + \varepsilon^{-4} \frac{\partial^2}{\partial X_{-2}^2}, \\
\frac{\partial^2}{\partial (t\omega)^2} &= \frac{\partial^2}{\partial T_0^2} + 2\varepsilon^{-2} \frac{\partial^2}{\partial T_0 \partial T_{-2}} + \varepsilon^{-4} \frac{\partial^2}{\partial T_{-2}^2}, \\
\frac{\partial^3}{\partial (t\omega)^3} &= \frac{\partial^3}{\partial T_0^3} + 3\varepsilon^{-2} \frac{\partial^3}{\partial T_0^2 \partial T_{-2}} + 3\varepsilon^{-4} \frac{\partial^3}{\partial T_0 \partial T_{-2}^2} + \varepsilon^{-6} \frac{\partial^3}{\partial T_{-2}^3}, \\
\frac{\partial^3}{\partial t\omega \partial (x\omega)^2} &= \frac{\partial^3}{\partial X_0^2 \partial T_0} + \varepsilon^{-2} \left(\frac{\partial^3}{\partial X_0^2 \partial T_{-2}} + 2 \frac{\partial^3}{\partial T_0 \partial X_0 \partial X_{-2}} \right) \\
&\quad + \varepsilon^{-4} \left(\frac{\partial^3}{\partial T_0 \partial X_{-2}^2} + 2 \frac{\partial^3}{\partial X_0 \partial X_{-2} \partial T_{-2}} \right) + \varepsilon^{-6} \frac{\partial^3}{\partial X_{-2}^2 \partial T_{-2}}.
\end{aligned} \tag{3.1.11}$$

It is precisely these variables that cause the equations [155, 166, 168, 170, 171], obtained within the framework of multiscale method [99, 105]

$$\begin{aligned}
O(\varepsilon^{+1}) &: \frac{\partial}{\partial T_0} \left(\frac{\partial^2 p}{\partial X_0^2} - c_f^{-2} \frac{\partial^2 p}{\partial T_0^2} + \alpha_f \frac{\partial^2 p^2}{\partial T_0^2} \right) = 0, \\
O(\varepsilon^0) &: \frac{\partial^2 p}{\partial X_0^2} - c_e^{-2} \frac{\partial^2 p}{\partial T_0^2} + \alpha_e \frac{\partial^2 p^2}{\partial T_0^2} = 0, \\
O(\varepsilon^{-1}) &: \left(\frac{\partial^3}{\partial X_0^2 \partial T_{-2}} + 2 \frac{\partial^3}{\partial T_0 \partial X_0 \partial X_{-2}} \right) p \\
&\quad - 3c_f^{-2} \frac{\partial^3 p}{\partial T_0^2 \partial T_{-2}} + 3\alpha_f \frac{\partial^3 p^2}{\partial T_0^2 \partial T_{-2}} = 0, \\
O(\varepsilon^{-2}) &: \frac{\partial^2 p}{\partial X_0 \partial X_{-2}} - c_e^{-2} \frac{\partial^2 p}{\partial T_0 \partial T_{-2}} + \alpha_e \frac{\partial^2 p^2}{\partial T_0 \partial T_{-2}} = 0, \\
O(\varepsilon^{-3}) &: \left(\frac{\partial^3}{\partial T_0 \partial X_{-2}^2} + 2 \frac{\partial^3}{\partial X_0 \partial X_{-2} \partial T_{-2}} \right) p \\
&\quad - 3c_f^{-2} \frac{\partial^3 p}{\partial T_0 \partial T_{-2}^2} + 3\alpha_f \frac{\partial^3 p^2}{\partial T_0 \partial T_{-2}^2} = 0, \\
O(\varepsilon^{-4}) &: \frac{\partial^2 p}{\partial X_{-2}^2} - c_e^{-2} \frac{\partial^2 p}{\partial T_{-2}^2} + \alpha_e \frac{\partial^2 p^2}{\partial T_{-2}^2} = 0, \\
O(\varepsilon^{-5}) &: \frac{\partial}{\partial T_{-2}} \left(\frac{\partial^2 p}{\partial X_{-2}^2} - c_f^{-2} \frac{\partial^2 p}{\partial T_{-2}^2} + \alpha_f \frac{\partial^2 p^2}{\partial T_{-2}^2} \right) = 0,
\end{aligned} \tag{3.1.12}$$

to be partially uncoupled. The two leading equations depend on T_0 and X_0 only, while the last two equations include the independent variables T_{-2} and X_{-2} only. Thus, the

low-frequency perturbations are described by the two leading equations, and the high-frequency perturbations — by the last two equations. An interaction between these perturbations is described by the three center equations.

Let us write out the equations of motion for low-frequency and high-frequency perturbations in the initial variables x and t . For low-frequency perturbations the main terms $\partial^2 p / \partial X_0^2$ and $c_e^{-2} \partial^2 p / \partial T_0^2$ (and only they) appear in the first and second equations of the system (3.1.12), while for high-frequency perturbations the main terms $\partial^2 p / \partial X_{-2}^2$ and $c_f^{-2} \partial^2 p / \partial T_{-2}^2$ (and only they) appear in the sixth and seventh equations of the system (3.1.12).

For low-frequency perturbations ($\tau_p \omega \ll 1$) propagating in one direction ($\partial / \partial x - c_e^{-1} \partial / \partial t \simeq 2 \partial / \partial x$), we obtain an evolution equation

$$\frac{\partial p}{\partial t} + c_e \frac{\partial p}{\partial x} + \alpha_e c_e^3 p \frac{\partial p}{\partial x} - \beta_e \frac{\partial^2 p}{\partial x^2} + \gamma_e \frac{\partial^3 p}{\partial x^3} = 0, \quad (3.1.13)$$

$$\alpha_e = \frac{1}{2V_0^2} \left. \frac{d^2 V_e}{dp^2} \right|_{p=p_0}, \quad \beta_e = \frac{c_e^2 \tau_p}{2c_f^2} (c_f^2 - c_e^2),$$

$$\gamma_e = \frac{c_e^3 \tau_p^2}{8c_f^4} (c_f^2 - c_e^2)(c_f^2 - 5c_e^2).$$

This equation can be derived in the following way. A dispersion relation for the linearized equation (3.1.4) can be written down with an accuracy $O(k^3)$ in the form $\omega = c_e k + i\beta_e k^2 - \gamma_e k^3$, if the terms $\partial p / \partial x$ and $c_e^{-1} \partial p / \partial t$ are the main ones. For this dispersion relation we write a linear equation in which a nonlinear term is reconstructed in agreement with the initial equation.

The equation (3.1.13) is the well-known KdVB equation. It is encountered in many areas of physics to describe nonlinear wave processes [3, 45, 37, 112, 107]. In [139] it was shown how hydrodynamic equations reduce to either the KdV or Burgers equation according to the choices for the state equation and the generalized force when analyzing the gasdynamical waves, waves in shallow water [139], hydrodynamic waves in cold plasma [48], and ion-acoustic waves in cold plasma [205].

As is known, the investigation of the KdV equation ($\beta_e = 0$) in conjunction with the nonlinear Schrödinger (NLS) and sine-Gordon equations give rise to the theory of solitons [3, 37, 43, 47, 63, 64, 107, 112, 139, 206]. These equations inherent the striking properties. This is above all the integrability. The equations can be integrated, for instance, by the inverse scattering method. The details on the study of the mentioned equations can be found in monographs [3, 37, 112]. Now let us clarify one of features, namely, the existence of the soliton solution. The soliton points to the distinctive features for these equations. The inverse scattering method, Hirota method, Bäcklund transformation, conservation laws and integrability are concerned with the nonlinear equations. Consequently, the finding of the soliton solutions for another equations involves a considerable interest.

For high-frequency perturbations ($\tau_p \omega \gg 1$), using the last two equations of the system (3.1.12), we get the following evolution equation:

$$\frac{\partial^2 p}{\partial x^2} - c_f^{-2} \frac{\partial^2 p}{\partial t^2} + \alpha_f c_f^2 \frac{\partial^2 p^2}{\partial x^2} + \beta_f \frac{\partial p}{\partial x} + \gamma_f p = 0. \quad (3.1.14)$$

$$\alpha_f = \frac{1}{2V_0^2} \left. \frac{d^2 V_f}{dp^2} \right|_{p=p_0}, \quad \beta_f = \frac{c_f^2 - c_e^2}{\tau_p c_e^2 c_f}, \quad \gamma_f = \frac{c_f^4 - c_e^4}{2\tau_p^2 c_e^4 c_f^2}.$$

In addition to the nonlinear term with coefficient α_f , the equation has dissipative $\beta_f \partial p / \partial x$ and dispersive $\gamma_f p$ terms. If $\alpha_f = \beta_f = 0$, this is a linear Klein-Gordon equation. There is a Green function for this equation [203] that enables us to find the solution in quadrature, at least. The numerical solutions of the Klein-Gordon equation modeling the propagation of high-frequency perturbations in gas-liquid media have been presented in [95]. A similar evolution equation for high-frequency perturbations was described in monograph by Whitham [208]. However, it coincides with Eq. (3.1.14) only when $\alpha_f = 0$ and $\gamma_f = 0$.

Landau and Lifshitz showed that for high frequencies the dissipative term under high transport of heat agrees with corresponding term in the equation (3.1.14) (see section 79 and 81 in [88]). Thus, the dynamic state equation (2.1.9) enables us to take into account the dissipative processes completely. But the form of the dissipative terms describing the inner exchange processes (transport of heat and momentum) are different for the high and low frequencies.

We call attention to the fact that the dispersion relations $\omega = \omega(k)$ for the linearized equations (3.1.13) and (3.1.14) have been restricted by the finite power series in k and in k^{-1} , respectively:

$$\omega = c_e k + i\beta_e k^2 - \gamma_e k^3, \quad \tau_p \omega \ll 1,$$

$$\omega^2 = c_f^2 k^2 (1 + i\beta_f k^{-1} - \gamma_f k^{-2}), \quad \tau_p \omega \gg 1.$$

At the time we were carrying out our research, it turned out that equation (3.1.14) had not been investigated much. It is likely that this is connected with the fact, noted by Whitham in Ref. [208], that high-frequency perturbations attenuate very quickly.

3.2 Evolution equation for high-frequency perturbations

The equation (3.1.14), which we are interested in,

$$\frac{\partial^2 p}{\partial x^2} - c_f^{-2} \frac{\partial^2 p}{\partial t^2} + \alpha_f c_f^2 \frac{\partial^2 p^2}{\partial x^2} + \beta_f \frac{\partial p}{\partial x} + \gamma_f p = 0$$

is written down in a dimensionless form. Let us restrict our consideration to the propagation of high-frequency waves in positive direction x , then with necessary accuracy we can write the operator

$$\frac{\partial^2}{\partial x^2} - c_f^{-2} \frac{\partial^2}{\partial t^2} = \left(\frac{\partial}{\partial x} - c_f^{-1} \frac{\partial}{\partial t} \right) \left(\frac{\partial}{\partial x} + c_f^{-1} \frac{\partial}{\partial t} \right) \rightarrow 2 \frac{\partial}{\partial x} \left(\frac{\partial}{\partial x} + c_f^{-1} \frac{\partial}{\partial t} \right).$$

In the moving coordinates system with velocity c_f , the equation has the form in dimensionless variables

$$\tilde{x} = \sqrt{\frac{\gamma_f}{2}} (x - c_f t), \quad \tilde{t} = \sqrt{\frac{\gamma_f}{2}} c_f t, \quad \tilde{u} = \alpha_f c_f^2 p$$

(tilde over variables $\tilde{x}, \tilde{t}, \tilde{u}$ is omitted) [153, 154, 157, 158]

$$\frac{\partial}{\partial x} \left(\frac{\partial}{\partial t} + u \frac{\partial}{\partial x} \right) u + \alpha \frac{\partial u}{\partial x} + u = 0. \quad (3.2.1)$$

The constant $\alpha = \beta_f / \sqrt{2\gamma_f}$ is always positive. The equation (3.2.1) without the dissipative term has the form of the nonlinear equation [119, 154]

$$\frac{\partial}{\partial x} \left(\frac{\partial}{\partial t} + u \frac{\partial}{\partial x} \right) u + u = 0. \quad (3.2.2)$$

Historically, the equation (3.2.2) has been called the Vakhnenko equation (VE) and we shall follow this name.

It is interesting to note that equation (3.2.2) follows as a particular limit of the following generalized Korteweg-de Vries equation

$$\frac{\partial}{\partial x} \left(\frac{\partial u}{\partial t} + u \frac{\partial u}{\partial x} - \beta \frac{\partial^3 u}{\partial x^3} \right) = \gamma u \quad (3.2.3)$$

derived by Ostrovsky [114] to model the small-amplitude long waves in a rotating fluid (γu is induced by the Coriolis force) of finite depth. Subsequently, the equation (3.2.2) was known by different names in the literature, such as the Ostrovsky-Hunter equation, the short-wave equation, the reduced Ostrovsky equation and the Ostrovsky-Vakhnenko equation.

The consideration here of equation (3.2.2) has interest not only from the viewpoint of the investigation of the propagation of high-frequency perturbations, but more specifically from the viewpoint of the study of methods and approaches that may be applied in the theory of nonlinear evolution equations. This equation was investigated in many papers, here we cite only some of them [102, 119, 153, 154, 157, 158, 162, 163, 179, 180, 181, 182, 183, 184, 185, 186, 187, 188, 189, 190, 191, 192].

3.2.1 The connection with the Whitham equation

Now we show how an evolution equation with hydrodynamic nonlinearity can be rewritten in the form of the Whitham equation. The general form of the Whitham equation is as follows [208]:

$$\frac{\partial u}{\partial t} + u \frac{\partial u}{\partial x} + \int_{-\infty}^{\infty} K(x-s) \frac{\partial u}{\partial s} ds = 0. \quad (3.2.4)$$

On the one hand, the equation (3.2.4) has the nonlinearity of hydrodynamic type; on the other hand, it is known (see, section 13.14 in [208]) that the kernel $K(x)$ can be selected to give the dispersion required. Indeed, the dispersion relation $c(k) = \omega(k)/k$ and the kernel $K(x)$ are connected by means of the Fourier transformation

$$c(k) = F[K(x)], \quad K(x) = F^{-1}[c(k)]. \quad (3.2.5)$$

Consequently, for the dispersion relation $\omega = -1/k$ corresponding to the linearized version of (3.2.2), the kernel is as follows

$$K(x) = F^{-1}[-1/k^2] = \frac{1}{2}|x|. \quad (3.2.6)$$

Thus, the VE (3.2.2) is related to the particular Whitham equation [208]

$$\frac{\partial u}{\partial t} + u \frac{\partial u}{\partial x} + \frac{1}{2} \int_{-\infty}^{\infty} |x-s| \frac{\partial u}{\partial s} ds = 0. \quad (3.2.7)$$

Since we can reduce the VE to the Whitham equation, we can assert that the VE shares interesting properties with the Whitham equation; in particular, it describes solitary wave-type formations, has periodic solutions and explains the existence of the limiting amplitude [208]. An important property is the presence of conservation laws for waves decreasing rapidly at infinity

$$\frac{d}{dt} \int_{-\infty}^{\infty} u dx = 0, \quad \frac{d}{dt} \int_{-\infty}^{\infty} u^2 dx = 0, \quad \frac{d}{dt} \int_{-\infty}^{\infty} \left(\frac{1}{3} u^3 + \widehat{K}u \right) dx = 0, \quad (3.2.8)$$

where by definition $\widehat{K}u = \int_{-\infty}^{\infty} K(x-s)u(s,t)ds$.

For equation (3.2.1) the kernel is $K(x) = \frac{1}{2}[\alpha(2\Theta(x) - 1) + |x|]$, where $\Theta(x)$ is the Heaviside function. Hence, (3.2.1) can be written down as

$$\frac{\partial u}{\partial t} + u \frac{\partial u}{\partial x} + \alpha u + \frac{1}{2} \int_{-\infty}^{\infty} |x-s| \frac{\partial u}{\partial s} ds = 0. \quad (3.2.9)$$

There is no derivative in the dissipative term αu of Eq. (3.2.9).

3.2.2 Loop-like traveling wave solutions

An important step in the investigation of nonlinear evolution equations is to find traveling wave solutions. These are solutions which are stationary with respect to a moving frame of reference. In this case, the evolution equation (a partial differential equation) becomes an ordinary differential equation which is considerably easier to solve.

For the VE (3.2.2) it is convenient to introduce a new dependent variable z and new independent variables η and τ defined by

$$z = (u - v)/|v|, \quad \eta = (x - vt)/|v|^{1/2}, \quad \tau = t|v|^{1/2}, \quad (3.2.10)$$

where v is a non-zero constant [119]. Then the VE becomes

$$z_{\eta\tau} + (zz_{\eta})_{\eta} + z + c = 0, \quad (3.2.11)$$

where $c = \pm 1$ corresponding to $v \gtrless 0$. We now seek stationary solutions of (3.2.11) for which z is a function of η only so that $z_{\tau} = 0$ and z satisfies the ordinary differential equation

$$(zz_{\eta})_{\eta} + z + c = 0. \quad (3.2.12)$$

After one integration (3.2.12) gives

$$\frac{1}{2}(zz_\eta)^2 = f(z), \quad (3.2.13)$$

$$f(z) = -\frac{1}{3}z^3 - \frac{1}{2}cz^2 + \frac{1}{6}A = -\frac{1}{3}(z - z_1)(z - z_2)(z - z_3).$$

A is a constant and for periodic solutions z_1 , z_2 and z_3 are real constants such that $z_1 \leq z_2 \leq z_3$. Since there is only one independent constant A in (3.2.13), one root is independent only, let it be z_3 . The two roots z_1 and z_2 can be defined through z_3

$$z_{2,1} = \frac{1}{2} \left(-q \pm \sqrt{q^2 - 4z_3q} \right), \quad q \equiv \frac{3}{2}v + z_3.$$

On using results 236.00 and 236.01 of [26], we may integrate (3.2.13) to obtain

$$\eta = \frac{\sqrt{6}z_1}{\sqrt{z_3 - z_1}} F(\varphi, m) + \sqrt{6(z_3 - z_1)} E(\varphi, m), \quad (3.2.14)$$

$$\sin \varphi = \frac{z_3 - z}{z_3 - z_2}, \quad m = \frac{z_3 - z_2}{z_3 - z_1}. \quad (3.2.15)$$

$F(\varphi, m)$ and $E(\varphi, m)$ are incomplete elliptic integrals of the first and second kind respectively. We have chosen the constant of integration in (3.2.14) to be zero so that $z = z_3$ at $\eta = 0$. The relations (3.2.14) give the required solution in parametric form with z and η as functions of the parameter φ .

An alternative route to the solution is to follow the procedure described in [142]. We introduce a new independent variable ζ defined by

$$\frac{d\eta}{d\zeta} = z \quad (3.2.16)$$

so that (3.2.13) becomes

$$\frac{1}{2}z_\zeta^2 = f(z). \quad (3.2.17)$$

By means of result 236.00 of [26], the equation (3.2.17) may be integrated to give $p\zeta = F(\varphi, m)$, where $p^2 = (z_3 - z_1)/6$. Thus, on noting that $\sin \varphi = \operatorname{sn}(p\zeta|w)$, where $\operatorname{sn}(\cdot)$ is a Jacobian elliptic function, we have

$$z = z_3 - (z_3 - z_2) \operatorname{sn}^2(p\zeta|w). \quad (3.2.18)$$

With result 310.02 of [26], the equations (3.2.16) and (3.2.18) give

$$\eta = z_1\zeta + \sqrt{6(z_3 - z_1)} E(p\zeta), \quad (3.2.19)$$

where $E(p\zeta) := E(\operatorname{am} p\zeta, m)$. Relations (3.2.18) and (3.2.19) are equivalent to (3.2.15) and (3.2.14) respectively and give the solution in parametric form with z and η in terms of the parameter ζ .

We define the wavelength λ of the solution as the amount by which η increases when φ increases by 2π ; from (3.2.14) we obtain

$$\lambda = \frac{2\sqrt{6}}{\sqrt{z_3 - z_1}} [z_1 K(m) + (z_3 - z_1) E(m)], \quad (3.2.20)$$

where $K(m)$ and $E(m)$ are complete elliptic integrals of the first and second kind respectively.

For $c = 1$ (i.e. $v > 0$), there are periodic solutions for $0 < A < 1$ with $\lambda < 0$, $z_2 \in (-1, 0)$ and $z_3 \in (0, 0.5)$; an example of such a periodic wave is illustrated by curve 2 in Fig. 3.2. $A = 1$ gives the solitary wave limit

$$u = \frac{3}{2}v \operatorname{sech}^2(\zeta/2), \quad \eta = -\zeta + 3 \tanh(\zeta/2) \quad (3.2.21)$$

as illustrated by curve 1 in Fig. 3.2. The periodic waves and the solitary wave have a loop-like structure as illustrated in Fig. 3.2.

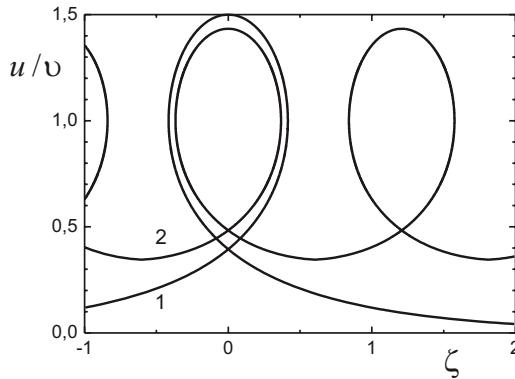


Figure 3.2: Traveling wave solutions with $v > 0$.

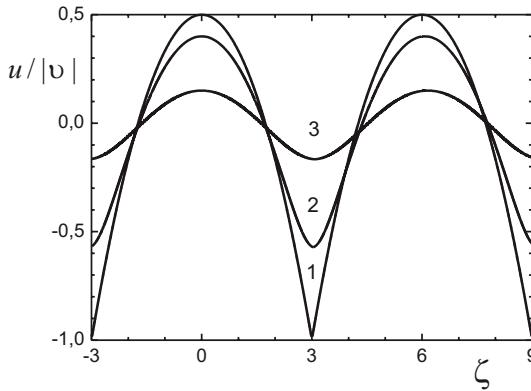
For $c = -1$ (i.e. $v < 0$), there are periodic waves for $-1 < A < 0$ with $\lambda > 0$, $z_2 \in (0, 1)$ and $z_3 \in (1, 1.5)$; an example of such a periodic wave is illustrated by curve 2 in Fig. 3.3. When $A = 0$ and $\lambda = 6$ the periodic wave solution simplifies to

$$u(\eta)/|v| = -\frac{1}{6}\eta^2 + \frac{1}{2}, \quad -3 \leq \eta \leq 3, \quad u(\eta + 6) = u(\eta). \quad (3.2.22)$$

This is shown by curve 1 in Fig. 3.3. For $A \simeq -1$ the solution has a sinusoidal form (curve 3 in Fig. 3.3). Note that there are no solitary wave solutions.

A remarkable feature of the equation (3.2.2) is that it has a solitary wave (3.2.21) which has loop-like form, i.e. it is a multi-valued function (see Fig. 3.2). Whilst loop solitary waves (3.2.21) are rather intriguing, it is the solution to the initial value problem that is of more interest in a physical context. An important question is the stability of the loop-like solutions. Although the analysis of stability does not link with the theory of solitons directly, however, the method applied in [119] is instructive, since it is successful in a nonlinear approximation.

We will prove (see subsection 3.3.3) that the solitary wave (3.2.21) is, in fact, a soliton.

Figure 3.3: Traveling wave solutions with $v < 0$.

3.3 Interaction of solitons

The multi-valued solutions obtained in the last section 3.2.2 obviously mean that the study of the VE (3.2.2) in the original coordinates (x, t) leads to certain difficulties. These difficulties can be avoided by writing down the VE in new independent coordinates. We have succeeded in finding these coordinates. Historically, working separately, Vyacheslav Vakhnenko in Ukraine and John Parkes in the UK independently suggested such independent coordinates in which the solutions become one-valued functions. It is instructive to present the two derivations here. In one derivation a physical approach, namely a transformation between Eulerian and Lagrangian coordinates, was used whereas in the other derivation a pure mathematical approach was used.

3.3.1 The Vakhnenko-Parkes equation

Let us define new independent variables (X, T) by the transformation

$$\varphi dT = dx - u dt, \quad X = t. \quad (3.3.1)$$

The function φ is to be obtained. It is important that the functions $x = \theta(X, T)$ and $u = U(X, T)$ turn out to be single-valued ones. In terms of the coordinates (X, T) the solution of the VE (3.2.2) is given by single-valued parametric relations. The transformation into these coordinates is the key point in solving the problem of the interaction of solitons as well as explaining the multiple-valued solutions [158]. The transformation (3.3.1) is similar to the transformation between Eulerian coordinates (x, t) and Lagrangian coordinates (X, T) . We require that $T = x$ if there is no perturbation, i.e. if $u(x, t) = 0$. Hence $\varphi = 1$ when $u(x, t) = 0$.

The function φ is the additional dependent variable in the equation system (3.3.3), (3.3.4) to which we reduce the original Eq. (3.2.2). We note that the transformation inverse to (3.3.1) is

$$dx = \varphi dT + U dX, \quad t = X, \quad U(X, T) \equiv u(x, t). \quad (3.3.2)$$

Then, by taking into account the condition that dx is an exact differential, we obtain

$$\frac{\partial \varphi}{\partial X} = \frac{\partial U}{\partial T}. \quad (3.3.3)$$

This equation, together with Eq. (3.2.2) rewritten in terms of $\varphi(X, T)$, $U(X, T)$, namely

$$\frac{\partial^2 \varphi}{\partial X^2} + U\varphi = 0, \quad (3.3.4)$$

is the main system of equations. The equation system (3.3.3), (3.3.4) can be reduced to a nonlinear equation in one unknown W defined by

$$W_X = U. \quad (3.3.5)$$

We study solutions U that vanish as $|X| \rightarrow \infty$ or, equivalently, solutions for which W tends to a constant as $|X| \rightarrow \infty$. From (3.3.3) and (3.3.5) and the requirement that $\varphi \rightarrow 1$ as $|X| \rightarrow \infty$ we have $\varphi = 1 + W_T$; then, by eliminating φ from (3.3.4) we arrive at the transformed form of the VE (3.2.2)

$$W_{XXT} + (1 + W_T)W_X = 0 \quad (3.3.6)$$

or, in equivalent form,

$$UU_{XXT} - U_X U_{XT} + U^2 U_T = 0. \quad (3.3.7)$$

Furthermore it follows from (3.3.2) that the original independent space coordinate x is given by

$$x = \theta(X, T) = x_0 + T + W, \quad (3.3.8)$$

where x_0 is an arbitrary constant. Since the functions $\theta(X, T)$ and $U(X, T)$ are single-valued, the problem of multi-valued solutions has been resolved from the mathematical point of view.

Alternatively, in a pure mathematical approach, we introduce new independent variables X, T defined by

$$x = \theta(X, T) = T + \int_{-\infty}^X U(X', T) dX' + x_0, \quad t = X, \quad (3.3.9)$$

where $u(x, t) = U(X, T)$, and x_0 is a constant. From (3.3.9) it follows that

$$\frac{\partial}{\partial X} = \frac{\partial}{\partial t} + u \frac{\partial}{\partial x}, \quad \frac{\partial}{\partial T} = \phi \frac{\partial}{\partial x}, \quad \text{with } \phi(X, T) = 1 + \int_{-\infty}^X U_T dX', \quad (3.3.10)$$

so that

$$\phi_X = U_T. \quad (3.3.11)$$

From (3.2.2) and (3.3.10) we obtain

$$U_{XT} + \phi U = 0. \quad (3.3.12)$$

By eliminating ϕ between (3.3.11) and (3.3.12) we obtain the equation (3.3.7) or, on introducing W , the equation (3.3.6).

The suggested transformation was originally derived in Refs. [102, 179, 181]. Following the papers [1, 42, 90, 94, 212], hereafter equation (3.3.6) (or in alternative form (3.3.7)) is referred to as the Vakhnenko-Parkes equation (VPE).

For example we will rewrite the solutions (3.2.15) and (3.2.14) for equation (3.2.2) in the transformed coordinates (X, T) , i.e. find the traveling wave solutions for equation (3.2.2) in new coordinates. Differentiating the relationship (3.2.14) with respect to X , we take

$$\begin{aligned} \pm \sqrt{\frac{2}{3}} \frac{\partial \eta}{\partial X} &= \pm \sqrt{\frac{2}{3}} \left(-v + \frac{\partial x}{\partial X} \right) = \pm \sqrt{\frac{2}{3}} (-v + W_X(X, T)) = \pm \sqrt{\frac{2}{3}} z \\ &= \frac{z}{\sqrt{(z - a_1)(z - a_2)(a_3 - z)}} \frac{\partial z}{\partial X}, \end{aligned}$$

or

$$\pm \sqrt{\frac{2}{3}} = \frac{1}{\sqrt{(z - a_1)(z - a_2)(a_3 - z)}} \frac{\partial z}{\partial X}.$$

Then after integration, we obtain

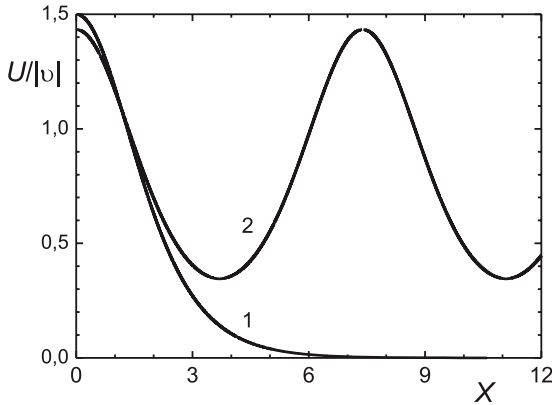


Figure 3.4: Traveling wave solutions with $v > 0$ in coordinates (X, T) .

$$\pm \sqrt{\frac{2}{3}} X = \int_z^{a_3} \frac{dz}{\sqrt{(z - a_1)(z - a_2)(a_3 - z)}} = \frac{2}{\sqrt{a_3 - a_1}} F(\varphi, k). \quad (3.3.13)$$

Together with $z = U(X, T) + v$ this relationship (3.3.13) determines the desired dependence $U(X, T)$ in parametrical form. Thus, we have the solution for equation (3.2.2) in new coordinates (X, T) .

The solutions for $v > 0$ in coordinates (X, T) are illustrated in Fig. 3.4. The curves 1, 2 in this figure relate to the curve 1, 2 in Fig. 3.2. The solutions in coordinates (X, T) for $v < 0$ are plotted in Fig. 3.5. The curves 1, 2, 3 in this figure relate to the curve 1, 2, 3 in Fig. 3.3.

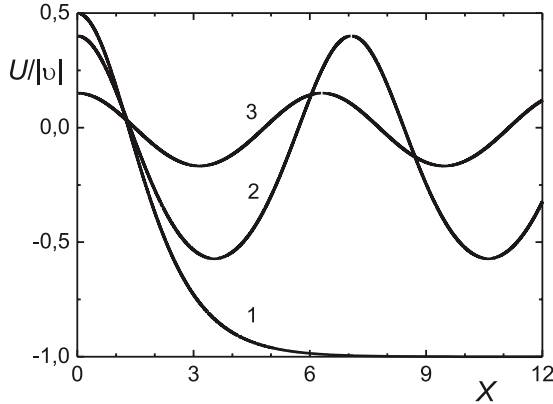


Figure 3.5: Traveling wave solutions with $v < 0$ in coordinates (X, T) .

On the one hand, we have attained the goal, namely, we have found the solutions in new coordinates in which the solutions become one-valued functions. On the other hand, it is important that periodical solution shown by curve 1 in Fig. 3.3, i.e. the solution consisting of parabolas becomes not periodical in new coordinates. Hence, we reveal some accordance between curve 1 in Fig. 3.4 and curve 1 in Fig. 3.5. This feature is important for finding the solutions by inverse scattering method [181, 184, 188, 190, 191, 192].

3.3.2 Hirota method

Various effective approaches have been developed to construct exact wave solutions of completely integrable equations. One of the fundamental direct methods is undoubtedly the Hirota bilinear method [63, 64, 65, 100], which possesses significant features that make it practical for the determination of multiple soliton solutions.

In the Hirota method the equation under investigation should first be transformed into the Hirota bilinear form [63]

$$F(D_X, D_T)f \cdot f = 0, \quad (3.3.14)$$

where F is a polynomial in D_T and D_X . Each equation has its own polynomial. The

Hirota bilinear D -operator is defined as (see section 5.2 in [63])

$$D_T^n D_X^m a \cdot b = \left(\frac{\partial}{\partial T} - \frac{\partial}{\partial T'} \right)^n \left(\frac{\partial}{\partial X} - \frac{\partial}{\partial X'} \right)^m a(T, X) b(T', X') \Big|_{T=T', X=X'} . \quad (3.3.15)$$

If the polynomial F satisfies conditions (see (5.41), (5.42) in [63])

$$F(D_X, D_T) = F(-D_X, -D_T), \quad F(0, 0) = 0, \quad (3.3.16)$$

then the Hirota method can be applied successfully. The dispersion relations is of importance in this method

$$F(2k_i, -2\omega_i) = 0, \quad i = 1, \dots, N. \quad (3.3.17)$$

In order to find the soliton solutions to the VPE (3.3.6)

$$W_{XXT} + (1 + W_T)W_X = 0$$

by using the Hirota method [63] we need to express (3.3.6) in the Hirota form [179]. The transformation (3.3.9) of the independent variables in the original equation (3.2.2) is a key step in finding an exact explicit N -soliton solution to (3.3.6) by use of the Hirota method, and hence an exact implicit N -soliton solution to (3.2.2). By taking

$$W = 6(\ln f)_X, \quad (3.3.18)$$

we find that

$$W_X = \frac{3D_X^2 f \cdot f}{f^2} \quad \text{and} \quad W_{XXT} + W_X W_T = \frac{3D_T D_X^3 f \cdot f}{f^2} \quad (3.3.19)$$

and the bilinear form of the VPE is as follows

$$F(D_X, D_T) f \cdot f = 0, \quad F(D_X, D_T) := D_T D_X^3 + D_X^2. \quad (3.3.20)$$

3.3.3 The one and two loop soliton solutions

The solution to (3.3.20) corresponding to one soliton is given by

$$f = 1 + e^{2\eta}, \quad \text{where} \quad \eta = kX - \omega T + \alpha, \quad (3.3.21)$$

and k , ω and α are constants. The dispersion relation (3.3.17) is $F(2k, -2\omega) = 0$ from which we find that $\omega = 1/4k$, and then

$$\eta = k(X - cT) + \alpha \quad \text{with} \quad c = 1/4k^2. \quad (3.3.22)$$

Substitution of (3.3.21) into (3.3.18) gives

$$W(X, T) = 6k(1 + \tanh \eta) \quad (3.3.23)$$

so that

$$U(X, T) = 6k^2 \operatorname{sech}^2 \eta. \quad (3.3.24)$$

The one loop soliton solution to the VE is given by

$$u(x, t) = U(t, T), \quad x = \theta(t, T), \quad \theta(X, T) = T + W(X, T) + x_0. \quad (3.3.25)$$

with (3.3.23) and (3.3.24). From (3.3.25) with $v = 1/c$ we have

$$x - vt = -v(X - cT) + 6k(1 + \tanh[k(X - cT) + \alpha]) + x_0. \quad (3.3.26)$$

Clearly, from (3.3.24) and (3.3.26), $U(X, T)$ and $x - vt$ are related by the parameter $\chi = X - cT$ so that $u(x, t)$ is a soliton that travels with speed v in the positive x -direction. That this soliton is a loop may be shown as follows. From (3.3.10) we have $u_x = \phi^{-1}U_T$, and on using (3.3.22) and (3.3.24) we also have $\phi = 1 - cU$ and $U_T = -cU_X$. Hence

$$u_x = -cU_X/(1 - cU). \quad (3.3.27)$$

Thus, as χ goes from ∞ to $-\infty$ in (3.3.26), so that $x - vt$ goes from $-\infty$ to $+\infty$, U_X changes sign once and remains finite, whereas u_x given by (3.3.27) changes sign three times and goes infinite twice. The one loop soliton solution may be written in terms of the parameter χ as

$$u = \frac{3v}{2} \operatorname{sech}^2\left(\frac{\sqrt{v}\chi}{2}\right), \quad x - vt = \tilde{x}_0 - v\chi + 3\sqrt{v} \tanh\left(\frac{\sqrt{v}\chi}{2}\right) \quad (3.3.28)$$

with $v(> 0)$ and \tilde{x}_0 arbitrary. The solution (3.3.28) is essentially the one loop soliton solution given by (3.2.21) (see [154, 119] too).

Usually it is assumed that the value α is real in order that the solution $U(X, T)$ is a real function. However, the real solution is obtained also at $\alpha = -i\pi + \tilde{\alpha}$ ($\tilde{\alpha}$ is real value). In this case the soliton solution (singular soliton solution) is discontinuous one [207]

$$U(X, T) = 6k^2 \sinh^{-2} \eta. \quad (3.3.29)$$

The solution to (3.3.20) corresponding to two solitons is given by

$$f = 1 + e^{2\eta_1} + e^{2\eta_2} + b^2 e^{2(\eta_1 + \eta_2)}, \quad \text{where } \eta_i = k_i X - \omega_i T + \alpha_i, \quad (3.3.30)$$

$$b^2 = -\frac{F[2(k_1 - k_2), -2(\omega_1 - \omega_2)]}{F[2(k_1 + k_2), -2(\omega_1 + \omega_2)]}, \quad (3.3.31)$$

and k_i , ω_i and α_i are constants. The dispersion relation is $F(2k_i, -2\omega_i) = 0$ from which we find that $\omega_i = 1/4k_i$, and then

$$\eta_i = k_i(X - c_i T) + \alpha_i \quad \text{with } c_i = 1/4k_i^2. \quad (3.3.32)$$

Without loss of generality we may take $k_2 > k_1$, and then

$$b = \frac{k_2 - k_1}{k_2 + k_1} \sqrt{\frac{k_1^2 + k_2^2 - k_1 k_2}{k_1^2 + k_2^2 + k_1 k_2}}. \quad (3.3.33)$$

Substitution of (3.3.30) into (3.3.18) gives the two soliton solution of the VPE. Following Hodnett and Moloney [66, 101], we may write $W(X, T)$ in the form

$$W = W_1 + W_2, \quad \text{where} \quad W_i = 6k_i(1 + \tanh g_i) \quad (3.3.34)$$

and

$$g_1(X, T) = \eta_1 + \frac{1}{2} \ln \left[\frac{1 + b^2 e^{2\eta_2}}{1 + e^{2\eta_2}} \right], \quad (3.3.35)$$

$$g_2(X, T) = \eta_2 + \frac{1}{2} \ln \left[\frac{1 + b^2 e^{2\eta_1}}{1 + e^{2\eta_1}} \right].$$

It follows that U may be written as

$$U = U_1 + U_2, \quad \text{where} \quad U_i = 6k_i \frac{\partial g_i}{\partial X} \operatorname{sech}^2 g_i. \quad (3.3.36)$$

The two loop soliton solution to the VE is given by (3.3.25) with (3.3.34) and (3.3.36) [179].

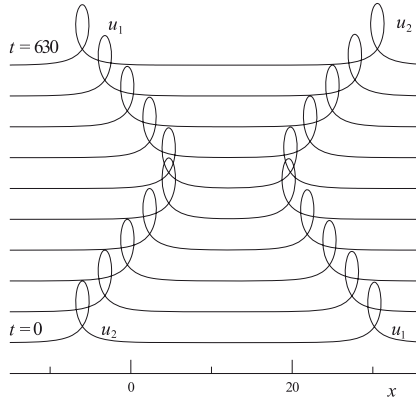


Figure 3.6: The interaction process for two loop solitons with $k_1 = 0.99$ and $k_2 = 1$ so that $\delta_1 < 0$.

In the interaction of two solitons for the VE [102, 179, 180, 181, 185] there are features that are not typical for the KdV equation (see Figs. 3.6–3.8). The larger soliton moving with larger velocity catches up with the smaller soliton moving in the same direction. For the sake of convenience in Figs. 3.6–3.8, the interactions of solitons are shown in coordinates moving with the speed of the centre mass. After the nonlinear interaction the solitons separate, their forms are restored, but phaseshifts arise. The larger soliton always has a forward phaseshift, while the smaller soliton can have three kinds of phaseshift. Note that this property is not typical for the KdV equation. There is a special value of the ratio $(k_1/k_2)_c = 0.88867$. The different kinds of phaseshift are illustrated in Figs. 3.6–3.8.

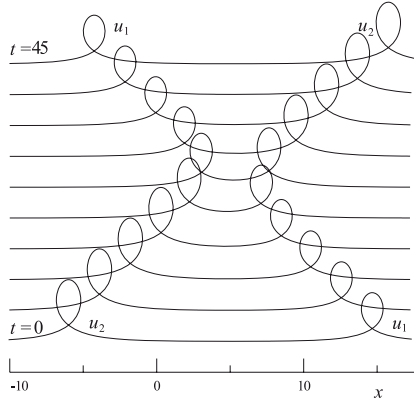


Figure 3.7: The interaction process for two loop solitons with $k_1 = 0.88867$ and $k_2 = 1$ so that $\delta_1 = 0$.

- For $k_1/k_2 > (k_1/k_2)_c$ the phaseshift of smaller soliton is in the opposite direction to the phaseshift of the larger soliton (Fig. 3.6).
- For $k_1/k_2 = (k_1/k_2)_c$ the smaller soliton has no phaseshift (Fig. 3.7).
- For $k_1/k_2 < (k_1/k_2)_c$ both solitons have phaseshifts in the same direction (Fig. 3.8).

3.4 Ambiguous solutions

The ambiguous structure of the loop-like solutions is similar to the loop soliton solution to an equation that models a stretched rope [76]. Loop-like solitons on a vortex filament were investigated by Hasimoto [60] and Lamb, Jr [87]. From the mathematical point of view an ambiguous solution does not present difficulties whereas the physical interpretation of ambiguity always presents some difficulties. In this connection the problem of ambiguous solutions is regarded as important. The problem consists in whether the ambiguity has a physical nature or is related to the incompleteness of the mathematical model, in particular to the lack of dissipation.

We will consider the problem related to the singular points when dissipation takes place (see Eq. (3.2.9)). At these points the dissipative term $\alpha \frac{\partial u}{\partial x}$ tends to infinity. The question arises: are there solutions of the equation (3.2.9) in a loop-like form? That the dissipation is likely to destroy the loop-like solutions can be associated with the following well-known fact [37]. For the simplest nonlinear equation without dispersion and without dissipation, namely

$$\frac{\partial u}{\partial t} + u \frac{\partial u}{\partial x} = 0, \quad (3.4.1)$$

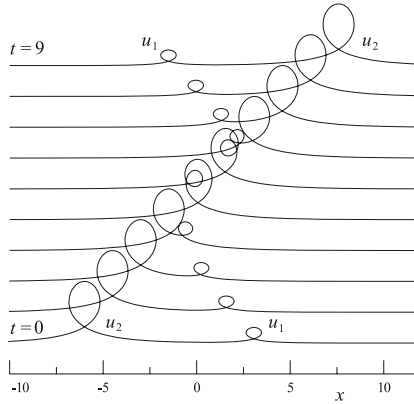


Figure 3.8: The interaction process for two loop solitons with $k_1 = 0.5$ and $k_2 = 1$ so that $\delta_1 > 0$.

any initial smooth solution with boundary conditions

$$u|_{x \rightarrow +\infty} = 0, \quad u|_{x \rightarrow -\infty} = u_0 = \text{const} > 0$$

becomes ambiguous in the final analysis. When dissipation is considered, we have the Burgers equation [25]

$$\frac{\partial u}{\partial t} + u \frac{\partial u}{\partial x} + \mu \frac{\partial^2 u}{\partial x^2} = 0.$$

The dissipative term in this equation is coincident with the dissipative term in equation (3.1.13) for low frequency. The inclusion of the dissipative term transforms the solutions so that they cannot be ambiguous as a result of evolution. The wave parameters are always unambiguous. What happens in our case for high frequency when the dissipative term has the form αu (see Eq. (3.2.9))? Will the inclusion of dissipation give rise to unambiguous solutions?

By direct integration of equation (3.2.1) (written in terms of the variables (3.2.10)) within the neighborhood of singular points $z = 0$ where $z_\eta \rightarrow \pm\infty$ and $z_r \ll z_\eta$, it can be derived (see Ref. [158]) that the dissipative term, with dissipation parameter less than some limit value α^* , does not destroy the loop-like solutions. Now we give a physical interpretation to ambiguous solutions.

Since the solution to the VE has a parametric form (3.2.14), (3.2.15) or (3.2.18), (3.2.19), there is a space of variables in which the solution is a single-valued function. Hence, we can solve the problem of the ambiguous solution. A number of states with their thermodynamic parameters can occupy one microvolume. It is assumed that the interaction between the separated states occupying one microvolume can be neglected in comparison with the interaction between the particles of one thermodynamic state. Even if we take into account the interaction between the separated states in accordance with the dynamic state equation (3.1.9) then, for high frequencies, a dissipative

term arises which is similar to the corresponding term in Eq. (3.1.14), but with the other relaxation time. In this sense the separated terms are distributed in space, but describing the wave process we consider them as interpenetrable. A similar situation, when several components with different hydrodynamic parameters occupy one microvolume, has been assumed in mixture theory (see, for instance [122, 138]). Such a fundamental assumption in the theory of mixtures is physically impossible (see [122], p.7), but it is appropriate in the sense that the separated components are multi-velocity interpenetrable continua.

Consequently, the following three observations show that, in the framework of the approach considered here, there are multi-valued solutions when we model high-frequency wave processes: 1) All parts of loop-like solution are stable to perturbations [119]. 2) The dissipation does not destroy the loop-like solutions. 3) The investigation regarding the interaction of the solitons has shown that it is necessary to take into account the whole ambiguous solution, and not just the separate parts.

Chapter 4

Waves in relaxing two-component medium

In this chapter we will simulate the wave fluids in media consisted of the uniform distributed gaseous and condensed components (solid particles, liquid, etc.). The gas-suspensions, foams, bubble media are the mixtures with regular structure.

Of special interest is the decrease of a shock wave action under propagation of shock waves in two-phase media [81, 83, 84, 164, 173, 174, 175, 177, 178]. The analysis of this phenomena shows that effectiveness of a medium as a means for shock wave location depends on capacity to retain heat in a condensed phase. The intensity of the heat transfer is determined by the complex physical chemical processes involved in the interaction between components.

Unfortunately, nowadays the experimental results on various interactions between components are insufficient in order to formulate the mechanisms of interaction and, consequently, to formalize them in mathematical models. There can be no doubt that the inner processes (although their mechanism is not known in details) manifest themselves in the behavior of a medium. We will study the action of inner processes on a change of macroparameters within the relaxation notations. As a result of inner interaction is the effect of the relaxation of macroparameters. Additionally the medium can be subject to the external actions, for example, wave perturbation, shock wave, dynamic loading, etc. The medium as a dynamic system is specified both the relaxation time and the time of propagation of the shock wave perturbation. We consider the wave processes when the relaxation time and time of an external action are the values of the same order. An irreversible energy loss in a gaseous component (a pressure of gas predetermines the pressure medium as a whole) through the heat transfer by radiation and/or by means of contact considerably influences on shock wave parameters. These processes, associated with the transfer of energy from one form that specifies a pressure in medium to another form that does not possess partial pressure, are definitely important for describing the attenuation of shock waves. We will consider these various processes from general point of view as the thermal relaxation. The processes of thermal relaxation will be described by dynamic state equation suggested in the next section 4.1.

4.1 Asymptotic averaged model for mixture with thermal relaxation

For mathematical modeling of dynamic behavior of a medium with thermal relaxation, we will consider the constitutive properties, basing upon following assumptions. The partial pressure of the condensed phase is negligibly small, while the medium pressure is specified by the gaseous component only. The gaseous component is generally the relaxing gas. The condensed components show the evidence of relaxation too.

Let us refine the asymptotic averaged model in order to remove the restriction connected with a barotropic medium (as it is studied in Chapter 2). The constitutive hydrodynamic equations for describing one-dimensional motions (2.1.1), (2.1.2)

$$\begin{aligned}\frac{\partial r^\nu}{\partial l^\nu} &= \frac{V}{V_0}, \quad \text{or} \quad \frac{\partial V}{\partial t} - \nu V_0 \frac{\partial r^{\nu-1} u}{\partial l^\nu} = 0, \\ u &= \frac{\partial r}{\partial t}, \\ \frac{\partial u}{\partial t} + V_0 \left(\frac{r}{l}\right)^{\nu-1} \frac{\partial p}{\partial l} &= 0.\end{aligned}$$

are added by the energy equation for each individual component

$$\frac{\partial E}{\partial t} + \frac{V_0 p}{l^{\nu-1}} \frac{\partial r^{\nu-1} u}{\partial l} = 0. \quad (4.1.1)$$

We analyze the longwave perturbations and assume that the velocities of gas and condensed phase are equal. Similarly to Chapter 2 let us apply the method of asymptotic averaging, whereas the variable E is expanded in series (see, for example, (2.2.2))

$$E(m, t) = E^{(0)}(s, t, \xi) + \varepsilon E^{(1)}(s, t, \xi) + \varepsilon^2 E^{(2)}(s, t, \xi) + \dots, \quad (4.1.2)$$

where $m = l^\nu/V_0$, $m = s + \varepsilon\xi$, s and ξ are slow and fast space variables, respectively.

The procedure similar to that in Section (2.2) enables us to obtain additionally the averaged energy equation (index (0) is omitted). Then the system of the equations in the Lagrangian coordinates (s, t) has the form

$$\begin{aligned}\frac{\partial r^\nu}{\partial s} &= \langle V \rangle, \quad \text{or} \quad \frac{\partial \langle V \rangle}{\partial t} - \nu \frac{\partial r^{\nu-1} u}{\partial s} = 0, \\ u &= \frac{\partial r}{\partial t}, \\ \frac{\partial u}{\partial t} + \nu r^\nu \frac{\partial p}{\partial s} &= 0, \\ \frac{\partial \langle E \rangle}{\partial t} + \nu p \frac{\partial r^{\nu-1} u}{\partial s} &= 0.\end{aligned} \quad (4.1.3)$$

Note that the averaged variables p , u , r , $\langle V \rangle$, $\langle E \rangle$ appear in Eqs. (4.1.3). Here variable r is a dependent value.

Now we can rewrite out the equations of motion in the Eulerian coordinates (r, t_E) (now r is an independent variable) (2.3.4)

$$dr^\nu = \langle V \rangle ds + \nu r^{\nu-1} u dt, \quad t_E = t.$$

Finally the averaged equations of motion in the slow Eulerian coordinate have the form (index E in t is omitted).

$$\begin{aligned} \frac{\partial \langle V \rangle^{-1}}{\partial t} - \frac{1}{r^{\nu-1}} \frac{\partial r^{\nu-1} \langle V \rangle^{-1} u}{\partial r} &= 0, \\ \frac{\partial u}{\partial t} + u \frac{\partial u}{\partial r} + \langle V \rangle \frac{\partial p}{\partial r} &= 0, \\ \left(\frac{\partial}{\partial t} + u \frac{\partial}{\partial r} \right) \langle E \rangle + \frac{p}{r^{\nu-1}} \frac{\partial r^{\nu-1} u}{\partial r} &= 0. \end{aligned} \tag{4.1.4}$$

Consequently, the equations of motion are reduced to the terms of the average values p , u , $\langle V \rangle$, $\langle E \rangle$ only. It is necessary to note that the structure of medium is evidently taken into account only in the equation of state, since the averaged state equation can not be reduced to the values p , u , $\langle V \rangle$, $\langle E \rangle$ only. This statement will be proved in Section 4.2.

It is worthwhile that at this point we can avoid the restriction in which the structure of medium should be strong periodic. The wavelength is long and covers many periods (see Fig. 1.1). In suggested approximation, the pressure p and mass velocity u are not changed over period. Let us imagine that in one of the structured sell the initial structure changes so that the period increases in two times. Obviously the field parameters in this case do not change. Determining the period size as arbitrarily small, we come to the conclusion that the averaged system of the equations is valid for medium with the constant concentrations of the components (statistic uniform distribution of the components).

4.2 Dynamic state equation for mixture with thermal relaxation

The practical interest in the gas-liquid-solid mixtures is connected with a capacity of such media to damp the shock waves. We focus our attention upon the study of such inner processes that reveal the transfer of a energy defining the medium pressure to the other energy that does not contribute in partial pressure. As a result of the existence of inner processes, we have that the functional dependence between energy E , specific volume V and pressure p (state equation) is ambiguous. For gas-liquid-solid mixture under the assumption of one-velocity approximation, the state equation can be justified from general notions on thermal relaxation.

It is convenient to write a state equation for each individual component in the form of dependence of specific energy E on a pressure p and specific volume V , i.e. $E = E(p, V)$. Let us use the gas-like form for this relation

$$E = \frac{pV}{\gamma - 1}, \tag{4.2.1}$$

which can successfully be applied both for gaseous component and for condensed component. Generally, both gas and condensed phase are relaxing components. Now we will derive the dynamic state equation for mixture with thermal relaxation [164, 173, 175, 177, 178]. For one-velocity model, there are two limiting cases: (i) full equilibrium between phases; (ii) lack of transfer of heat between phases. Let us introduce the notations for fast and slow processes for the two components.

1. For gaseous component

$$E_g = \frac{pV}{\gamma_{gf} - 1}, \quad \tau_{Eg}\omega \gg 1, \quad E_g = \frac{pV}{\gamma_{ge} - 1}, \quad \tau_{Eg}\omega \ll 1. \quad (4.2.2)$$

2. For condensed component

$$E_s = \frac{pV}{\gamma_{sf} - 1}, \quad \tau_{Es}\omega \gg 1, \quad E_s = \frac{pV}{\gamma_{se} - 1}, \quad \tau_{Es}\omega \ll 1. \quad (4.2.3)$$

According to the formalism [209, 210, 211], we can write a dynamic state equation for each individual component (see Section 3.1)

$$\tau_{Ei} \frac{d}{dt} \left(E - \frac{pV}{\gamma_{if} - 1} \right) + \left(E - \frac{pV}{\gamma_{ie} - 1} \right) = 0, \quad i = g, s. \quad (4.2.4)$$

It is clear that at $\tau_{Ei}\omega \gg 1$ and $\tau_{Ei}\omega \ll 1$ we have respective equations (4.2.2), (4.2.3). The procedure of the asymptotic average leads to the dynamic state equation that describes the thermal relaxation in mixture

$$d\langle E \rangle = -dp \left\langle \frac{V}{\gamma_f - 1} \right\rangle - \left\langle \frac{E}{\tau_E} \right\rangle dt - p \left\langle \frac{V}{\tau_E(\gamma_e - 1)} \right\rangle dt. \quad (4.2.5)$$

Hence the dynamic state equation (4.2.5) is not reduced to the variables p , u , $\langle V \rangle$, $\langle E \rangle$ only.

However, in particular case it is possible to simplify the dynamic state equation (4.2.5). The appropriate conditions are realized in the two-components medium with gaseous component and incompressible component. Indeed, for this medium $\gamma_{sf} = \gamma_{se} = 1$ and then time relaxation τ_{Es} can be defined arbitrarily. For the sake of convenience we define $\tau_{Es} = \tau_{Eg} = \tau_E$. We consider the heat transfer from gas to the some inner reservoir. Hence, the specific heat of gaseous component is not constant, i.e. gas is the relaxing component. It is clear that the mentioned reservoir is the condensed phase, whereas, on the one hand, this phase is incompressible, on the other hand, the partial pressure of this phase is negligibly small. It is convenient hereafter to introduce the new notations $\Gamma_0 = \gamma_{ge}$, $\gamma = \gamma_{gf}$. Note that for gas-containing mixture the parameter

$$\Gamma_0 = \gamma \frac{\sigma_g + \sigma_s c / c_{pg}}{\sigma_g + \gamma \sigma_s c / c_{pg}} \quad (4.2.6)$$

is close to 1, while the inequality $\Gamma_0 > 1$ always holds. In the relationship (4.2.6) the values σ_s and c are mass concentration and specific heat of the condensed component;

the values σ_g and c_p are mass concentration and specific heat at constant pressure of the gaseous component, respectively.

Now the averaged dynamic state equation (4.2.5) can be reduced to the form

$$\tau_E \frac{d}{dt} \left[\langle E \rangle - \frac{p \langle V \rangle (1 - \varepsilon)}{\gamma - 1} \right] + \left[\langle E \rangle - \frac{p \langle V \rangle (1 - \varepsilon)}{\Gamma_0 - 1} \right] = 0, \quad (4.2.7)$$

where ε is a volume fraction of the condensed phase, whereas this value is uniquely defined through $\langle V \rangle$

$$\varepsilon = \varepsilon_0 \frac{\langle V_0 \rangle}{\langle V \rangle}. \quad (4.2.8)$$

The equation (4.2.7) describes the nonequilibrium transition of a mixture from one state

$$\langle E \rangle = \frac{p \langle V \rangle (1 - \varepsilon)}{\gamma - 1} + \text{const} \quad (4.2.9)$$

to other state

$$\langle E \rangle = \frac{p \langle V \rangle (1 - \varepsilon)}{\Gamma_0 - 1}. \quad (4.2.10)$$

Rudinger [127, 128, 129] was the first who established the equilibrium state equation for mixture with incompressible component (4.2.10).

Thus, the equation (4.2.7) together with equations (4.1.4) constitutes the closed system of equations. For this system of the differential equations the initial and boundary conditions depending on problem being studied should be given.

The suggested asymptotic averaged model allows one to analyze the influence of relaxation under the wave propagation in gas-liquid-solid media.

4.3 Similarity in motions of gas and two-phase medium with incompressible component

In this section we compare the motion of a perfect gas and that of a two-phase medium with any volume occupied by the incompressible condensed component. It is known [9, 127, 128, 129] that in one-velocity approach at low volume portion of the condensed phase ε , the motion of a two-phase medium is similar to the motion of gas. To describe the motion of two-phase medium without restriction on a value of the volume portion ε , it is necessary to introduce this value ε as additional variable in the system of the hydrodynamic equations in contrast to the usual gas-dynamic equations. In approaches of other authors [117, 141] such an extended system of equations have been treated by solving it separately for each particular ε .

We focus our attention on transformation between the equations for a perfect gas and the equations describing, in one-velocity approach, the two-phase medium with any volume occupied by the incompressible phase [83, 159, 160, 174, 177]. It shall be proved that the motion of a two-phase medium in the transformed coordinate system

is similar with certain accuracy to that of a perfect gas. It means that the solutions obtained for perfect gas can be used to solve the wave problems for media with incompressible component. There is no necessity directly to solve the problem for medium with incompressible component, and it is only sufficient to transform the known solution of the similar problem for a homogeneous medium. Thus, the solutions of many hydrodynamic problems for multi-component media with incompressible phase can be obtained without solving the original system of equations. The scope for the suggested transformation is demonstrated by reference to the strong explosion in a two-phase medium.

4.3.1 System of equations in the Lagrangian coordinates

One of a concept consists in analyzing the considered problem in the Lagrangian coordinates (ζ, τ) . Let us consider a two-phase medium consisting of a condensed phase and a gaseous phase uniformly distributed in a volume. The incompressible condensed component can occupy an arbitrary partial-specific volume ε . We assume the following: (a) the condensed phase is incompressible; (b) the partial pressure of the condensed phase is negligibly small; (c) the velocities of the condensed phase and gaseous phase equal each other. The conservation laws for mass, momentum, and energy give us the following system of the equations for the one-dimensional motions in the Lagrangian coordinates [78, 134] (see equations (2.2.4) in the Chapter 2):

$$\begin{aligned} \frac{r^{\nu-1}}{\zeta^{\nu-1}} \left(\frac{\partial r}{\partial \zeta} \right)_\tau &= \frac{v}{v_0}, & u &= \left(\frac{\partial r}{\partial \tau} \right)_\zeta, \\ \left(\frac{\partial u}{\partial \tau} \right)_\zeta + v_0 \left(\frac{r}{\zeta} \right)^{\nu-1} \left(\frac{\partial p}{\partial \zeta} \right)_\tau &= 0, \\ \frac{\partial E}{\partial \tau} + p v_0 \zeta^{1-\nu} \left(\frac{\partial r^{\nu-1} u}{\partial \zeta} \right)_\tau &= 0. \end{aligned} \tag{4.3.1}$$

For convenience of the description, we here introduce new notations for independent variables $t \rightarrow \tau$, $s \rightarrow \zeta^\nu/v_0$ as well as for dependent variables $\langle V \rangle \rightarrow v$, $\langle E \rangle \rightarrow E$.

The parameter ν that determines the symmetry of the two-phase flow is equal to 1, 2, and 3 correspondingly for planar, cylindrical and spherical symmetries. Index 0 relates the variables to the unperturbed state of medium. Note that the Eulerian space coordinate $r = r(\zeta, \tau)$ is a dependent variable. Within the accepted assumptions the state equation for the two-phase medium is conveniently written in the form [84, 117, 127]

$$E = \frac{pv(1-\varepsilon)}{\gamma-1}. \tag{4.3.2}$$

Since the state equation (4.3.2) contains value of the volume portion as additional value, then

$$\varepsilon = \varepsilon_0 \frac{v_0}{v}. \tag{4.3.3}$$

Eq. (4.3.2) does not coincide with the state equation for a perfect gas with certain effective adiabatic parameter γ . Considering the adiabatic flow γ to be constant, the equation for energy can be reduced to the form [78]:

$$\left(\frac{\partial p (v - \varepsilon_0 v_0)^\gamma}{\partial \tau} \right)_\zeta = 0. \quad (4.3.4)$$

Thus, the closed system of the equations consists of first three equations of system (4.3.1) and equations (4.3.3), (4.3.4).

Since the Eulerian space coordinate $r = r(\zeta, \tau)$ is a dependent variable, we write this dependence through the Lagrangian independent coordinates (ζ, τ)

$$dr = \frac{\zeta^{\nu-1} v}{r^{\nu-1} v_0} d\zeta + u d\tau. \quad (4.3.5)$$

We now show that (i) for planar motions ($\nu = 1$), (ii) for stationary motions of any symmetry, and (iii) for self-similar flows at $\nu \neq 1$ but with certain accuracy, one can find new variables in which all equations (4.3.1), (4.3.3), (4.3.4) coincide with equations for a perfect gas and are explicitly independent of ε .

The following physical background provides a basis for eliminating the volume portion ε from (4.3.1)–(4.3.4). Indeed, if the condensed phase does not vary its volume (condition (a)) and does not contribute into partial pressure (condition (b)), and moves along the paths of the compressible gaseous phase (condition (c)), then we can assume that eliminating of the volume occupied by the condensed phase ε should substantially simplify the mathematical description of motion.

4.3.2 Similarity of stationary flows

We need to reduce the system of equations (4.3.1)–(4.3.4) to the system of equations describing the motion of a perfect gas (hereafter the notations for gas primed)

$$\begin{aligned} \left(\frac{r'}{\zeta'} \right)^{\nu-1} \left(\frac{\partial r'}{\partial \zeta'} \right)_{\tau'} &= \frac{v'}{v'_0}, & u' &= \left(\frac{\partial r'}{\partial \tau'} \right)_{\zeta'}, \\ \left(\frac{\partial u'}{\partial \tau'} \right)_{\zeta'} + v'_0 \left(\frac{r'}{\zeta'} \right)^{\nu-1} \left(\frac{\partial p'}{\partial \zeta'} \right)_{\tau'} &= 0, & \left(\frac{\partial p' (v')^\gamma}{\partial \tau'} \right)_{\zeta'} &= 0. \end{aligned} \quad (4.3.6)$$

For the latter system (4.3.6) the relation between the Eulerian space coordinate and the Lagrangian coordinates is as follows:

$$dr' = \left(\frac{\zeta'}{r'} \right)^{\nu-1} \frac{v'}{v'_0} d\zeta' + u' d\tau'. \quad (4.3.7)$$

One of the key requirements is as follows: the time should be equivalently running in all systems of coordinates $t = \tau = \tau'$.

The perturbations in incompressible component propagate with infinite velocity. Hence, the volume occupied by incompressible phase can be eliminated, then the connection between the equation (4.3.4) and the last equation (4.3.6) is presented in the form

$$v' = v - \varepsilon_0 v_0, \quad (4.3.8)$$

$$p' = p. \quad (4.3.9)$$

The relationship (4.3.8) indicates that the volume occupied by incompressible component is eliminated, and all masses of the medium are distributed over the residual volume of the compressible component.

Comparing the mass equations with each other, i.e. first equations from system (4.3.1) and system (4.3.4), the condition

$$\varepsilon_0 + (1 - \varepsilon_0) \left(\frac{r'}{\zeta'} \right)^{\nu-1} \left(\frac{\partial r'}{\partial \zeta'} \right)_{\tau'} = \left(\frac{r}{\zeta} \right)^{\nu-1} \left(\frac{\partial r}{\partial \zeta} \right)_{\tau}. \quad (4.3.10)$$

should be satisfied.

We need also to make consistent the momentum equations (i.e. third equation in (4.3.1) and third equation in (4.3.6)). The required condition after several reductions can be written as

$$\left(\frac{\partial u}{\partial \tau} \right)_{\zeta} - \gamma p_0 \left(\frac{r}{\zeta} \right)^{\nu-1} \left(\frac{v'_0}{v'} \right)^{\gamma+1} \frac{1}{1 - \varepsilon_0} \left(\frac{\partial v'}{\partial \zeta} \right)_{\tau} = 0, \quad (4.3.11)$$

$$\left(\frac{\partial u'}{\partial \tau'} \right)_{\zeta'} - \gamma p'_0 \left(\frac{r'}{\zeta'} \right)^{\nu-1} \left(\frac{v'_0}{v'} \right)^{\gamma+1} \left(\frac{\partial v'}{\partial \zeta'} \right)_{\tau'} = 0. \quad (4.3.12)$$

For deriving (4.3.11) we use the relation

$$\left(\frac{\partial p}{\partial \zeta} \right)_{\tau} = -\gamma p_0 \frac{v_0^{\gamma}(1 - \varepsilon_0)^{\gamma}}{(v - \varepsilon_0 v_0)^{\gamma+1}} \left(\frac{\partial v}{\partial \zeta} \right)_{\tau} = -\gamma p_0 \left(\frac{v_0}{v'} \right)^{\gamma+1} \frac{1}{v_0(1 - \varepsilon_0)} \left(\frac{\partial v'}{\partial \zeta} \right)_{\tau},$$

which follows from

$$p(v - \varepsilon_0 v_0)^{\gamma} = p_0(v_0 - \varepsilon_0 v_0)^{\gamma}.$$

Let us take advantage of key relationship between the independent variables in the Eulerian coordinates

$$dr' = (1 - \varepsilon)dr + \varepsilon u dt \quad (4.3.13)$$

appearing in the transformation for planar motion ($\nu = 1$) [83, 174, 177]. Owing to the relation (4.3.5) the terms with ε collected together in (4.3.13) yield the value $\varepsilon dr - \varepsilon u dt = \varepsilon_0 d\zeta$. Then the relation (4.3.13) has a form $dr' = dr - \varepsilon_0 d\zeta$ that confirms the physical interpretation for (4.3.13), namely, the volume (in planar symmetry ($\nu = 1$) the distance) occupied by the incompressible component $\varepsilon_0 d\zeta$ can be eliminated.

The suggestion (4.3.13) enables us to assume that the connection between variables r and r' for any symmetry could be presented in the form:

$$r'^{\nu-1} dr' = r^{\nu-1} dr - \varepsilon_0 \zeta^{\nu-1} d\zeta. \quad (4.3.14)$$

Thus we satisfy the important condition: the value dr' is an exact differential. That in turn enable us to rewrite the relationship (4.3.14) in the integral form:

$$r'^{\nu} = r^{\nu} - \varepsilon_0 \zeta^{\nu}. \quad (4.3.15)$$

The connection between the mass velocities follows immediately from (4.3.14)

$$r'^{\nu-1}u' = r^{\nu-1}u. \quad (4.3.16)$$

Substitution of the relation (4.3.15) directly into the condition (4.3.10) reduces this condition to the transformation

$$\zeta'^{\nu} = (1 - \varepsilon_0)\zeta^{\nu}. \quad (4.3.17)$$

Trying to transform Eq. (4.3.11) into (4.3.12) we can obtain new equation in which in addition to all terms of the equation (4.3.12) we get unfortunately the additional term

$$u' \left(\frac{r'}{r} \right)^{\nu-1} \left(\frac{\partial (r/r')^{\nu-1}}{\partial \tau} \right)_{\zeta}. \quad (4.3.18)$$

The additional term (4.3.18) vanishes for stationary flows as well as for any flows with planar symmetry, and possibly for self-similar motions.

Consequently, the transformation (4.3.8), (4.3.9), (4.3.15)–(4.3.17) between the systems of equations (4.3.1)–(4.3.4) and (4.3.6) is valid (i) at least for stationary flows, i.e. one can state that for cylindrical ($\nu = 2$) and spherical ($\nu = 3$) symmetries, the stationary motion of the two-phase medium is completely similar to the stationary motion of gas as well as (ii) there is a similarity in motions for all planar flows.

In the next Subsection 4.3.3 we analyze the transformation (4.3.8), (4.3.9), (4.3.15)–(4.3.17) between equation systems (4.3.1), (4.3.4) for self-similar motions in order to estimate the error included in the term (4.3.18).

4.3.3 Self-similar motions with shock waves

The above-mentioned transformation allows one to use its advantage for describing the self-similar problems. Let us apply the method for solving the problem related to the strong explosion stage in a two-phase medium.

Let a finite amount of energy E_0 be instantaneously deposited in an infinitely small volume of a two-phase medium. We restrict ourselves to distances from the explosion source where the wave can be considered as strong one, i.e. when we can neglect the initial internal energy of the medium in comparison with E_0 . We consider the propagation of the shock wave moving with velocity

$$D = \frac{dr_f}{dt}, \quad (4.3.19)$$

where r_f is a place of the shock wave front, $r_f = r_f(t)$ is a function of time only. Note that $\zeta_f = r_f$.

Let us define new dimensionless variables for the equation systems describing the two-phase flow (4.3.1), (4.3.3), (4.3.4)

$$\begin{aligned} P = v_0 p / D^2, \quad U = u / D, \quad \mathcal{V} = v / v_0, \quad \mu = \zeta / \zeta_f, \\ \eta = r / \zeta_f, \quad \chi = \zeta_f / \tau_0 D, \quad z = \frac{\zeta_f}{D^2} \frac{dD}{d\tau}, \end{aligned} \quad (4.3.20)$$

and gas (4.3.6)

$$\begin{aligned} P' &= v'_0 p' / D'^2, \quad U' = u' / D', \quad \mathcal{V}' = v' / v'_0, \quad \mu' = \zeta' / \zeta'_f, \\ \eta' &= r' / \zeta'_f, \quad \chi' = \zeta'_f / \tau_0 D', \quad z' = \frac{\zeta'_f}{D'^2} \frac{dD'}{d\tau'}, \quad D' = \frac{d\zeta'_f}{d\tau}. \end{aligned} \quad (4.3.21)$$

According to (4.3.15) we write

$$r'_f{}^\nu = (1 - \varepsilon_0) r_f{}^\nu, \quad r'_f{}^{\nu-1} D' = (1 - \varepsilon_0) r_f{}^{\nu-1} D. \quad (4.3.22)$$

At strong explosion in a two-phase medium the self-similar motion is realized, whereas, the derivatives with respect to χ are equal to zero, and $z = z' = -\nu/2$ (see, for example, [78, 117, 134, 141]). Then we can rewrite the systems of equations for the two-phase medium as

$$\begin{aligned} \frac{\eta^{\nu-1}}{\mu^{\nu-1}} \frac{d\eta}{d\mu} &= \mathcal{V}, \quad zU - \mu \frac{dU}{d\mu} + \frac{\eta^{\nu-1}}{\mu^{\nu-1}} \frac{dP}{d\mu} = 0, \\ P(\mathcal{V} - \varepsilon_0)^\gamma \mu^\nu &= \text{const} \end{aligned} \quad (4.3.23)$$

with boundary conditions at shock wave front [117, 141])

$$U = P = \frac{2(1 - \varepsilon_0)}{\gamma + 1}, \quad \mathcal{V} = \frac{\gamma - 1 + 2\varepsilon_0}{\gamma + 1},$$

and for the homogeneous medium (perfect gas) in the form

$$\begin{aligned} \left(\frac{\eta'}{\mu'} \right)^{\nu-1} \frac{d\eta'}{d\mu'} &= \mathcal{V}', \quad z'U' - \mu' \frac{dU'}{d\mu'} + \left(\frac{\eta'}{\mu'} \right)^{\nu-1} \frac{dP'}{d\mu'} = 0, \\ P'\mathcal{V}'^\gamma \mu'^\nu &= \text{const} \end{aligned} \quad (4.3.24)$$

with boundary conditions

$$U' = P' = \frac{2}{\gamma + 1}, \quad \mathcal{V}' = \frac{\gamma - 1}{\gamma + 1}.$$

We prove the last equation in (4.3.23) only. Let us consider the sequence of relations taking into account (4.3.4) and (4.3.20),

$$\begin{aligned} \left(\frac{\partial P(\mathcal{V} - \varepsilon_0)^\gamma \mu^\gamma}{\partial \tau} \right)_\zeta &= \left(\frac{\partial v_0 p D^{-2} (v - \varepsilon_0 v_0)^\gamma v_0^{-\gamma} (\zeta / \zeta_f)^\nu}{\partial \tau} \right)_\zeta \\ &= v_0^{1-\gamma} D^{-2} (\zeta / \zeta_f)^\nu \left(\frac{\partial p (v - \varepsilon_0 v_0)^\gamma}{\partial \tau} \right)_\zeta + v_0^{1-\gamma} \zeta^\nu p (v - \varepsilon_0 v_0)^\gamma \left(\frac{\partial D^{-2} \zeta_f^{-\nu}}{\partial \tau} \right)_\zeta \\ &= 0 + v_0^{1-\gamma} \zeta^\nu p (v - \varepsilon_0 v_0)^\gamma \left(-2\zeta_f^{-\nu} D^{-3} \frac{dD}{d\tau} - \nu \zeta_f^{-\nu-1} D^{-2} \frac{d\zeta_f}{d\tau} \right) \\ &= v_0^{1-\gamma} \zeta^\nu p (v - \varepsilon_0 v_0)^\gamma (-2\zeta_f^{-\nu-1} D^{-1} z - \nu \zeta_f^{-\nu-1} D^{-1}) = 0. \end{aligned}$$

The transformation (4.3.8), (4.3.9), (4.3.15)–(4.3.17) is easily reduced to the dimensionless form

$$(1 - \varepsilon_0) \mathcal{V}' = \mathcal{V} - \varepsilon_0, \quad (1 - \varepsilon_0) P' = P, \quad (4.3.25)$$

$$(1 - \varepsilon_0) \left(\frac{\eta'}{\eta} \right)^{\nu-1} U' = U, \quad \eta'^{\nu} = (1 - \varepsilon_0) \eta^{\nu} + \varepsilon_0 \mu^{\nu}, \quad \mu = \mu'.$$

It turns out that for self-similar motion with shock wave (in contrast to the stationary flow) the transformation between systems (4.3.22) and (4.3.23) is not succeeded in finding. Anyway for $\nu \neq 1$ there is the difference between system (4.3.22) and system appeared from (4.3.23) by means of transformation (4.3.25). The transformed system contains the additional term

$$U' \eta' \left(\frac{\eta'}{\eta} \right)^{\nu-1} \frac{d(\eta/\eta')^{\nu-1}}{d\eta}.$$

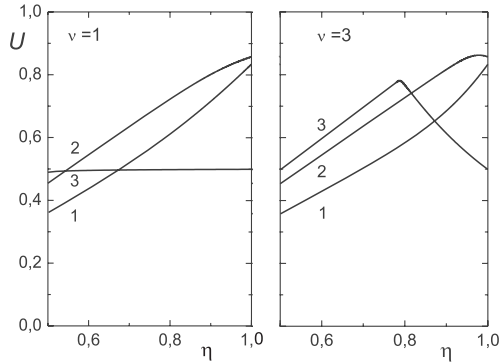


Figure 4.1: The profiles of dimensionless velocity U . The solutions calculated by two methods equal each other.

Using the point explosion as an example, we estimate the error introduced by the additional term. The results of the calculations for strong explosion are demonstrated in Figs. 4.1–4.4. We calculate the dimensionless specific volume \mathcal{V} , velocity U and pressure P by two methods. First, the system of equations (4.3.23) is directly solved at some particular values ε_0 . This is the exact solution \mathcal{V} , U , P . For the sake of convenience we use the dimensionless density $R = \mathcal{V}^{-1}$ instead of the dimensionless specific volume \mathcal{V}^{-1} . In Figs. 4.1–4.3 the variables U , R , P are plotted by curves 1, 2, 3. Second, the variables U , R , P are found by means of the transformation (4.3.25) of the solution U' , R' , P' for perfect gas (4.3.24). The solution thus obtained U , R , P are the approximate solution of the equation system (4.3.23). The approximate solutions are illustrated by curves 2', 3'. In Figs. 4.1–4.4 the curves 1 relate to gas ($\varepsilon_0 = 0$, $\gamma = 1, 4$), curves 2, 2' and 3, 3' — to two-phase media with $\varepsilon_0 = 0.1$, $\gamma = 1, 1$

and $\varepsilon_0 = 0.5$, $\gamma = 1,005$, respectively. It is very important that complete agreement is observed for U , R calculated by two methods, therefore, in Figs. 4.1, 4.2 the curves 2', 3' are not plotted, they completely coincide with curves 2, 3, respectively. While for the values P at $\nu \neq 1$ (see Fig. 4.1) the distinction between the exact solutions (curves 2, 3) and the approximate solutions (curves 2', 3') are largest. We note that for curves 3, 3' the initial volume portion is $\varepsilon_0 = 0.5$, i.e. one-half of the initial volume is occupied by the incompressible component. At small $\gamma - 1 \ll 1$ almost all mass of the condensed phase is accumulated near the front of shock wave (see Fig. 4.4).

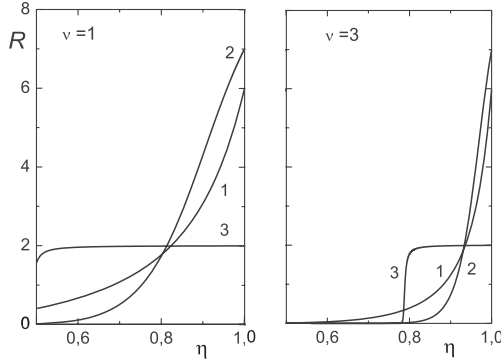


Figure 4.2: The profiles of dimensionless density $R = \mathcal{V}^{-1}$. The curves calculated by two methods coincide with each other.

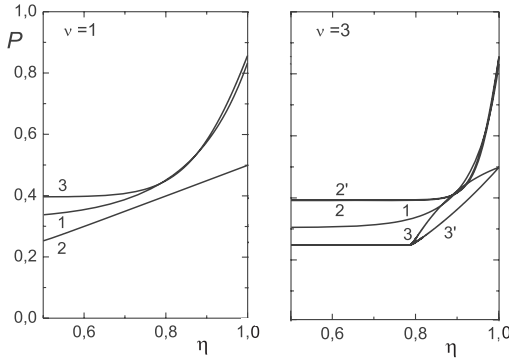


Figure 4.3: The profiles of dimensionless pressure P . Curves 2 and 3 are the exact solutions. Curves 2' and 3' are the approximate solutions.

Thus, since for a problem of strong explosion in gas the self-similar solution is known in forms of analytical dependencies [78, 134] and tabulated data [73], one can obtain with certain accuracy the solution for strong explosion in two-phase medium with

incompressible component. Moreover, the solution obtained in this manner has the analytical dependencies on value of volume portion of incompressible phase ε_0 . Hence, the influence of value ε_0 on two-phase flows can be estimated through the analytical dependencies.

We present below the example of successful applying the analytical transformation to estimate the velocity of shock wave propagation in two-phase medium [83, 174, 177].

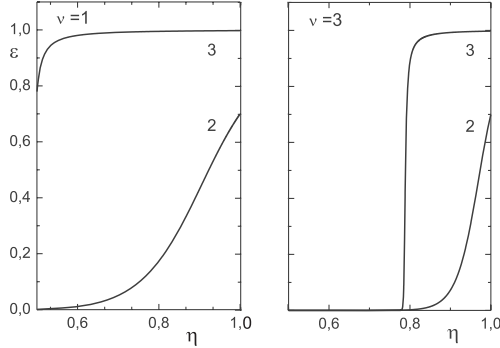


Figure 4.4: The distributions of volume portion of incompressible component ε_0 in shock wave.

4.3.4 Shock front parameters

It is fairly simple to establish analytically the effects of the volume portion of condensed phase on the motion of the shock wave and the shock front parameters without finding the distributions P , \mathcal{V} and R [164]. We need to trace only the energy balance in volume of medium involved by the shock wave

$$E_0 = \sigma(\nu) \int_0^{r_f} \left(\frac{p(1-\varepsilon)}{\gamma-1} + \rho \frac{u^2}{2} \right) r^{\nu-1} dr, \quad (4.3.26)$$

where $\sigma(\nu) \equiv 2(\nu-1)\pi + (\nu-2)(\nu-3)$. For this purpose we transform (4.3.26) by means of (4.3.25) as follows:

$$\begin{aligned} E_0 &= \sigma(\nu) \rho_0 D^2 r_f^\nu \int_0^1 \left(\frac{P(1-\varepsilon)}{\gamma-1} + R \frac{\mathcal{V}^2}{2} \right) (\eta)^{\nu-1} d\eta \\ &= \sigma(\nu) \rho_0 D^2 r_f^\nu \frac{(1-\varepsilon_0)^2}{\gamma-1} \int_0^1 \left(P' + \frac{\gamma-1}{2} R' (\mathcal{V}')^2 \right) (\eta')^{\nu-1} d\eta'. \end{aligned} \quad (4.3.27)$$

The dimensional method [134] allows us to obtain the equation for the shock wave

$$r_f = \left(\frac{E_0}{\alpha \rho_0} \right)^{1/(\nu+2)} \left(\frac{\tau}{1 - \varepsilon_0} \right)^{2/(\nu+2)}, \quad (4.3.28)$$

$$D = \frac{2}{(\nu + 2)(1 - \varepsilon_0)} \sqrt{\frac{E_0}{\alpha \rho_0}} r_f^{-\nu/2},$$

$$\alpha = \frac{4\sigma(\nu)\psi}{(\nu + 2)(\gamma - 1)}, \quad \psi = \int_0^1 \left(P' + \frac{\gamma - 1}{2} R'(\mathcal{V})^2 \right) (\eta')^{\nu-1} d\eta'.$$

For $\gamma \rightarrow 1$ the integral ψ tends to a finite limit and for $\gamma = 1$ we have $\psi = (2\nu)^{-1}$. If we derive ψ from the available theoretical and tabulated data such as in [73], we find that in the entire range in γ from 1.1 to 1.4 the value of the integral is close to the limiting value $\psi = (2\nu)^{-1}$ and differs from it by $\pm 3\%$. Then the expression for α can be put as

$$\alpha = \left(\frac{2}{\nu + 2} \right)^2 \frac{\sigma(\nu)}{2\nu(\gamma - 1)}. \quad (4.3.29)$$

We use (4.3.28), (4.3.29) and (4.3.20) to get a relation between the shock front pressure and the distance from the explosion center:

$$p = \frac{2(1 - \varepsilon_0)}{\gamma + 1} \rho_0 D^2 = \frac{4\nu}{\sigma(\nu)} \frac{\gamma - 1}{\gamma + 1} \frac{E_0}{1 - \varepsilon_0} r_f^{-\nu}. \quad (4.3.30)$$

These equations indicate that the increase in the shock wave parameters when the medium contains an incompressible phase is due to the increase in the shock wave velocity by a factor $(1 - \varepsilon_0)^{-1}$ in comparison with $\varepsilon_0 \rightarrow 0$ for a given ratio of the mass concentrations. In the limiting case $\varepsilon_0 \rightarrow 1$ the shock wave velocity tends to infinity. This feature is evident from the physical viewpoint because the velocity of the perturbation tends to infinity for an incompressible medium.

It follows from (4.3.30) that the minimum pressure occurs at a given distance from the explosion center in a medium having the maximal shock compressibility for the gas phase (by definition $(\gamma + 1)/(\gamma - 1)$) with the minimum value of ε_0 . Therefore, in the general case of arbitrary ε_0 the pressure field and the shock wave velocity in a two-phase medium are dependent not only on the density ρ_0 , the explosion energy E_0 , and α [50] but also on the volume portion of condensed phase ε_0 .

Consequently, we have suggested the transformation that allows one to obtain the wave fields in two-component media with arbitrary volume portion of the incompressible component from the similar problem for perfect gas. The solutions of many hydrodynamic problems for mixtures with incompressible component can be obtained without solving the original system of equations. The scope for the suggested transformation is shown through the analysis of the strong explosion in a two-phase medium.

Chapter 5

Blast waves in medium with structure

The features of dynamic behavior of two-component media, the influence of interphase interaction under the wave propagation can be elucidated by means of solution of a problem related to the strong explosion in a two-phase medium. This problem attracts interest also in practical possibility to estimate the efficiency of a medium for localizing the shock wave action. The expanded range of pulsed materials processing requires the development of means for localizing the effect of high-power energy sources used to excite the shock waves in the surrounding medium. In addition to the special chambers, recently the multiphase media (bubble screens in liquids [49, 152], gas-liquid foam [82, 84], foam plastics [75], etc.) have been used for damping of the shock waves. The studies have shown that the energy of explosions is most efficiently absorbed by the water foam [75].

A qualitative theoretical analysis of strong shock waves in two-phase media with a small volume fraction of condensed material shows that the potential capacity of foam to damp the shock waves is greater. It turns out that the estimated parameters of shock waves at a fixed distance can be below the parameters found in experiments [50, 84]. It is noticed that the failure to reach the calculated parameters can apparently be explained by means of the fact that the characteristic time of interphase relaxations, which describe the conversion of thermal energy from the gaseous component (which determines the pressure of a medium) to the internal energy of the condensed phase (which does not contribute to the pressure), are substantially greater than the time required to peak the pressure at the shock front. We will clarify that the properties of own medium determine the attenuation of shock waves. We will analyze the dependence of the shock wave attenuation on the thermal relaxation time in order to understand the damping of shock waves by such media and find out their effectiveness as localizing media as well. Besides, it is of interest to define the dependence of the shock wave attenuation on a shock loading, in particular, on an explosion energy [164].

In many problems of blasting, the formation of cracks in a rock under the explosion action is of decisive importance. The crack formation exerts an influence on the change in physical mechanical rock properties, particularly, the rock-mass permeability. As the permeability in the near-well zone of the productive strata rises, the producing well discharge increases. One of a perspective method is the method of controlled change

in mechanical properties of rocks using the pulse action, including explosion energy. The model of rock fracture is suggested with due regard for the attenuation of wave loading governed by the geometrical divergence of wave and irreversible losses in rock. The obtained analytical relations enables us, on the one hand, to indicate the blast wave characteristics which affect the fracture process and, on the other hand, to lay the theoretical foundations for estimating the blast wave properties by means of the known fracture area.

5.1 System of equations for describing the strong explosion

The molecular relaxation following an explosion in a gaseous or liquid medium proceeds so fast that the perturbation front can be regarded as a discontinuity surface (a shock wave). This makes it correct to use the self-similar theory of point explosion [73, 78, 134] for describing the evolution of a shock wave during the high-intensity stage of the explosion process also at distances where the shape of the energy source does not play a significant role. Hence, in this classical case where there are no relaxation processes in flow behind the front of a shock wave, the unsteady motion of a medium induced by the instantaneous release of energy at a point is described by a self-modeling solution [73, 78, 134]. Then the pressure and velocities of the wave flows are uniquely determined by the energy of explosion and the thermophysical properties of the gas surrounding the energy source.

However, there are media in which the relaxation processes occur in flow behind the shock front. If the medium possesses the relaxation processes with characteristic time compared with a time of wave propagation, the parameters behind the front depend significantly on the completeness of relaxation processes in a medium. One glowing example of these media is the gas-liquid foam. After explosion in a two-phase medium only the gaseous component reaches equilibrium immediately, owing to the inertia of condensate particles at a wave front. There is the wide relaxation zone behind the shock front, since the equalization time between the parameters of the phases is well long than the relaxation time in a gas [82, 84]. Consequently, formation of a shock wave after explosion in two-phase medium cannot any more be regarded as occurring within an infinitesimally short time, and the relaxation processes in wave should be taken into account [84] to define the shock wave.

This chapter is concerned with the effect of thermal relaxation behind the shock front on the evolution of a shock wave. For example, the attenuation of shock waves in gas-liquid foam generated by the condensed explosive charge shall be described in terms of a relaxed heat transfer from the gas phase into the condensed phase [83, 84, 173, 175, 178]. Let an explosion occur in this medium and, as a result, an energy E_0 producing a shock wave be released instantaneously within an infinitesimally small volume. The problem consists in defining a flow behind the shock front as a dependence on thermophysical properties of a medium as well as on completeness of relaxation processes. The existence of relaxation processes makes considerably more complicated the calculations of strong shock because the flow is not a self-similar one. This means that a time-dependent system of differential equations must be solved. Analyzing the

shock flows in two-phase media, we made the following assumptions : (a) components in two-phase media are uniformly in volume; (b) density and specific heat of the condensed phase are constant; (c) gaseous phase obeys the state equation for an ideal gas; (d) there are no mass transitions between phases; (e) gaseous phase and the condensate phase move at the same velocity; (f) energy of the mixture is an additive quantity; (g) time for thermal relaxation between gas and condensed component is constant; (h) transfer of perturbations from the relaxation zone to the front of the shock wave obeys the hydrodynamics laws.

On the basis of these assumptions, the fundamental system of equations for describing the shock-wave flows at point explosion in mixture (spherical symmetry $\nu = 3$) will be put in the form of the asymptotic averaged model (4.1.4), (4.2.7) created in Sections 4.1, 4.2.

$$\frac{\partial \langle V \rangle^{-1}}{\partial t} - \frac{1}{r^2} \frac{\partial r^2 \langle V \rangle^{-1} u}{\partial r} = 0, \quad (5.1.1)$$

$$\frac{\partial u}{\partial t} + u \frac{\partial u}{\partial r} + \langle V \rangle \frac{\partial p}{\partial r} = 0, \quad (5.1.2)$$

$$\left(\frac{\partial}{\partial t} + u \frac{\partial}{\partial r} \right) \langle E \rangle + \frac{p}{r^2} \frac{\partial r^2 u}{\partial r} = 0, \quad (5.1.3)$$

$$\tau_E \frac{d}{dt} \left[\langle E \rangle - \frac{p \langle V \rangle (1 - \varepsilon)}{\gamma - 1} \right] + \left[\langle E \rangle - \frac{p \langle V \rangle (1 - \varepsilon)}{\Gamma_0 - 1} \right] = 0. \quad (5.1.4)$$

The dynamic state equation (5.1.4) relates to the certain mass of medium, thereby the full derivative with respect of time t is to be $d/dt = \partial/\partial t + u\partial/\partial r$. The volume fraction of a condensed phase ε is one-valued function of an averaged specific volume $\langle V \rangle$ (4.2.8)

$$\varepsilon = \varepsilon_0 \langle V_0 \rangle / \langle V \rangle.$$

Since there is an additional variable $r_f = r_f(t)$ (or velocity of a shock wave $D = dr_f(t)/dt$), the system of equations is supplemented by the balance equation of the total energy: the energy of the medium bounded by the shock wave is equal to the initial energy of the medium $E(p_0, \rho_0)$ and the energy of the explosion E_0

$$\begin{aligned} E_0 + \frac{4}{3} \pi \rho_0 E(p_0, \rho_0) r_f^3 &= \frac{4}{3} \pi \int_0^{r_f} \langle E + \frac{1}{2} u^2 \rangle ds \\ &= 4\pi \int_0^{r_f} \left(\frac{\langle E \rangle}{\langle V \rangle} + \frac{u^2}{2 \langle V \rangle} \right) r^2 dr. \end{aligned} \quad (5.1.5)$$

The state equation can be formally rewritten down in a form

$$\langle E \rangle = \frac{p \langle V \rangle (1 - \varepsilon)}{\hat{\Gamma} - 1}, \quad \hat{\Gamma} = \gamma - (\gamma - \Gamma) \left/ \left(1 + \tau_E \frac{d}{dt} \right) \right. . \quad (5.1.6)$$

The physical sense of the operator $\hat{\Gamma}$ concerns in that it specifies the thermophysical properties of a medium as well as their changes due to internal relaxation processes. It

can vary between $\hat{\Gamma} = \gamma$ for flows with the frozen thermal processes, and $\hat{\Gamma} = \Gamma_0$ for the equilibrium flows. For most processes we have $\Gamma_0 < \gamma$. As was noted for two-phase gas-containing mixtures, Γ_0 is usually close to 1, though not exactly equal to it.

For wave propagation it is succeeded to reduce the form $\hat{\Gamma}$ by introducing an additional assumption. The nonequilibrium between phases is considered to arise in shock front only (here $\hat{\Gamma} = \gamma$). The wide zone relaxation follows behind shock front, where the progressive equalization of temperatures between the components takes place. We assume that in flow behind the shock front, an additional nonequilibrium is not introduced between the components medium. In this case the expression (5.1.6) can be reduced assuming that the time relaxation τ_E is a constant value. Although this approximation on flow is not faithful, however, it allows one to present the relationship (5.1.6) in an algebraic form, and hence, the analysis of wave propagation is essentially simplified for describing the relaxation processes.

The parameter $\hat{\Gamma}$ corresponds to the completeness of relaxation processes, hence, it is to be depended on the lifetime of a microscopic volume in the shock wave τ' . Then in the shock front we have $\tau' = 0$ and $\hat{\Gamma} = \gamma$, while at $\tau' \rightarrow \infty$ we get $\hat{\Gamma} \rightarrow \Gamma_0$. At these conditions from (5.1.6) it is easy to obtain the algebraic expression for the effective parameter Γ to describe the relaxation process [84, 173, 175]

$$\Gamma = \Gamma_0 + (\gamma - \Gamma_0) \exp(-\tau'/\tau_E). \quad (5.1.7)$$

In general, τ' is a function of the time t and space coordinate r , i.e. $\tau' = \tau'(r, t)$, and satisfies the differential equation

$$\frac{\partial \tau'}{\partial t} + u \frac{\partial \tau'}{\partial r} = 1 \quad (5.1.8)$$

with $\tau' = 0$ for $t = 0$ and $r = r_f$.

We shall restrict ourselves the consideration of the strong shock wave where the initial internal energy of the gas can be neglected $\frac{4}{3}\pi r_f^3 \rho_0 E(p_0, \rho_0) \ll E_0$ in Eq. (5.1.5). Then the boundary conditions at the shock front and center symmetry take the following form [117]

$$\begin{aligned} u &= 0 \quad \text{at} \quad r = 0, \\ u_f &= \frac{2(1 - \varepsilon_0)}{\gamma + 1} D, \quad p_f = \frac{2(1 - \varepsilon_0)}{\gamma + 1} \rho_0 D^2, \\ \langle V \rangle_f^{-1} &= \frac{\gamma + 1}{\gamma - 1 + 2\varepsilon_0} \rho_0 \quad \text{at} \quad r = r_f, \end{aligned} \quad (5.1.9)$$

In the case of a point source of energy E_0 the initial conditions for the system of equations can be found from the self-similar solution of the problem [78, 134].

Since the dependence on the volume fraction of a condensed phase ε , as it has been proved in Sec. 4.3, can be considered separately, the system of equations shall be solved at the condition $\varepsilon_0 = 0$.

Consequently, we have obtained a closed system of equations (5.1.1)-(5.1.3), (5.1.5)-(5.1.8) with boundary conditions (5.1.9) for the motion of a two-phase medium including the thermal nonequilibrium behind the shock front. This system consists of seven equations which have seven unknown variables: $\langle V \rangle$, u , p , $\langle E \rangle$, Γ , τ' , r_f .

The system of equations (5.1.1)-(5.1.3), (5.1.5)-(5.1.8) is reduced to the dimensionless form by means of transformation of the dependent variables

$$R = \frac{\langle V \rangle_0}{\langle V \rangle}, \quad U = \frac{u}{D}, \quad P = \frac{p \langle V \rangle_0}{D^2}, \quad \theta = \frac{\tau'}{\tau_E} \quad (5.1.10)$$

and independent variables

$$\eta = \frac{r}{r_f}, \quad \chi = \frac{r_f}{\tau_E D}, \quad \tau_E \frac{d\chi}{dt} = 1 - z, \quad z = \frac{r_f}{D^2} \frac{dD}{dt} \quad (5.1.11)$$

as follows:

$$\begin{aligned} (1-z)\chi \frac{\partial R}{\partial \chi} + (U-\eta) \frac{\partial R}{\partial \eta} + \frac{R}{\eta^{\nu-1}} \frac{\partial \eta^{\nu-1} U}{\eta} &= 0, \\ (1-z)\chi \frac{\partial U}{\partial \chi} + (U-\eta) \frac{\partial U}{\partial \eta} + zU + \frac{1}{R} \frac{\partial R}{\eta} &= 0, \\ \left((1-z)\chi \frac{\partial}{\partial \chi} + (U-\eta) \frac{\partial}{\partial \eta} + 2z \right) \frac{P}{\Gamma-1} \\ &+ \frac{\Gamma P}{(\Gamma-1)\eta^{\nu-1}} \frac{\partial \eta^{\nu-1} U}{\eta} = 0, \\ (1-z)\chi \frac{\partial \theta}{\partial \chi} + (U-\eta) \frac{\partial \theta}{\partial \eta} &= \chi, \\ (1-z)\chi \frac{d\psi}{d\chi} + (2z+\nu)\psi &= 0, \\ \psi = \int_0^1 \left(\frac{P}{\Gamma-1} + R \frac{U^2}{2} \right) \eta^{\nu-1} d\eta, \\ \Gamma = \Gamma_0 + (\gamma - \Gamma_0) \exp(-\theta). \end{aligned} \quad (5.1.12)$$

We have seven equations for seven unknown variables $R, U, P, \theta, \psi, \Gamma, z$.

The boundary conditions for this system take the form

$$\begin{aligned} U = 0 \quad \text{at} \quad \eta = 0, \\ U_f = \frac{2}{\gamma+1}, \quad P_f = \frac{2}{\gamma+1}, \quad R_f = \frac{\gamma+1}{\gamma-1} \quad \text{at} \quad \eta = \eta_f = 1. \end{aligned} \quad (5.1.13)$$

In the limiting case without relaxation processes ($\Gamma = \gamma = \text{const}$) the dimensionless variables R, U, P are self-similar, whereas $z(t=0) = -3/2$. These self-similar distributions R, U, P on $0 \leq \eta \leq 1$ are considered to determine the initial conditions.

The system of equations (5.1.12) differs from the self-similar system of equation by the dependence of Γ on time χ and space coordinate η . This difference occurs only in equation (5.1.12) containing the additional term

$$\left((1-z)\chi \frac{\partial}{\partial \chi} + (U-\eta) \frac{\partial}{\partial \eta} \right) \ln(\Gamma-1).$$

It is clearly that at time instant $\chi \simeq 0$ and long time $\chi \gg 1$ this additional term becomes negligible small. It means that the solution at these times is close to the self-similar solution, but with different parameters: $\Gamma = \gamma$ at $\chi \simeq 0$ and $\Gamma = \Gamma_0$ at $\chi \gg 1$.

5.2 Calculation of shock waves

The finding of solution for the equations system is sufficiently complicated by singularities that take place at initial instant of time $\chi \simeq 0$ and in vicinity of symmetry center $\eta = 0$. At $\eta = 0$ we meet a singularity of a saddle-point type. Moreover, at time instant under transition from $\chi = 0$ (here the initial conditions have been specified) to the time $\chi > 0$, the order of the system of equations (5.1.12) increases. Indeed, at $\chi = 0$ we have the system of the ordinary differential equations (there is one independent variable η only), while at $\chi > 0$ we have the system of partial differential equations. To avoid the singularity concerned with vanishing the terms which include the partial derivative with respect to χ , we have suggested the following method. For times less than a certain value χ^* , i.e. at $\chi < \chi^*$, when the relaxation processes change insignificantly the flow with respect to the self-similar flow, all deviations of the dependent variables from the self-similar values can be defined in form of the linear corrections (the self-similar variables are denoted by subscript 0)

$$R = R_0(1 + \delta_{Rt}/\tau_E), \quad U = U_0(1 + \delta_{Ut}/\tau_E), \quad P = P_0(1 + \delta_{Pt}/\tau_E). \quad (5.2.1)$$

After the linearization the linear system has been solved by the numerical method. For $\eta < \eta^*$ (η^* is some value selected at numerical experiment) we use the asymptotic approximation to avoid the singularity of the saddle-point type at $\eta = 0$. Hence, we can obtain the solutions which hold true until certain χ^* , i.e. at $\chi \leq \chi^*$.

For $\chi > \chi^*$ the method of solution is based on the implicit finite-difference schemes analogous to those given in [135]. With an implicit scheme it is possible to avoid the strict limitation on the time step. The differential equations (5.1.12) can be approximated to the first order by an implicit finite-difference scheme of the triangular type (running calculation). The calculation starts from the shock front, where all the flow parameters are known. The implementation of the implicit scheme is complicated by the nonlinearity of the equations and therefore the variables were found using the method [40], adopted to the case of two independent variables. It is essential at numerical calculation that the integral relation in (5.1.12) and the boundary condition $U = 0$ are to be satisfied simultaneously. By varying the value of z , these two requirements can be satisfied using the method of successive approximations. A singularity of the saddle-point type near the center of symmetry was crossed by varying z . Starting from a certain η^* , when the lowest values of the density are reached, the value of the velocity is extrapolated by the linear dependence $U = U(\eta^*)\eta/\eta^*$ for $0 \leq \eta \leq \eta^*$ in order to avoid the significant errors at calculation of the kinetic energy.

In order to suppress the possible high-frequency computational oscillations in the finite-difference procedure we have used the smoothing method (see Ref. [73]). The resulting smoothing coefficients (0.002 for the density and 0.005 for the pressure and velocity) lead to the desired result and do not accumulate errors in the flow parameters.

The occurrence of thermal relaxation is shown to make the description of the shock waves more complicated [164]. The features arise in form of changes of profiles for pressure P , mass velocity U and density R . The relaxation in medium affects on rate of damping shock wave, on ratio between kinetic and internal energies, on impulse of the pressure in transient shock wave. In general case the shock wave parameters depend on properties of a medium ρ_0 , γ , Γ_0 , τ_E and explosion energy E_0 . The principal features of flow in the relaxing medium appear even at initial time instant.

The calculations show that at the initial time $\chi \leq \chi^*$ the flow parameters deviate linearly, with an accuracy of 15%, from the self-similar parameters of a flow in a nonrelaxing medium. The more rapid damping of the shock velocity under thermal relaxation leads to an increase of the relative velocity U as compared with the self-similar solution. Because of this the relative fraction of the mass in the central region decreases, but increases near the front. The pressure at the shock front decreases monotonically. The deviations from the self-similar parameters given by the formulas (5.2.1) are shown in Fig. 5.1 for $\gamma = 1.4$ and $\Gamma_0 = 1.01$.

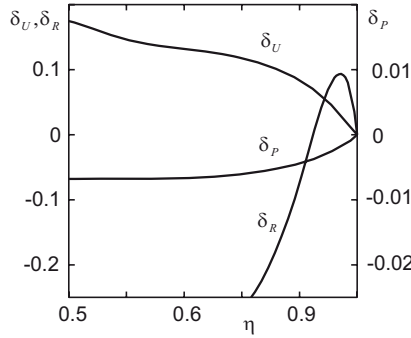


Figure 5.1: Distributions of the corrections to the self-similar solution for the density δ_R , mass velocity δ_U , and pressure δ_P .

The effect of heat exchange on the attenuation of pressure in the shock wave is conveniently characterized by the parameter s which relates the pressure at the shock front p_f to the distance from the center of the energy source in a form $p \sim r_f^{-s}$. If kinematic equilibrium exists between components we get

$$s = -\frac{d \ln p}{d \ln r_f} = -2 \frac{d \ln D}{d \ln r_f}. \quad (5.2.2)$$

It should be noted that for strong shocks, in which the relaxation processes occur within the shock front, the variable s is a constant, whereas, in particular, for spherical symmetry we have the value $s_0 = 3$. Then the reduction in the pressure drop with distance is related only to the geometric divergence of the flow. At the same time, for a medium in which the shock is damped more rapidly than in a uniform medium, the parameter s must exceed the value s_0 related to the self-similar solution. The deviation

from the self-similar value s_0 for $t < \tau_E$ is conveniently characterized by the quantity

$$\delta_s = \frac{s - s_0}{s_0} \frac{t}{\tau_E}. \quad (5.2.3)$$

Table 5.1 shows the computed corrections δ_s for spherical symmetry. We note that the correction δ_s characterizes the rate of damping of the shock at initial time.

Table 5.1: Correction δ_s

Γ_0	δ_s for γ			
	1.1	1.2	1.4	1.66
1.2	–	0.0	0.505	0.655
1.1	0.0	0.560	0.760	0.800
1.05	0.610	0.840	0.885	0.870
1.01	1.095	1.065	0.985	0.925
1.001	1.205	1.115	1.010	0.940

The dependence of pressure attenuation on the relative distance $\tilde{R} = r_f/E_0^{1/3}$ (E_0 is energy of explosive charge) with different dimension parameters ρ_0 , E_0 , γ , Γ_0 , τ_E at initial instant of time, is represented in Figs. 5.2. From Fig. 5.2a it follows that for $\tau_E = \text{const}$ the reduction of Γ_0 by changing the mass concentration of the condensed phase leads to a substantially more rapid damping of the wave than for the same values of Γ_0 at the lower mass concentrations, however, in the limiting case without heat exchange ($\tau_E \rightarrow \infty$) the shock parameters are the same in both cases.

This effect is explained by the fact that, despite of the heat exchange, the enhanced concentration of the condensed phase leads to a attenuation of the velocity of shock wave. When a heat exchange occurs in the medium, then the time required for the shock to travel a fixed distance increases and, consequently, this leads to the more completeness of the thermal relaxation between the phases.

For given ρ_0 , γ , Γ_0 , and τ_E (see Fig. 5.2b) an increase of the energy by a factor of 10 and 100 causes a reduction by factor of 1.2 and 1.45, respectively, for the distance where a pressure exceeds a value 5 MPa. The influence of the characteristic heat-exchange time on the pressure variation with distance is shown in Fig. 5.2c. As would be expected, the attenuation should be more rapid at more intense heat exchange (all other conditions are the same). The variation of the initial value γ (the adiabatic index of the gaseous phase) leads, on one hand, to the different initial pressures and, on the other, to the more rapid attenuation for smaller γ (see Fig. 5.2d).

For $\chi > \chi^*$ the deviations from the self-similar solution do not obey the linear relations. It is necessary to solve the nonlinear system (5.1.12). The numerical method we used was described in Sec. 5.1.

At $t \gg \tau_E$ the basic features of the evolution of strong shock waves in a relaxing medium are shown in Figs. 5.3-5.6. The effect of the relaxation process on the change of the pressure profile is shown in Fig. 5.3. In the central region a decrease in P is observed at the initial instant of time, but later, as the average thermodynamic

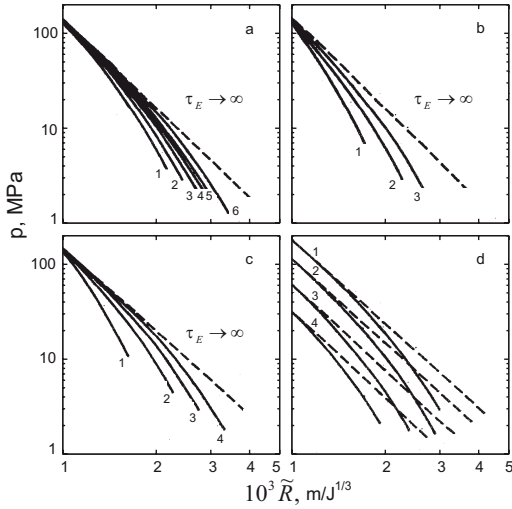


Figure 5.2: Dependence of the pressure attenuation on the relative distance for different Γ_0 , ρ_0 , E_0 , τ_E and γ : (a) $\gamma = 1.4$, $E_0 = 10^7$ J, $\tau_E = 150 \mu\text{sec}$, (1) $\Gamma_0 = 1.01$, $\rho_0 = 50 \text{ kg/m}^3$, (2) $\Gamma_0 = 1.01$, $\rho_0 = 20$, (3) $\Gamma_0 = 1.001$, $\rho_0 = 10$, (4) $\Gamma_0 = 1.01$, $\rho_0 = 10$, (5) $\Gamma_0 = 1.1$, $\rho_0 = 10$, (6) $\Gamma_0 = 1.01$, $\rho_0 = 2 \text{ kg/m}^3$; (b) $\gamma = 1.4$, $\rho_0 = 10 \text{ kg/m}^3$, $\Gamma_0 = 1.01$, $\tau_E = 150 \mu\text{sec}$, E_0 in J: (1) 10^9 , (2) 10^8 , (3) 10^7 ; (c) $\gamma = 1.4$, $E_0 = 10^7$ J, $\rho_0 = 10 \text{ kg/m}^3$, $\Gamma_0 = 1.01$, τ_E in μsec : (1) 30, (2) 80, (3) 150, (4) 300; (d) $E_0 = 10^7$ J, $\rho_0 = 10 \text{ kg/m}^3$, $\Gamma_0 = 1.01$, $\tau_E = 150 \mu\text{sec}$, γ : (1) 1.67, (2) 1.4, (3) 1.2, (4) 1.1.

equilibrium is reached, the pressure increases and approaches to the value related to the self-similar flow with Γ_0 .

The parameter Γ represented in the form (5.1.7) can be considered as a relaxation function describing the heat exchange in two-phase medium. If the thermodynamic equilibrium exists between the phases, Γ_0 is identical to the ratio of the specific heats of the medium at constant pressure and constant volume [108]. In this case a decrease

The parameter Γ represented in the form (5.1.7) can be considered as a relaxation function describing the heat exchange in two-phase medium. If the thermodynamic equilibrium exists between the phases, Γ_0 is identical to the ratio of the specific heats of the medium at constant pressure and constant volume [108]. In this case a decrease of Γ_0 is equivalent to an increase of the concentration and/or the specific heat of the condensed phase (the other conditions are the same).

The presence of the relaxation process leads to a qualitative change in the nature of the attenuation of the shock wave. Unlike the case of a nonrelaxing medium, where the pressure and propagation velocity of the shock wave vary according to the power laws ($p \sim r_f^{-s}$, $D \sim r_f^{-0.5s}$) with a constant exponent $s_0 = 3$, the presence of relaxation leads to a variation of the exponent. The maximum absolute value s_{\max} exceeds (for the other parameters held constant) later s_0 in a medium with a smaller value of Γ_0 .

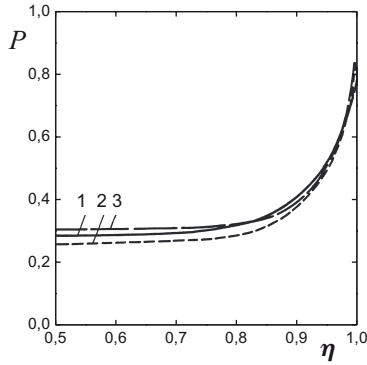


Figure 5.3: The pressure profile of shock wave at different time propagation. For all curves $\gamma = 1.4$, $\Gamma_0 = 1.2$. Curve (1) relates to $t/\tau_E = 0$; (2) — $t/\tau_E = 1$; (3) — $t/\tau_E = 6$.

Table 5.2: The time t/τ_E for maximum value s_{\max} at specific values of Γ_0 and at fixed $\gamma = 1.4$

Γ_0	1.2	1.05	1.01
s_{\max}	3.6	6.6	12.2
t/τ_E	3.2	5.4	7.8

In Table 5.2 we show the dimensionless time t/τ_E at which the maximum value s_{\max} is reached for specific values of Γ_0 and for fixed $\gamma = 1.4$. Far from the energy source and for $t \gg \tau_E$ the relaxation processes do not really affect the nature of damping of the velocity and pressure on the shock front. In this case s asymptotically approaches its limiting value $s_0 = 3$, corresponding to the self-similar solution. Indeed, if wave propagates over a long time ($t \gg \tau_E$) and it remains yet strong shock wave ($p \gg p_0$), then all relaxation processes take place in zone near to the shock front only. The flow behind this zone can be described with necessary accuracy by means of self-similar solution but with equilibrium parameter Γ_0 . This is illustrated in Fig. 5.4 where the dependence of the pressure on the wave front $P_f = p\tau_E^{6/5}(\rho_0 A^2)^{-1}$ is shown as a function of the dimensionless distance $l = r_f(\tau_E^{2/5} A)^{-1}$ ($A = (E_0/\alpha\rho_0)^{1/5}$ see (4.3.28)). As is seen from Fig. 5.4 the curves approach the asymptotic value at the same distance from the energy source. We note that the increase of the exponent s larger than the self-similar value $s_0 = 3$ is purely a relaxation effect. This effect is typical for the propagation of strong shock waves for a wide class of multiphase media (foam [50, 81, 84, 175], soil [91, 92], bubble-like materials [49, 104, 111, 120]).

An important characteristic related to the attenuation of the shock wave in the medium with relaxation is the variation of the ratio of the internal energy to the kinetic one during the relaxation process. The dependence of the energy redistribution

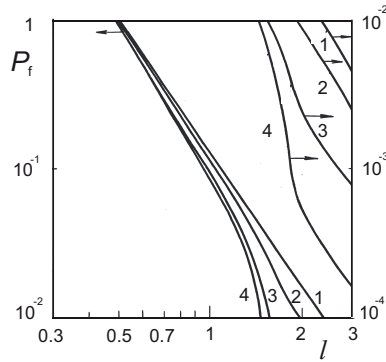


Figure 5.4: The pressure on the wave front $P_f = p\tau_E^{6/5}(\rho_0 A^2)^{-1}$ as a function of the dimensionless distance $l = r_f(\tau_E^{2/5} A)^{-1}$. Curve (1) relates to $\Gamma_0 = 1.4$; (2) — $\Gamma_0 = 1.2$; (3) — $\Gamma_0 = 1.05$; (4) — $\Gamma_0 = 1.01$. For all curves $\gamma = 1.4$.

from the explosion between the internal and kinetic energies of the medium on the dimensionless time is shown in Fig. 5.5. We see that the energy redistribution in

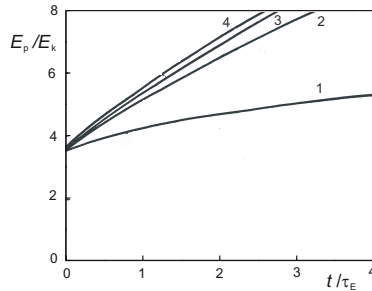


Figure 5.5: The dependence of the energy redistribution from the explosion between the internal E_p and kinetic E_k energies of the medium on the dimensionless time t/τ_E . For all curves $\gamma = 1.4$. Curve (1) relates to $\Gamma_0 = 1.2$; (2) — $\Gamma_0 = 1.05$; (3) — $\Gamma_0 = 1.01$; (4) — $\Gamma_0 = 1.0$.

time also reaches a limiting value corresponding to thermodynamic equilibrium in the medium, and this process occurs more rapidly for larger value of the parameter Γ_0 . However, at any fixed time instant, in a medium with a smaller value Γ_0 the ratio of the internal energy to the kinetic energy is always larger. But at the decrease of Γ_0 the difference in the energy redistribution decreases, and finally the ratio of energies approaches the dependence which is realized for the limiting value $\Gamma_0 = 1.0$ (curve 4).

The attenuation of shock waves in a relaxing medium is intimately connected with the need to decrease their intensity in order to avoid the breakup of the structures and objects. In practice, a breakup is determined in the most cases either by the impulse

of the shock wave or by a quantity involving the impulse and the pressure on the shock front [61]. Since the relaxing multiphase media are so widely used in the damping of shock waves, the knowledge how the impulse of the shock wave changes throughout relaxation processes is of current interest. This is shown in Fig. 5.6 as the dependence of the dimensionless impulse of the pressure

$$J = I\tau_E^{1/5}(\rho_0 A)^{-1}, \quad I = \int_{t(r_1)}^{\infty} p(r_1, t) dt \quad (5.2.4)$$

on the distance $l = r_f(\tau_E^{2/5} A)^{-1}$. For constant ρ_0 , a decrease of the parameter Γ_0 leads to a decrease of the impulse of pressure at a fixed relative distance. It must be pointed

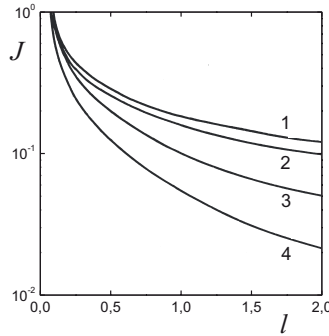


Figure 5.6: The dependence of the dimensionless impulse of the pressure J on the dimensionless distance l . Curve (1) relates to $\Gamma_0 = 1.4$; (2) — $\Gamma_0 = 1.2$; (3) — $\Gamma_0 = 1.05$; (4) — $\Gamma_0 = 1.01$. For all curves $\gamma = 1.4$.

out that an increase of the density of the medium (all other properties being equal) can lead to an increase of the impulse of pressure I even larger than the value for a less dense nonrelaxation medium (see Fig. 5.6), in spite of the decrease of the peak pressure p (Fig. 5.4).

5.3 Blast waves in foam

Nature of the relaxation interaction between gas and liquid must be understood in order to predict the parameters of shock waves generated by the ignition of explosive in foam. At the explosion in foam the degree of completion of relaxation processes depends both upon the thermophysical properties of phases and the energy of the explosion determining the wave attenuation [164].

Considering the attenuation of shock waves generated by nonpoint energy sources, such as chemical explosives, it should be noted that the increase of the density of the condensed phase in medium for purposes to reduce the shock wave parameters simultaneously causes a decrease of the shock formation region and, hence, an increase of the

shock parameters at the interface between the two-phase medium and the explosion products. It is natural to assume that in some region of shock wave formation the pressure amplitude at the shock front in the two-phase medium will also be greater than in a gas.

5.3.1 Experimental study

To find the nature of the relaxation interaction between the phases and to obtain quantitative estimates of shock attenuation in the formation region for the shock waves generated by solid explosives, we have studied experimentally both the velocity field of shock waves (see Fig. 5.7) and the pressure at front (see Fig. 5.8) in an air foam with a mass concentration of liquid of 10–15 kg/m³. The experimental results for air from Refs. [6, 7, 10, 23, 24, 130] are also represented in Fig. 5.7 and Fig. 5.8.

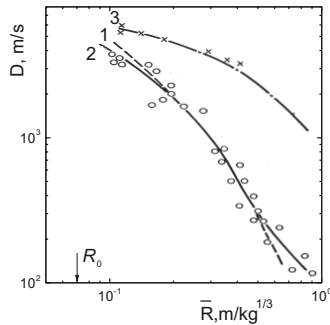


Figure 5.7: The velocity of the wave front D as a function of the reduced distance $\bar{R} = r_f/Q^{1/3}$. Curve (1) is the calculated curve; (2) — experiment in foam; (3) — experiment in air. R_0 is radius of explosive charge.

The experiments were conducted with spherical explosive charges having a bulk mass of 0.5–2.8 kg ($E_0 = 5.4$ MJ/kg) and using electrical contact probes. Figure 5.7 shows the observed variation of the shock velocity with the reduced radius $\bar{R} = r_f/Q^{1/3}$ (Q is mass of explosive charge) in foam and in air [6]. It can be seen that at closer distances from the charge, there is a sharp reduction in the differences between the shock velocities in the foam and gas.

For $R > 0.4$ m/kg^{1/3} where the direct measurements of the pressure were performed (a continuous curve in Fig. 5.8) with charges having a mass of 0.5–2.8 kg the difference between the measured values of the pressure and those calculated from the velocity lies within the measurement error of 20–30%. Hence, analysis of the experimental data indicates that the relationship between the Mach number and the ratio of the maximum pressure in a shock wave p_f to the initial pressure p_0 is

$$\frac{p_f}{p_0} \simeq M^2. \quad (5.3.1)$$

Here $M = D/c_0$ is the Mach number, and $c_0^2 = \Gamma_0 \frac{p_0}{\rho_0(1 - \varepsilon_0)}$ is the equilibrium sound velocity in foam. In the zone nearest to the explosion charge the pressure ratio at the wave front is close to the ratio for kinematic equilibrium between the phases. Thus, we

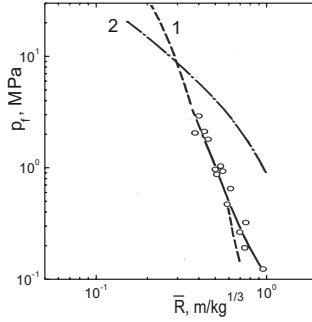


Figure 5.8: The pressure on the wave front p_f as a function of the reduced distance $\bar{R} = r_f/Q^{1/3}$. Solid curve is experiment in foam. Curve (1) is the calculated curve; (2) — experiment in air.

may assume with this accuracy that the kinematic interphase equilibrium exists in the shock front. The curve 1 of Fig. 5.8 represents the pressure field of a point explosion in foam taking the thermal relaxation into account. As can be seen in Fig. 5.8, when $R \approx 0.3 \text{ m/kg}^{1/3}$ the pressure in a foam becomes comparable to the pressure at a shock front in air and sharply increases as the charge is approached, whereas at the boundary of charge, judging from the shock velocity, the pressure must be $p = 500 \text{ MPa}$. These data agree with the predictions of the initial parameters of a shock wave at the interface explosion products of RDX-foam. From the analysis of shock adiabat for foam at $\sigma = 15 \text{ kg/m}^3$ and isentrope of the expansion of the RDX explosion products for $D = 6000 \text{ m/s}$ and $p = 500 \text{ MPa}$, the parameters of the wave weakly depend upon a degree of the completion of thermal relaxation between the phases. Thus, the attenuation does not occur near the explosive charge and furthermore in this zone the shock wave parameters in foam can be larger than those in air. This fact must be taken into account when using a foam as a damping medium.

It is important that there are the abrupt reductions of the wave parameters both for pressure

$$p \sim R^{-s_p}, \quad s_p = -\frac{d \ln p}{d \ln R} = 4 \quad (5.3.2)$$

and for propagation velocity

$$D \sim R^{-s_D}, \quad s_D = -\frac{d \ln D}{d \ln R} = 2 \quad (5.3.3)$$

in foam with distance. Note that for nonrelaxation medium these exponents can not exceed the values $s_p = 3$ and $s_D = 3/2$.

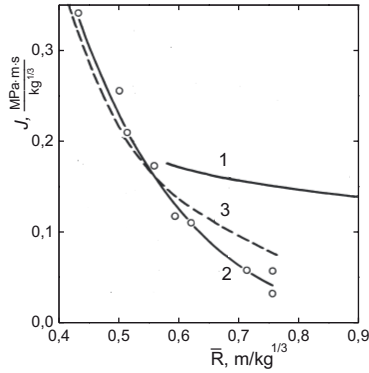


Figure 5.9: The reduced impulse of the pressure J as a function of the reduced distance $\bar{R} = r_f/Q^{1/3}$. Curve (1) is experiment in air; (2) — experiment in foam; (3) — the calculated curve.

The experimental dependencies of the reduced impulse of the pressure J (5.2.4) on the reduced distance \bar{R} are shown in Fig. 5.9. At distance, where we have carried out the experimental study, there is a monotone reduction of the impulse. The comparison with experimental data in air (curve 1 in Fig. 5.9) points up the different dependencies of impulse of the pressure in these media. The dependence observed in air [6, 7] relates to the shock wave formation. Simultaneously, the monotone dependence of the impulse in foam points up the more near formation of the shock wave to the explosive charge. The experimental results confirm that the gas-liquid foam is one of media in which the relaxation phenomena are more pronounced usually.

The abrupt attenuation of the wave observed in foam in comparison with attenuation in gas is associated with the processes of heat exchange between liquid and gas. In this case the increase of attenuation of the shock wave parameters, depending on a distance, enables us to make the conclusion that the thermal relaxation occurs more slowly than the kinematic equilibrium is established between phases.

5.3.2 The comparison of the calculation with experiment

The correlation between the experimental results for the wave velocity D and the pressure at front p_f , as we have already noted, points up that with accuracy of experimental error the relationship (5.3.1) takes place. In order to the relationship (5.3.1) be valid, it is important to reach the kinematic equilibrium in contrast to the thermal equilibrium. Indeed, $c_0^2 = \Gamma_0 \frac{p_0}{\rho_0(1 - \varepsilon_0)}$ is slightly dependent on the exchange of Γ_0 for γ , i.e. on the completeness of thermal relaxation, while this value c_0 essentially depends on the density of a medium. Hence, to satisfy the relationship (5.3.1) it is sufficient to reach the kinematic (without thermal) equilibrium between phases. Thus, if the relationship (5.3.1) is true, then we can believe that velocities of the two phases are equal. It means that the profile of wave behind the shock front is determined by

other interphase processes. These above-mentioned arguments enable us to apply the one-velocity model for describing the relaxation effects.

The results of Ref. [51] confirm the suggested approach. It is noted [51] that in dusty gas at initial time instant the particles lag from the gas. However, henceforth the gas flow involves the particles and the velocity of particles increases. Furthermore, the geometrical divergence of gas flow provides the decrease of its velocity and as a result the particles velocity can exceed the gas velocity. The particles involved by flow move to the shock front, whereas their velocity becomes sufficient to sustain the shock wave.

The process of formation and propagation of a shock wave generated by chemical explosion can be imagined as follows. At explosion of a charge the explosive products with high pressure transmit gradually the energy to the surrounding medium. Since the shock wave velocity is lower in two-component medium (the foam) than in gas, the transfer of energy from explosive products to a foam occurs more fast than to a gas possessing lesser density. Thus, the shock wave in foam should be formed nearer to a charge than the shock wave in gas. Here, we point out once again that the formation of the shock wave in near zone to a charge in foam confirms by the experiments on the pressure impulse in foam and air (see Fig. 5.9). On the basis of the experimental results, we can claim that in zone, where the direct measurements of pressure and impulse have been performed, the shock wave had already been formed.

After the formation of shock wave, the mechanism which energetically supports the wave perturbation is likely to be caused by both the pressure of a gas phase and the kinetic energy of a condensed phase. This last process is considered to lead to the equalization of velocities between phases in flow behind the shock front.

The more near formation of the shock wave to the explosive charge enables us to use the assumption on the kinematic equilibrium, and, thus, to estimate the pressure through the Mach number in zone, where the direct measurements of pressure have not been performed (dashed line 1 in Fig. 5.8). The estimations point that here pressure in foam exceeds the pressure in air.

In flow behind front, where the kinematic equilibrium is considered to take place, the relaxation effects concern with other interphase interactions such as heat exchange, radiation, partial mass exchange between phases, etc. Such internal processes evidently lead to the loss of energy determining the pressure of medium. The process of thermal relaxation is slow in a comparison with the time to attain a maximal pressure at wave front. The effect from the energy transfer caused by above-mentioned processes in flow behind shock front is not immediately manifested in front parameters of wave. The hydrodynamic laws constitute the transmission of information on the loss of heat in gas phase from the deepness of flow to the shock front. Consequently, in order to describe the propagation of shock wave, it is necessary to solve the time-dependent hydrodynamic equations. The simulation of propagation of the shock waves generated by point explosive charge has been carried out in Secs. 5.1, 5.2.

Now we compare computer calculation with experimental results on the propagation of shock waves in the foam possessing the relaxation effects. The assumption on the ideal energy source (i.e., the point charge and the instantaneous energy release) does not allow us to compare directly numerical data with experimental results where waves have been generated by the real chemical explosion. For example, the comparison

of the pressure in air from point charge and real one shows that at distances where the dependence $p \sim R^{-3}$ is valid, the energy equivalent of point charge accounts for 60% of energy of a real charge [24]. Hence, it is necessary (i) whether to define the energy equivalent of point charge, (ii) or to compare the relative values, i.e. the values of variables in flow in the relaxing medium related to the appropriate values in the nonrelaxation medium. In the second case it is naturally to compare the experimental and numerical values of wave parameters in the foam and in the medium which is described by the state equation for ideal gas without relaxation processes. First of all, such a medium can be a gas. For instance, the known results on the explosion in air can be attracted [6, 7, 10, 23]. The energy part of real source forming directly the shock wave (energy of point source) is estimated from a comparison of the calculated value $p_f l^3$ and experimental value $p \bar{R}^3$, whereas the value $p \bar{R}^3$ is to be defined in the vicinity of charge where the relaxation effects are negligible, but the shock wave has already been formed. For gas-liquid foam the energy equivalent of point charge accounts for 50-60% of energy of real source. The characteristic time for heat exchange between the gas and liquid in foam can be estimated by determining the parameter s_p (5.3.2) from the curve slope for dependence of pressure on distance (see Fig. 5.8). For $\bar{R} = 0.5 \text{ m/kg}^{1/3}$, where the shock wave can still be regarded as strong one, we have $s_p = 4$. Given $\delta_s = 1$ for gas-water foam with mass concentrations of the condensed phase $\sigma \approx 15 \text{ kg/m}^3$ ($\gamma = 1.4$, $\Gamma_0 = 1.01 - 1.001$) and knowing the time propagation of the shock from the surface of the explosive charge to the specified distance, the equation (5.2.4) can be easily used to define the characteristic heat exchange time, which is estimated as $\tau_E = 150 - 180 \mu\text{s}$. At the calculated energy equivalent accounted for 50-60% of the real energy explosion and the characteristic time of relaxation $\tau = 150 - 180 \mu\text{s}$, the experimental and theoretical dependencies for the shock front velocity D as well as for the pressure at shock front p_f are in agreement with each other within appropriate accuracy. In Figs. 5.7, 5.8 the calculated values of mentioned variables are illustrated by dashed lines. In the vicinity of charge $\bar{R} < 0.15 \text{ m/kg}^{1/3}$, the calculated values of the wave velocity in foam exceed the measured values in air. It means that a zone of the shock wave formation in foam is smaller than in air. For the distances $\bar{R} > 0.7 \text{ m/kg}^{1/3}$, where we do not take into account the internal energy of medium (or counterpressure) in calculations, the calculated values for pressure and wave velocity are smaller than the measured values. The neglect of the counterpressure in calculation of the impulse of pressure causes the larger errors than errors in the calculated pressure and wave velocity. It is concerned with the different pressure profiles at large distances. Nevertheless, at distances, where $\Delta p \simeq p_0$, at measurement of the impulse of pressure J , the errors caused by the account of a counterpressure p_0 and a wave rarefaction are partly mutually compensated. As a result at the distances, where we have performed the direct measurements of the impulse of pressure, we observe the agreement between the calculated and measured values for the impulse of pressure (see Fig. 5.9).

Apart from the comparison of absolute values, we have compared the relative values related to the appropriate values in air. It is interesting to compare the change in pressure for a transient wave in relaxing medium (foam) and in nonrelaxation one (for example, in air). Such a value can be the pressure attenuation coefficient. As usually, by definition the pressure attenuation coefficient is the ratio of the pressure in nonrelaxation medium to the pressure in relaxing medium at a fixed distance.

Since the pressure attenuation coefficient under conditions of the kinematic equilibrium between phases depends only on the heat transfer between phases, then it becomes possible to deduce the trend of thermal relaxation in a two-phase medium, without distortion, from experimental data on attenuation of shock waves. In order to establish the model kinetics here, it is appropriate to compare the experimental curves of shock wave attenuation in foam and in medium describable in terms of the state equation for gas without relaxation properties. Since such a medium can, specifically, serve gas, then the available data on explosion in air [6, 7] can be used for this purpose.

From these experimental data one calculates the pressure attenuation coefficient as the ratio of pressure in air to pressure in foam at the fixed dimensionless distance. It must be taken into consideration that in the zone where the energy source cannot be regarded as a point source, the pressure attenuation coefficient K is lower than coefficient calculated theoretically. Indeed, in denser medium (foam) the shock wave begins to "disregard" the nonideality of the energy source nearer to it than in air [6, 7]. The pressure at the front of shock wave attributable to nonideality of the energy source within the zone of shock wave formation should be higher in foam than in air.

To predict the shock wave attenuation in foam on the basis of the suggested model, one needs to have an experimental point as reference, inasmuch as the parameter τ_E is involved. In this study the value $\bar{R} = 0.4 \text{ m/kg}^{1/3}$ was used as the reference point for calculations. A better agreement between the pressure attenuation coefficient calculated from the experimental results (see Fig. 5.8) and estimated theoretically is observed for $\tau_E = 150 - 180 \mu\text{s}$ and the energy equivalent accounted for 50-60% of the energy explosion (see Fig. 5.10).

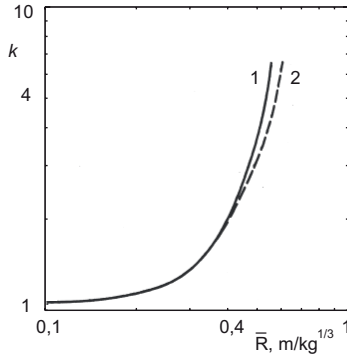


Figure 5.10: Pressure attenuation coefficient for a blast wave in foam. The estimated values are represented by curve (1); the experimental values — by curve (2).

Figure 5.10 depicts the dependence of the pressure attenuation coefficient on the reduced distance $\bar{R} = r_f/Q^{1/3}$, according to experiment (dash line) and according to theory (solid line). A comparison of these curves indicates that it is possible to describe the trend of shock wave attenuation in a two-phase medium with $\Gamma_0 \approx 1$ and to evaluate the parameters of a shock wave during the strong stage of the explosion by means of the suggested model. The disregard of the counterpressure results, as was to be expected,

in an overestimation of the pressure attenuation coefficient at $\bar{R} > 0.6 \text{ m/kg}^{1/3}$.

The represented analysis showed that thermal relaxation significantly changes the flow parameters and increases the attenuation of strong shock waves in two-phase media. The dependence of the shock attenuation coefficient on the inner heat-exchange processes in medium has been demonstrated. It has been found that the parameters of shock waves in foam are enhanced in comparison with the parameters in gas near a nonpoint energy source because of the conditions under which energy is transferred from the source to the medium.

Since the thermal relaxation times obtained by two independent methods correlate, it appears that an adequate description of the relaxation processes in foam is possible within the framework of the suggested theory. The results of experimental and theoretical investigations of the relaxation phenomena which accompany the propagation of shock waves in foam indicate that within the scope of relaxation hydrodynamics it is possible to explain the observed phenomena and estimate the efficiency of medium as localizer of the shock wave action.

5.4 Estimation of fracture area in rock under blast

The problem of increasing discharge of a productive well is closely connected with the increase of filtering properties in the rock surrounding the productive well. The crack exerts an influence on the physical mechanical rock properties, in particular, the gas and/or oil permeability of rock. As the permeability in the near-well zone of the productive strata rises, the producing well discharge increases. However, at exploitation of the productive well, the different deposits are accumulated in filtering channels of medium. The well discharge and the coefficient of carbohydrate extraction from the medium are decreased. It is known that chemical acids, surface-active substances, solvents, different thermal processing, etc are widely applied for intensifying the stratum permeability [13]. One of a perspective method is the method of controlled change in mechanical properties of rocks using a powerful impulse action, in particular, the energy of an explosion [98].

At the present time, there is a number of mathematical models, in the frameworks of which the action of explosion on rocks and crack formation are described [125, 126]. The Rodionov's zoned model is the most adequate one, since it takes into account both the rock properties and the features of fracture [125, 126]. For real conditions, the theoretical description of crack formation under explosion is a sufficiently complicated problem. This is associated with the fact that rock is inhomogeneous, and the blast loading is the highly intensive nonlinear actions causing the irreversible processes within the medium. Based on the solution of system of differential equations with the postulated state equation, the wave field can be determined only for certain model media [14, 78, 91]. For real media, it is impossible to calculate the parameters of nonlinear wave fields and the change in the physical mechanical properties in each case.

In this section, the method for estimating the region of crack formation under the action of intensive wave loading is suggested [176]. To describe the rock fracture in propagating blast wave, we select the energy criterion. In model the change of a wave spectrum is considered, where the geometrical divergence of a wave and the irreversible losses in the medium take into account. The investigations confirm the

functional dependence of fracture area on the explosion energy. Moreover, the obtained analytical relations enables us to indicate the blast wave characteristics which affect the fracture process as well as to lay the theoretical foundations for estimating the blast wave properties by means of the known fracture area.

5.4.1 Model of wave disturbance attenuation

During propagation in the medium with complex internal exchange processes, the wave attenuates. This attenuation is governed not only by its geometrical divergence, but also by irreversible losses of energy, in particular, spent for crack formation. Physically, the functional independence of the first and second processes is possible only in acoustical approximation. In general case, as the cracks form, the loading is such that the waves are nonlinear, hence, these two processes are dependent. Therefore, we restrict ourselves only to the estimation of the shattering area, and for mathematical description of wave field, we assume that these two processes are functionally independent.

We suppose that for one-dimensional motion in medium without energy losses, the dependence of the blast wave front pressure p_f on the distance r is determined by the relation [14]

$$p_f = A \left(\frac{Q^{1/\nu}}{r} \right)^\mu, \quad (5.4.1)$$

where Q is the explosion energy; the parameter ν determines the type of symmetry: $\nu = 1, 2, 3$ are the plane, cylindrical, and spherical symmetries, respectively; μ is the constant value; constant A is the dimension factor depending on the medium properties. It is assumed that after a shock wave arrives at distance r at the moment $t = t_1$, the pressure in this space point varies with time t according to the exponential law [14].

$$p(r, t) = \theta(t - t_1) p_f(r) \exp\left(\frac{t - t_1}{\tau}\right). \quad (5.4.2)$$

Here $\theta(t)$ is Heaviside function. For convenience, we accept $t_1 = 0$ if it does not reduced uncertainty.

In wave process without energy losses in medium, the characteristic time of the wave loading action has the following functional dependence on distance r and explosive energy Q [14]

$$\tau(r, Q) = BQ^{1/\nu} \left(\frac{r}{Q^{1/\nu}} \right)^\beta, \quad (5.4.3)$$

where B is the dimension factor. Since the displacement of medium is insignificant as compared with the distance considered, we can state that relations (5.4.2) and (5.4.3) are valid for a particular medium microvolume, i.e., in the absence of energy losses the microvolume of medium has a pressure, which can be described by dependence (5.4.2). The values of the constants μ and β are interconnected. This fact can be established from the condition that the energy flow W through the closed surface (for a spherical case this value is equal to $4\pi r^2$) is independent of distance

$$r^{\nu-1} W(r) = \text{const}. \quad (5.4.4)$$

For weak nonlinear shock waves, the flow energy through the surface unite is as follows [88]

$$W(r) = \int_{t_1}^{\infty} \frac{p^2(r, t)}{\rho c} dt, \quad (5.4.5)$$

where ρ is the medium density; c is the sound velocity. With the value of $r^{\nu-1}W(r)$ required to be independent of distance, we obtain the connection between constants μ and β

$$\beta = 1 - \nu + 2\mu. \quad (5.4.6)$$

Note that functional dependence (5.4.3) is known for water [14, 31]. At the same time, for geophysical medium, the empirical relationship (the spherical case) is used

$$\tau = aQ^{1/3} + br. \quad (5.4.7)$$

The coefficients a and b are defined from the experimental data [14, 91, 98]. The calculation of time of the shock wave action τ by the two formulas (5.4.3) and (5.4.7) showed that these values are close for $r \leq 20r_0$, where r_0 is explosive charge radius. We note once again, that from the physical point of view, the functional dependence (5.4.3) is more preferable.

Relations (5.4.2) and (5.4.3) are obtained for blast wave without energy absorption by the medium, i.e., at condition (5.4.4). In general case, under intensive wave loads which are the blast waves, the irreversible nonequilibrium processes occur in the medium and lead to the additional wave attenuation. The experimental investigations indicate that the high-frequency disturbances attenuate faster than the low-frequency ones. We use one of the most frequently applied dependences describing the change in the spectrum density of pulse loading [103]

$$S(r, \omega) = S_0(\omega) \exp(-\alpha|\omega|r). \quad (5.4.8)$$

Physically, this relationship implies that the monochromatic wave with the frequency ω attenuates exponentially. In this case, the energy is absorbed by the medium and not redistributed between different frequencies in wave. Usually the spectrum density of the wave disturbance is determined by Fourier transformation; for (5.4.2) it has the form

$$S_0(\omega) = F[p(t)](\omega) = \int_{-\infty}^{\infty} \theta(t) p(t) \exp(i\omega t) dt = \frac{pf}{\tau^{-1} - i\omega}. \quad (5.4.9)$$

The inverse Fourier-transformation $F^{-1}[S(\omega)](t)$ defines the dependence of pressure in the medium $p(r, t)$ on distance and time. The spectral representation of the wave perturbation allows one to analyze the time evolution of the wave and its distance dependence, arising from the geometrical divergence of the wave (5.4.9) and the irreversible losses to the medium (5.4.8).

5.4.2 Energy criterion of crack formation

For estimation of rock shattering in propagating blast wave, the energy criterion is selected [176]: the crack formation occurs until the energy absorbed by the medium exceeds a certain limiting value. In order to determine the energy remained in the medium after the propagation of blast wave, we calculate first the total energy flow through the unit surface by formula (5.4.5)

$$W(r) = \frac{1}{\rho c} \int_0^\infty p^2(r, t) dt = \frac{p_f^2}{\pi \rho c} \int_0^\infty \frac{\exp(-2\alpha\omega r)}{\omega^2 + \tau^{-2}} d\omega. \quad (5.4.10)$$

This relationship follows from Parseval theorem [74].

The value of the integral

$$I(r, \omega) = \int_0^\infty \frac{\exp(-2\alpha\omega r)}{\omega^2 + \tau^{-2}} d\omega \quad (5.4.11)$$

can be expressed through the special functions. However, such notation is ponderous and uninformative. The approximation, where integral (5.4.11) is estimated by the saddle point method, is more effective. This integral (5.4.11) can be reduced to the following functional dependence on r and τ

$$I = e^{-1} \sqrt{2\pi} \tau \arctan(\tau/2\alpha r). \quad (5.4.12)$$

Indeed, integral (5.4.11) can be rewritten down in a form convenient for applying the saddle point method

$$\begin{aligned} I &= \int_0^\infty d\omega \frac{\exp(-2\alpha\omega r)}{\omega^2 + \tau^{-2}} = \tau \arctan(\tau\omega) \exp(-2\alpha\omega r) \Big|_0^\infty \\ &+ 2\alpha r \tau \int_0^\infty d\omega \arctan(\tau\omega) \exp(-2\alpha\omega r) \\ &= \tau \int_0^\infty d\omega \frac{\arctan(\tau\omega)}{\omega} \exp(-2\alpha\omega r + \ln(2\alpha r\omega)). \end{aligned}$$

At the point $\omega_1 = (2\alpha r)^{-1}$, the exponential function has the maximum. In the vicinity of this point, the required integral receives basic contribution, and according to the saddle point method, it is following

$$\begin{aligned} I &\approx 2\alpha r \tau \arctan(\tau\omega) \int_{-\infty}^\infty d\omega \exp(-1 - 2\alpha^2 r^2 (\omega - \omega_1)^2) \\ &= \frac{\sqrt{2\pi}}{e} \tau \arctan \frac{\tau}{2\alpha r}. \end{aligned}$$

The numerical calculations show that the deviation of the exact value of integral (5.4.11) from approximate value (5.4.12) does not exceed 8%. It is important, that as result we have the analytical dependence of the integral I on τ and r (5.4.12).

Consequently, the whole energy flow passing through the surface $\sigma(\nu) r^{\nu-1}$ equals

$$G(r) \equiv \sigma(\nu) r^{\nu-1} W(r) = \sigma(\nu) D \frac{Q}{\rho c} \arctan \frac{\tau(r, Q)}{2\alpha r}, \quad (5.4.13)$$

$$\sigma(\nu) = 2\pi(\nu - 1) + (\nu - 2)(\nu - 3), \quad D = e\sqrt{2/\pi} A^2 B.$$

Using (5.4.13), we can estimate the energy remained in the medium layer $\sigma(\nu) r^{\nu-1} dr$ after the propagation of the blast wave

$$G(r) - G(r + dr) = -\sigma(\nu) \frac{dr^{\nu-1} W(r)}{dr} dr.$$

According to the accepted fracture criterion, the crack formation takes place if the k -share of the energy exceeds a certain admissible value. If the maximum admissible energy of crack formation per unite volume is denoted as γ_ν , when the crack formation criterion has a form

$$-k\sigma(\nu) \frac{dr^{\nu-1} W(r)}{dr} \geq \sigma(\nu) r^{\nu-1} \gamma_\nu. \quad (5.4.14)$$

Note that in general case, the specific energy γ_ν of fracture depends on symmetry of a shock wave ν , because the fracture mechanism can vary for these cases. For example, the tangential stresses, which are considerable in rock fracture under the action of the cylindrical or spherical waves, are absent in the plane case.

We proceed to the investigation of the coefficient k . As mentioned above, it has the following sense. The k -share of the blast wave energy absorbed by the medium is spent for crack formation. It is evident that in fracture area, the value of k can be dependent on distance. We can regard that with the certain accuracy the energy γ_ν is to be the same for different Q on the boundary of crack formation region. Therefore, on these boundaries the values of k are assumed to coincide at different Q .

Substituting (5.4.13) into (5.4.14), we derive the equation connecting Q and the size of fracture area r_b

$$\frac{Q^{2-\frac{2}{\nu}} r_b^{2(1+\mu-\nu)}}{(2\alpha r_b)^2 + \tau^2(r_b, Q)} = \frac{\gamma_\nu}{H}, \quad H = k2e^{-1} \sqrt{2/\pi} (1 - \beta) \frac{\alpha A^2 B^2}{\rho c}. \quad (5.4.15)$$

By forward substitution, the solution of this equation takes the form

$$r_b = RQ^{1/\nu}, \quad (5.4.16)$$

where, as follows from (5.4.15), the dimensional constant R satisfies the equation

$$\frac{R^{2(1+\mu-\nu)}}{(2\alpha R)^2 + (BR^\beta)^2} = \frac{\gamma_\nu}{H}. \quad (5.4.17)$$

Thus, the obtained relations allow to confirm the following statements. Firstly, equation (5.4.16) previously established experimentally [38, 98, 103] is theoretically substantiated. Moreover, the conformity of the theoretical and experimental results indicates the correct choice of the model proposed for the physical phenomenon of crack formation in a rock. Secondly, expression (5.4.17) enables us to estimate the coefficient R through properties of medium and explosive charge. Moreover, using (5.4.17), we can consider the inverse problem and calculate the blast wave parameters, as well as the medium properties, if we know the fracture area, i.e. we can determine α , γ_ν , A , and B through the value of R .

5.4.3 Geometric similarity of the explosive fracture area

As is stated in [103], the areas of crushing and crack formation should satisfy conditions $r_b \sim Q^{1/3}$. In other words it means that there is a geometric similarity. However, there is no strong proof this statement in [103]. Indeed, the relation (5.4.1) can be scaled (i.e. it can be reduced to the dimensionless form) by the chosen value $r_0 Q^{-1/\nu}$, while the relation (5.4.3) can not be rewritten down in same scale (i.e. it can not be reduced to the dimensionless form only through value $r_0 Q^{-1/\nu}$). We can not neglect the relation (5.4.3), when we consider the physical phenomena related to the absorption of shock wave energy by the medium. Therefore arguments pointed out in [103] is insufficient to state about geometric similarity $r_b \sim Q^{1/\nu}$. Nevertheless, proceeding from the distribution in shock wave (5.4.1) – (5.4.2), (5.4.8), we came to the result (5.4.16), which directly specifies geometric similarity on the explosion energy. Thus, Mosints's statement about similarity $r_b \sim Q^{1/3}$ [103] has been received the strong mathematical substantiation.

5.4.4 Estimation of region of crack formation

Let us examine the dependence of crack formation region on the required energy for crack formation γ_ν at fixed explosion energy Q . We rewrite the relationship (5.4.17) in the dimensionless form

$$\frac{l^{1-\nu-\beta}}{l^{2(1-\beta)} + 1} = \Omega \quad (5.4.18)$$

Here, $\Omega = \gamma_\nu B^{1-\nu/(1-\beta)} \rho c / \left(2e^{-1} \sqrt{2/\pi} (1-\beta) k A^2 \alpha^{\nu/(1-\beta)} \right)$ and $l = (2\alpha/B)^{1/(1-\mu)} R$ are the dimensionless values. Figures 5.11 and 5.12 present the dependence $\Omega(l)$ at different β (or μ , see (5.4.6)) for the cylindrical ($\nu = 2$) and spherical ($\nu = 3$) cases, respectively.

Rewriting (5.4.18) as $\Omega^{-1} = l^\nu (l^{1-\beta} + l^{-(1-\beta)})$, we note that $\Omega^{-1} = l^\nu - |\beta - 1|$ at $l \ll 1$, and $\Omega^{-1} = l^{\nu+|\beta-1|}$ when $l \gg 1$. In logarithmic coordinates, they are the straight lines going through the point $l = 1, \Omega = 0.5$ (dark-colored points in Figs. 5.11, 5.12). Provided $\beta = 1$, both asymptotic forms coincide; if $\beta \neq 1$, the curves are convex upwards. Pay attention to the fact that with $|\beta_1 - 1| = |\beta_2 - 1|$, the curves coincide for any pair of μ_1, μ_2 satisfying the relationship $\mu_1 + \mu_2 = \nu$. It is obvious from Fig. 5.11 that curve 3 corresponds both to $\mu = 0.5$ and $\mu = 1.5$. The same is observed in Fig. 5.12, namely, curve 3 corresponds simultaneously to the values $\mu = 1$ and $\mu = 2$.

In the different domains $\Omega > 1$ and $\Omega < 1$, the same relative energy change required for rock fracture leads to the various changes in size of the fracture area. For example, the decrease of Ω in the domain $\Omega > 1$ by a factor of 2 causes more considerable increase in the fracture area as compared with the same decrease of Ω in $\Omega < 1$.

It is necessary to note that in real physical process the values l and Ω are close to $l = 1, \Omega = 0.5$. For example, for explosion in a granite, the values $2\alpha r_b$ and $\tau(r_b, Q)$ exactly coincide, i.e. $l = 1$. This implies that the physics of process is determined simultaneously both by characteristic time of action of shock wave τ on microvolume and by characteristic time of wave attenuation $2\alpha r$ at the distance. When $l \ll 1$, the process of crack formation is determined by τ , while at $l \gg 1$ the most important feature is the degree of the blast wave attenuation on distance.

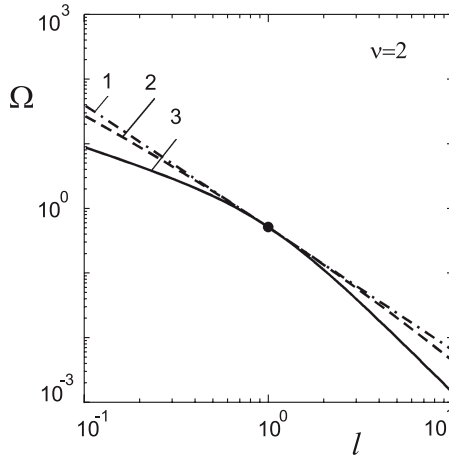


Figure 5.11: Dependence $\Omega(l)$ for $\nu = 2$: 1 — $\beta = 1$; 2 — $\beta = 1 \pm 0.44$; and 3 — $\beta = 1 \pm 1$.

5.4.5 Comparison with the experiment

Theoretical dependence (5.4.16) of the crack formation region size on the explosive energy contains only one unknown parameter R . Thus, to find R and the dependence $r_b = r_b(Q)$, it is sufficient to carry out only one experiment on explosion in the studied medium; in the experiment, for assigned Q , the size r_b of the fractured region is obtained. The comparison of the experimental results [97, 103] and (5.4.16) is shown in Fig. 5.13. To calculate R , we specified a fiducial point whose values for granite and limestone are presented in Table 5.3.

In logarithmic coordinates, the dependence (5.4.16) represents a straight line passing through a fiducial point. The fiducial points are darkened in Fig. 5.13.

In Table 5.3 the blast wave parameters are presented for TNT for two media: granite and limestone. The dimension factor B is established from the condition of coincidence of the values τ calculated by (5.4.3) and (5.4.7) at a distance equal to the charge radius. In (5.4.1), the dimensional constant A is connected with A' from Table 5.3 by the relation $A' = A \left(Q_0^{1/3} / r_0 \right)^\mu$, where $Q_0 = 1$ kg, $r_0 = 0.054$ m.

In fact, relation (5.4.16) is not a new result. However, the coincidence of the theoretical dependence $r_b Q^{1/3}$ and the experimental data indicates that the assumptions in the model are admissible. In this case, value R functionally depends on ρ , c , α , μ , A , B , γ_ν (but without Q), i.e., on the properties of the medium only. Using (5.4.17), we can solve both the direct problem, in which the value R is defined through values mentioned above and the inverse problem, in which the value γ_ν (or another value from the listed ones) is defined through the known value R .

In inverse problem, the energy density γ_ν/k is estimated. This is energy that is absorbed by the medium near the boundary of crack formation region. The ratio γ_ν/k

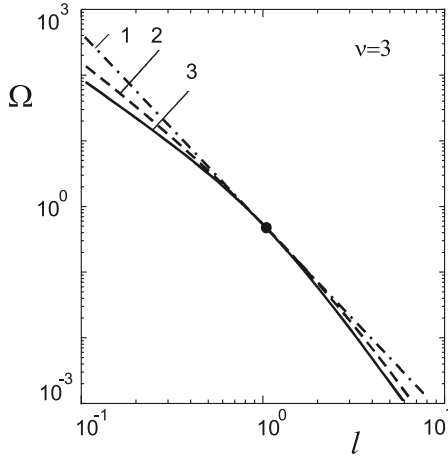


Figure 5.12: Dependence $\Omega(l)$ for $\nu = 3$: 1 — $\beta = 1$; 2 — $\beta = 1 \pm 0.74$; and 3 — $\beta = 1 \pm 1$.

Table 5.3: Parameters for Eqs. (5.4.15)–(5.4.17)

medium	properties			blast wave				fiducial point		calculation	
	ρ kg/m ³	c m/s	$\alpha \cdot 10^5$ m/s	μ	$A' \cdot 10^{-8}$ Pa	$a \cdot 10^5$ s/kg ^{1/3}	$b \cdot 10^4$ s/m	Q kg	r_b m	R m/kg ^{1/3}	γ_ν J/m ³
granite	2600	5720	2	1.13	1.09	3.6	0.18	1	2.4	2.4	0.67
limestone	2580	4650	6	1.13	0.30	4.1	4.69	1	2.0	2.0	0.19

obtained from (5.4.17) is presented in Table 5.3.

At the same time, the direct problem, in which R is calculated through the energy γ_ν , allow to use additional theoretical and experimental results which are not pertinent directly to explosion. In this case, apart from the well-known values ρ, c, μ, A, B and α [38] (Table 5.3), it is required to know γ_ν and k or γ_ν/k . Knowing γ_ν and k , we can estimate R by (5.4.16) without carrying out an experiment. Currently, the problem on finding the values of γ_ν and k from the other theoretical and experimental data remains unsolved.

The model of crack formation under the action of blast wave is developed [176]. In this model the change in the wave loading, which is governed by both geometric divergence of wave and irreversible losses in the medium, is considered. The energy criterion was selected for fracture of rock. The geometric similarity of fracture area caused by the explosion energy is proved. The accordance of the theoretical and experimental results indicates the correct choice of the basic assumptions for the suggested model of crack formation in rock. On the basis of the assigned properties of the medium and

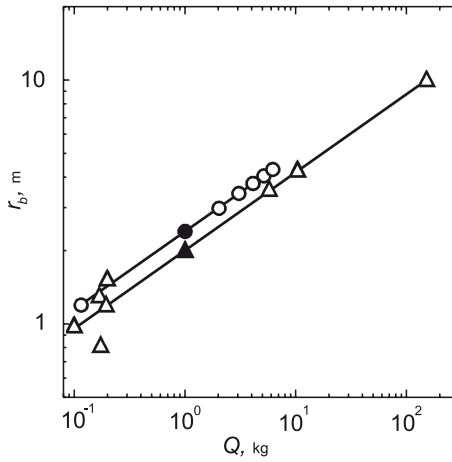


Figure 5.13: Size of crack formation region as explosion energy function (theoretical results — straight lines; experiment: \circ — granite, \triangle — limestone).

explosion, the analytical dependences enable one, on the one hand, to estimate the crack formation area (the direct problem) as well as, on the other hand, to lay the foundation for determining the blast wave parameters and the medium properties by the known fracture area (the inverse problem).

Chapter 6

Diagnostics of medium by long nonlinear waves

In chapter 2 we proved that the long wave with finite amplitude responds to the structure of medium. At the same time, a question appears, namely, is there a sufficient information in the wave field to reconstruct the structure of medium? It turns out that the knowledge on the evolution of nonlinear waves enables one to define with certain accuracy the concentrations of medium components.

6.1 The increase of nonlinearity in medium with structure

In this section we shall prove the statement that the structure of medium always exalts the nonlinear effects under the propagation of long waves. At first, let us consider the sound velocity in homogeneous c_{hom} and heterogeneous c_{eff} media. Now we will show that in the general case with pressure increase the velocity of the sound becomes greater in a structured medium than in a homogeneous one

$$c_{\text{eff}} \geq c_{\text{hom}}. \quad (6.1.1)$$

For the sake of clarity, we consider a medium in which the sound velocities of individual components are independent of the pressure

$$c \neq f(p), \quad dc/dp = 0. \quad (6.1.2)$$

The equality sign is fulfilled (a) for an initial pressure, by virtue of the normalization, and also (b) for a special structured medium in which the relation $V(\xi)/c^2(\xi)$ is not a function on the fast variable ξ . We must prove which case results in an equality and which gives the inequality.

Let us write the relations (6.1.2) for homogeneous medium consisting only one component

$$c_{\text{hom}} \neq f(p), \quad dc_{\text{hom}}/dp = 0. \quad (6.1.3)$$

For multicomponent medium the derivative dc_{eff}/dp is defined from relationship

$$\frac{dc_{\text{eff}}}{dp} = \frac{2\langle V \rangle}{\langle V^2/c^2 \rangle} \left(\langle V \rangle \left\langle \frac{V^3}{c^4} \right\rangle - \left\langle \frac{V^2}{c^2} \right\rangle^2 \right) \geq 0. \quad (6.1.4)$$

This last inequality follows from the well-known Cauchy-Schwarz inequality (see, for instance, [77]). Therefore, with the increase of pressure, the sound velocity c_{eff} increases. Consequently, we have the inequality (6.1.1) at $p \geq p_0$.

Moreover, at $p > p_0$ the shock adiabatic curve for the medium with a structure always lies above that for the homogeneous medium (they touch only at the initial point $p = p_0$)

$$\frac{d^2p}{d\langle V \rangle^2} \geq \left(\frac{d^2p}{dV^2} \right)_{\text{hom}}. \quad (6.1.5)$$

Indeed, a ratio of these derivatives is equal to

$$\begin{aligned} \frac{d^2p}{d\langle V \rangle^2} / \left(\frac{d^2p}{dV^2} \right)_{\text{hom}} &= \frac{\langle V^3/c^4 \rangle \langle V^2/c^2 \rangle^{-3}}{c_{\text{hom}}^2 \langle V \rangle^3} \\ &= \frac{\langle V^3/c^4 \rangle \langle V \rangle c_{\text{eff}}^2}{c_{\text{hom}}^2 \langle V^2/c^2 \rangle^2} \geq \frac{\langle V^3/c^4 \rangle \langle V \rangle}{\langle V^2/c^2 \rangle^2} \geq 1. \end{aligned}$$

Hence, a long wave with a finite amplitude responds to the structure of the medium, and the nonlinear effects increase as compared with those in the homogeneous medium. The nonlinearity takes place even if individual components are described by the linear evolution equation (i.e. at condition (6.1.2)).

The exception, as it was noted already, is a medium with the properties of structure $V(\xi)/c^2(\xi) \neq f(\xi)$. For this medium only the equality sign is correct in the inequalities (6.1.1) and (6.1.5). Particular elements of the structure respond to the pressure variations, but the relative structure does not change, i.e. the ratio $V(\xi, p)/V(\xi, p_0)$ does not depend on ξ . In this case, the value $c_{\text{eff}} = \sqrt{\langle c^2 \rangle}$ is an averaged characteristic (see Eq. (2.4.5)). Therefore, the system of equations may be presented using the averaged variables $p, u, \langle V \rangle, c_{\text{eff}} = \sqrt{\langle c^2 \rangle}$. Heterogeneity does not introduce an additional nonlinearity for this medium, and the structure of medium does not affect the wave motion.

In addition to the analysis of the sound velocity in homogeneous and heterogeneous media, we consider now the evolution equations with nonlinear term and compare the coefficients of nonlinearity in these media. Let us derive the evolution equation with a weak nonlinearity. First of all, we have to note that the mass velocity u is related to the pressure p by means of [172]

$$u = \int_{p_0}^p \sqrt{\langle V^2/c^2 \rangle} dp. \quad (6.1.6)$$

A functional dependence of an average specific value on the pressure increment $p' = p - p_0$ with the accuracy $O(p'^2)$ can be presented as a series

$$\langle V \rangle(p) = \langle V \rangle_0 + \left. \frac{d\langle V \rangle}{dp} \right|_{p=p_0} p' + \frac{1}{2} \left. \frac{d^2\langle V \rangle}{dp^2} \right|_{p=p_0} p'^2.$$

In this case the system of equations (2.3.6) for planar symmetry $\nu = 1$ can be written as

$$\langle V \rangle_0 \frac{\partial u}{\partial x} + \left\langle \frac{V^2}{c^2} \right\rangle_0 \frac{\partial p'}{\partial t} - \frac{1}{2} \frac{d^2 \langle V \rangle}{dp^2} \Big|_{p=p_0} \frac{\partial p'^2}{\partial t} = 0,$$

$$\frac{\partial u}{\partial t} + \langle V \rangle_0 \frac{\partial p'}{\partial x} = 0.$$

The relationship $u \frac{\partial p'}{\partial x} = p' \frac{\partial u}{\partial x}$ follows from Eq. (6.1.6) with the assumed accuracy $O(p'^2)$ and was used for derivation of the first equation. The evolution equation for one variable assumes the form

$$\langle V \rangle_0^2 \frac{\partial^2 p'}{\partial x^2} - \left\langle \frac{V^2}{c^2} \right\rangle_0 \frac{\partial^2 p'}{\partial t^2} + \frac{1}{2} \frac{d^2 \langle V \rangle}{dp^2} \Big|_{p=p_0} \frac{\partial^2 p'^2}{\partial t^2} = 0. \quad (6.1.7)$$

Now let us consider the waves propagating in one direction, then with the indicated accuracy we can write (hereinafter index 0 is omitted)

$$-\frac{\sqrt{\langle V^2/c^2 \rangle}}{\langle V \rangle} \frac{\partial}{\partial t} + \frac{\partial}{\partial x} \rightarrow 2 \frac{\partial}{\partial x}$$

(see, for example, Section 93 in Ref. [88]). Thus, after factorization of Eq. (6.1.7) we get

$$\frac{\partial p'}{\partial t} + c_{\text{eff}} \frac{\partial p'}{\partial x} + \frac{1}{2} \langle V \rangle \left\langle \frac{V^2}{c^2} \right\rangle^{-3/2} \frac{d^2 \langle V \rangle}{dp^2} p' \frac{\partial p'}{\partial x} = 0. \quad (6.1.8)$$

The coefficient of nonlinearity α_p for the structured medium, when the sound velocities in the individual components are independent of the pressure $c \neq f(p)$, can be presented as

$$\alpha_p \equiv \frac{1}{2} \langle V \rangle \left\langle \frac{V^2}{c^2} \right\rangle^{-3/2} \frac{d^2 \langle V \rangle}{dp^2} = \frac{d(u + c_{\text{eff}})}{dp} = \langle V \rangle \left\langle \frac{V^3}{c^4} \right\rangle \left\langle \frac{V^2}{c^2} \right\rangle^{-3/2}.$$

For all cases we take $\alpha_p > 0$. For a homogeneous medium with $dc/dp = 0$ we have $\alpha_{p \text{ hom}} = V/c$.

In certain media the value V/c^2 does not change within the period. The individual elements of the structure respond to the pressure variations so that a relative structure does not change, i.e. the ratio $V(\xi, p)/V(\xi, p_0)$ does not depend on ξ . In this case, the value $c_{\text{eff}} = \sqrt{\langle c^2 \rangle}$ derived from Eq. (2.4.5) is the averaged characteristic. Consequently, the system of equations may be presented in the averaged variables p , u , $\langle V \rangle$, $c_{\text{eff}} = \sqrt{\langle c^2 \rangle}$. Heterogeneity does not introduce the additional nonlinearity for these media. Such media behave like the homogeneous media under the action of the nonlinear wave perturbations.

For media when the sound velocity is independent of the pressure ($c \neq f(p)$) it is possible to show that a heterogeneity of the medium, in the general case, introduces the additional nonlinearity. Let us consider the ratio of the nonlinearity coefficients

for heterogeneous and homogeneous media. In the space of dimensionless normalized variables this implies that at $p = p_0$ we have $\langle V \rangle_0 = 1$ as well as $\langle V^2/c^2 \rangle_0 = 1$ for the compared media.

Using the conditions (2.4.5) we can obtain

$$\frac{\alpha_p}{\alpha_{p\text{hom}}} = \langle V \rangle \left\langle \frac{V^3}{c^4} \right\rangle \left\langle \frac{V^2}{c^2} \right\rangle^{-2} \geq 1. \quad (6.1.9)$$

This inequality is the well-known Cauchy-Schwarz inequality (see formula (15.2-3) in Ref. [77]). Since $\langle V \rangle \geq 0$ and $\langle V/c^2 \rangle \geq 0$, we prove

$$\begin{aligned} \langle V \rangle \langle V^3/c^4 \rangle &\equiv \int_{-\infty}^{\infty} V d\xi \cdot \int_{-\infty}^{\infty} \frac{V^3}{c^4} d\xi = \int_{-\infty}^{\infty} \frac{V^2}{c^2} \left(\frac{V}{c^2} \right)^{-1} d\xi \cdot \int_{-\infty}^{\infty} \frac{V^2 V}{c^2 c^2} d\xi \\ &\geq \left(\int_{-\infty}^{\infty} \sqrt{\frac{V^2}{c^2} \left(\frac{V}{c^2} \right)^{-1}} \cdot \sqrt{\frac{V^2 V}{c^2 c^2}} d\xi \right)^2 \\ &= \left(\int_{-\infty}^{\infty} \frac{V^2}{c^2} d\xi \right)^2 \equiv \langle V^2/c^2 \rangle^2. \end{aligned}$$

It only remains to find the condition for equality sign in (6.1.9). For this purpose we apply the Cauchy-Schwarz inequality in vector form (see formula (15.2-5) in Ref. [77])

$$|(\vec{a}, \vec{b})|^2 \leq (\vec{a}, \vec{a})(\vec{b}, \vec{b}).$$

Whereas the equality sign is realized if and only if the vectors \vec{a} and \vec{b} are linearly dependent, i.e. $\vec{a} = k\vec{b}$ ($k = \text{const}$). By designating $(\vec{a}, \vec{a}) \equiv V/c^2$, $(\vec{b}, \vec{b}) \equiv V^2/c^2$, it is easy to notice that the equality sign is realized if and only if

$$\sqrt{\frac{V^2}{c^2} \left(\frac{V}{c^2} \right)^{-1}} \Big/ \sqrt{\frac{V^2 V}{c^2 c^2}} = \text{const.}$$

(see sections 14.2-6 in Ref. [77]), i.e. when the value $V/c^2 = \text{const}$ does not vary within the period ($V(\xi)/(c(\xi))^2 \neq f(\xi)$). This heterogeneous medium has been considered above. For all other heterogeneous media for which the value V/c^2 changes within period, the inequality is realized in Eq. (6.1.9). So, in a heterogeneous medium the value α_p is always greater than $\alpha_{p\text{hom}}$ in a homogeneous medium. Thus, it is proved that, in the general case, the heterogeneities in a medium introduce the additional nonlinearity. This effect provides the basis for a new method of diagnostics to define the properties of multicomponent media using the propagation of long nonlinear waves in such media.

6.2 Fundamentals of new diagnostic method

The structure of medium affects the wave field. There are different methods which allow the detection of gas bubbles and/or cracks in liquid [44], concrete [133] and ice cover [41] by means of the nonlinear effects.

In this section we describe our new diagnostic method for the properties of medium. The features of the motion of finite-amplitude long waves and the effect of the increase of nonlinearity in the heterogeneous medium in comparison with homogeneous medium form the basis for the development of theoretical fundamentals of the diagnostic method. In this method the properties of individual components are defined by long waves of finite amplitudes; more specifically, the dependence $V/c^2 = V/c^2(\zeta)$ on the fast Eulerian coordinate ζ (see Eq. (2.3.7)) is defined. Thus, the nonlinear wave evolution allows one to obtain the structure of the medium with an inherent accuracy. As a final result, the mass concentrations of the individual components can be found using this method.

It should be kept in mind that the period of the structure of medium is infinitely small in the longwave model, so it is not always possible to indicate reliably the location of the structure elements inside the period. Hence, the media with the different

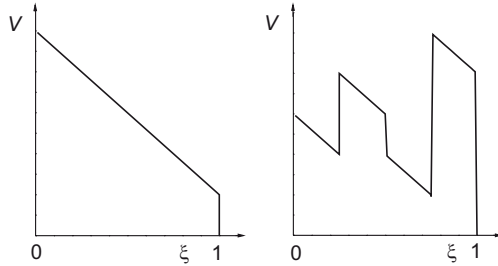


Figure 6.1: The equivalent distributions of the specific volume in elementary sell for diagnostic method.

structures plotted in Fig. 6.1, for example, affect identically on wave fields. These two media are indistinguishable in the framework of the suggested method. Taking into account this indefiniteness, we consider the function $V/c^2 = V/c^2(\zeta)$ that is to be the decreasing, integrable, mutually one-valued function on the interval $\zeta \in [0, 1]$ and equals to zero outside of this interval.

Now we represent the theoretical fundamentals for new method of diagnostics of medium by means of the long nonlinear waves. Let us prove the principal relation which enables us to obtain the inverse function $\zeta = \zeta(V/c^2)$ for the desired function $V/c^2 = V/c^2(\zeta)$ through the inverse Fourier transformation [156, 167, 169]

$$\zeta(Vc^{-2}) = F^{-1} \left[\sum_{n=0}^{\infty} \frac{\langle V(Vc^{-2})^{n+1} \rangle}{(n+1)! \langle V \rangle} i^n q^n \right] (Vc^{-2}). \quad (6.2.1)$$

It is known from theory of probability that the distribution function $f(x)$ (any one-valued, integrable, positive function) can be expressed by its central moments

$$\alpha_n = \int_{-\infty}^{\infty} x^n f(x) dx. \quad (6.2.2)$$

Indeed, by using the characteristic function

$$\chi(q) = F[f(x)](q), \quad (6.2.3)$$

any positive integrable function $f(x)$ can be written as follows

$$f(x) = F^{-1}[\chi(q)](x), \quad (6.2.4)$$

where $F[\cdot]$ is the Fourier transformation, $F^{-1}[\cdot]$ is the inverse Fourier transformation.

We take into account the important fact from the theory of probability: the characteristic function $\chi(q)$ is uniquely determined by the central moments α_n

$$\chi(q) = \sum_{n=0}^{\infty} \alpha_n i^n \frac{q^n}{n!}. \quad (6.2.5)$$

Hence, the function $f(x)$ can be found by means of the inverse Fourier transform

$$f(x) = F^{-1} \left[\sum_{n=0}^{\infty} \alpha_n i^n \frac{q^n}{n!} \right] (x), \quad (6.2.6)$$

if series $\sum_{n=0}^{\infty} |\alpha_n| (s^n/n!)$ converges absolutely for some value $s > 0$ (see Section 18.3.7 in Ref. [77]).

These facts from the theory of probability are used to prove such a statement: if $V/c^2 = V/c^2(\zeta)$ is a decreasing positive integrable function on the interval $\zeta \in [0, 1]$ and equals to zero outside of it, then the inverse function $\zeta = \zeta(V/c^2)$ for the required function $V/c^2 = V/c^2(\zeta)$ can be written as (6.2.1) in the averaged values

$$\langle V(V/c^2)^n \rangle \equiv \int_{-\infty}^{\infty} V(V/c^2)^n d\xi. \quad (6.2.7)$$

Indeed, for the monotonic one-valued function $V/c^2 = V/c^2(\zeta)$ we find the integral in (6.2.7) by integrating the inverse function $\zeta = \zeta(V/c^2)$, since the transformation Jacobian is not equal to zero. We have the chain of identifies

$$\begin{aligned} \langle V(V/c^2)^n \rangle &= \int_0^1 V(\xi) \left(\frac{V}{c^2} \right)^n d\xi = \langle V \rangle \int_0^1 V \left(\frac{V}{c^2} \right)^n \rho d\zeta \\ &= \langle V \rangle \int_{-\infty}^{\infty} \left(\frac{V}{c^2} \right)^n \frac{d\zeta}{d(V/c^2)} d(V/c^2). \end{aligned} \quad (6.2.8)$$

In the geometric sense this relation signifies that the integral (in our case it is an area between the curve $V/c^2 = V/c^2(\zeta)$ and axes $O\zeta$ and $O(V/c^2)$) can be calculated either over ζ or over V/c^2 (see Fig. 6.1). Whereas, the inequality is realized for the monotonic decreasing function $V/c^2 = V/c^2(\zeta)$.

For a function defined on a finite interval, if this function is positive and bounded above, we have

$$\begin{aligned} \langle V(V/c^2)^n \rangle &= \langle V \rangle \int_{-\infty}^{\infty} \left(\frac{V}{c^2} \right)^n \frac{d\zeta}{(dV/c^2)} d(V/c^2) \\ &= -n \langle V \rangle \int_{-\infty}^{\infty} \left(\frac{V}{c^2} \right)^{n-1} \zeta d(V/c^2). \end{aligned} \quad (6.2.9)$$

This relation provides the connection between the central moment α_n and the value $\langle V(V/c^2)^n \rangle$

$$\langle V(V/c^2)^n \rangle = -n \langle V \rangle \alpha_{n-1}. \quad (6.2.10)$$

Then the characteristic function $\chi(q)$ for the inverse function $\zeta = \zeta(V/c^2)$ is expressed through $\langle V(V/c^2)^n \rangle$. By applying the inverse Fourier transformation, finally, we find the required relationship (6.2.1).

The physical value Vc^{-2} is bounded by some constant M , hence

$$\alpha_n = \int_{-\infty}^{\infty} (Vc^{-2})^{n-1} \zeta d(V/c^2) \leq \int_0^M (Vc^{-2})^n d(V/c^2) = \frac{M^{n+1}}{n+1}.$$

The series $\sum_{n=0}^{\infty} |\alpha_n| (s^n/n!) \leq \sum_{n=0}^{\infty} M^{n+1} s^n / (n+1)!$ converge at $s < M^{-1}$. Consequently, the power series (6.2.1) also converges.

The coefficients $\langle V(V/c^2)^n \rangle$ ($n = 3, 4, \dots$) in Eq. (6.2.1) can be easily calculated, if we know the functional dependence $\langle V \rangle(p)$ or $\langle V^2/c^2 \rangle(p)$. Indeed, they can be successively defined by the recurrence relation

$$\frac{d \langle V(Vc^{-2})^n \rangle}{dp} = -(n+1) \langle V(Vc^{-2})^{n+1} \rangle, \quad (6.2.11)$$

that follows directly from the equation of state. With mentioned accuracy it is possible to diagnose the structural properties of the medium.

We have proved the principal relation (6.2.1) for method of diagnostics that allows one to find the properties of the individual components in structured media by means of the long nonlinear waves.

6.3 The governing wave parameters for diagnostic method

markright6.3. The wave parameters for diagnostic method First way that is evidently the simplest one for experimental finding of the dependence $\langle V \rangle(p)$ is a procedure in which a specific volume (or density) of a tested sample is found under different pressure. Then the recurrence formula (6.2.11) enables one to obtain the required series $\langle V(Vc^{-2})^n \rangle$ for $n \geq 2$ in order to apply the constitutive relationship (6.2.1). Nevertheless, the application of this procedure has the restriction, for instance, for a geophysical medium in the natural conditions. At the same time at these conditions the required coefficients for the constitutive relation (6.2.1) can be obtained from the features of wave field evolution. The advantages of medium testing by the waves are the convincing. This approach is considered to be particularly of the promising for media with the complex inner structure, specifically for a geophysical medium.

A possible way to obtain the functional dependence of $\langle V \rangle$ on p is to perform an experiment to define the parameters of shock waves. The shock wave velocity in the Lagrangian mass coordinates $D = ds/dt$ (dimension [D] is kg/s) and/or mass velocity

u as well as pressure p in the shock wave front can be experimentally measured. The value $\langle V \rangle(p)$ is calculated from the relationships on the shock front (2.4.12)

$$D = \sqrt{(p - p_0) / (\langle V_0 \rangle - \langle V \rangle)},$$

$$u - u_0 = \sqrt{(p - p_0)(\langle V_0 \rangle - \langle V \rangle)}.$$

After the measurement of the shock wave parameters for various pressures p we can obtain the dependence $\langle V \rangle = \langle V \rangle(p)$. Then the recurrence formula (6.2.11) is applied to obtain $\langle V(Vc^{-2})^n \rangle$ at $n \geq 2$ for Eq. (6.2.1).

The self-similar rarefaction wave can be considered as a universal instrument to define the coefficients $\langle V(Vc^{-2})^n \rangle$. Let us observe the features of rarefaction wave propagating in two-components periodic medium for the purpose of applying these features to test the properties of medium. In Fig. 6.2, for example, the profiles of

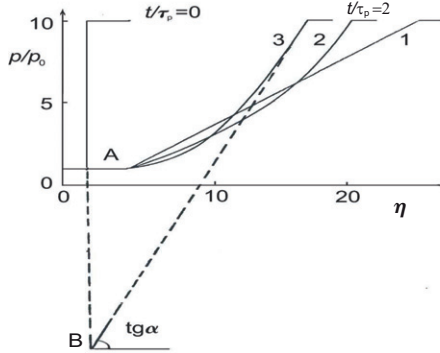


Figure 6.2: The self-similar rarefaction wave in different media: curve 1 in a homogeneous medium; curve 2 — two-component periodic medium with $c_1/c_2 = \sqrt{2}/5$; curve 3 — two-component periodic medium with $c_1/c_2 = 5/\sqrt{2}$.

the rarefaction waves are plotted for some two-component periodic media. The ratio of the pressure p to the initial pressure p_0 equals to $p/p_0 = 10$. The elementary cell consists of two layer with equal sizes in the Lagrangian mass coordinates ($\varkappa = 0.5$) and $V_1/V_2 = 2$ ($V_1 = 4/3$, $V_2 = 2/3$). For comprising the results in different media, we need to normalize to the averaged specific volume as well as to the velocity of small perturbations. In dimensionless variables it means $\langle V \rangle = \langle V^2/c^2 \rangle = 1$ at $p = p_0$. The relation between mass velocity and pressure is described by Eq. (6.1.6). The profiles of rarefaction waves calculated from Eq. (2.4.8) are shown in Fig. 6.2 in form of dimensionless dependence of pressure p/p_0 on the Lagrangian mass coordinate $\eta = s/\tau_p(p_0/\langle V \rangle)^{1/2}$.

At high pressure the velocities of different points of the wave profile (for fixed level of the pressure) ds_p/dt can be written as

$$\frac{ds_p}{dt} = \frac{s_p}{t} = \frac{\Delta p}{\sqrt{\langle c^2 \rangle}} + \frac{\langle c^4/V_0 \rangle}{(\langle c^2 \rangle)^{3/2}}. \tag{6.3.12}$$

Then at $p \gg \langle V^2/c^2 \rangle^{-1/2}$ the profile slope tends to the value $\tan \alpha = \sqrt{\langle c^2 \rangle}/t$ (see Fig. 6.2). Hence, the profile slope enables one to obtain the value $\sqrt{\langle c^2 \rangle}$.

In a special case for medium, in which the value $\langle V/c^2 \rangle$ is independent of ξ (i.e. for a medium with $V_1/V_2 = 2$ at $c_1/c_2 = \sqrt{2}$), the profile of the self-similar rarefaction wave is to be a straight line like for the homogeneous medium (curve 1 in Fig. 6.2). Therefore these media in this sense do not differ by the suggested method of diagnostics. For other periodic media, the profiles of rarefaction waves (curves 2 and 3 in Fig. 6.2) deviate from a straight line. The initial properties for these media were selected so as the averaged characteristics $\langle c^2 \rangle$ be the same at $p \rightarrow \infty$. It means that the asymptotics to curves 2 and 3 have the same slope. However, it is seen that for the moderate pressures, the profiles of the curves 2 and 3 are different as a result of the action of the nonhomogeneity.

Consequently, the self-similar rarefaction wave is to be considered as a universal instrument to define the required variables for diagnostic method. The self-similar motion of the rarefaction wave, as appears from relationship (2.4.8)

$$\frac{ds}{dt} = \pm \left\langle \frac{V^2}{c^2} \right\rangle^{-1/2},$$

allows one to obtain the value $\langle V/c^2 \rangle$ from the propagation velocity ds/dt of the separate parts of the wave profile under various pressures. The evolution of the profile of the rarefaction wave makes it possible to define the dependence $\langle V/c^2 \rangle = \langle V/c^2 \rangle(p)$ and then the values $\langle V(Vc^{-2})^n \rangle$ at $n \geq 2$ which can be found from Eq. (6.2.11).

We pointed out a few ways by means of which, from our point of view, it is possible to find the required dependence $\langle V/c^2 \rangle(p)$ from the experimental rarefaction waves. Certain difficulties for the calculation of the dependence $\langle V/c^2 \rangle(p)$ can be connected with the following fact. Indeed, the experimental data are always defined with some accuracy, hence, the application of Eq. (6.2.11) will lead to the increase of the relative error for high-order derivatives. This requires that a limited number of the terms should be used in series (6.2.1). Consequently, it is necessary to study the accuracy at the reconstruction of the structure of medium in the case when we know only several first terms in series (6.2.1).

6.4 Approximation of diagnosed medium by layer medium

Diagnostics of the structured medium properties by the long nonlinear waves is connected with the definition of values $\langle V(V/c^2)^n \rangle$. As indicated above, there is a problem related to the accuracy of the description of the structure by finite series (6.2.1).

Now, we shall show that the partial sum of series (6.2.1) is a step-function and approximates the desired function $\zeta = \zeta(V/c^2)$ with certain accuracy, namely the diagnosed medium can be approximated by a layer medium. Let us write down the

chain of the identities for any integrable function

$$\begin{aligned} 2\pi f(-x) &= F[F[f(x)](q)](x) = F\left[\sum_{n=0}^{\infty} \frac{i^n q^n}{n!} \alpha_n\right] \\ &= \sum_{n=0}^{\infty} \frac{i^n \alpha_n}{n!} 2\pi(-i)^n \delta^{(n)}(x). \end{aligned}$$

Here we used the known relationships for the Fourier transform [77]

$$F[F[f(x)](q)](x) = 2\pi f(-x),$$

$$F[q^n](x) = 2\pi(-i)^n \delta^{(n)}(x).$$

Hence, any integrable function can be represented by a series

$$f(-x) = \sum_{n=0}^{\infty} \frac{\alpha_n}{n!} \delta^{(n)}(x). \quad (6.4.1)$$

We will prove that the finite series (6.2.1) approximates the desired function $f(x)$ by step-function. Consider the step-function $f_1(x)$ consisting of N steps:

$$f_1(x) = \begin{cases} \varphi_1, & 0 < x \leq b_1, \\ \varphi_2, & b_1 < x \leq b_2, \\ \vdots & \vdots \\ \varphi_N, & b_{N-1} < x \leq b_N \end{cases} \quad (6.4.2)$$

in order to approximate the desired function $f(x)$. The relation (6.4.2) can be written down through the Heavyside functions as follows

$$\begin{aligned} f_1(x) &= \varphi_1[\Theta(x) - \Theta(x - b_1)] + \varphi_2[\Theta(x - b_1) - \Theta(x - b_2)] + \dots \\ &\quad + \varphi_N[\Theta(x - b_{N-1}) - \Theta(x - b_N)], \end{aligned} \quad (6.4.3)$$

Evidently, by increasing the number of steps N and choosing the values φ_i, b_i , any integrable function $f(x)$ can be approximated by the step-function $f_1(x)$. It is convenient to use a notation

$$\begin{aligned} f_1(-x) &= \varphi_1[\Theta(x + b_1) - \Theta(x)] + \varphi_2[\Theta(x + b_2) \\ &\quad - \Theta(x + b_1)] + \dots + \varphi_N[\Theta(x + b_N) - \Theta(x + b_{N-1})], \end{aligned} \quad (6.4.4)$$

that follows immediately from (6.4.3) after substitution

$$\Theta(x) = 1 - \Theta(-x).$$

The Heavyside function $\Theta(x + b)$ can be expanded into a Taylor series in the neighborhood of point x

$$\Theta(x + b) = \Theta(x) + \sum_{n=1}^{\infty} \frac{b^n}{n!} \Theta^{(n)}(x). \quad (6.4.5)$$

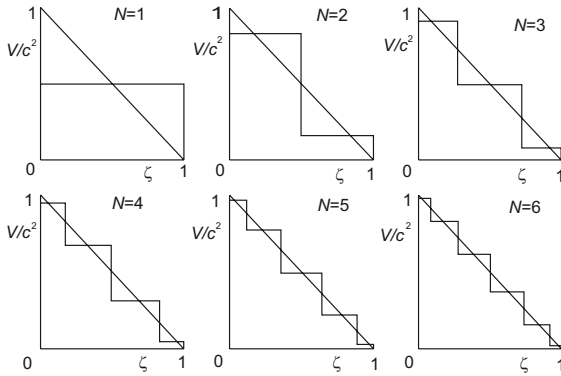


Figure 6.3: Approximation of the diagnosed medium $V/c^2 = 1 - \zeta$ by N -component media.

layer medium, for which $V/c^2 \neq f(\zeta)$, in particular, this medium can be a homogeneous one.

According to the asymptotic averaged model of a structured medium the period of the structure is infinitely small, and this diagnostic method cannot give the exact location of the structure elements inside the period. Hence, using this method, only the mass contents of the particular components can be determined.

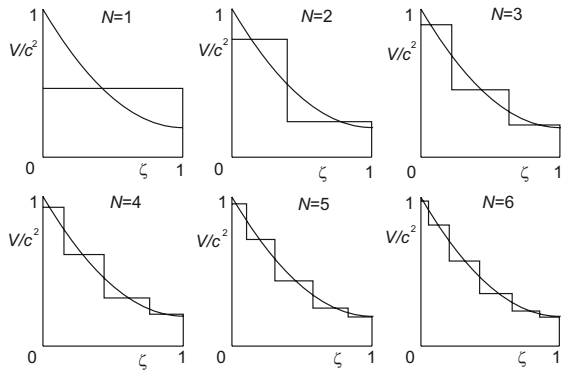


Figure 6.4: Approximation of the diagnosed medium $V/c^2 = 0.2 + 0.8(1 - \zeta)^2$ by N -component media.

We present as an example the results of the calculation to define the structure of layer media which can properly approximate the diagnosed medium. The structure of the diagnosed media is $V/c^2 = 1 - \zeta$ as well as $V/c^2 = 0.2 + 0.8(1 - \zeta)^2$ in Fig. 6.3 and Fig. 6.4, respectively. In order to approximate the diagnosed medium by layer periodic medium, which has N layers within the period, it is necessary to know $2N - 1$

values $\langle V(Vc^{-2})^n \rangle$ for finite series (6.2.1). If we regard that the $2N - 1$ averaged characteristics $\langle V(Vc^{-2})^n \rangle$ coincide for the diagnosed medium and for the layer medium, these averaged values at $n \leq 2N - 1$ can be calculated from the known distributions $V/c^2 = 1 - \zeta$ and $V/c^2 = 0.2 + 0.8(1 - \zeta)^2$ for Fig. 6.3 and Fig. 6.4, respectively. At $n > 2N - 1$ the values $\langle V(Vc^{-2})^n \rangle$ for diagnosed medium and for approximated layer medium are different. The distributions of $V/c^2(\zeta)$ within the period for diagnosed medium and for approximated media with N components are shown in Figs. 6.3, 6.4. On the one hand, the calculated distributions for layered media are the best approximation for the medium we test. On the other hand, we have illustrated the accuracy of the approximation of the diagnosed medium by the finite series (6.2.1).

Thus, the new method for the diagnostics of the medium characteristics by long nonlinear waves is suggested on the basis of the asymptotic averaged model of structured medium. The mass contents of the particular components can be denoted by the above-mentioned diagnostic method.

Chapter 7

State equation for Berea sandstone under slow loading

The typical stress-strain dependences for rocks under quasistatic loading measurements point out their essentially nonlinear behavior. The results by Adams and Coker [5], Boitnott [21], Hilbert *et al.* [62] and Darling *et al.* [36] on repeatable hysteretic loops in stress-strain curves are well known and can be regarded as the classical experiments. By modeling the dependence of strain on stress we generally obtain the state equation. Dealing only with macroparameters such as stress and strain while the processes on a microlevel still remain unknown makes it very difficult to create a model that adequately describes these properties. The recent experiments [36] showed that the most remarkable stress-strain properties of rocks are determined by a small volume of material at grain contacts. However, it is unclear how the interior equilibration processes in rocks under quasistatic loading can be studied in detail. In the literature, there are a number of models that qualitatively describe the relationships between macroparameters such stress and strain. First of all, there are two models, the Hertz-Mindlin model [109] and the Preisach-Mayergoyz model [53, 93]. However, with these approaches, there is some difficulty in assigning a set of model hysteretic elements to the real physical processes. While these approaches can duplicate experimental observations, the incorrectly formulated connection between the distribution of auxiliary elements and maximum stress levels leads to their limited predictive power.

A set of experimental results [21, 36, 53, 55, 57, 62] can be described within the model we suggested [161, 193, 198, 199]. We consider three appropriately formalizing mechanisms that appear to actually occur in rocks under quasistatic loading: (i) 'standard solid relaxation' mechanism; (ii) 'sticky-spring' mechanism; (iii) 'permanent plastic deformation' mechanism. A suitable combination of these mechanisms enables us to derive some general stress-strain relations, although without a detailed description of interior equilibration processes. As a result, we can obtain a phenomenological model that allows us to simulate qualitative and quantitative stress-strain characteristics and to reproduce the distinctive features typical of the basic experimental observations by Boitnott [21], Hilbert *et al.* [62] and Darling *et al.* [36] for Berea sandstone.

7.1 Analysis of experimental data

In order to facilitate analysis of three groups of fundamental experimental data for Berea sandstone by Boitnott (Fig. 1 in Ref. [53]), Hilbert *et al.* (Fig. 2 in Ref. [53]), and Darling *et al.* (Fig. 1 in Ref. [36]), we place them in a common format. Because in different experiments the origins of strain coordinates were introduced in different ways, it is an advantage to combine all experimental stress-strain curves in a single picture. We proceed from the assumption that for all three experimental curves, the

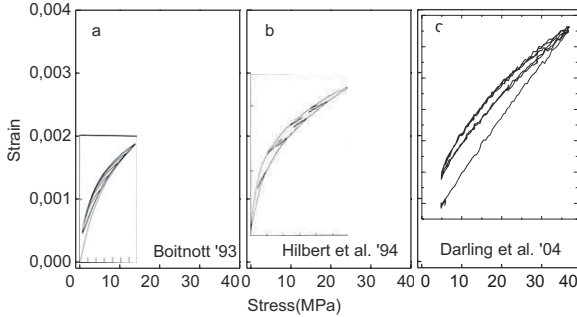


Figure 7.1: Experimental results for Berea sandstone: (a) Boitnott (Ref. [21]), (b) Hilbert *et al.* (Ref. [62]), (c) and Darling *et al.* (Ref. [36]). Stress-strain trajectories with their original coordinate meshes are placed within common coordinates. The systematic strain shifts caused by the apparatus adjustments are 0 for the data of Boitnott, 0.00042 for the data of Hilbert *et al.*, and 0.00097 for the data of Darling *et al.*

points relating to maximum stress should be placed somewhere on the longest of the available unconditioned curves, i.e., on the bottom curve of Fig. 7.1(c), while the origin for the common strain coordinate should be chosen from Fig. 7.1(a), where the starting point of the unconditioned (bottom) curve is documented. In this terminology, "unconditioned" refers to an initial curve that starts at zero stress on a sample that has been undisturbed for a long period (of the order of many hours or a day) as is the case in Fig. 7.1(a). In contrast, the curves of Fig. 7.1(b) are "conditioned", that is, have undergone multiple stress cycles. In this case, the starting point is not shown and, except for the final, highest point, the unconditioned curve is absent. The original experimental figures have different scales, and in Fig. 7.1, we have placed the experimental curves (omitting the scale numbers for clarity) into common coordinates. In this procedure Fig. 7.1(a) preserves its coordinates, while Figs. 7.1(b) and 7.1(c) are shifted to include zero strain positions; the strain shift for Fig. 7.1(a) is 0, for Fig. 7.1(b) is 0.00042, and for Fig. 7.1(c) is 0.00097.

It is pertinent to note that this approach for introducing common coordinates is not ideal inasmuch as it essentially treats the actual position of the initial (unconditioned) curve as independent of the rate of increase of the applied stress, which, in general, is not the case. However, experimentally, such a rate dependence is mainly detectable at high stresses and, to first (but rather good) approximation, can be neglected without

practical consequences within the common frame of reference.

The first effect that arises within a detailed analysis of given experimental data as in Fig. 7.1 is the manifestation of some internal relaxation process that appears as a characteristic looplike retardation in strain response upon external loading and unloading stresses. Indeed, the experiment involving transient stress steps [56, 118] clearly displays this effect. The relaxation component in the strain response can also be observed in other stress-strain dependences for various sandstones [36], especially for Meule sandstone. In particular, we see that after the moment when the stress becomes constant, the strain still changes for some time. Recently, several theoretical approaches have been developed to model time dependence in sandstone behavior near the high frequency vibrational resonance [15, 145, 194, 195] (see Chap. 8) as well as dispersion and absorption of sound in microinhomogeneous materials [59]; nevertheless, none of them seems to apply to the present case of comparatively slow loading. Hence, we will describe the relaxation features of sandstones in alternative terms of a phenomenological standard solid relaxation mechanism arising from a nonlinear generalization [158] of well-established relaxation modeling in the framework of a standard linear solid [213].

Second, the stress cycling gives rise to hysteresis loops in stress-strain curves. The observation of the experimental dependences from Ref. [36] (particularly Fig. 1 in Ref. [36]) reveals that opposite sides of each loop are not entirely stuck together even at infinitely slow loading, that is, the loops persist independent of loading time. Hence, there must be specific irreversible interior changes responsible for loop formation, i.e., those cannot be attributed simply to relaxation. We presume that some sort of friction has to be involved in any mechanism responsible for this effect. Therefore, we are forced to take into account a second mechanism, referred to here as a sticky-spring mechanism, for describing this aspect of sandstone stress-strain properties.

Finally, the whole conception would be incomplete without including a third mechanism called here a permanent plastic deformation. This third mechanism is needed to explain the observation that unconditioned and conditioned experimental curves differ from each other due to a permanent deformation, that is, a strain offset.

The next section provides a comprehensive treatment of these three mechanisms in order to model the interior processes that arise in rock samples under quasistatic compression.

7.2 Mechanisms for quasistatic loading

In this chapter we treat uniaxial compression of a rock sample restricted to quasistatic loading. As a consequence, the equation of motion for the bulk of the sample can be written using a single spatial coordinate

$$\rho\ddot{u} = \partial\sigma/\partial x \tag{7.2.1}$$

and can be simplified by putting the left-hand-side (inertial) term to zero. As usual, this approximation is valid when the wave propagation time $\tau_L = L/c$ (where L is the sample length and c is sound velocity) is sufficiently less than the loading time $\tau_\sigma = \sigma/\dot{\sigma}$, i.e., $\tau_L \ll \tau_\sigma$. Here, stress σ relates to strain $\varepsilon \equiv \partial u/\partial x$ through both elastic

and anelastic mechanisms, which are obtained beforehand from analysis of experimental data. Moreover, in this (slow loading) approximation, the stress turns out to be uniform along a sample and is determined by the absolute value of external loading, which plays the role of an external governing parameter. For the latter reason, we assign both σ and ε to be positive quantities as they are usually regarded in quasistatic compression experiments.

The fact, that for interpretation of quasistatic experiments it is sufficient to operate directly with the stress-strain relation, provides a good basis for understanding the main mechanisms of anelasticity and elasticity, especially nonlinear ones, as well as to formalize and verify them. As mentioned previously, we consider separately three mechanisms to account for interior processes in a rock sample under quasistatic loading: (i) the standard solid relaxation mechanism, (ii) the sticky-spring mechanism, (iii) the permanent plastic deformation mechanism.

7.2.1 Standard solid relaxation mechanism

The first part ε^r of the total strain ε to be considered is associated with a relaxation mechanism caused by an interior equilibration process. We use the superscript index r to distinguish ε^r from other contributions to ε . According to the analysis of experimental curves in Sec. 7.1, ε^r may depend on time not only implicitly through the governing stress σ but also explicitly through relaxation $\varepsilon^r = \varepsilon^r(\sigma(t), t)$. Thus, in general, strain can have different values at the same stress. However, the main hypothesis, which will be confirmed *a posteriori*, consists in assuming that the strain also responds to stress variation in time or, more precisely, to the time derivative $\dot{\sigma}$.

The most general linear theory taking into account all of the above-mentioned effects (i.e., explicit strain relaxation in time as well as implicit time dependence through both σ and $\dot{\sigma}$) is readily derived from the Zener phenomenological model of a standard linear solid [213]

$$\tau \dot{\varepsilon}^r + \varepsilon^r = \frac{\sigma}{M_e} + \frac{\dot{\sigma} \tau}{M_f}. \quad (7.2.2)$$

The theory deals with three material parameters: a relaxation time τ and two elastic moduli, relaxed M_e and unrelaxed M_f . Considering the quasistatic loading, we restrict our description to the condition $\tau_L \ll \tau$. Its main result is that a steady-state strain response (i.e., response at $t/\tau \gg 1$) to a periodically oscillating stress $\sigma = \sigma_a \cos(\omega t + \varphi)$ can exhibit two different regimes, namely, a relaxed $\varepsilon^r = \sigma/M_e$ at low frequencies $\omega\tau \ll 1$ and an unrelaxed $\varepsilon^r = \sigma/M_f$ at high frequencies $\omega\tau \gg 1$.

Unfortunately, another basic result

$$\varepsilon^r = \frac{\sigma_0}{M_e} \frac{t}{t_0} - \sigma_0 \frac{M_f - M_e}{M_f M_e} \frac{\tau}{t_0} \quad (7.2.3)$$

describing the steady-state strain response (i.e., response at $t/\tau \gg 1$) to a stress growing linearly with time $\sigma = (\sigma_0/t_0)t$ is usually misinterpreted due to a neglect of the small second term. Meanwhile, the similar "small" terms can play crucial roles in a complete understanding of quasistatic loading experiments and should be accurately taken into account. It is remarkable that the steady-state strain response (see Eq. (7.2.3)) reveals

two contributions that are distinct in origin. The first term contains the elastic contribution σ/M_e usually measured under infinitesimally slow loading, whereas the second term yields the regular anelastic shift proportional to the difference $M_f - M_e$, to τ , and to the loading rate σ_0/t_0 . In contrast, the instantaneous strain response (i.e., response at $t/\tau \ll 1$) on the same stress $\sigma = (\sigma_0/t_0)t$ exhibits only the elastic contribution σ/M_f and is characterized by the unrelaxed elastic modulus M_f :

$$\varepsilon^r = \frac{\sigma_0}{M_f} \frac{t}{t_0}. \quad (7.2.4)$$

As for a possible physical background to model the standard linear solid, researchers often appealed to a hidden interior relaxation process [88, 96]. Its main distinguishing feature consists of allowing the equilibrium state to shift linearly subject to an external influence, in particular, the subject to applied external pressure and its time derivative [88].

To better visualize the manifestation of interior relaxation in macroparameters under quasistatic loading, we consider the strain-stress dependences calculated from Eq. (7.2.2) (see Fig. 7.2). The strain-stress trajectories under loading with a fixed

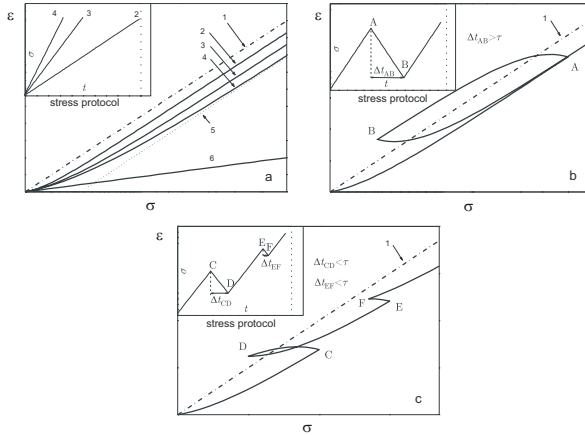


Figure 7.2: Strain-stress trajectories for standard linear solid [213]. Curve 1 is equilibrium line, 2–4 are calculation data for different loading speed, 5 is asymptotics, 6 is fast loading.

speed $\dot{\sigma} = \text{const}$ tend asymptotically to the lines that are parallel to the equilibrium line (dash-dotted line in Fig. 7.2). Note that the shift of asymptotics Δt from the equilibrium line is proportional to a loading speed $\dot{\sigma}$ and relaxation time τ , i.e. $\Delta \sim \tau \dot{\sigma}$. The initial condition is of no consequence to the time $\Delta t > \tau$. Indeed, the strain-stress trajectory tends to the asymptotics during the time $\Delta t \approx \tau$ (see Fig. 7.2a). There are the hysteretic loops (see Fig. 7.2b) at unloading with the time interval $\Delta t_{AB} \gg \tau$, whereas they are the closed loop in turning point A. Nevertheless, at unloading time

$\Delta t_{CD} < \tau$, $\Delta t_{EF} < \tau$ in Fig. 7.2c the loops either are not realized or are closed above the turning point C (see Fig. 7.2c).

In order to extend the basic ideas of a standard linear solid and its physical justification, a more general theory to describe the additional effects of nonlinear elasticity was developed several years ago [158]. The appropriate dynamic state equation becomes

$$\tau \frac{d}{dt} [\varepsilon^r - \varepsilon_f^r(\sigma)] + \varepsilon^r - \varepsilon_e^r(\sigma) = 0. \quad (7.2.5)$$

The suggested relation between strain ε^r , stress σ , and their time derivatives $\dot{\varepsilon}^r$ and $\dot{\sigma}$ is distinguished to include nonlinearities by means of two essentially nonlinear functions $\varepsilon_e^r(\sigma)$, and $\varepsilon_f^r(\sigma)$. These functions are responsible for a true thermodynamic equilibrium state at infinitely slow loading and for a frozen pseudoequilibrium state at infinitely fast loading, respectively. Both slow and fast terms are understood in relation to the typical time of the hidden internal relaxation process τ . Formally speaking, the curve $\varepsilon_e^r = \varepsilon_e^r(\sigma)$ could be thought as the state equation in the limit of instantaneous relaxation $\tau \rightarrow 0$, whereas the curve $\varepsilon_f^r = \varepsilon_f^r(\sigma)$ is the state equation in the limit of no relaxation $\tau \rightarrow \infty$.

It is necessary to note that, just as for the linear theory, the interior equilibration processes need not be specified concretely in the derivation of equation (7.2.5), but the macroscopic characteristics $\varepsilon_e^r(\sigma)$, $\varepsilon_f^r(\sigma)$, and τ in this approach are chosen to be a satisfactory combination for the overall model description. Of course, the macroscopic parameters involved, as well as the particular forms of functional dependences $\varepsilon_e^r(\sigma)$ and $\varepsilon_f^r(\sigma)$ themselves, should be selected to match known experimental results.

We term the model incorporated in the dynamical state equation (7.2.5) as the standard solid relaxation mechanism in view of its generic property of interconnection of two different nonlinear elastic state equations mediated through the hidden interior relaxation processes similar to the interconnection of two linear state equations in the theory of standard linear solid. In what follows, the equilibrium state function $\varepsilon_e^r(\sigma)$ is determined by the ordinary formula

$$\varepsilon_e^r(\sigma) = (E_e(\sigma))^{-1}\sigma, \quad (7.2.6)$$

and the stress-dependent Young modulus $E_e(\sigma)$ is written according to the empirical relationship

$$E_e(\sigma) = E_e^+ + (E_e^- - E_e^+) \exp(-D\sigma) \quad (7.2.7)$$

obtained as approximations that fit a number of experiments (see, e.g., Ref. [72] and references therein). The constants E_e^- , E_e^+ , and D are selected via numerical trials, and their values are close to those listed in Ref. [72]. For completeness, we define the frozen state function by the approximation

$$\varepsilon_f^r(\sigma) = a\varepsilon_e^r(\sigma), \quad (7.2.8)$$

where the factor a is a constant lying within the interval $0 < a < 1$. For example, in the linear theory, a relationship such as Eq. (7.2.8) finds its justification in stating that the ratio of the equilibrium sound velocity to the frozen one is independent of stress. When the time dependence of loading $\sigma = \sigma(t)$ (i.e., the stress protocol) is

known, then Eq. (7.2.5) can be solved. As a rule, we use an initial condition in the form $\varepsilon^r(t=0) = \varepsilon_e^r(\sigma(t=0))$.

Figure 7.3 illustrates the relaxation mechanism. The stress protocols for Fig 7.3 qualitatively correspond to the loading in works by Boitnott (see Fig. 1 in Ref. [53]) and Hilbert *et al.* (see Fig. 2 in Ref. [53]) accordingly. The constants in the state equations

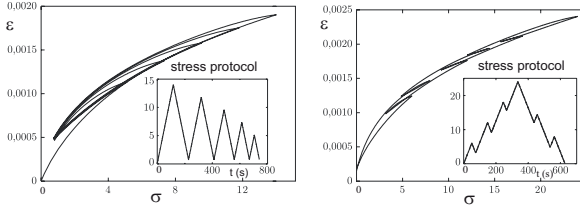


Figure 7.3: Modeling the Boitnott experiment (Ref. [21]) using only the standard solid relaxation mechanism (a). Modeling the experiment of Hilbert *et al.* (Ref. [62]) using only the standard solid relaxation mechanism (b). The theoretical curve for the unconditioned state is not shown here because its experimental counterpart with Fig. 7.1b is not available.

(7.2.5)–(7.2.8) are taken to be the same for both pictures. The best correspondence with experiments was obtained for relaxation time τ of 18 s; the other constants are $E_e^- = 1.5$ GPa, $E_e^+ = 32$ GPa, $D = 0.05$ MPa $^{-1}$, and $a = 0.7$. Modeling the Boitnott experiment leads to almost ideal results. In contrast, the experiment of Hilbert *et al.* cannot be adequately described by the sole relaxation mechanism, inasmuch as it does not close the small loops through the stress-strain cusps for any assignment of constants in the state equations. Thus, the relaxation mechanism by itself does not explain the end-point memory.

7.2.2 Sticky-spring mechanism

In order to develop the approach to explain the end-point memory of the stress-strain curves mentioned above, it is necessary to examine the stress-strain curves for Meule sandstone in the work by Darling *et al.* [36]. For this purpose, we select only important parts of the data of Darling *et al.* and depict them qualitatively in Fig. 7.4. Points corresponding to each other in the stress protocol picture (Fig. 7.4b) and stress-strain picture (Fig. 7.4a) are marked by the same capital letters and are unprimed and primed, respectively. In the time intervals AB , CD , and EF , stress is constant. The fact that the points A' , C' , and E' do not coincide with the respective points B' , D' , and F' can be explained by relaxation alone. Indeed, relaxation by itself should inevitably lead the experimentally distinct points D' and F' (and even B') to coincide. To resolve this problem and understand the discrepancy, it is necessary to include an additional mechanism. A principal feature of this mechanism should be its capacity to describe the hysteresis of a strain-stress trajectory, on the one hand, and this mechanism in contrast to the relaxation mechanism should be independent of speed of loading, on the other hand. We call this additional process as sticky-spring mechanism and, for the sake of convenience, formulate it separately from the other mechanisms.

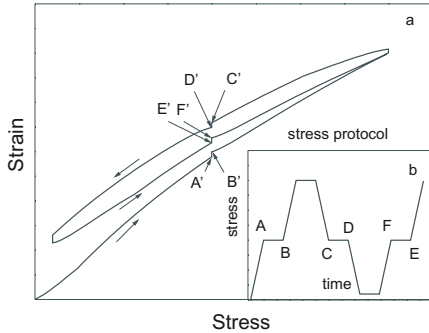


Figure 7.4: Features of the stress-strain relations for Meule sandstone (Ref. [36]) (qualitative picture).

A prototype system to illustrate this mechanism is given in Fig. 7.5. The system consists of a closed cylinder containing a cork plug. The quantity of gas in the closed

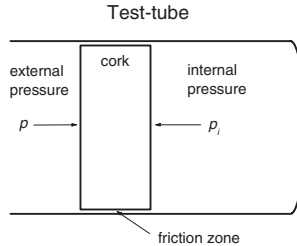


Figure 7.5: Analog model to illustrate the sticky-spring mechanism.

end is fixed, and its pressure p_i supplies the elastic restoring force. In addition, there is a friction between cork and tube walls. We treat this friction as independent of cork velocity. Such a friction arises in thermodynamical systems when the interior equilibration process is slow in comparison with the typical time of loading [158].

In terms of the cork-tube device, the maximum frictional force is taken to be proportional to the threshold pressure p_t (a positive value) that must be overcome by external pressure p against an internal p_i (or vice versa) in order for the cork to be pushed from one position into another. If we assume the cork to be massless, its displacement χ along the tube as a function of time t obeys the following first-order differential equation

$$\frac{d\chi}{dt} = \theta(\dot{p})\theta(\chi_-(p) - \chi) \frac{d\chi_-(p)}{dp} \dot{p} + \theta(-\dot{p})\theta(\chi_+(p) - \chi) \frac{d\chi_+(p)}{dp} \dot{p}, \tag{7.2.9}$$

in which the functions

$$\chi_-(p) \equiv \chi_m(p - p_t), \quad \chi_+(p) \equiv \chi_m(p + p_t) \tag{7.2.10}$$

are determined by

$$\chi_m(p) = l_0 - \frac{p_0 l_0}{p}. \quad (7.2.11)$$

Here, $\theta(z)$ is the Heaviside step function, $p_0 l_0$ is a constant characterizing the quantity of gas in a working volume of the cylinder, and l_0 is a length that fixes the working point of the cork-tube nonlinear device. Thus, $l_0 - \chi$ is simply the running position of the cork with respect to the back of the tube.

Some aspects of the sticky-spring mechanism are presented in Fig. 7.6, which illustrates the dependence of cork displacement χ on external pressure p . For this purpose, Eq. (7.2.9) has been numerically integrated from the initial condition $\chi(t = 0) = 0$ using the pressure protocol given in Fig. 7.6b. The essential feature of the sticky-spring

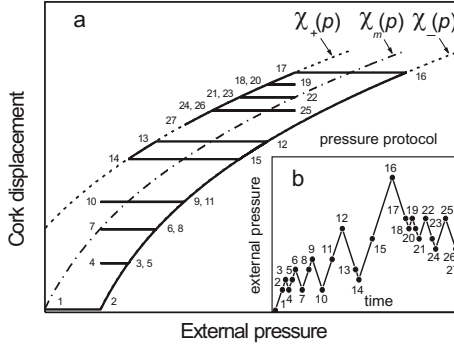


Figure 7.6: Cork displacement in response to external pressure. The curve of marginal equilibrium $\chi = \chi_m(p)$ is marked by a dash-dotted line.

mechanism consists in producing a stripe-like continuum of stationary states between the curves $\chi = \chi_-(p)$ and $\chi = \chi_+(p)$ as in Fig. 7.6. Only in the limit of very small threshold pressure $p_t \rightarrow +0$ do these curves come together and give rise to a single curve $\chi = \chi_m(p)$. This medial curve turns out to bisect the stripe and can be thought as the equilibrium curve of the process in the limiting case of $p_t \rightarrow +0$. Another essential part of this mechanism is its elastic component manifested through the inclination of stripe $\chi_-(p) < \chi < \chi_+(p)$ with respect to the p axis.

Summarizing the principal features of the sticky-spring mechanism (Eqs. (7.2.9) and (7.2.9)) as applied to sandstones, we postulate the stress-strain relation to be

$$\frac{d\varepsilon^s}{dt} = \theta(\dot{\sigma})\theta(\varepsilon_-(\sigma) - \varepsilon^s)\frac{d\varepsilon_-}{d\sigma}\dot{\sigma} + \theta(-\dot{\sigma})\theta(\varepsilon^s - \varepsilon_+(\sigma))\frac{d\varepsilon_+}{d\sigma}\dot{\sigma}. \quad (7.2.12)$$

Here, the partial strain ε^s is associated with the sticky-spring contribution to the total strain ε , while the functions $\varepsilon_-(\sigma)$ and $\varepsilon_+(\sigma)$ are determined via the medial equilibrium state function $\varepsilon_m(\sigma)$ and two positive threshold stresses σ_+ and σ_- as follows:

$$\varepsilon_-(\sigma) \equiv \varepsilon_m^s(\sigma - \sigma_-), \quad \varepsilon_+(\sigma) \equiv \varepsilon_m^s(\sigma + \sigma_+). \quad (7.2.13)$$

We note that no restrictions are imposed on the threshold values σ_- and σ_+ that are responsible for the friction. In principle, they can be functions of stress σ .

For the function $\varepsilon_m^s(\sigma)$ we assume

$$\varepsilon_m^s(\sigma) = \varepsilon_e^r(\sigma). \quad (7.2.14)$$

In accord with thermodynamic principles, Eq. (7.2.14) thus requires that the final position of a truly equilibrium state be independent of the origin of the internal processes that led to this equilibrium.

Within the Preisach-Mayergoyz approach [93], the qualitative distribution $\rho^s(P_c, P_0)$ for the sticky-spring mechanism can be written as

$$\begin{aligned} \rho^s(P_c, P_0) = & A'(P_c, P_0)[\theta(P_c - \sigma_+)\theta(\sigma_+ + \sigma_- - P_c)\delta(P_0) \\ & + \theta(P_c - (\sigma_+ + \sigma_-))\theta(\sigma_+ + \sigma_- - P_c) \\ & \times \delta(P_c - P_0 - (\sigma_+ + \sigma_-))], \end{aligned} \quad (7.2.15)$$

where notations are taken from Ref. [93].

Because the sticky-spring mechanism employs fewer adjustable parameters (constants) than do the Preisach-Mayergoyz models, we use this mechanism to describe quasistatic loading in rocks. Furthermore, if we consider the possible physical interpretations of the sticky-spring effects, it seems plausible that they capture the most essential features in opening-closing of sticky microcracks.

In Sec. 7.3 we show that, in the proper combination, the standard solid relaxation mechanism and the sticky-spring mechanism enable us to model relaxation steps on the conditioned curves under a fixed load (Fig. 7.4) and the effect of end-point memory, respectively. However, to include the unconditioned portion of the curves we must invoke a mechanism that takes the plastic deformation into account.

7.2.3 Permanent plastic deformation mechanism

We note that the permanent plastic deformation mechanism can, in principle, be treated within the relaxation mechanism, provided we include an additional set of relaxation parameters. However, because the permanent plastic deformation mechanism is responsible for the difference between the unconditioned and conditioned states, we prefer to separately extract it as an appropriately adjusted relaxation mechanism.

Taking into account the intuitively understandable features of permanent plastic deformation, we postulate that under compression, i.e., during increasing initial loading $\dot{\sigma} > 0$, the sample, on one hand, must contract with a permanent plastic contribution ε^p to total strain to obey a linear Hooke-like law $\varepsilon^p = \sigma/E_p$ (where the appropriate Young modulus E_p is presumed to be stress independent). On the other hand, it must simultaneously experience the interior irreversible deformations. Conversely, when external loading decreases, $\dot{\sigma} < 0$, the plastic component ε^p must remain fixed. To formalize the above-mentioned statements, the state equation for the permanent plastic deformation mechanism can be described as

$$\frac{d\varepsilon^p}{dt} = \theta(\dot{\sigma})\theta(\sigma/E_p - \varepsilon^p)\dot{\sigma}/E_p. \quad (7.2.16)$$

According to this mechanism, once a peak loading is achieved, the possible store of plastic deformation in the rock sample becomes saturated. Thereafter, when loading is less than the peak stress, the permanent plastic deformation mechanism does not appear as subsequent cycles. Through the Heaviside function, only an unconditioned curve manifests the permanent plastic deformation, while, on conditioned curves, it does not contribute.

Similar to the sticky-spring mechanism, the distribution in the Preisach-Mayergoyz space (see Fig. 2(a) in Ref. [93]) for permanent plastic deformation mechanism can be obtained from

$$\rho^p(P_c, P_0) = A^p(P_c, P_0)\delta(P_0). \quad (7.2.17)$$

It is necessary to note that the sticky-spring mechanism and the permanent plastic deformation mechanism can be considered as independent of each other, as are individual elements in Preisach-Mayergoyz space.

The separation of the sticky-spring mechanism and the permanent plastic deformation mechanism can have a physical interpretation. In the experimental results [21, 36, 53, 62], each increment of stress (starting at zero stress) beyond the previous highest stress produces irreversible changes in the rock fabric as crack surfaces slide and asperities are crushed. The permanent plastic mechanism is a means to incorporate these irreversible changes. In a regime where stress cycles at stresses less than the maximum previously achieved, the sticky-spring mechanism is applied. It may be that the Preisach-Mayergoyz approach can cover the whole stress range, yet there is a utility in the present approach where the damaging stresses are separated from a regime in which stress cycles are associated with reversible changes in the rock.

It is interesting to observe that Belinskiy has experimentally revealed the pure permanent plastic deformation under collision of steel balls in chain with plumbum layers [34].

7.3 Simulation of stress-strain relations

In the previous section, we have suggested three mechanisms by which interior interaction processes in sandstones are assumed to be described. Because the physical origins of these processes have not been well established, we use a phenomenological approach in which they are not concretely defined. In computing the counterparts of the available experimental data, the processes modeled by both the standard solid relaxation and the sticky-spring mechanisms can be treated using only a minimal number of phenomenological parameters, i.e., the number adopted in Secs. 7.2.1 and 7.2.2. However, when describing the more precise experiments, the suggested models have the potential to be modified by extending the number of relaxation and sticky-spring processes.

Taking into account all three developed mechanisms (standard solid relaxation, sticky-spring and permanent plastic deformation), we rely upon the minimum number of processes, i.e., only a single process for each mechanism. For loading by a given stress protocol, we can solve Eqs. (7.2.5), (7.2.12) and (7.2.16) with the initial conditions $\varepsilon^r(t=0) = \varepsilon^s(t=0) = \varepsilon^p(t=0) = 0$ and find the total strain ε as a linear combination of partial strains:

$$\varepsilon = b(\varepsilon^r + \varepsilon^p) + (1 - b)(\varepsilon^s + \varepsilon^p). \quad (7.3.1)$$

Here, the constant b is bounded inside the interval $0 \leq b \leq 1$. Clearly, at $b = 1$, we have the relaxation mechanism with permanent plastic deformation only, while at $b = 0$, we retain only the sticky-spring mechanism plus the permanent plastic deformation. Choosing relation (7.3.1) as a linear combination and keeping in mind the definition (7.2.14), we are able to tune the single parameter b to obtain a physical condition such that the true equilibrium state is independent of any type of interior relaxation process. Since in Ref. [28] it is experimentally proved that there are the different slopes between the minor loop and the major stress-strain loop, while these slopes have a large jump, the value b can be estimated through suitable angles of the loop slopes as it has been suggested in Ref. [161].

If the stress is fixed at one moment, then the relaxation mechanism moves the whole system to some new equilibrium during a characteristic relaxation time. Owing to the sticky-spring mechanism plus the permanent plastic deformation mechanism, there can be several equilibrium states at the same stress. The ambiguity of equilibrium state dependence on stress has been written in Ref. [59].

The best fits of the calculated results as applied to all three groups of experiments on Berea sandstone [21, 36, 53, 62] (see also Fig. 7.1) were obtained with the parameters listed in Table 7.1. Note that these parameters are applied when we consider the combination of all three mechanisms in contrast to the parameters applied in Sec. 7.2.1 for Figs. 7.2 and 7.3, when only the relaxation mechanism was analyzed.

Table 7.1: Fitting parameters

τ	E_e^-	E_e^+	D	σ_-	σ_+	E_p	a	b
s	GPa	GPa	MPa ⁻¹	MPa	MPa	GPa		
3	5	23	0.03	4	4	70	0.2	0.8

Results of the numerical simulation are presented in Fig. 7.7. Comparing the calculated curves (Fig. 7.7) with experimental data (Fig. 7.1), we observe an acceptable coincidence of these results both qualitatively and quantitatively. First, we find the small loops in curve b of Fig. 7.7 that simulates the experiment of Hilbert *et al.* [62]. These loops are closed at the cusps. Unfortunately, in experimental curves for Berea sandstone, it is difficult to reveal the features that are present in Meule sandstone (Fig. 1 in Ref. [36]), i.e., to precisely observe the steps caused by sample relaxation under fixed load, e.g., in Fig. 7.4. This difficulty could be explained by the exceptional smallness of typical relaxation times for Berea sandstone as compared with typical times in the experimental stress protocol. For this reason, Berea sandstone features related to relaxation under fixed load are simply not seen in our theoretical curve c of Fig. 7.7 that models the experiment of Darling *et al.* [36]. However, the relaxation mechanism cannot be completely removed because it plays an important role in describing the end-point memory as manifested by the small loops on the theoretical curve b in Fig. 7.7, which reproduces the experiment of Hilbert *et al.* [62]. On the one hand, it is precisely the effect of small but finite relaxation time that enables one to close a small loop through a cusp (see curve b in Fig. 7.7 once again). On the other hand, the relaxation provides the means to produce the small loops in the modeling.

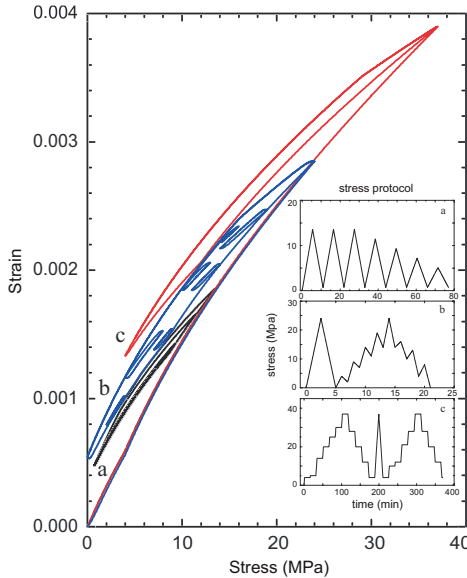


Figure 7.7: Computer simulation of stress-strain trajectories for Berea sandstone. Curve *a* relates to the experiment of Boitnott (Ref. [21], curve *b* models the experiment of Hilbert *et al.* (Refs. [53, 62]), and curve *c* reproduces the experiment of Darling *et al.* (Ref. [36]).

7.4 Dissipation of energy in rock under cyclic loading

Much is known about the qualitative and quantitative nonlinear response of rock [56]. The experimental measurements of repeatable hysteretic loops in stress-strain trajectory at slow loading have been studied in Refs. [21, 36, 53, 62] (see, also, sections 7.1–7.3). The investigation of the behavior of sandstones under mechanical loading is aimed at construction of the state equation for these media. Experiments [36] have shown that the most remarkable stress-strain properties of rocks are determined by a small volume of material at grain contacts. Understanding of the internal processes on a mesoscopic level under mechanical loading provides a mean for both physical and mathematical simulations.

The study in details of all complicated internal processes is impossible at this time that in its turn hampers the development of models. However, it is important to know not internal processes in itself, but their effect on the connection between macroparameters of medium. For mechanical loading, it is the dependence of strain on stress, in other words, the equation of state.

In sections 7.1–7.3 (see, also, Refs. [193, 198, 199]) we have suggested the model of the dynamic behavior of rocks under quasistatic mechanical loading. The response of

the internal exchanged processes appeared as a result of the intensive external loading, is simulated on macrolevel by three appropriately formalizing mechanisms: (i) a standard solid relaxation mechanism, (ii) a sticky-spring mechanism, and (iii) a permanent plastic deformation mechanism. A suitable combination of these mechanisms has enabled us to derive some general stress-strain relations and to reproduce the distinctive features typical of the basic experimental observations for Berea sandstone [21, 36, 62].

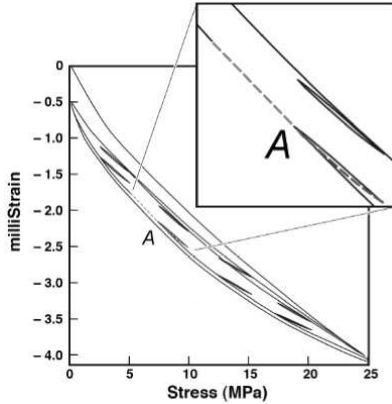


Figure 7.8: Experimental stress-strain trajectories for Berea sandstone. Figure is taken from [28].

Additional experimental data on the mechanical deformation of the Berea sandstone are represented in [28]. They were obtained after the development of model we suggested. First of all, in this paper [28] authors have observed (a) a discontinuity between slopes of the main loop and the inner small loops in endpoint *A* (see Fig. 7.8 and also Fig. 2 and Fig. 3 in [28]); (b) the main loop area as a function of the sweep rate (see Fig. 7.9 and also Fig. 1 in this paper [28]); (c) the congruence of the inner loops (see Fig. 4 in the paper [28]). Owing only to the precise measurements, some insight into the details of the stress-strain trajectory has been gained in [28].

7.4.1 The slopes of main and inner hysteretic loops

Let us consider the slopes of the inner small hysteretic loops with respect to the major hysteretic loop (see Fig. 7.8). In endpoint *A* there is no smooth passage between inner and external hysteretic loops, but there is the jump of the slopes between these loops. The discontinuity at the endpoint *A* can be explained [161] by means of the sticky-spring mechanism together with relaxation mechanism within the model [198]. For convenience of explanation only, we regard that the equilibrium curve is a straight line, and the relaxation mechanism is reduced to the elastic deformation (it is true at passing in Eq. (7.2.5) to the limit $\tau \rightarrow 0$ or $\tau \rightarrow \infty$). It is noted that at cyclic loading after the first attainment of a maximum stress, the third mechanism, namely,

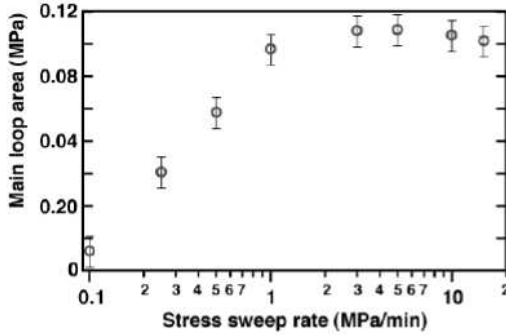


Figure 7.9: Main loop area as a function of experimental measurement sweep rate. Figure is taken from [28].

the permanent plastic deformation mechanism does not produce the contribution into dependence of strain on stress.

Now let us consider the combination of the sticky-spring mechanism and the relaxation mechanism. The stress-strain curve for the sticky-spring mechanism is shown qualitatively in Fig. 7.6. This mechanism with the elastic mechanism at series prototype elements (as in left upper corner in Fig. 7.10) has such qualitative stress-strain trajectory as in Fig. 7.10. It is easily to understand that an angle α is associated

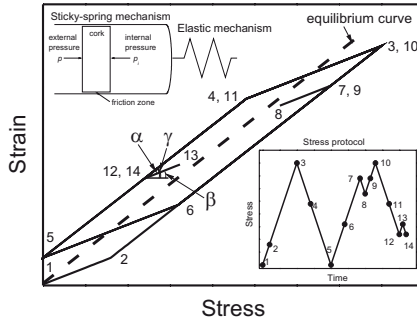


Figure 7.10: Qualitative stress-strain trajectory for sticky-spring mechanism with elastic mechanism.

with the angle measured in the experiments [28] between the slopes of main and inner hysteretic loops. Thus, the jump of the slopes between these loops observed in the experiments [28] finds its explanation within the model [198]. Moreover, the angle α enables us to determine the constant b for the relationship (7.3.1), i.e. the balance between the sticky-spring mechanism and the relaxation mechanism

$$b = \frac{\tan \beta}{\tan \gamma},$$

where the angles β and γ are defined as in Fig. 7.10 and $\alpha = \gamma - \beta$.

It should be noted that the value b is independent on the friction in prototype element of the sticky-spring mechanism (see Fig. 7.5). Hence, the constant b that in section 7.3 was chosen by means of best coincidence of computer modeling with experimental data, now receives other sense and can be estimated from the jump of slopes for major and inner hysteretic loops. Since in model approach for determining the angle α the relaxation is not considered here that contributes some mistake, we can only estimate the value b . However, the effect of relaxation on the mutual slope of the major and inner loops is not considered in details here.

The congruence of the inner loops observed in the experiment [28] can be explained [161] within the suggested model (see sections 7.1–7.3 and, also, Ref. [198]) in the following way. It is obvious that in Fig. 7.10 the intervals of stress-strain trajectory between the points (1,2), the points (3,4), the points (5,6), the points (7,8), the points (8,9), the points (10,11), the points (12,13), the points (13,14) are parallel each other. The inner loops appear around the intervals (7,8) and (12,13) as a result of relaxation. Consequently, the inner loops should be congruent each other.

7.4.2 Energy dissipation

The dissipation of energy caused by internal processes in sandstone is estimated through the area bounded by hysteretic stress-strain curve. Thus, the dependence of the area on the form of loading is important characteristics which illuminates the sandstone properties under quasistatic loading.

At first, let us study qualitatively the possibility for appearing the dependence of hysteretic loop area on sweep rate in a form observed in experiments (see Fig. 7.9). The experimental values of loop area in this figure attain maximum value, i.e. the area becomes constant. This fact can be explained in frames of the suggested model (see sections 7.1–7.3 and, also, Refs. [193, 198, 199])

Consider the relaxation mechanism in details (see Fig. 7.2). From Fig. 7.2 a we see how the curves approach to the asymptotics at different sweep rates $\dot{\sigma}$. If $\dot{\sigma}$ is constant, the curve tends to the asymptotics that is parallel line to the equilibrium line. The sweep rate $\dot{\sigma}$ is larger, the departure of the asymptotics from the equilibrium line is larger.

As a function of sweep rate, the area of hysteretic loop, at first, increases (see Fig. 7.11 a,b), later leads to a maximum (see Fig. 7.11 b,c), and finally if $\sigma_{max} = \text{const}$, the area should decrease (see Fig. 7.11 c,d). For each next picture in Fig. 7.11, the sweep rate is redoubled, i.e. $\sigma = \sigma_0$ in Fig. 7.11 a, $\sigma = 2\sigma_0$ in Fig. 7.11 b, $\sigma = 4\sigma_0$ in Fig. 7.11 c, and $\sigma = 8\sigma_0$ in Fig. 7.11 d. The increase of the loop area is associated with the effect of the relaxing exchanged processes, while the attainment of maximum as well as the decrease later of the loop area is the result of the limitation for maximum level of loading σ_{max} . As in experiments, here we regard that the maximum level of loading is constant $\sigma_{max} = \text{const}$ for all pictures in Fig. 7.11. Thus, in contrast to a conclusion from [28], namely, that for Berea sandstone at sweep rate above 3 MPa/min, the relaxation can not be taken into account, we become to a result that the relaxation exists always and gives a contribution into the area of hysteretic loops. While the decrease of the loop area is connected with another factor, namely, with the limitation

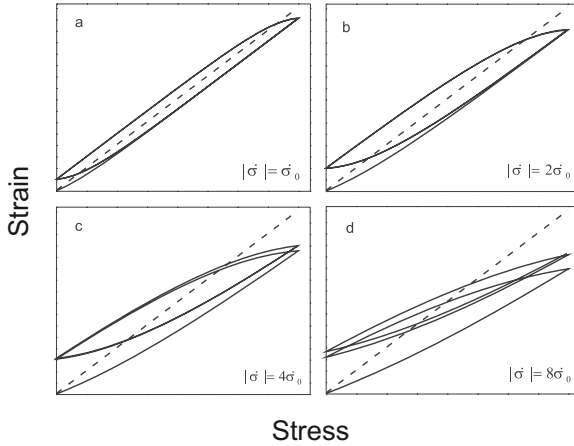


Figure 7.11: Hysteretic stress-strain curves under cyclic loading at different $|\dot{\sigma}|$ and $\sigma_{max} = \text{const}$. The dash lines determine the equilibrium states.

of the maximum level of loading $\sigma_{max} = \text{const}$ exerted to a sandstone sample.

We confirm this qualitative exploration by computer calculations (see Fig. 7.12), using the suggested model for describing the dynamic behavior of sandstone under quasistatic loading (see sections 7.1–7.3 and, also, Refs. [193, 198, 199]). The model parameters for Berea sandstone are borrowed from Table 7.1. The stress protocols have the form of the repeated triangulars. The modulus of the sweep rate $|\dot{\sigma}|$ for each picture in Fig. 7.12 are different. It is seen that as in qualitative analysis of the physical phenomena (see Fig. 7.11), the area of the hysteretic loop, at first, increases (Fig. 7.12 a,b), later at high rate of loading the loop area decreases (Fig. 7.12 b,c).

In Fig. 7.13 we plot the calculated dependence of the hysteretic loop area on the sweep rate $|\dot{\sigma}|$. The curve 2 in Fig. 7.13 simulates the experimental data (see Fig. 7.9) represented in [28]. Note that the theoretical and experimental results coincide not only qualitatively, but also quantitatively with appropriate accuracy. We predict that at high sweep rate the dissipation of energy determined as area of the main loop should decrease [161]. The confirmation of this fact by experimental observation could be the additional argument for further application of the suggested model [193, 198, 199], on the one hand, and, on the other hand, such experimental dependences could stimulate to the improvement and development of new models.

We call attention that all parameters for Berea sandstone have been taken from Table 7.1 and in no way have been picked up for this experiments [28]. So, model we suggested in sections 7.1–7.3 (see, also, Refs. [193, 198, 199]). additionally to the results represented in the papers [193, 198, 199], can describe new experiments [28]. For trustworthiness of model it is significant that the experiments [28] simulated here were carried out after we had suggested the model of the dynamical behavior of sandstone with the determined recent parameters in the state equation i.e. in the stress-strain

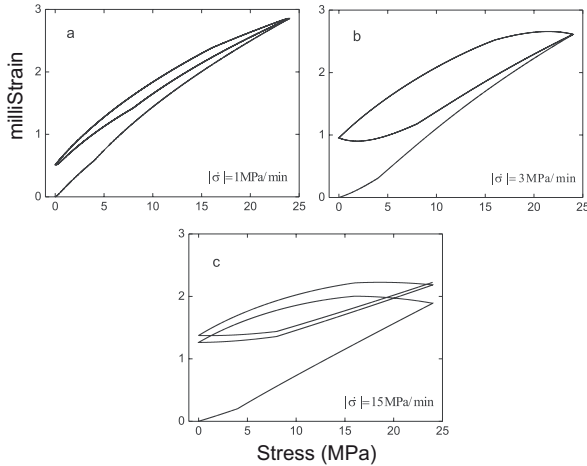


Figure 7.12: The calculated stress-strain trajectory at different sweep rates and $\sigma_{max} = 24$ MPa for Berea sandstone.

relation [198].

7.5 Conclusions

In this chapter we have suggested a phenomenological model to describe the stress-strain properties of Berea sandstone under quasistatic loading. Analysis of experimental observations has demonstrated the need to invoke several mechanisms that are responsible for interior equilibration processes in sandstone: the standard solid relaxation mechanism, the sticky-spring mechanism, and the permanent plastic deformation mechanism. To justify these mechanisms we have used an approach in which the interior processes in a sample are not explicitly defined. This approach drastically simplifies the mathematical description. Only by properly combining all three mechanisms we have been able to obtain the acceptable simulation. Moreover, it was shown that each of first two mechanisms (the relaxation and sticky-spring ones) can be restricted to one process. The resulting treatment reproduces extremely complex stress-strain trajectories with only nine adjustable parameters. However, if it is required to describe other, more precise experiments, then the model can be properly modified because it is possible to invoke a number of relaxation times for the standard solid relaxation mechanism and friction parameters for the sticky-spring mechanism. As for the permanent plastic deformation mechanism, we presently do not know how it could be generalized to include more than one phenomenological parameter.

Owing to the proposed treatment of quasistatic stress-strain relations, it becomes possible to produce an adequate and self-consistent simulation that both qualitatively and quantitatively describes the principal features of experimental data by Boit-

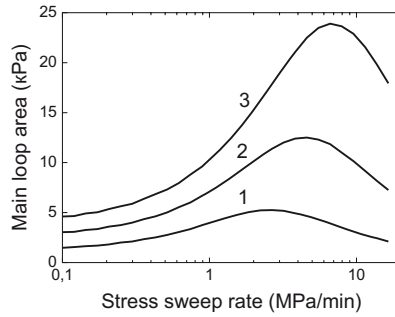


Figure 7.13: The calculated area of main loop as a function of the sweep rate for Berea sandstone. Curve 1 has $\sigma_{max} = 14$ MPa, 2 — $\sigma_{max} = 24$ MPa, 3 — $\sigma_{max} = 37$ MPa.

nott [21], Hilbert *et al.* [62] and Darling *et al.* [36] for Berea sandstone. The model correctly reproduces both the large loops and, equally important, the small loops in stress-strain trajectories (the end-point memory effect). We have predicted effect of decrease of the energy dissipation at high sweep rate.

Chapter 8

Dynamics of a sandstone bar under resonance loading

Apart from their distinctive quasistatic characteristics (see Chap. 7) as one of earth materials, sandstones have been shown to demonstrate a number of unexpected and even surprising dynamical properties. In this chapter we consider the numerous experimental results on nonlinear resonant response exhibited by sandstone rods in forced longitudinal oscillations that appear even at extremely small forcing levels and consequently at small dynamic strain.

Sedimentary rocks, particularly sandstones, are distinguished by their grain structure [32, 39, 148] in which the core of each grain is much harder than the intergrain cementation material [55, 57]. The imperfect intergrain cementation partially appears as porosity [32, 39, 148], a property governing rock permeability that is essential, e.g., for petroleum production [32, 39]. In addition, porosity facilitates a penetration of water into areas of intergrain contacts [55, 57] causing a dramatic impact on elastic moduli [2, 29, 214] and seismic dissipation factors [2, 29, 214, 149]. The peculiarities of grain and pore structures give rise to a variety of remarkable nonlinear mechanical properties demonstrated by rocks, both at quasistatic and alternating dynamic loading. Thus, the hysteresis, earlier established for the stress-strain relation in samples subjected to quasistatic loading-unloading cycles [33, 52], has also been discovered for the relation between acceleration amplitude and driving frequency in bar-shaped samples subjected to an alternating external drive that is frequency swept through resonance [68, 71, 143, 146]. At strong drive levels there is an unusual, almost linear decrease of resonant frequency with strain amplitude [58, 71, 145], and there are the long-term relaxation phenomena [143, 146, 147] such as nearly logarithmic recovery (increased of resonant frequency) after the large conditioning drive has been removed [143, 145].

The fragmentary understanding of these observations [54, 145] has stimulated us to look into the whole problem, usually characterized as "slow dynamics", more systematically and to propose a closed-form theory. This is based upon an explicit, physically motivated formalization of a sandstone bar system as two coupled nonlinear subsystems, one of which breaks the symmetry of system response to an alternating external drive and acts as a sort of soft ratchet or leaky diode [194, 195]. We specify these subsystems as a fast subsystem of longitudinal displacements and a slow subsystem of

ruptured intergrain and/or interlamina cohesive bonds.

In this chapter we present a detailed development of a model [194, 195, 196, 201] as well as inspect its ability to explain the numerous experimental observations seen in forced longitudinal oscillations of sandstone bars. We demonstrate that a broad set of experimental data can be understood as various facets of the same internally consistent approach. Furthermore, the suggested theory will be shown to predict the dynamical realization of hysteresis with end-point memory, figuratively resembling its well-known quasistatic prototype [33, 52] (see also more recent publications [55, 57, 68]). Our theoretical predictions have been confirmed by experimental measurements performed at the Los Alamos National Laboratory (LANL) by Ten Cate and Shankland.

8.1 Analysis of experimental data

Over the past several years, rocks have been shown to be elastically nonlinear. The majority of quantitative measurements for rocks have been performed with resonant bar experiments [55, 57, 69, 71, 116, 143, 146, 147, 145]. Due to the amplification that resonance provides, it is perhaps the most sensitive manner by which to observe nonlinear behavior, even at extremely small dynamic strains, as low as 10^{-7} .

The nonlinear resonance measurements have been performed to understand the mechanisms that produce the observed nonlinearity. The typical experimental apparatus used to obtain the resonance curves is shown in Fig. 8.1. The experimental

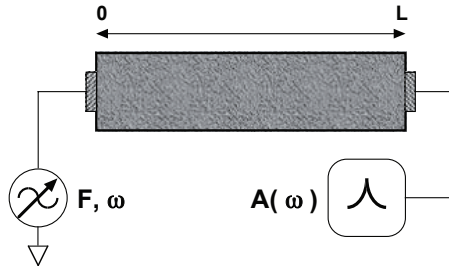


Figure 8.1: Experimental configuration for resonance bar experiments. In a typical resonant bar experiment, the bar is driven at one end and the strain field or its functional equivalent is detected at the other end. It is usual to fix the drive amplitude F and sweep the frequency ω over a resonance. The measured acceleration is denoted as $A(\omega)$. Figure is taken from [55].

method is to drive a cylindrical sample of rock in the fundamental longitudinal elastic mode (Young mode), with a piezoelectric force transducer cemented between one end of the sample and a massive backload. Acceleration of the opposite end of the sample is measured with a lightweight accelerometer and processed with a lock-in amplifier referenced to the driving signal. The driving force is a harmonic acoustic wave, incremented through the fundamental resonance frequency of the bar, to produce the frequency-dependent lumped-parameter response function of the resonant bar.

The sample, 50 mm in diameter and 0.3 m long, had a low-amplitude resonance at $f_r \approx 3920$ Hz (the strain at resonance of order 10^{-8}). Fig. 8.2 shows the experimental resonance curves as the dependence of an acceleration on the driving frequency from Ref. [146]. In Fig. 8.2a the first curve made when the rock was in its recovered state

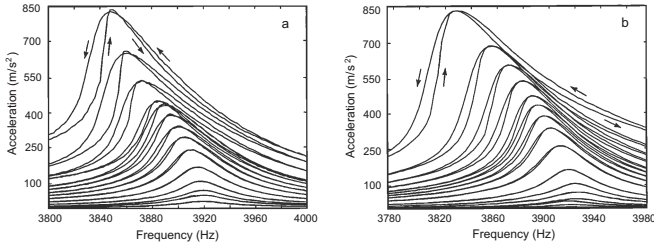


Figure 8.2: Resonance bar data [146]. (a) Unconditioned resonance curves measured at successively higher amplitudes. (b) Resonance curves at successively higher amplitudes only after a few up and down sweeps were made first (conditioning). Arrows on highest pair of curves indicate the sweep direction. Figures are taken from [146].

differed from the subsequent curves. Figure 8.2b shows a set of conditioned resonance curves obtained after two frequency sweeps were performed at each drive level to achieve repeatable curves. As the resonance was swept over ((up followed by down) 3800 to 4000 Hz to 3800 Hz in 2-Hz steps (200 frequency points) at 300 ms per step) with increasing drive amplitude, the resonance frequency was seen to shift to lower values, for example, $f_r = 3850$ Hz when the strain at resonance was of order 10^{-5} . A frequency sweep of 3800 to 4000 Hz was different from a frequency sweep of 4000 to 3800 Hz.

The first resonance curve made on a 'recovered' sample differed from the following curves. Figures 8.3a, 8.3b show these initial curves (indicated on each figure) and several successive up/down or down/up sweeps. Figure 8.3a represents a set of curves beginning at 3800 Hz and sweeping up, Fig. 8.3b represents a set starting at 4000 Hz and going down. If the first sweep reaches the resonance frequency f_r (independently on sweep direction), it alters the response of the rock so that at the repeated cycling conditions, the sample has the same resonance curves. Amplitudes of the repeatable curves all lie above the initial curve at frequencies below the resonance frequency (Fig. 8.3a); they lie below the initial curve for downward sweeps at frequencies above the resonance frequency (Fig. 8.3b). Hence, the sample has a 'memory' on the maximum strain amplitude already reached. Most importantly, the same maximum value of the strain amplitude is reached at the same resonance frequency f_r irrespective of whether the sweep direction was down/up or up/down for both unconditioned and conditioned curves.

Fig. 8.4 (see also Fig. 6 in [146]) shows the relaxation changes of acceleration amplitude at fixed frequency. Here, it is illustrated how a rock gradually loses memory of the highest strain. At repeatable up or down sweep, the sweep was stopped (drive still on) and time-dependence of acceleration was recorded for nearly 10 minutes. As shown in Fig. 8.4, the measured acceleration gradually decreased for the experiments where the stopping frequency was lower than the resonance frequency f_r , while increased

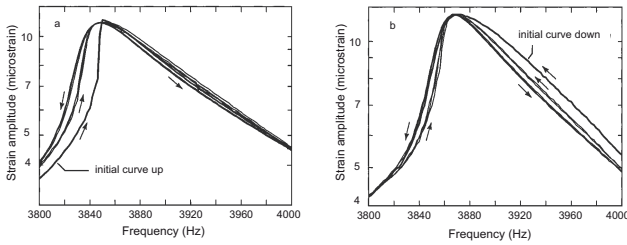


Figure 8.3: First sweep at constant drive level (a) up from 3800 Hz or (b) down from 4000 Hz and repeating; repetitions show the approach to a conditioned response. Figures are taken from [146].

when the stopping frequency was higher than f_r . After several minutes, both levels approached the same long term level.

In order to examine another relaxation features of rocks in the next experiments in addition to the previous experiment, in which the sweep had been stopped, the drive has been shut off for 30 s. Figure 8.5 shows the faster response for both sides of the resonance curve. In both cases the sample was conditioned by driving at the resonance frequency for this strain level (3850 Hz) for 2 min. At constant drive amplitude, starting at resonance frequency f_r , the frequency is swept over the resonance down to 3825 Hz for Fig. 8.5a, and up to 3900 Hz for Fig. 8.5b, where the drive is turned to zero for 30 s. The original drive voltage had been reestablished, and the frequency sweep has been completed. Results are clearly seen as discontinuities on the curves. At frequencies lower than resonance f_r , the resonance curve jumps down, while at frequencies higher than resonance f_r , the resonance curve jumps up. Comparison of figures 8.4 and 8.5 reveals that memory of the highest strain is lost more quickly, if the drive is turned off. In Ref. [146] it is noted that a qualitative explanation of jumps can be received from the nonlinear change of bar modulus E with amplitude. After a period of high intensity, the rock resonance curve shifts downward in frequency (i.e., the modulus decreases). If the drive is then turned off, the resonance curve moves back (i.e., the modulus increases) as memory of the high strain is lost.

The experimental results shown in Figs. 8.4 and 8.5 point out that rocks reveal the relaxation properties under dynamic loading, i.e. at fixed frequency, the resonance curves depend on a time not only indirectly throughout drive amplitude, but also explicitly.

Much of the interesting nonlinear behavior observed in the medium strain region can be attributed to slow dynamics. At high enough strains, the excitation (reversibly) changes the rock's modulus. It doesn't recover immediately from the high strain; often it takes hours, even days to return to its pre-excitation state. In experiments a sample was driven at a high intensity for a fairly long period of time. One manner in which to observe the nonlinear behavior is to monitor the resonance frequency before and after large excitation [143, 145, 147]. The low-amplitude resonant peak is then monitored until the resonant peak has returned to its original frequency. Figure 8.6b shows fractional resonant frequency shift per unit conditioning strain, as a function

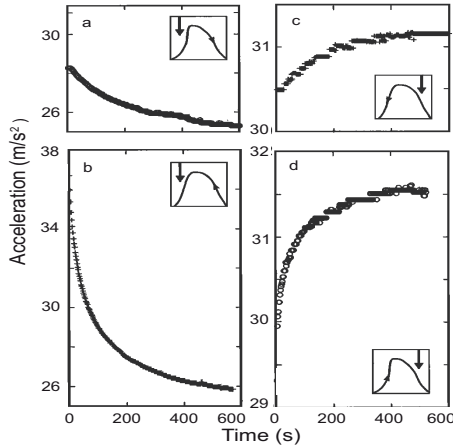


Figure 8.4: Measurement of acceleration decay at fixed frequency. Frequencies are 3825 Hz, upward going (a) or downward going (b), and 3900 Hz downward going (c) or upward going (d). Note that (a) and (b) end up at nearly the same acceleration; a similar observation holds for (c) and (d). Figures are taken from [146].

of time t after the conditioning drive is turned off, for the six samples studied. The slow dynamical scaling of the resonance frequency recovery in time is logarithmic [145]. The $\log(t)$ time dependence is usually associated with the operation of phenomena that involve a broad range of time scales. As is noted in Ref. [55], it seems unavoidable that this attention must be a part of any serious experimental exploration. Now we point out only that developing model for dynamics of rocks, suggested below in Sec. 8.2.2, we have taken into account a broad spectrum of time scales.

Conclusively, we have to emphasize that in the vicinity of bar resonant frequency the longitudinal alternating drive produces strong essentially nontrivial nonlinear responses:

- At high drive levels the effective width of resonance curves depends on the direction of frequency sweep; it is narrower for upward sweeps (i.e., from lower to higher frequencies) than at downward sweeps (i.e., from higher to lower frequencies) [146]. This effect proves to be a typical manifestation of slow dynamics and can be treated as hysteresis both on low- and high-frequency slopes of a resonance curve.
- The resonance peak is shifted toward the lower frequency almost linearly with an increase of driving amplitude [55, 57, 71, 146].
- At constant level of drive amplitude the peak of resonance curves is the same for different direction of sweep frequency and it is independent of either unconditioned or conditioned state of a sample [146].

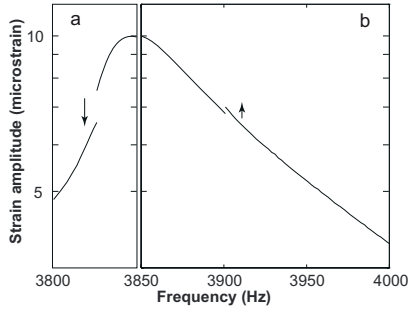


Figure 8.5: Stopping resonance curve sweep, turning off the drive for 30 s and then continuing the sweep. Stopping frequencies are 3825 Hz and 3900 Hz. The arrows indicate the direction the measured amplitude jumps that take place during the time the drive is off. Figure is taken from [146].

- The resonance curves depend on a time not only indirectly through stress $\sigma(t)$ but also explicitly. This dependence is a manifestation of relaxation behavior of sample in dynamic process.
- Other evidence of slow dynamics comprises gradual recovery (increase) of resonant frequency to its original value as defined at extremely low drive level after the sample has been conditioned at a high drive level. The time-dependence of the shift of resonance frequency is almost logarithmic $\delta f \sim \log(t/t_0)$ [143, 145, 147].

8.2 Model of sandstone dynamics at resonance

The above-mentioned facts cannot be understood in the framework of standard theories of resonant nonlinear response [20] and imply memory of peak strain history [146]. Some aspects of the problem have been explained by the interpretation of Guyer *et al.* [54] in the framework of a McCall-Guyer quasistatic model [93]. This approach uses the concept of auxiliary hysteretic elements that allows the introduction of an additional nontrivial nonlinear term in the dynamical equation for the field of longitudinal displacements. However, this theoretical treatment lacks completeness in that it initially neglects the dynamics of hysteretic elements and postulates temporal evolution of the amplitude-frequency characteristic (the key point of claimed results) to be developed afterwards. Although Capogrosso-Sansone and Guyer recently suggested dynamical realization of the McCall-Guyer quasistatic model [27], evaluating its adequacy to explain experimental data turns out to be difficult.

In approach we suggested, we omit the idea of auxiliary hysteretic elements as the sole approach for treating all peculiar hysteretic phenomena. We will carry out the analysis of experimental data in details and give reasons for physical motivated approach to describe the resonance behavior of rocks.

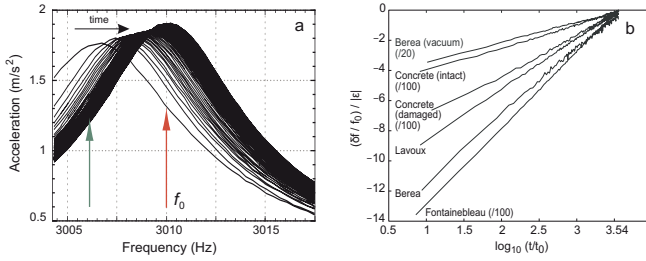


Figure 8.6: Slow dynamical response. (a) Successive resonance sweeps made after a long conditioning sweep. Initial resonance frequency before experiment is at 3010 Hz, resonance frequency immediately after conditioning strain is at 3007 Hz [147]. (b) The time-dependent shift δf of the recovering resonant frequency, normalized to the asymptotic value f_0 , per unit conditioning strain $|\epsilon|$, in several rock types and in concrete [145].

8.2.1 Physical notions on resonance bar dynamics

We have suggested the model of the dynamic behavior of rocks on experimental grounds [194, 195, 196, 201]. The resonance peak shift toward lower frequencies with an increase of driving amplitude is pointed out to be a result of decrease of the Young modulus E . For the sake of convenience the resonance curve for a constant elastic modulus E is presented in Fig. 8.7a. Fig. 8.7b illustrates two resonance curves for two different constants $E_1 > E_2$, whereas the curve L_2 related to a modulus E_2 has a shift down the abscissa axis (frequency).

Henceforth, we explain the resonance curves for dynamic process, when there are some internal exchanged processes in rock's sample under external action, resulting in change of elastic properties of a sample, namely, in change of Young modulus. It is assumed that the value E decreases with the increase of a strain. At first let us consider a case, when the internal processes are in equilibrium with external stress. It is clear that resonance curve at low stress, i.e. away from resonance frequency f_r , is close to the curve L_1 with E_1 . Whereas in the vicinity of a resonance frequency, where stress and strain have maximum values, the resonance curve is to be traced along curve L_2 with E_2 . Hence, when the internal processes are in equilibrium with external loading, then the resonance curve has qualitative form as curve L_3 in Fig. 8.7c.

We need now to take into account the relaxation essence of the internal exchanged processes. Under natural conditions the internal processes have insufficiently time to be in equilibrium with external action. As a result of nonequilibrium between external and internal processes, the strain change has not kept pace with stress change. This effect is known as a relaxation. The connection between macroparameters (in this case between stress and strain) depends additionally on internal processes. Consequently, there is ambiguous connection between macroparameters. From mathematical viewpoint this feature can be described by an explicit time-dependence of a relation between macroparameters. At fixed drive loading (independent macroparameter) the strain (dependent macroparameter) can, nevertheless, have the different values if a

nonequilibrium takes place, i.e. if the internal exchanged processes occur in the sandstone bar under resonance loading.

Developing the model of dynamic behavior of rocks, now we take into account the experimental fact noted in the page 127, namely, that at constant drive amplitude all resonance curves have the same resonance peak, i.e. maximal resonance strain amplitude and resonance frequency. Whereas, the resonance peak does not depend on a

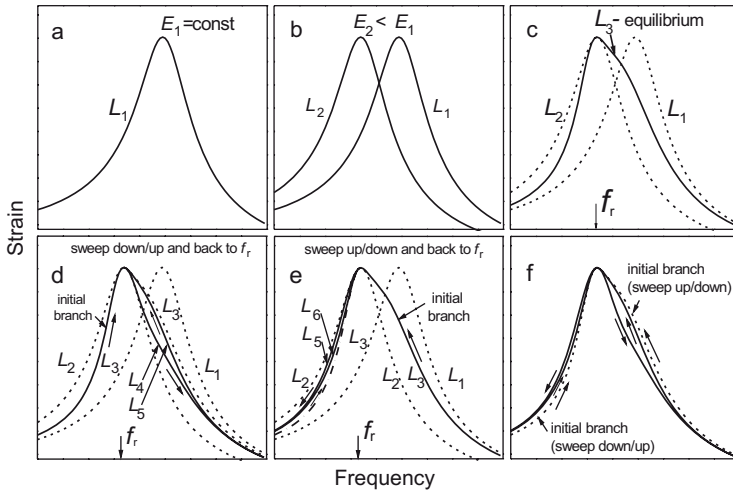


Figure 8.7: Resonance curves: (a) classic case $E_1 = \text{const}$, (b) for case $E_2 < E_1$, (c) equilibrium case for E depended on stress, (d) unconditioned sample with relaxation under frequency sweep from down to up and back to f_r , (e) unconditioned sample with relaxation under frequency sweep from up to down and back to f_r , (f) qualitative resonance curves for modeling experiments.

direction of frequency sweep and on a sample state (unconditioned state or conditioned one). To satisfy this feature and retain the relaxation effects we should make the following assumption. When the driving frequency tends to the resonance frequency f_r (a process in which the strain increases), we assume full equilibrium between stress and strain, while at frequency sweep from resonance frequency f_r (a process in which the strain decreases), we assume that a strain has not kept pace with a stress. It is necessary to draw special attention to the mentioned assumption, because it is sufficiently different from ordinary description, for example, of chemical reactions (low of mass action), where the rate of approach to the equilibrium does not depend on the direction of this approach, i.e. either from high concentration to a equilibrium or from slow concentration to a equilibrium concentration.

With regard for all mentioned above features, we plot the qualitative resonance curves for unconditioned bar under frequency sweep from down to up (see Fig. 8.7d). For a left side of resonance curve, the resonance curve falls on curve L_3 (see Fig. 8.7d). Passing the resonance frequency f_r , on descendant branch, where the sample is in the

conditioned state, the resonance curve L_4 passes between curves L_2 and L_3 , since the relaxation process realizes the gradual approach of curve L_4 to the curve L_3 . If next the frequency sweep comes back, i.e. from up to down, the resonance curve L_5 passes above branch L_4 , however, underlies the curve L_3 (see Fig. 8.7d).

Similarly to the case shown in Fig. 8.7d, we plot resonance curves for process where the initial sweep (unconditioned bar state) begins from up to down (see Fig. 8.7e). The qualitative resonance curve for this case has the form illustrated in Fig. 8.7e. For driving frequencies higher than the resonance frequency ($f > f_r$), the resonance curve passes over curve L_3 , while for frequencies f below f_r , the resonance curve should lie between curves L_2 and L_3 as a result of relaxation. Sweeping the frequency back from lower frequencies to the resonance frequency f_r , we have the resonance curve L_6 between L_3 and L_5 (Fig. 8.7e).

We have proved that the resonance curves shown in Fig. 8.7g can be realized. These resonance curves are qualitatively similar to the curves appeared in experiments (see Fig. 8.2). Finally, we have substantiated the physical model for describing the resonance behavior of sandstone bar.

8.2.2 Kinetics of ruptured cohesive bonds

The experimental resonance curves show that the increase of a strain causes the change of elastic properties of a sandstone bar, so that the Young modulus E decreases. We regard that a direct influence of strain $\partial u \partial x$ on Young modulus E is absent. Meanwhile, the indirect effect of strain on Young modulus, namely the impact mediated by the concentration c of ruptured intergrain cohesive bonds, will be incorporated in our theory as the main source of all nontrivial phenomena mentioned in Sec. 8.1. Here the significant issue is apparently not in excessive (presumably unclaimed) details of all plausible mechanisms that might modify the Young modulus in a qualitatively similar way, but in their reasonable concise formalization by means of a minimal number of slow fields.

Any dynamical model dealing exclusively with a single subsystem of longitudinal displacements is incapable of reproducing the entire suite of phenomena exhibited by sandstones in resonant bar experiments without invoking speculative assumptions (e.g., temporal evolution of the amplitude-frequency characteristic [54]) that does not follow from the original equation or without incorporating auxiliary quantities (e.g., maximum strain excursion [54]) that can be justified only for the quasistatic theory. When holding this position one is unable to depart from an incomplete, fragmentary description. At best, one may have to appeal to a hypothetical slow subsystem only in a rather artificial way [54, 145], i.e., without explicit specification of all relevant (dynamic or kinetic) independent variables and their governing evolution equations, not to mention the mutual feedback between the slow subsystem and the fast elastic one.

We overcome the difficulties of single-subsystem modeling by introducing along with the fast elastic subsystem a slow subsystem of ruptured intergrain cohesive bonds via their concentration c . At any given stress σ (tensile or compressive) the quantity c must evolve to its stress-dependent equilibrium value c_σ . In order to achieve reliable consistency between theory and experiment such an evolution has to be treated as being

nearly logarithmic rather than exponential, on the one hand, and as being sensitive to the sign of the applied stress on the other. Both of these aspects can be readily included in the concept of blended kinetics which is believed to find more or less natural physical justification in consolidated materials. The idea consists in presenting the actual concentration of defects c as some reasonable superposition of constituent concentrations g , where each particular g is proved to obey rather simple kinetics.

We start with considering a set of constituent concentrations. Every particular concentration g in this set is assumed to evolve to its stress-dependent equilibrium value g_σ with the velocity $\partial g/\partial t$ that in the lowest order approximation should be proportional to the difference $g_\sigma - g$. Thus, at $g > g_\sigma$ the ruptured bonds are becoming restored ($\partial g/\partial t < 0$) while at $g < g_\sigma$ the unruptured bonds are becoming broken ($\partial g/\partial t > 0$). Denoting the restoring rate as $\mu = \mu_0 \exp(-U/kT)$ and the rupturing rate as $\nu = \nu_0 \exp(-W/kT)$ we can formalize the earlier statements in terms of the following kinetic equation

$$\partial g/\partial t = -[\mu\theta(g - g_\sigma) + \nu\theta(g_\sigma - g)](g - g_\sigma), \quad (8.2.1)$$

where U and W are the activation barriers for the processes of bond restoration and bond rupturation, respectively, k is the Boltzmann constant, and $\theta(z)$ designates the Heaviside step function.

There is a question whether the rates μ and ν should be the same or different and why. We argue that the parameters μ and ν have to differ substantially inasmuch as the volume attributed to generate a single crack turns out to be essentially mesoscopic although confined to an intergrain space.

Indeed, under a tensile loading there are an immense number of spatial ways for a mesoscopic intergrain cementation contact to be broken with the same basic result: creation of an intergrain crack. Here we understand that any relevant macroscopic characteristic of rock is bound to be insensitive to the particular position of a crack between given neighboring grains but should essentially depend on the cumulative area of cracks per unit volume which can serve as an appropriate measure for the concentration of defects. Similarly, there are various ways for an already existing crack in equilibrium to be further expanded when surplus tensile loading is applied. However, under compressive loading a crack, once formed, has only one spatial way to be annihilated or contracted. These are the key observations that imply a large disparity $\nu_0 \gg \mu_0$ between the rates ν_0 and μ_0 regardless of the cohesive properties of the cementation material. Moreover, because of possible water intercalation and/or fine fragmentation of cementation material between opposite faces of a crack, we can expect the typical value of U to exceed that of W . In combination all these factors might sustain an even greater disparity $\nu \gg \mu$ between the actual rates ν and μ of defect creation and defect annihilation that may amount to many orders. This conclusion, which relies on the mesoscopic scale of the structural elements involved, finds a natural analogy on the macroscopic level when samples once having been broken remain broken practically forever.

Up to now we specified only a particular constituent concentration of defects g that can be labeled by the pair of fixed activation parameters U and W . In reality, any small but still macroscopic volume of sandstone contains a huge variety of structural elements distinguished by size, composition, natural cleavage, etc. As a result, activation barriers

for the process of cohesion restoration U and the process of cohesion rupture W have to be distributed over some ranges, which we denote as $U_0 \leq U \leq U_0 + U_+$ and $W_0 \leq W \leq W_0 + W_+$, respectively. Although the types of these distributions are unknown, their characteristics U_0, U_+ and W_0, W_+ must be insensitive to a particular choice of bar's cross-section in accordance with specimen homogeneity (similarity) on the macroscopic scale. Of course, the very number of these characteristics is insufficient to specify the set of constituent concentrations constructively, i.e., we still lack a definite recipe for how (with what weight) any constituent concentration of defects g should contribute to the actual (averaged) concentration of defects c . Thus, to proceed further some additional assumptions about the distributions of activation barriers must be added. For the sake of definiteness we approximate the barriers U and W as distributed independently and uniformly within the intervals given earlier. Thus, the relative number of restoration barriers in the interval dU surrounding U at W being fixed is taken to be $\theta(U - U_0)\theta(U_0 + U_+ - U)dU/U_+$, while the relative number of rupture barriers in the interval dW surrounding W at U being fixed is taken to be $\theta(W - W_0)\theta(W_0 + W_+ - W)dW/W_+$. As a consequence the actual concentration of ruptured cohesive bonds c is determined by the constituent concentration g via the formula

$$c = \frac{1}{U_+W_+} \int_{U_0}^{U_0+U_+} dU \int_{W_0}^{W_0+W_+} g dW. \quad (8.2.2)$$

This expression does not contradict the next assumption

$$g_\sigma = c_\sigma, \quad (8.2.3)$$

relating the equilibrium value of actual concentration of ruptured bonds c_σ to the equilibrium value of constituent concentration of ruptured bonds g_σ , where both c_σ and g_σ are prescribed by the stress σ . As a matter of fact, only the quantity c_σ might find a legitimate place in standard thermodynamical estimations [79, 80, 113], whereas in dealing with g_σ we must lean upon more or less plausible conjecture, e.g. as established by formula (8.2.3).

According to Kosevich [79, 80] the equilibrium concentration of defects associated with a stress σ is given by the expression

$$c_\sigma = c_0 \exp(v\sigma/kT), \quad (8.2.4)$$

where the parameter $v > 0$ stands for a typical volume accounting for a single defect and characterizes the intensity of dilatation. Although the formula (8.2.4) should supposedly be applicable to the ensemble of microscopic defects in crystals, it was derived in the framework of continuum thermodynamic theory that does not actually need any specification of either the typical size of elementary defect or the particular structure of the crystalline matrix. For this reason we believe it should also work for an ensemble of mesoscopic defects in consolidated materials, provided that for a single defect we shall understand some elementary rupture of intergrain cohesion. The equilibrium concentration of defects in an unstrained, completely recovered bar c_0 has to be some function of temperature T and water saturation s . The particular character of these dependences does not follow from first principles and needs to be extracted from experiments.

At this point we introduce a phenomenological relationship between defect concentration c and Young modulus E . Intuition suggests that E must be some monotonically decreasing function of c , which can be expanded in a power series with respect to a small deviation of c from its unstrained equilibrium value c_0 . In the lowest approximation we can drop all powers except the zeroth and first and as a result safely rearrange the required relation into the form

$$E = (1 - c/c_{\text{cr}}) E_+. \quad (8.2.5)$$

Here c_{cr} and E_+ are the critical concentration of defects and the maximum possible value of Young modulus, respectively. Both of these parameters we take to be independent of temperature and water saturation.

According to the relationship (8.2.5) the actual concentration of defects c is incorporated as normalized by its critical value c_{cr} . For this reason there is no need to supply the quantities c , c_σ , and c_{cr} by any particular units, though the units must be the same for all three quantities. As for the units of the running and equilibrium constituent concentrations g and g_σ it is sufficient to know only their relationship to the units of actual concentration given by the expression (8.2.3).

At constant loading, the kinetic equation (8.2.1) ensures that the concentration c tends to its equilibrium value c_σ given by formula (8.2.4), and as a consequence the Young modulus (8.2.5) attains the magnitude

$$E_\sigma = [1 - (c_0/c_{\text{cr}}) \exp(v\sigma/kT)] E_+. \quad (8.2.6)$$

It is worth noticing that the resulting functional dependence of E_σ on σ almost exactly matches the experimentally established fitting formula for elastic moduli as a function of an applied loading $P \sim -\sigma > 0$ (see, e.g., Ref. [72], and references therein). Furthermore, the relation (8.2.6) taken at zero stress $s=0$ allows us to reconstruct the temperature and saturation dependences of the unstrained equilibrium concentration of defects c_0 using available experimental data for the Young modulus E_0 in unstrained, recovered samples. Thus, if we take into account the Sutherland temperature extrapolation [140, 213] and analyze temperature-dependent data at zero saturation [144] plus saturation-dependent data at room temperature [2] (selected for Berea sandstone), we are able to suggest the following fitting formula:

$$c_0 = c_{\text{cr}} \left(\frac{T}{T_{\text{cr}}} \right)^2 \left[\cosh^2 \alpha - \exp \left(-\frac{\beta s}{1-s} \right) \sinh^2 \alpha \right], \quad (8.2.7)$$

where saturation s varies within the interval $0 \leq s \leq 1$. The fitting parameters relevant for Berea sandstone are as follows $T_{\text{cr}} = 1475^{\circ}\text{K}$, $\cosh^2 \alpha = 16$, $\beta = 10$. At $s \neq 0$ our approximation is expected to work at least within the temperature range between irreversible damage thresholds of sedimentary rocks, namely between the freezing-point of pore water ($\approx 273^{\circ}\text{K}$) and the baking point of interstitial clays ($\approx 345^{\circ}\text{K}$).

The significant issue of our approach is contained in the kinetic equation (8.2.1) that can be applied to both static and dynamic regimes of external loading. In the latter case, however, for c_σ and g_σ we must consider the would-be equilibrium quantities, i.e., quantities given by formulas (8.2.4) and (8.2.3) where the stress σ is taken to be dynamical one.

At small dynamical stresses $|\sigma| \ll kT/v$ the exponent $\exp(v\sigma/kT)$ dominating the expression (8.2.4) for c_σ can be readily approximated by the two first terms in its expansion. Because of relation (8.2.3) a similar approximation applies for g_σ . Nevertheless, this fact does not indicate a zero-valued, long-term correction to g_0 in the solution g of the kinetic equation (8.2.1) as might be roughly expected. On the contrary, the great disparity $\nu \gg \mu$ between the rate of defect creation ν and the rate of defect annihilation μ turns out to provide the physical mechanism that breaks the symmetry of system response to an alternating external drive and acts as a sort of soft ratchet or leaky diode. It is the core of this modeling.

In contrast, earlier theories of inelastic relaxation developed for crystalline solids [113] rely upon a symmetric form of the kinetic equations (corresponding to $\nu \equiv \mu$ in our notations) and do not assume the equilibrium value of the internal relaxation parameter (corresponding to g_σ in our notations) to be driven dynamically. Also, earlier theories of crack formation [123] differ from our approach in that they neglect the possibility of crack recuperation (i.e., they assume $\mu = 0$ in our notations) and do not incorporate a variable concentration of defects into the right-hand side of the appropriate kinetic equation.

8.2.3 Motion equations. Problem on bar resonance

For describing the experiments on bar resonance [54, 55, 57, 71, 143, 145, 146, 147], we assume that the alternating strain configuration inside the bar is principally longitudinal, and has to be treated as kinematically excited [202]. For the evolution equation for the field of longitudinal displacements (referred to also as the elastic subsystem) we write the most general form

$$\rho \frac{\partial^2 u}{\partial t^2} = \frac{\partial \sigma}{\partial x} + \frac{\partial}{\partial x} \left[\frac{\partial \mathcal{F}}{\partial (\partial^2 u / \partial x \partial t)} \right], \quad (8.2.8)$$

evaluating its content step-by-step. Thus, the dissipative function \mathcal{F} must be some even function of strain velocity $\partial^2 u / \partial x \partial t$ in order to ensure both the positiveness and the internal character of dissipation. Here we restrict ourselves to the Stokes internal friction [137] associated with the dissipative function

$$\mathcal{F} = (\gamma/2) [\partial^2 u / \partial x \partial t]^2. \quad (8.2.9)$$

The quantities ρ and γ are, respectively, the mean density of sandstone and the coefficient of internal friction in an elastic subsystem. In what follows, the dependences of ρ and γ in Eqs. (8.2.8) and (8.2.9) on temperature T , water saturation s , and strain $\partial u / \partial x$ will be ignored. The stress-strain relation ($\sigma - \partial u / \partial x$) we adopt in the form

$$\sigma = \frac{E \operatorname{sech} \eta}{(r-a) [\cosh \eta \partial u / \partial x + 1]^{a+1}} - \frac{E \operatorname{sech} \eta}{(r-a) [\cosh \eta \partial u / \partial x + 1]^{r+1}} \quad (8.2.10)$$

which at $r > a > 0$ allows one to block the bar compressibility at strain $\partial u / \partial x$ tending toward $+0 - \operatorname{sech} \eta$. Thus, the parameter $\cosh \eta$ is assigned for a typical distance

between the centers of neighboring grains divided by the typical thickness of intergrain cementation contact, while the exponents r and a characterize the repulsive and the attractive parts of intergrain interaction, respectively. In other words, we approximate the potential of grain-grain interaction by the empirical Mie potential. At small strains $|\partial u/\partial x| \ll \text{sech } \eta$ we obtain

$$\begin{aligned} \frac{\sigma}{E\partial u/\partial x} &\approx 1 - \frac{1}{2}(r+a+3) \text{sech } \eta \partial u/\partial x \\ &\quad + \frac{1}{6}(r^2+ar+a^2+6r+6a+1)(\text{sech } \eta \partial u/\partial x)^2, \end{aligned} \quad (8.2.11)$$

and, hence, the parameters r , a , $\cosh \eta$ are seen to completely specify the nonlinear corrections to Hooke law, provided that a direct influence of strain $\partial u/\partial x$ on Young modulus E is absent. The indirect effect of strain on Young modulus is considered to associate with the concentration c of ruptured intergrain cohesive bonds (see Sec. 8.2.2)

The relevant boundary conditions for the field of longitudinal displacements u that conform to the resonant loading in experiments [202]:

$$u(x=0|t) = D(t) \cos \left(\varphi + \int_0^t d\tau \omega(\tau) \right), \quad (8.2.12)$$

$$\sigma(x=L|t) + \gamma \frac{\partial^2 u}{\partial x \partial t}(x=L|t) = 0, \quad (8.2.13)$$

where t is time and x denotes the running longitudinal Lagrange coordinate of the bar with $x=0$ and $x=L$ marking its driven and free ends, respectively. As a rule, the driving amplitude $D(t)$ is set to be basically constant except for the moments when the driving device is switched on, is switched into another constant driving level, or is switched off, whereas the time dependence of cyclic driving frequency $\omega(t)$ is prescribed by the type of frequency sweep. Another kind of experiment where the parts played by the driving amplitude $D(t)$ and the driving frequency $\omega(t)$ are reversed would also be informative.

The only thing remaining to be specified is the initial conditions. They must depend on the sample's prehistory. Thus, for the unstrained, completely recovered bar the initial conditions are written as follows:

$$u(x|t=0) = 0, \quad \frac{\partial u}{\partial t}(x|t=0) = 0, \quad g(x|t=0) = c_0, \quad (8.2.14)$$

where $0 < x < L$.

Summarizing the content of Sec. 8.2, we have formulated the principal theoretical propositions of our model and have formalized them in terms of two coupled, essentially nonlinear subsystems. First, we have suggested a dynamical equation for the field of longitudinal displacements (8.2.8) with the appropriate specification of the dissipative function (8.2.9), the stress-strain relation (8.2.10), and the impact of defect concentration on Young modulus (8.2.5). Second, we have developed a soft-ratchet-type kinetic equation for the constituent concentration of defects (ruptured intergrain cohesive bonds) (8.2.1) with the appropriate specifications of stress-guided, would-be equilibrium constituent concentration of defects (8.2.3) and would-be equilibrium actual concentration of defects (8.2.4) and have adopted a reasonable relation between

the constituent concentration and the actual concentration of ruptured intergrain cohesive bonds (8.2.2). We also have presented boundary and initial conditions for the field of longitudinal displacements (8.2.12) and (8.2.13) allowing us to formalize the effect of the transducer on the whole bar system.

8.3 Soft-ratchet kinetics under harmonic drive

In this section we illustrate two different kinetic regimes of defect creation and annihilation under an alternating drive that can be the basic to qualitative understanding of experimental results as well as their computerized replicas. For this purpose we introduce a quantity (the surplus constituent concentration)

$$G \equiv g - g_0, \quad (8.3.1)$$

that measures the excess $G > 0$ or shortage $G < 0$ of defects relative to the unstrained background g_0 , and we approximate the impact of the dynamic subsystem onto the kinetic subsystem by a single harmonic

$$G_\sigma \equiv g_\sigma - g_0 = A \sin(\omega t + \delta), \quad (8.3.2)$$

where A and δ are some functions of the longitudinal coordinate x . Their particular forms do not need to be specified because at each fixed x the quantity G obeys the ordinary differential equation

$$dG/dt = -[\mu\theta(G - G_\sigma) + \nu\theta(G_\sigma - G)](G - G_\sigma). \quad (8.3.3)$$

Note, however, that to the lowest order the amplitude A is proportional to the amplitude ε of strain

$$\frac{\partial u}{\partial x} = \varepsilon \sin(\omega t + \delta), \quad (8.3.4)$$

taken in the same single mode approximation. The proportionality coefficient $\nu c_0 E/kT$ can be readily extracted from expressions (8.3.2) and (8.3.4) with the approximate stress-strain relation $\sigma = E\partial u/\partial x$ and formulas (8.2.3), (8.2.4) for g_σ and c_σ . Here for the sake of simplicity we ignore the time dependence of Young modulus through the total concentration of defects.

Starting from the zeroth value $G(t = 0) = 0$ the kinetic equation (8.3.3) and the sinusoidal drive (8.3.2) cause surplus constituent concentration G to grow in each cycle $2\pi/\omega$ in a nearly steplike fashion for $\mu \ll \nu \leq \omega/2\pi$ (Fig. 8.8). Time intervals of fast increase controlled by rate ν are determined from the inequality

$$A \sin(\omega t + \delta) - G(t) > 0, \quad (8.3.5)$$

whereas time intervals of slow decrease controlled by rate μ are determined from the opposite inequality

$$A \sin(\omega t + \delta) - G(t) < 0. \quad (8.3.6)$$

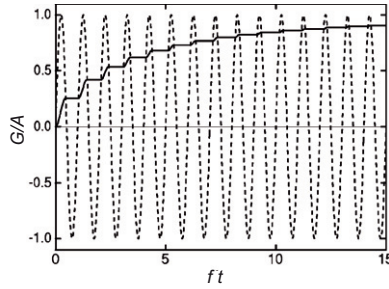


Figure 8.8: Normalized solution G/A of the soft-ratchet kinetic equation (8.3.3) with sinusoidal stimulation (8.3.2) at $\mu = 1 \text{ s}^{-1}$, $\nu = 4000 \text{ s}^{-1}$, $f = \omega/2\pi = 4000 \text{ Hz}$, $\delta = 0$, and the initial condition $G(t = 0) = 0$ (solid steplike line). The dashed line indicates the normalized sinusoidal stimulation $G_\sigma/A = \sin \omega t$. Time along the abscissa is normalized to the oscillation period $1/f$.

A time interval of increase is followed by a time interval of decrease and vice versa, yielding a net full step in each cycle $2\pi/\omega$.

Although the kinetic equation (8.3.3) could be integrated analytically at every time interval where either inequality (8.3.5) or (8.3.6) holds, it is impractical to match such piecewise solutions into a concise expression suitable for qualitative analysis. Instead, even a quick look at the computer solutions (Fig. 8.9) is sufficient to evaluate the mean (time-averaged) magnitude H of the steady-state solution for G in comparison with the amplitude A as well as to estimate the effective rate λ of cyclic buildup of surplus constituent concentration G under an oscillating loading in comparison with the rate ν of monotonic growth of G under a constant tensile loading. In preparing Fig. 8.9 we

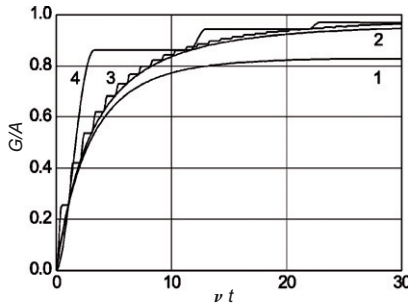


Figure 8.9: Normalized solution G/A of the soft-ratchet kinetic equation (8.3.3) under sinusoidal stimulation (8.3.2). Curves $j = 1, 2, 3, 4$ correspond to successively higher rates of defect creation $\nu_j = 4 \cdot 10^j \text{ s}^{-1}$ with all other parameters from Fig. 8.8 being preserved. Time on the abscissa is normalized to the inverse rate of defect creation $1/\nu$ separately for each curve.

took the rate μ to coincide with its maximum value $\mu_0 \exp(-U_0/kT) = 1 \text{ s}^{-1}$, which

in Sec. 8.4 will be adopted for interpreting experimental results on slow dynamics. The frequency $f \equiv \omega/2\pi$ was chosen to be 4000 Hz, and the rate ν was tested at four essentially different values 40, 400, 4000, and 40 000 s⁻¹ (Fig. 8.9, curves 1, 2, 3, and 4, respectively). All four curves strongly indicate that for $\nu \geq 0.01f$ the effective rate λ of cyclic buildup does not drop more than five or six times below the rate ν . Moreover, at $\nu \geq 0.01f$ the ratio H/A always exceeds value of 0.8 and rapidly approaches unity as the ratio ν/f increases. Another significant observation consists in the almost total suppression of periodical fluctuations of steady-state solution G around its mean value H (Fig. 8.10).

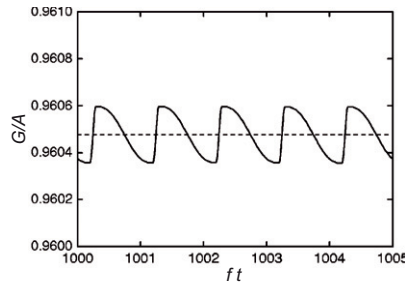


Figure 8.10: Normalized solution G/A of the soft-ratchet kinetic equation (8.3.3) at an essentially steady stage of its evolution (solid line). The dashed line represents the mean value H/A of the normalized steady-state solution. Conditions used for calculations of curve 2 from Fig. 8.9 are preserved. Time along the abscissa is normalized to the oscillation period $1/f$.

The results presented in the subsection 8.2.2 can be readily applied to the case when the amplitude A is not constant but grows with time sufficiently slowly such that $0 < \dot{\varepsilon}/\varepsilon \ll \lambda \sim 0.2\nu$; the overdot denotes the derivative with respect to time t . Then at $\nu \geq 0.01f$ we can safely treat the surplus defect concentration G as a time dependent quantity that effectively tracks amplitude A . There is a reason to believe that both the above requirements are fulfilled in resonant bar experiments as frequency sweeps toward a resonance. Thus, the inequality $0 < \dot{\varepsilon}/\varepsilon \ll 0.2\nu$ is maintained by the fact that typical sweeps around resonance [146] are unable to sustain the rate $|\dot{\varepsilon}|/\varepsilon$ by more than 0.5 s^{-1} . As for the inequality $0.01f \leq \nu$, it seems to be in line with our hypothesis of strong inequality $\mu \ll \nu$ secured by many orders as given in Sec. 8.2.

We now inspect the regime of slow relaxation in the subsystem of intergrain ruptured bonds. This regime occurs after the surplus constituent concentration G has been pumped to some steady-state magnitude B and then the conditioning oscillating drive is drastically reduced at time $t = t_c$. In this case (at $t > t_c$) the strong inequality $B \gg A$ holds, and the elastic subsystem serves only for probing the resonant frequency, while its impact on the subsystem of ruptured bonds can be totally neglected. Thus, we omit the term G_σ through the kinetic equation (8.3.3) and obtain

$$dG/dt = -\mu G, \quad (8.3.7)$$

bearing in mind that the regime of interest starts at $t = t_c$ with $G(t = t_c) = B$. Here the quantity B is estimated to be

$$B = c_0 \left[\exp \left(\frac{v\sigma_+}{kT} \right) - 1 \right], \quad (8.3.8)$$

where $\sigma_+ > 0$ stands for the maximum stress determined by the amplitude of stress oscillations under dynamical conditioning.

The approach just formulated is undoubtedly valid to describe the process of relaxation after tensile static conditioning when σ_+ should be understood as the positive end-point stress. We expect it could be also applied to treat relaxation phenomena after an abrupt thermal disturbance provided σ_+ is identified with some effective rupturing stress predetermined by the absolute value of thermal shock.

The kinetic equation (8.3.7) for surplus constituent concentration G yields an exponential decay

$$G = B \exp[-\mu(t - t_c)]. \quad (8.3.9)$$

at $t \geq t_c$. However, this by no means causes the actual surplus of defect concentration $c - c_0$ to diminish exponentially. On the contrary, inserting the solution (8.3.9) into the formula (8.2.2) with the use of definition (8.3.1) we easily obtain

$$c = c_0 + \frac{B}{\chi} \{E_1[\tau \exp(-\chi)] - E_1(\tau)\}. \quad (8.3.10)$$

Here

$$\tau \equiv \mu_0 \exp(-U_0/kT)(t - t_c) \quad (8.3.11)$$

denotes a unitless time, whereas

$$\chi \equiv U_+/kT \quad (8.3.12)$$

determines a unitless width of energy interval occupied by the distribution of activation barriers for the process of cohesion restoration. Finally

$$E_1(z) = \int_1^{\infty} \frac{dy}{y} \exp(-zy) \quad (8.3.13)$$

designates the integral exponential function [77].

Despite its name, $E_1(z)$ initially behaves logarithmically as clearly seen in its analytic expansion for $z < 1$ [77]

$$E_1(z) = -C - \ln z - \sum_{n=1}^{\infty} (-1)^n \frac{z^n}{n \cdot n!}, \quad (8.3.14)$$

where $C \simeq 0.577\,215\,7$ stands for the Euler-Mascheroni constant. In its final stages $z > 1$, however, use of the asymptotic series [77]

$$E_1(z) = \frac{\exp(-z)}{z} \left[1 + \sum_{n=1}^{\infty} (-1)^n \frac{n!}{z^n} \right] \quad (8.3.15)$$

turns out to be appropriate.

We apply expansions (8.3.14) and (8.3.15) to the most plausible case of $\exp(\chi) \gg 1$ and approximate the difference $E_1(\tau \exp(-\chi)) - E_1(\tau)$ controlling the temporal restoration of defect concentration (8.3.10) by the following piecewise formula:

$$E_1(\tau \exp(-\chi)) - E_1(\tau) \approx \begin{cases} \chi - \tau + \tau^2/4 + \tau \exp(-\chi), & \tau < \xi_- \\ \chi - C - \ln \tau + \tau \exp(-\chi), & \xi_- \leq \tau \leq \xi_+ e^\chi \\ \frac{\exp(-\tau \exp(-\chi))}{\exp(-\chi)}, & \xi_+ e^\chi < \tau. \end{cases} \quad (8.3.16)$$

Here the constants $\xi_- \simeq 1.391\,099\,0$ and $\xi_+ \simeq 0.928\,630\,6$ are determined as the solutions of transcendental equations

$$-\xi_- + \xi_-^2/4 = -C - \ln \xi_- \quad (8.3.17)$$

and

$$-C - \ln \xi_+ + \xi_+ = \frac{\exp(-\xi_+)}{\xi_+}, \quad (8.3.18)$$

respectively. Equations (8.3.17) and (8.3.18) supply matching conditions to ensure that the piecewise representation (8.3.16) will be a continuous function at points $\tau = \xi_-$ and $\tau = \xi_+ \exp(\chi)$, respectively. The larger is the inequality $\exp(\chi) \gg 1$, the longer becomes the interval of almost logarithmic time-dependence in formula (8.3.16).

Formulas (8.3.8), (8.3.10), and (8.3.16) substituted into the linear relationship (8.2.5) between Young modulus E and the concentration of defects c allow us to analytically reproduce the slow, nearly logarithmic recovery (increase) of Young modulus

$$E = \left(1 - \frac{c_0}{c_{cr}}\right) E_+ - E_+ \frac{c_0}{c_{cr}} \left[\exp\left(\frac{v\sigma_+}{kT}\right) - 1 \right] \\ \times \left\{ 1 - C \frac{kT}{U_+} - \frac{kT}{U_+} \ln \left[\mu_0 \exp\left(-\frac{U_0}{kT}\right) (t - t_c) \right] \right. \\ \left. + \frac{kT}{U_+} \mu_0 \exp\left(-\frac{U_0 + U_+}{kT}\right) (t - t_c) \right\} \quad (8.3.19)$$

over the very wide time interval

$$\frac{\xi_-}{\mu_0} \exp\left(\frac{U_0}{kT}\right) < t - t_c < \frac{\xi_+}{\mu_0} \exp\left(\frac{U_0 + U_+}{kT}\right). \quad (8.3.20)$$

This type of recovery is experimentally observed by monitoring temporal variation of resonant frequency after the conditioning drive has been removed [145].

The idea supporting the logarithmic recovery of Young modulus had earlier been advocated by Ten Cate, Smith and Guyer [145], although without identifying the proper time interval (8.3.20) where the logarithmic dependence holds and omitting the small linear correction (the last term in parentheses of expression (8.3.19)) to the leading logarithmic pattern. It is interesting to note that logarithmic kinetics have been also attributed to the process of moisture-induced aging in granular media [19].

8.4 Modeling of resonant nonlinear effects

The vast majority of experimental results on forced longitudinal oscillations of sandstone bars use the slow, stepwise frequency sweeps over one of the bar resonant frequencies [54, 55, 57, 71, 145, 146, 147]. A rough estimation based on the linear theory of kinematic excitation yields the fundamental frequencies

$$f_0(l) = \frac{2l-1}{4L} \sqrt{E_0/\rho} \quad (l = 1, 2, 3, \dots), \quad (8.4.1)$$

where E_0 is the Young modulus in an unstrained, recovered sample given by formula (8.2.6) at $\sigma = 0$, and attenuation γ is taken to be negligible. The relative

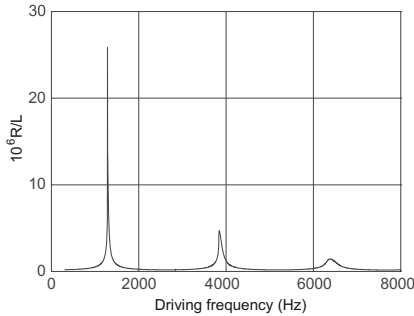


Figure 8.11: Calculated resonance curve illustrating the relative positions of the first three resonance peaks under longitudinal kinematic excitation for a rock bar.

positions of fundamental frequencies at finite attenuation as calculated for slow upward frequency sweep are displayed in Fig. 8.11. Here the resonance curve shows the dependence of response amplitude R (taken on free end of the bar $x = L$) on drive frequency $f = \omega/2\pi$ at very small drive amplitude $D = 7.6 \cdot 10^{-9}L$ and with the model parameters as assumed for the next figure.

Figure 8.12 shows typical hysteretic resonance curves calculated in the vicinity of the second resonant frequency at successively higher drive amplitudes D . In order to achieve repeatable hysteresis each successive pair of curves was calculated following two preliminary sweep calculations. Such curves are usually referred to as being conditioned [146]. Arrows on the two highest curves indicate sweep directions. The cycle time for an up plus down sweep over the frequency interval 3700–4100 Hz was chosen to be 120 s. Model parameters were adopted to fit the experimental conditions and the experimental data as observed by Ten Cate and Shankland in experiments on Berea sandstone [146]. In particular, the ratio $E_+/\rho = 7.439 \cdot 10^6 \text{ m}^2/\text{s}^2$ was estimated from relationships (8.4.1), (8.2.6), and (8.2.7) with the second order frequency, bar length, temperature, and saturation as follows $f_0(l = 2) = 3920 \text{ Hz}$, $L = 0.3 \text{ m}$, $T = 297^{\circ}\text{K}$, and $s = 0.25$. The ratio $\gamma/\rho = 1.851 \text{ m}^2/\text{s}$ characterizing internal friction was chosen from the best fit of low amplitude theoretical curve (Fig. 8.12) to its experimental prototype [146] via comparison of quality factors. The parameters

$\mu_0 \exp(-U_0/kT) = 1 \text{ s}^{-1}$ and $U_+/k = 2525^\circ\text{K}$ determining the character of slow relaxation were estimated in accordance with experimental measurements of temporal relaxation of response acceleration amplitude at fixed frequency [146] and observations of recovering resonant frequency as a function of time [145]. Due to the rather slow typical regimes of frequency sweep corresponding to actual experiments there is neither the experimental possibility nor the theoretical need to designate particular values for parameters $\nu_0 \exp(-W_0/kT)$ and W_+/k that are responsible for defect creation kinetics. This is because above some critical value depending on driving frequency the combination $\nu_0 \exp(-(W_0 + W_+)/kT)$ gives rise to results indistinguishable from those obtained assuming the combination to be infinite. According to the estimations of previous section the condition that the kinetics of defect creation could be treated as practically instantaneous (i.e., formally characterized by infinite rate ν) is fulfilled already provided the inequality $0.01 f_0 \leq \nu_0 \exp(-(W_0 + W_+)/kT)$ holds. The combination of parameters $\nu E_+/k \cosh \eta = 275^\circ\text{K}$ was chosen to quantitatively reproduce hysteretic phenomena in the sweep regimes typical of actual experiments [146]. Finally, the nonlinearity parameters $\cosh \eta = 2300$, $r = 4$, $a = 2$ were estimated to map the true asymmetry of experimental resonance curves [146]. It is significant that the chosen model parameters from Figs. 8.12 are suitable to describe all other known experimental results. This fact counts in favour of the suggested theory.

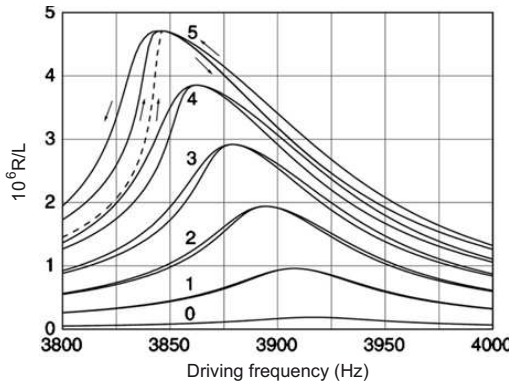


Figure 8.12: Resonance curves $j = 0, 1, 2, 3, 4, 5$ at successively higher driving amplitudes $D/L = 3.8(j + 0.5\delta_{j0}) \cdot 10^{-8}$. The dashed line represents an unconditioned state, and the solid line represents the conditioned states. Arrows on the two highest curves indicate sweep directions. The absolute value of sweep rate is $|du_f/dt| = 400 \text{ Hz/min}$. Water saturation is taken to be $s = 0.25$.

From Fig. 8.12 we clearly see that at each level of external drive the effective width of resonance peak depends on the direction of frequency sweep being narrower for upward sweep (i.e., from lower to higher frequencies) than for downward sweep (i.e., from the higher to lower frequencies). As a result we observe the hysteretic loops formed by upward and downward curves both on their low and high-frequency slopes. Historically this effect proved to be the first manifestation of slow dynamics [146] caused according

to our theory by the net creation of intergrain defects when the driving frequency closely approaches to resonance (i.e., when the amplitude of alternating stress increases) and rather slow their annihilation when the driving frequency departs from resonance (i.e., when the amplitude of alternating stress decreases). It is worth noticing that in the case of conditioned curves considered above annihilation of intergrain defects persists even when the driving frequency approaches resonance from far away until the amplitude of alternating stress overcomes some threshold above which defect creation prevails.

The resonance curves in Figs. 8.13a and 8.13b were calculated without any preliminary conditioning but with all model parameters for Fig. 8.12 preserved. The drive amplitude was chosen to be the same as for two highest curves on Fig. 8.12. Thus

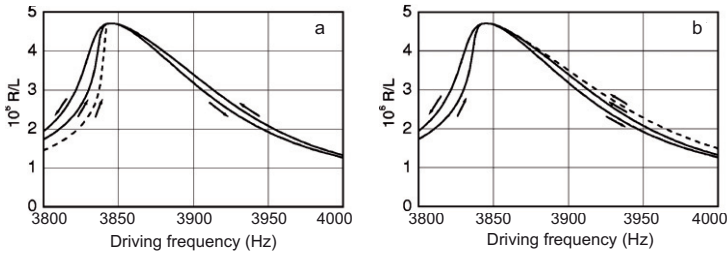


Figure 8.13: Resonance curves at driving amplitude $D = 1.9 \cdot 10^{-7} L$. Arrows indicate sweep directions. The absolute value of sweep rate is $|df/dt| = 400 \text{ Hz/min}$. The dashed line in Fig. 8.13a represents the unconditioned initial curve made on the upward sweep. The dashed line in Fig. 8.13b represents the unconditioned initial curve made on the downward sweep.

Fig. 8.13a demonstrates three resonance curves obtained during the three successive (upward-downward-upward) frequency sweeps beginning with an upward sweep. The initial, unconditioned, curve marked by the dashed line lies below the two subsequent curves. Figure 8.13b demonstrates three resonance curves obtained during the three successive (downward-upward-downward) frequency sweeps beginning with a downward sweep. The initial curve marked by the dashed line lies above two subsequent curves. The curves marked by the solid lines in Figs. 8.13a and 8.13b are practically repeatable and coincide with the respective two highest curves on Fig. 8.12. All these results are in complete agreement with experimental observations [146]. The reason why the conditioned curve does not coincide with its unconditioned (initial) counterpart in the sweep interval between the starting frequency and the resonant frequency lies in the softer value of conditioned Young modulus caused by an unrelaxed excess of defects created during the initial sweep.

As sweep rate decreases, the mentioned differences become less pronounced thanks to the additional time for relaxation at each spanning frequency. This point is illustrated in Figs. 8.14a and 8.14b where the sweep rate was a hundred times slower than for Figs. 8.13a and 8.13b. Nevertheless, even in this supposedly nonhysteretic case the memory of the highest strain amplitude still persists. The latter result characterized after its experimental detection [146] as "perhaps surprising" can be readily explained by the long-term recovery of Young modulus dictated by the slow, almost logarithmic ki-

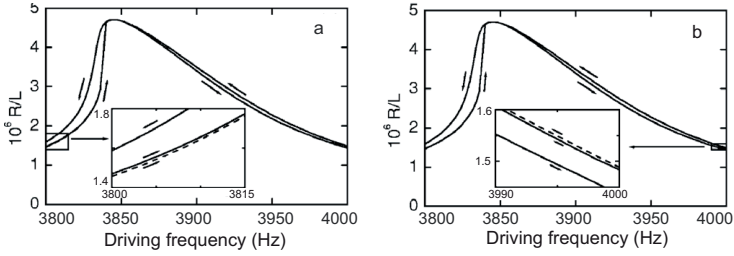


Figure 8.14: Resonance curves at driving amplitude $D = 1.9 \cdot 10^{-7}L$. The absolute value of sweep rate is slowed to $|df/dt| = 4\text{ Hz/min}$. Arrows indicate sweep directions. The dashed line in Fig. 8.14a resolvable only in the magnified inset represents the unconditioned initial curve made on the upward sweep. The dashed line on Fig. 8.14b resolvable in the magnified inset represents the unconditioned initial curve made on the downward sweep.

netics of defect annihilation (see formulas (8.3.19), (8.3.20), (8.3.10) and (8.3.16) from Sec. 8.3). With still slower sweep times exceeding one day all three curves become indistinguishable regardless of direction of the initial sweep. This theoretical result corroborates an indirect experimental indication in fixed-frequency measurements of acceleration that a sweep time of a few days in carefully controlled conditions would produce the same up and down resonance curves [146].

Figure 8.15 compares the shifts of resonant frequency as functions of driving amplitude at two different values of dilatation parameter v while other parameters were kept the same as in Fig. 8.12. Thus curve 1 calculated at $vE_+/k \cosh \eta = 275^\circ\text{K}$, for which

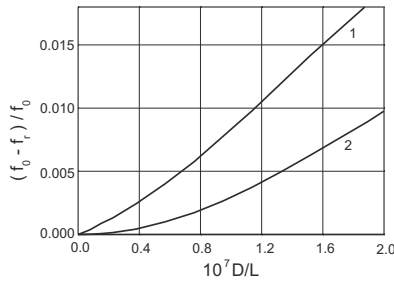


Figure 8.15: Negative value of the shift $f_r - f_0$ of peak frequency f_r from its asymptotic value f_0 as a function of normalized driving amplitude D/L for a hysteretic nonlinear material (curve 1) and for a classical nonlinear material with $v = 0$ (curve 2).

strain-induced feedback between the slow and fast subsystems is substantial, demonstrates the almost linear dependence typical of materials with nonclassical nonlinear response, i.e., materials that possess the basic features of slow dynamics. In contrast, curve 2 calculated at $v = 0$, when strain-induced excitation of the slow subsystem is absent and, hence, the mutual feedback between the slow and the fast subsystems

is totally broken, demonstrates the almost quadratic dependence typical of materials with classical nonlinear response [20]. Closer inspection indicates that curve 1 can be approximated by the linear and the quadratic terms, which are in line with the second-order polynomial fit of Young modulus extracted by Smith and Ten Cate from the experiments [136].

Apart from the reason mentioned earlier, measurements of temporal relaxation of acceleration amplitude at fixed frequency provide experimental documentation of how a rock gradually loses memory of the highest strain [146], and they thus elucidate the most interesting aspects of bond restoration kinetics. Figures 8.16 shows theoretical relaxation curves that correctly reproduce the main features of the experiments [146]. While making a repeatable up or down resonance curve (with all model parameters

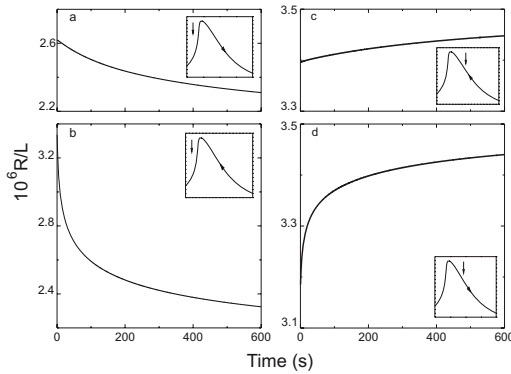


Figure 8.16: Decay of response amplitude R at driving amplitude $D = 1.9 \cdot 10^{-7}L$. (a), (b) a fixed frequency $f_s=3825$ Hz, lower than the peak frequency at $f_r=3846$ Hz. In Fig. 8.16a the sweep was stopped while making a repeatable upward sweep. In Fig. 8.16b the sweep was stopped while making a repeatable downward sweep. (c), (d) a fixed frequency $f_s=3900$ Hz, higher than the peak frequency at $f_r=3846$ Hz. In Fig. 8.16c the sweep was stopped while making a repeatable downward sweep. In Fig. 8.16d the sweep was stopped while making a repeatable upward sweep.

the same as for the two highest curves of Fig. 8.12) we stopped the sweep at time t_s (drive still on) and calculated the amplitude of response R as a function of time $t - t_s$. As in the experiments the simulated response amplitude gradually decreased when the stopping frequency was lower than the resonant frequency (see Figs. 8.15a and 8.15b) and increased when the stopping frequency was higher (see Figs. 8.15c and 8.15d). Moreover, after approximately 10 min of relaxation the relaxation curves at a particular stopping frequency approached a long term level corresponding to the unconditioned part of the initial resonance curve whether or not the upward or downward preceding sweep was selected.

To reproduce another experimental facet of recovery time [146] we varied the previous simulations by stopping the sweep and simultaneously turning off the drive for 30 s with the sweep moving downward (see Fig. 8.17a) or upward (Fig. 8.17b) from an

already conditioned resonance. In a relatively short time (tens of seconds) the memory of the high strain amplitude rock had experienced at resonance diminished far more quickly than when the drive was left on. According to the kinetic equation (8.2.1) this distinction finds its rational explanation in a more favorable regime for defect annihilation under zero stress $\sigma = 0$ in comparison with the regime governed by the oscillating stress of a considerable amplitude (though lesser than that at resonance). Figures 8.17a and 8.17b were prepared using the same model parameters as for Fig. 8.12. Also, drive amplitude and sweep rate (except the short time interval of drive and sweep stopping) were set to the same values as for the two highest curves in Fig. 8.12. Figure 8.17a displays the resonance curves obtained by the continuous sweep in upward followed by a sectionally continuous sweep downward. Figure 8.17b shows the complementary curves obtained by a continuous sweep downward followed by a sectionally continuous sweep upward. Effects of quick recovery (increase) of bar modulus E while sweep and drive were stopped are clearly seen as discontinuities in the curves. At stopping frequencies

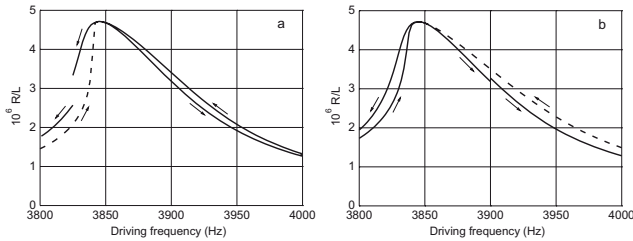


Figure 8.17: (a) Resonance curves obtained by a continuous upward sweep and subsequent sectionally continuous downward sweep. During the downward sweep both drive and sweep were turned off simultaneously for 30 s at fixed frequency $f_s=3825$ Hz, lower than the peak frequency at $f_s=3846$ Hz. (b) Resonance curves obtained by continuous downward sweep and subsequent sectionally continuous upward sweep. During the upward sweep drive and sweep were turned off simultaneously for 30 s at fixed frequency $f_s=3900$ Hz, higher than the peak frequency at $f_s=3846$ Hz. For both pictures the driving amplitude and the absolute value of sweep rate when being turned on were $D = 1.9 \cdot 10^{-7} L$ and $|df/dt| = 400$ Hz/min, respectively.

below resonance one f_r , the response amplitude drops closer to the first (recovered) upward-swept curve marked by the dashed line in Fig. 8.17a. At stopping frequencies above resonance one f_r , the response amplitude jumps closer to the first (recovered) downward-swept curve marked by the dashed line in Fig. 8.17b. A qualitative view of these jumps comes from the indirect impact of strain on bar modulus through the concentration of defects. During the period of time when the sweep is approaching and passing resonance frequency f_r , the strain intensity becomes substantial one, causing a corresponding generation of defects, and the modulus decreases. This effect is manifested as a shift of resonance curve downward in frequency when the sweep has already passed resonance. If the drive and sweep are then turned off, the strain vanishes causing progressive annihilation of defects so that modulus increases. As a consequence the part of resonance curve, tracked after drive and sweep have been resumed, moves back

(i.e., upward in frequency) as memory of the high strain is lost.

8.4.1 Water saturation

Another interesting experimental observation is the dramatic suppression of hysteresis with decreasing water saturation [2]. According to our theory this effect can be understood by noting that equilibrium defect concentration in a recovered sample c_0 (8.2.7) drops more than three times in magnitude when water saturation decreases from $s = 0.25$ to $s = 0.05$. Indeed, it is precisely the equilibrium defect concentra-

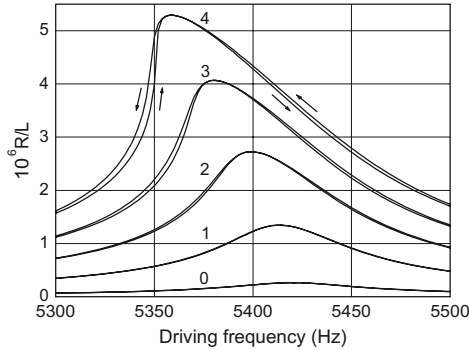


Figure 8.18: Conditioned resonance curves $j = 0, 1, 2, 3, 4$, at successively higher driving amplitudes $D_j = 3.8(j + 0.2\delta_{j0}) \cdot 10^{-8}L$. Arrows on the two highest curves indicate sweep directions. The absolute value of sweep rate is $|df/dt| = 400$ Hz/min, and water saturation is $s = 0.05$.

tion (8.2.7) that controls variation of elastic modulus (8.2.5) through strain-induced variation of nonequilibrium defect concentration c as follows from the kinetic equation (8.2.1) and formulas (8.2.2)-(8.2.4). This conclusion has been confirmed by direct computation with saturation $s = 0.05$ being the only model parameter changed from the parameters adopted for Fig. 8.12. The results shown in Fig. 8.18 contrast in hysteresis with those of Fig. 8.12. Figure 8.18 also demonstrates a substantial increase of resonant frequency f_r in comparison with Fig. 8.12 as a result of the monotonic growth of Young modulus with decreasing saturation (seen already at $s = 0$ from expression (8.2.6) combined with formula (8.2.7)). Due to this fact the interval of frequency sweep for producing Fig. 8.18 was shifted to 5200–5600 Hz.

In addition, we have observed a monotonic decrease in quality factor Q (defined here as resonant frequency f_r divided by the resonance curve width at $\sqrt{2}/2$ of peak height at low-amplitude drive) with increase of water saturation s . This trend is well-documented in numerous experiments [2, 29, 149, 214]. In the present theory it derives from the drop of resonant frequency f_r with water saturation s as seen from the low amplitude analytical estimation at $\sigma = 0$ and $\gamma = 0$ when the expressions (8.4.1), (8.2.6), and (8.2.7) are combined. Figure 8.19 illustrates the theoretical dependence of quality factor Q on saturation s with all model parameters except the variable s as given in Fig. 8.12.

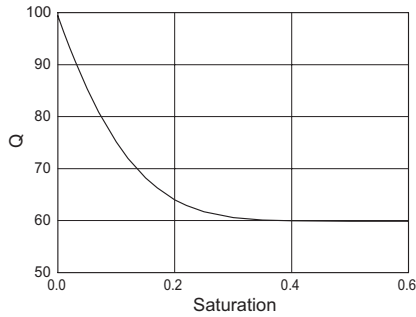


Figure 8.19: Quality factor Q as a function of water saturation s . The fixed model parameters were assumed to be the same as for Fig. 8.12.

8.5 Simulation of slow dynamics

In this section we will carry out the simulation of slow dynamics effect revealed in experiments [143, 145, 147] (see Fig. 8.6 in Sec. 8.1). Figure 8.20 shows the gradual recovery of resonant frequency f_r to its maximum limiting value f_0 after the bar was subjected to high amplitude conditioning and then conditioning was stopped. Conditioning was performed by multiple short-range sweeps over the resonance at the drive level used to obtain the third pair ($j = 3$) of curves in Fig. 8.12. We have plotted

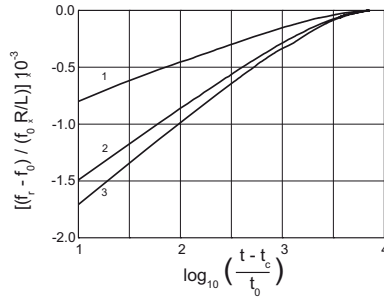


Figure 8.20: Time-dependent recovery of peak frequency f_r to its asymptotic value f_0 . Curves $j=1, 2, 3$ correspond to successively higher saturations $s_j = 0.05(2j - 1)$. The frequency shift $f_r - f_0$ is normalized by both the asymptotic frequency f_0 and the effective conditioning strain ε_{eff} . Here ε_{eff} is defined as the value of dimensionless response amplitude R/L which had been attained during high-amplitude conditioning tuned to the frequency of resonance.

three different curves corresponding to three different saturations with all other model parameters used for Fig. 8.12 being retained. The net frequency shift $f_r - f_0$ consists of two different parts, namely (i) the expected dynamic shift caused by strain nonlinearity at high levels of excitation [20] and (ii) the shift caused by the slow subsystem.

However, only the second part can actually be observed during the recovery process because the first part vanishes almost instantaneously on switching off the high amplitude drive. Hence, the visible recovery should be governed by the slow kinetics of restoring intergrain cohesive bonds. From Fig. 8.20 we clearly see the very wide time interval $10t_0 \leq t - t_c \leq 1000t_0$ of logarithmic recovery of resonant frequency f_r in complete agreement with experimental results [145] and analytical calculations summarized by formulas (8.3.19) and (8.3.20) from Sec. 8.2.2. Here t_c is the moment when the conditioning was switched off and $t_0 = 1$ s is the time scaling constant.

The process of low amplitude probing of recovering resonant frequency to determine f_r as a function of time follows the same procedure either experimentally or theoretically. After the high-amplitude conditioning drive is stopped, a low-amplitude drive remains on to repeatedly sweep the resonance curve and monitor the moving position of resonant frequency f_r . Figure 8.21 illustrates the set of successive resonance curves corresponding to the time-dependent recovery of resonant frequency given by curve 3 of Fig. 8.20. At each successive sweep the curves shift upward in frequency and gradually

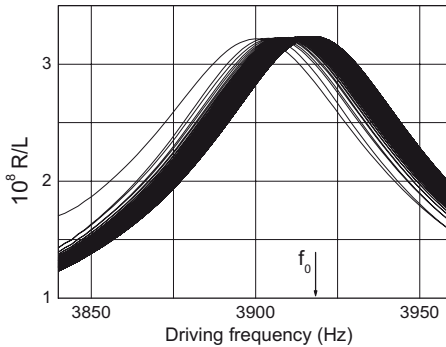


Figure 8.21: The set of successive resonance curves obtained by means of back and forth sweeps around the recovering resonance after the high-amplitude conditioning drive was stopped. The arrow indicates the asymptotic resonant frequency. Water saturation, amplitude of probing drive, and absolute value of sweep rate are $s = 0.25$, $D = 1.14 \cdot 10^{-9}L$, and $|df/dt| = 400$ Hz/min.

approach an asymptotic curve with the asymptotic resonant frequency f_0 indicated by an arrow. Only a fraction of the successive resonance curves calculated over the time interval $t - t_c > 1$ s are clearly distinguishable because separation between neighboring curves progressively diminishes with successive sweeps. The amplitude of the probing drive was taken to be as small as $D = 1.14 \cdot 10^{-9}L$.

8.6 Dynamical realization of end-point memory

The suggested model enables us to describe correctly a wide class of experimental facts concerning the unusual dynamical behavior of such mesoscopically inhomogeneous media as sandstones [146, 145, 147]. Moreover, as it is shown below, we have predicted

the phenomenon of hysteresis with end-point memory in its essentially dynamical hypothesis [195]. These theoretical findings were confirmed experimentally in Los Alamos National Laboratory by Ten Cate and Shankland [197, 200].

Figures 8.12-8.14 and Fig. 8.18 demonstrate a dynamical realization of hysteretic phenomena in the case of only two reversing points in the driving frequency protocol. The question arises whether an effect similar to the end-point (discrete) memory that is observed in quasistatic experiments with a multiply-reversed loading-unloading protocol [21, 33, 52, 53, 55, 57, 71] could also be manifested in resonating bar experiments with a multiply-reversed frequency protocol.

We studied this problem theoretically and show the results in Fig. 8.22, where the model parameters including the absolute value of sweep rate coincide with those of the two highest resonance curves in Fig. 8.12, while the sweep range is taken within the low-frequency slopes of these curves. End-point memory, defined here as the memory of the previous maximum amplitude of alternating stress, is seen to be pronounced in the form of small loops inside the big loop. The starting and final points of each small loop in Fig. 8.22 coincide, what is the typical manifestation of end-point memory. A small closed loop can be produced anywhere on the unconditioned (dashed) curve,

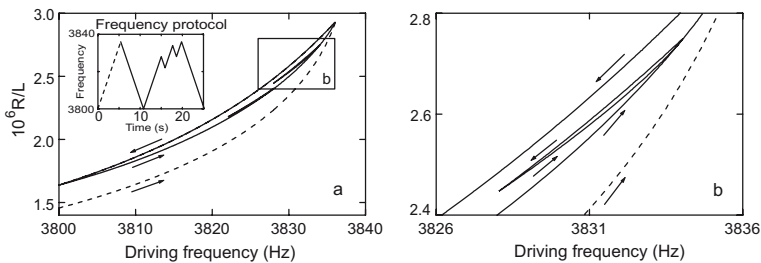


Figure 8.22: Manifestation of end-point memory in dynamic response with a multiply-reversed frequency protocol. Model parameters, including the absolute value of sweep rate, coincide with those for the two highest resonance curves in Fig. 8.12. The range of frequency sweep is on the low-frequency slopes of the two highest resonance curves from Fig. 8.12. R is the response amplitude taken at the free end of the bar.

but the situation on the conditioned up-going curve looks more complicated. Thus, the closeness of an extremely small loop can be achieved only on the upper part of the conditioned up-going curve. The reason for such behavior is the existence of a threshold stress amplitude (depending on previous history) that must be surmounted in order for the kinetics of the slow subsystem to be switched from defect annihilation at lower amplitudes to defect creation at higher amplitudes. This restriction can be substantially relaxed provided the linear size of the inner loop becomes comparable with that of the big outer loop. Direct calculations (not shown) confirm the earlier statement, and the chance to find the inner loop being closed increases progressively with the growth of its size irrespective of whether the inner loop was produced on an up-going or on a down-going curve of the big outer loop.

Following the theoretical prediction, shown in Fig. 8.22, our colleagues Ten Cate and Shankland have performed experimental measurements to verify this prediction [197,

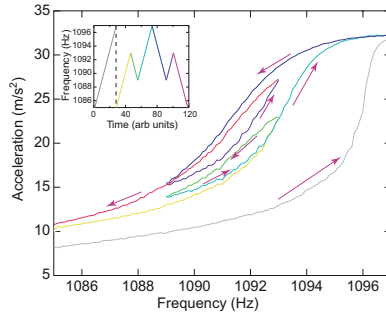


Figure 8.23: The low frequency sides of experimental resonance curves for Fontainebleau sandstone. Exclusive experimental results by Ten Cate and Shankland (LANL).

200]. The sample bar was a Fontainebleau sandstone and the drive level produced a

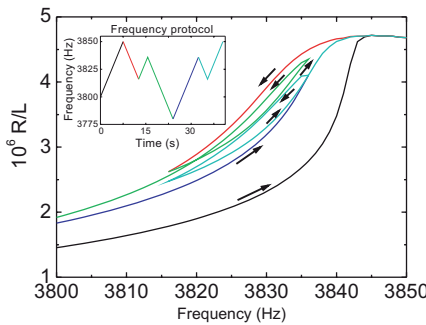


Figure 8.24: The low frequency sides of the resonance curves calculated for Berea sandstone.

calculated strain of about $2 \cdot 10^{-6}$ at the peak. Figure 8.23 shows the low frequency sides of resonance curves that correspond to the frequency protocol given on inset of Fig. 8.23. We clearly see that the beginning and end of each inner loop coincide, i.e., a major feature of end-point memory.

Exclusive experimental results obtained at Los Alamos National Laboratory stimulate us to carry out additional modeling calculations. The experimental results for the Fontainebleau sandstone shown in Fig. 8.23 [197, 200] were reproduced by using our model equations though with constants (including a state equation) developed for Berea sandstone [194, 195, 196, 200, 201]. We note the good qualitative agreement between the experimental (see Fig. 8.23) and the theoretical (see Fig. 8.24) curves suggesting that our physical model is appropriate for both sandstones.

Let us make some important remarks to note the physical adequacy of the suggested model. First, the model parameters, chosen once for describing only one experiment,

namely, the resonance curves (see Fig. 8.12), are suitable to describe all known experiments both qualitatively and quantitatively. Second, after the development of model was completed and new experimental results have appeared later, this model enables us to successfully describe these new results. Consequently, the model we developed can adequately reproduce the experimental results and can be applied for future researches.

Bibliography

- [1] Abazari, R. (2010) Application of (G'/G) -expansion method to travelling wave solutions of three nonlinear evolution equation. *Computers and Fluids*, **39**, 1957–1963.
- [2] Van Den Abeele, K.E.-A., Carmeliet, J., Johnson, P.A. and Zinszner, B. (2002) Influence of water on the nonlinear elastic mesoscopic response in earth materials and the implications to the mechanism of nonlinearity. *J. Geophys. Res.*, **107**, 2121–2142.
- [3] Ablowitz, M. and Segur, H. (1981) *Solitons and the inverse scattering transform*, SIAM, Philadelphia.
- [4] Achenbach, J.D. (1973) *Wave propagation in plastic solids*, North-Holland, Amsterdam.
- [5] Adams, F.D. and Coker, E.G. (1906) *An investigation into the elastic constants of rocks, more especially with reference to cubic compressibility*, Carnegie Institute of Washington, Washington.
- [6] Adushkin, V.V. (1963) On shock wave forming and explosion products flying away. *J. Appl. Mech, Techn. Phys.*, N5, 107–120 (in Russian).
- [7] Adushkin, V.V. and Korotkov, A.I. (1961) Shock wave parameters near chemical explosion in air. *J. Appl. Mech, Techn. Phys.*, N5, 119–123 (in Russian).
- [8] Aki, K. and Richards, P.G. (1980) *Quantitative seismology. Theory and methods*, Vol. I and II, W.H. Freeman, San Francisco.
- [9] Arutyunyan, G.M. (1979) Condition for applying on the hydrodynamics of a perfect gas to dispersed media. *Izv. Akad. Nauk SSSR, Mekh. Zhidk. Gasa*, N1, 15–160.
- [10] Baker, W.E., Cox, P.A., Westine, P.S., Kuzesz, J.J. and Strehlow, R.A. (1983) *Explosion hazards and evaluation*, Elsevier Scientific Publishing Company, Amsterdam-Oxford-New York.
- [11] Bakhvalov, N.S. and Panasenko, G.P. (1984) *Averaging of processes in periodic media*, Nauka, Moscow, (in Russian).

- [12] Bakhvalov, N.S. and Eglit, M.E. (1983) Processes in periodic media not described in terms of averaged characteristics. *Dokl. Akad. Nauk SSSR (transl. as Soviet Math. Dokl.)*, **268**, 836–840.
- [13] Balakirov, Yu.A. and Bugai Yu.N. (2000) *Innovation technologies in oil-and-gas production*, MNTU, Kiev, (in Russian).
- [14] Baum, F.A., Orlenko, L.P., Stanyukovich, K.P., et al. (1975) *Physics of explosion*, Nauka, Moscow, (in Russian).
- [15] Bentahar, M., Aqra, H.El., Guerjouma, R.El., Griffa, M. and Scalerandi, M. (2006) Hysteretic elasticity in damaged concrete: quantitative analysis of slow and fast dynamics. *Phys. Rev. B*, **73**, 014116.
- [16] Berdichevsky, V.L. (2010) *Variational principles of continuum mechanics*, Springer-Verlag, Berlin-Heidelberg.
- [17] Bereznev, I.A. and Nikolaev, A.V. (1988) Experimental investigations of nonlinear seismic effects. *Phys. Earth Planetary Int.*, **50**, 83–87.
- [18] Biot, M.A. (1956) Theory of propagation of elastic waves in a fluid-saturated solid. I. Low-frequency range. *J. Acoust. Soc. Am.*, **28**, 168–178.
- [19] Bocquet, L., Charlaix, E., Ciliberto, S. and Crassous, J. (1998) Microscopic derivation of non-markovian thermalization of a Brownian particle. *Nature (London)*, **396**, 735–737.
- [20] Bogolyubov, N.N. and Mytropol'skiy, Yu.A. (1974) *Asymptoticheskie metody v teorii nelineynykh kolebaniy*, Nauka, Moscow.
- [21] Boitnott, G.N. (1993) Fundamental observations concerning hysteresis in the deformation of intact and jointed rock with applications to nonlinear attenuation in the near source region, in: *Proceedings of the Numerical Modeling for Underground Nuclear Test Monitoring Symposium*. Report LA-UR-93-3839 *Los Alamos Natl. Lab. Rev.*, 121–137.
- [22] Bonner, B.P. and Wanamaker, B.J. (1991) Acoustic nonlinearities produced by a single macroscopic fracture in granite, in *Review of Progress in Quantitative NDE*, (eds. D.O. Thompson and D.E. Chimenti), Plenum, New York, **10B**, 1861–1867.
- [23] Brode, H.I. (1955) Numerical solutions of spherical blast waves. *J. Appl. Phys.*, **26**(6), 766–775.
- [24] Brode, H.I. (1976) *Point explosion in air, mechanics, numerical solutions of explosions*, Mir, Moscow, **4**, pp. 7–70.
- [25] Burgers, J.M. (1948) A mathematical model illustrating the theory of turbulence, in *Advances in Applied Mechanics*, (eds. Richard von Mises, Theodore von Kármán), Academic Press Inc., New York, N. Y., pp. 171–199.

- [26] Byrd, P.F. and Friedman, M.D. (1971) *Handbook of Elliptic Integrals for engineers and scientists*, SatiswKr, Berlin.
- [27] Capogrosso-Sansone, B. and Guyer, R.A. (2002) Dynamic model of hysteretic elastic systems. *Phys. Rev. B*, **66**, 224101(12).
- [28] Claytor, K.E., Koby, J.R. and TenCate, J.A. (2009) Limitations of Preisach theory: Elastic aftereffect, congruence, and end point memory. *Geophys. Res. Lett.*, **36**, L06304(4).
- [29] Clark, V.A., Tittmann, B.R. and Spencer, T.W. (1980) Effect of volatiles on attenuation (Q-1) and velocity in sedimentary rocks. *J. Geophys. Res. B*, **85**, 5190–5198.
- [30] Clarke, J.E. (1984) Lectures on plane waves in reacting gases. *Ann. Phys. Fr.*, **9**, 211–306.
- [31] Cole, R.H. (1948) *Underwater explosions*, Princeton Univ. Press, Princeton.
- [32] Collins, R.E. (1961) *Flow of fluids through porous materials*, Reinhold, New York.
- [33] Cook, N.G.W. and Hodgson, K. (1965) Some detailed stress-strain curves for rock. *J. Geophys. Res.*, **70**, 2883–2888.
- [34] Danylenko, V.A., Belinskiy, I.V., Grzhibovskiy, V.V. and Lemeshko, V.A. (2010) Experimental research of a deformation of the elastic-plastic structured medium and the formation of compactons in it. *Rep. NAS Ukr.*, N10, 93–101.
- [35] Danylenko, V.A., Sorokina, V.V. and Vladimirov, V.A. (1993) On the governing equations in relaxing models and self-similar quasiperiodic solutions. *J. Phys. A*, **26**, 7125–7135.
- [36] Darling, T.W., TenCate, J.A., Brown, D.W., Clausen, B. and Vogel, S.C. (2004) Neutron diffraction study of the contribution of grain contacts to nonlinear stress-strain behavior. *Geophys. Res. Lett.*, **31**, L16604.
- [37] Dodd, R.K., Eilbeck, J.C., Gibbon, J.D. and Morris, H.C. (1984) *Solitons and nonlinear wave equations*, Academic Press, London.
- [38] Drukovanny, N.F. (1973) *Methods of explosion control in pits*, Nedra, Moscow, (in Russian).
- [39] Dullien, F.A.L. (1979) *Porous media. Fluid transport and pore structure*, Academic Press, New York.
- [40] Dushin, V.K. (1973) Method of numerical solution of the equations of chemical kinetics, in *Scientific Proceedings of the Mechanics Institute of Moscow State University*, N21, pp. 35–39.
- [41] Ekimov, A.E., Lebedev, A.V., Ostrovskii, L.A. and Sutin, A.M. (1996) Nonlinear acoustic effects due to cracks in ice cover. *Akust. Zhurnal*, **42**, 61–64 (in Russian).

- [42] Estévez, P.G. (2009) Reciprocal transformations for a spectral problem in 2+1 dimensions. *Theor. Math. Physics*, **159**, 763–769.
- [43] Faddeev, L.D. and Takhtajan, L.A. (1987) *Hamiltonian methods in the theory of solitons*, Springer-Verlag, Berlin, Heidelberg and New York.
- [44] Fenlon, F.H. (1980) On the amplification of modulated acoustic waves in gas-liquid mixtures, in *Cavitation and Inhomogeneities in Underwater Acoustics* (ed. W. Lauterborn), Springer, Heidelberg, pp. 141–150.
- [45] Gabov, S.A. (1988) *Introduction in theory of nonlinear wave*, MGU Press, Moscow.
- [46] Gamburtseva, N.G., Nikolaev, A.V., Khavroshkin, A.B. and Tsyplakov, V.V. (1986) Soliton properties of teleseismic wave. *Transactions (Doklady) of the USSR Academy of Sciences, Earth Sci. Sect.*, **291**, 30–32.
- [47] Gardner, C.S., Greene, J.M., Kruskal, M.D. and Miura, R.M. (1967) Method for solving the Korteweg-de Vries equation. *Phys. Rev. Lett.*, **19**, 1095–1097.
- [48] Gardner, C.S. and Morikawa, G.K. (1960) Similarity in the asymptotic behaviour of collision free hydromagnetic wave and water waves. Tech. report. *New York University Report NYU-9082, Courant Inst. Math. Scien.*
- [49] Gel'fand, B.E., Gubanov, A.V. and Gubin, S.A. (1977) Attenuation of shock waves in a two phase liquid-gas-bubble medium. *Izv. Akad. Nauk SSSR, Mekh. Zhidk. Gaza*, N1, 173–176.
- [50] Gel'fand, B.E., Gubanov, A.V. and Timofeev, E.I. (1981) Features of shock-wave propagation in foams. *Fiz. Goreniya Vzryva*, **17**(4), 129–136.
- [51] Gekber, N. and Bartos, J.M. (1974) Strong spherical blast waves in a dust-laden gas. *AIAA Journal*, **12**, 120–122.
- [52] Gordon, R.B. and Davis, L.A. (1968) Velocity and attenuation of seismic waves in imperfectly elastic rock. *J. Geophys. Res.*, **73**, 3917–3935.
- [53] Guyer, R.A., McCall, K.R., Boitnott, G.N., Hilbert, L.B. Jr, and Plona, T.J. (1997) Quantitative implementation of Preisach-Mayergoyz space to find static and dynamic elastic moduli in rock. *J. Geophys. Res.*, **102**, 5281–5293.
- [54] Guyer, R.A., McCall, K.R. and Van Den Abeele, K. (1998) Slow elastic dynamics in a resonant bar of rock. *Geophys. Res. Lett.*, **25**, 1585–1588.
- [55] Guyer, R.A. and Johnson, P.A. (2009) *Nonlinear mesoscopic elasticity: the complex behaviour of rocks, soil, concrete*, Wiley-VCH Verlag GmbH and Co. KGaA, Weinheim.
- [56] Guyer, R.A. and Johnson, P.A. (2000) Hysteresis, energy landscape and slow dynamics: A survey of the elastic properties of rocks. *J. Mater. Process. Manuf. Sci.*, **9**, 14–26.

- [57] Guyer, R.A. and Johnson, P.A. (1999) Nonlinear mesoscopic elasticity: Evidence for a new class of materials. *Physics Today*, **52**, 30–35.
- [58] Guyer, R.A., Ten Cate, J. and Johnson, P.A. (1999) Hysteresis and the dynamic elasticity of consolidated granular materials. *Phys. Rev. Lett.*, **82**, 3280–3283.
- [59] Gusev, V., Lauriks, W. and Thoen, J. (1998) Dispersion of nonlinearity, nonlinear dispersion, and absorption of sound in micro-inhomogeneous materials. *J. Acoust. Soc. Am.*, **103**, 3216–3226.
- [60] Hasimoto, H. (1972) A soliton on a vortex filament. *J. Fluid Mech.*, **51**, 477–85.
- [61] Held, M. (1983) Blast waves in free air, in *Propellants, Explosives, Pyrotechnics*, **8**(1/7), 1–7.
- [62] Hilbert, L.B. Jr, Hwang, T.K., Cook, N.G.W., Nihei, K.T. and Myer, L.R. (1994) Effects of strain amplitude on the static and dynamic nonlinear deformation of Berea sandstone, in *Rock mechanics models and measurements challenges from industry*, (eds. P.P. Nelson and S.E. Laubach), Netherlands, Rotterdam, pp. 497–515.
- [63] Hirota, R. (1980) Direct methods in soliton theory, in *Solitons*, (eds. R.K. Bullough and P.J. Caudrey), Springer, New York, Berlin, pp. 157–176.
- [64] Hirota, R. (2004) *The direct method in soliton theory*, Cambridge University Press, Cambridge.
- [65] Hirota, R. and Satsuma, J. (1976) A variety of nonlinear network equations generated from the Bäcklund transformation for the Toda lattice. *Suppl. Progr. Theor. Physics*, N59, 64–100.
- [66] Hodnett, P.F. and Moloney, T.P. (1989) On the structure during interaction of the two-soliton solution of the Korteweg-de Vries equation. *SIAM J. Appl. Math.*, **49**, 1174–1187.
- [67] Johnson, P.A. and McCall, K.R. (1994) Observation and implications of nonlinear elastic wave response in rock. *Geophys. Res. Lett.*, **21**, 165–168.
- [68] Johnson, P.A. and Rasolofosaon, P.N.J. (1996) Manifestation of nonlinear elasticity in rock: convincing evidence over large frequency and strain intervals from laboratory studies. *Nonlinear Processes Geophys.*, **3**, 77–88.
- [69] Johnson, P. and Sutin, A. (2005) Slow dynamics and anomalous nonlinear fast dynamics in diverse solids. *J. Acous. Soc. Am.*, **117**, 124–130.
- [70] Johnson, P.A., Shankland, T.J., O’Connell, R.J. and Albright, J.N. (1987) Nonlinear generation of elastic waves in crystalline rock. *J. Geophys. Res.*, **92**, 3597–3602.
- [71] Johnson, P.A., Zinszner, B. and Rasolofosaon, P.N.J. (1996) Resonance and nonlinear elastic phenomena in rock. *J. Geophys. Res.*, **101**, 11553–11564.

- [72] Kaselow, A. and Shapiro, S.A. (2004) Stress sensitivity of elastic moduli and electrical resistivity in porous rocks. *J. Geophys. Eng.*, **1**, 1–11.
- [73] Kestenboim, Kh.S., Roslyakov, G.S. and Chudov, L.A. (1974) *Point explosion. Methods of calculation. Tables*, Nauka Press, Moscow.
- [74] Kharkevich, A.A. (1962) *Spectra and analysis*, Fizmatizd., Moscow, (in Russian).
- [75] Kherrmann, V. (1976) Governing equations for compressible porous materials, in *Mechanics (New results in foreign science). Problems in the theory of plasticity*, N7, Mir, Moscow, pp. 178–216 (in Russian).
- [76] Konno, K., Ichikawa, Y.H. and Wadati, M. (1981) A loop soliton propagating along a stretched rope. *J. Phys. Soc. Japan*, **50**, 1025–1026.
- [77] Korn, G. and Korn, T. (1961) *Mathematical handbook for scientists and engineers*, McGraw-Hill, New York-Toronto-London.
- [78] Korobeinikov, V.P. (1991) *Problems of point-blast theory*, American Institute of Physics, New York.
- [79] Kosevich, A.M. (1972) *Osnovy mekhaniki kristallicheskoy reshetki*, Nauka, Moscow.
- [80] Kosevich, A.M. (1981) *Fizicheskaya mekhanika realnykh kristallov*, Naukova Dumka, Kyiv.
- [81] Kudinov, V.M. and Palamarchuk, B.I. (1976) Parameters of shock waves under explosion of explosive charge in form. *Soviet Physics Doklady*, **228**, 555–557.
- [82] Kudinov, V.M., Palamarchuk, B.I., Gel'fand, B.E. and Gubin, S.A. (1976) The use of foam for damping shock-waves at welding and cutting by explosion. *Avtomaticheskaya Svarka (Automatic Welding)*, **69**(3), 12–16.
- [83] Kudinov, V.M., Palamarchuk, B.I. and Vakhnenko, V.A. (1983) Attenuation of a strong shock wave in a two-phase medium. *Soviet Physics Doklady*, **272**, 1080–1083.
- [84] Kudinov, V.M., Palamarchuk, B.I., Vakhnenko, V.A., Cherkashin, A.V., Lebed, S.G. and Malakhov, A.T. (1983) Relaxation phenomena in a foamy structure, in *Shock Waves, Explosions, and Detonations*, (eds. J.R. Bowen, N. Manson, A.K. Oppenheim and R.I. Soloukhin), American Institute of Aeronautics and Astronautics, New York, pp. 96–118.
- [85] Kudryavtsev, L.D. (1971) *Mathematical analysis*, Volume II, Nauka, Moscow.
- [86] Kutateladze, S.S. and Nakoryakov, V.E. (1984) *Heat exchange and waves in gas-liquid systems*, Nauka, Novosib. (in Russian).
- [87] Lamb, G.L. Jr. (1977) Solitons on moving space curves. *J. Math. Phys.*, **18**, 1654–1661.

- [88] Landau, L.D. and Lifshitz, E.M. (1988) *Fluids Mechanics*, Pergamon, New York.
- [89] Lavrentiev, M. and Chabat, B. (1980) *Effets hydrodynamiques et modèles mathématiques*, Traduction franc. Éditions Mir, Moscow.
- [90] Liu, X.H. and He, C. (2013) New traveling wave solutions to the Vakhnenko-Parkes equation. *ISRN Mathematical Physics*, 1–4, doi.org/10.1155/2013/178648.
- [91] Lyakhov, G.M. (1974) *Fundamentals of the dynamics of blast waves in soils and rocks*, Nedra Press, Moscow (in Russian).
- [92] Lyakhov, G.M. (1982) *Waves in soils and porous multicomponent media*, Nauka, Moscow (in Russian).
- [93] McCall, K.R. and Guyer, R.A. (1994) Equation of state and wave propagation in hysteretic nonlinear elastic materials. *J. Geophys. Res.*, **99**, 23,887–23,898.
- [94] Majida, F., Triki, H., Hayat, T., Aldossaryd, O.M. and Biswase, A. (2012) Solitary wave solutions of the Vakhnenko-Parkes equation. *Nonlinear Analysis: Modelling and Control*, **17**(1), 60–66.
- [95] Malykh, K.V. and Ogorodnikov, I.L. (1977) On application of the Klein-Gordon equation for describing the structure of impulse of the compression in a liquid with the bubbles of gas, in *Dynamics of Continuous Media*, Hydrodynamics Institute Press, Novosibirsk, pp. 140–148 (in Russian).
- [96] Mandel'shtam, L.I. and Leonovich, M.A. (1937) To the theory of a sound attenuation in liquids. *J. Exper. Theor. Phys.*, **3**(7), 438–449 (in Russian).
- [97] Mikhalyuk, A.V. (1980) *Rocks under nonuniform dynamic loads*, Naukova Dumka, Kiev, (in Russian).
- [98] Mikhalyuk, A.V. (1986) *Shooting and pulse hydraulic fracturing of seams*, Naukova Dumka, Kiev, (in Russian).
- [99] Mitropolsky, Yu.A., Samoilenko, A.M. and Martinyuk, D.I. (1993) *Systems of evolution equations with periodic and quasiperiodic coefficients*, Kluwer Academic, Dordrecht.
- [100] Miura, R.M. (ed) (1976) *Bäcklund transformations, the inverse scattering method, solitons, and their applications*, Springer, New York.
- [101] Moloney, T.P. and Hodnett, P.F. (1989) A new perspective on the N -soliton solution of the KdV equation. *Proc. R. Ir. Acad.*, **89A**(2), 205–217.
- [102] Morrison, A.J., Vakhnenko, V.O. and Parkes, E.J. (1999) The N loop soliton solution of the Vakhnenko equation. *Nonlinearity*, **12**, 1427–1437.
- [103] Mosinets, V.N. (1976) *Shattering and seismic effect produced by explosion in rocks*, Nedra, Moscow, (in Russian).

- [104] Nakoryakov, V.E., Pokusaev, B.G. and Shreieber, I.R. (1993) *Wave propagation in gas-liquid media*, Begell House, New York.
- [105] Nayfeh, A.H. (1973) *Perturbation methods*, Wiley-Interscience, New York.
- [106] Nesterenko, V.F. (2001) *Dynamics of heterogeneous materials*, Springer-Verlag, New York.
- [107] Newel, A.C. (1985) *Solitons in mathematics and physics*, SIAM, Philadelphia.
- [108] Nigmatulin, R.I. (1987) *Dynamics of multiphase media*, Vol. I and II, Nauka, Moscow (in Russian).
- [109] Nihei, K.T., Hilbert, L.B. Jr, Cook, N.G.W., Nakagawa, S. and Myer, L.R. (2000) Frictional effects on the volumetric strain of sandstone. *Int. J. Rock Mech. Min. Sci. Geomech. Abstr.*, **37**, 121–132.
- [110] Nikolaevskii, V.N. (1985) Viscoelasticity with internal oscillators as a possible model of seismoactive medium. *Dokl. Akad. Nauk SSSR*, **283**, 1321–1324 (in Russian).
- [111] Noordrij, L. and van Wijngaarden, L. (1979) Relaxation effects, caused, by relative motion, on shock waves in gas bubble liquid mixtures. *J. Fluid. Mech.*, **66**, 1–9.
- [112] Novikov, S.P., Manakov, S.V., Pitaevskii, L.P. and Zakharov, V.E. (1984) *Theory of solitons. The inverse scattering methods*, Plenum Publishing Corporation, New York–London.
- [113] Nowick, A.S. and Berry, B.S. (1972) *Anelastic relaxation in crystalline solids*, Academic Press, New York.
- [114] Ostrovsky, L.A. (1978) Nonlinear internal waves in a rotating ocean. *Okeanologia*, **18**, 181–191.
- [115] Ostrovsky, L.A. (1991) Wave processes in media with strong acoustic nonlinearity. *J. Acoust. Soc. Am.*, **90**, 3332–3337.
- [116] Ostrovsky, L.A. and Johnson, P. (2001) Dynamic nonlinear elasticity in geomaterials. *Riv. Nuovo Cimento*, **24**, 1–46.
- [117] Pai, I., Menon, S. and Fan, Z.Q. (1980) Similarity solution of a strong shock wave propagating in a mixture of gas and dusty particles. *Int. J. Eng. Sci.*, **18**(12), 1365–1378.
- [118] B.I. Pandit and J.C. Savage, Experimental test of Lomnitz's theory of internal friction in rock, *J. Geophys. Res.*, 78 (1973) 6097–6099.
- [119] Parkes, E.J. (1993) The stability of solutions of Vakhnenko's equation. *J. Phys. A: Math Gen.*, **26**, 6469–6475.

- [120] B.R. Parkin, F.R. Gilmore and G. L. Broud, Shock waves in water with bubbles of air, in: *Underwater and Underground Explosions* (Russian translation), Mir, Moscow, 1974, 152–258.
- [121] Raats, P.A.C. (1984) Applications of the theory of mixtures in soil physics, in *Rational thermodynamics*, (ed C. Truesdell), Springer, New York, pp. 326–343.
- [122] Rajagopal, K.R. and Tao, L. (1995) *Mechanics of mixtures*, World Scientific Publishing, Singapore.
- [123] Robotnov, Y.N. (1980) *Elements of hereditary solid mechanics*, Mir, Moscow.
- [124] Rodionov, V.N. (1979) Dissipative structures in geomechanics. *Uspekhi Mekhan.*, **4**(2), 47–111.
- [125] Rodionov, V.N., Adushkin, V.V., Kostyuchenko, V.N., Nikolaevskii, V.N., Romashov, V.N. and Tsvetkov, V.I. (1971) *Mechanical effect of underground explosion*, Nedra Press, Moscow (in Russian).
- [126] Rodionov, V.N., Sizov, I.A. and Tsvetkov, V.M. (1986) *Fundamentals of geomechanics*, Nedra Press, Moscow (in Russian).
- [127] Rudinger, G. (1965) Some effects of finite particle volume on the dynamics of gas-particle mixtures. *AIAA Journal*, **3**, 1217–1222.
- [128] Rudinger, G. (1964) Some properties of shock relaxation in gas plows garring small particles. *The Phys. Fluids*, **7**(5), 658–663.
- [129] Rudinger, G., and Chang, A. (1964) Analysis of nonsteady two-phase flow. *Phys. Fluids*, **7**(11), 1747–1754.
- [130] Sadovsky, M.A. and Pisarenko, G.F. (1991) *Seismic process in block medium*, Nauka, Moscow (in Russian).
- [131] Sadovsky, M.A. (ed) (1989) *Discrete properties of geophysics medium*, Nauka, Moscow (in Russian).
- [132] Sanchez-Palencia, E. (1980) *Non-homogeneous media and vibration theory*, Springer, New York.
- [133] Schkolnik, I. (1993) Nondestructive testing of concretes: new aspects. *Nondestr. Test. Eval.*, **10**, 351–358.
- [134] Sedov, L.I. (1993) *Similarity and dimensional methods in mechanics*, CRC Press, Boca Raton.
- [135] Shidlovsky, V.P. (1977) Effect of dissipative phenomena on the evolution of shock waves. *AIAA Journal*, **15**(1), 33–38.
- [136] Smith, E. and Ten Cate, J.A. (2000) Sensitive determination of nonlinear properties of Berea sandstone at low strains. *Geophys. Res. Lett.*, **27**, 1985–1988.

- [137] Stokes, G.G. (1845) On the theories of internal friction of fluids in motion. *Transactions of the Cambridge Philosophical Society*, **8**, 287–305.
- [138] Struminskii, V.V. (1980) *Mechanics and technical progress*, Nauka, Moscow (in Russian).
- [139] Su, C.H. and Gardner, C.S. (1969) Korteweg-de Vries equation and generalizations. III. Derivation of Korteweg-de Vries equation and Burgers equation. *J. Math. Phys.*, **10**, 536–539.
- [140] Sutherland, W. (1891) A kinetic theory of solids with an experimental introduction *Philos. Mag.*, **32**(194), 31–43.
- [141] Suzuki, T., Ohyagi, S., Higashino, F. and et al. (1976) The propagation of reacting blast waves through inert particle clouds. *Acta Astronaut.*, **3**, 517–529.
- [142] Takahashi, D. and Satsuma, J. (1988) Explicit solutions of magma equation. *J. Phys. Soc. Japan*, **57**, 417–421.
- [143] TenCate, J.A. (2011) Slow dynamics of Earth materials: An experimental overview. *Pure Appl. Geophys.*, **168**, 2211–2219.
- [144] Ten Cate, J.A., Duran, J. and Shankland, T.J. (2002) Nonlinearity and slow dynamics in rocks: Respons to changes of temperature and humidity, in *Proceedings of the 16th International Symposium on Nonlinear Acoustics*, (eds. O.V. Rudenko, O.A. Sapozhnikov), MSU, Moscow, **2**, 767–770.
- [145] Ten Cate, J.A., Smith, E. and Guyer, R.A. (2000) Universal slow dynamics in granular solids. *Phys. Rev. Lett.*, **85**, 1020–1023.
- [146] Ten Cate, J.A. and Shankland, T.J. (1996) Slow dynamics in the nonlinear elastic response of Berea sandstone. *Geophys. Res. Lett.*, **23**, 3019–3022.
- [147] Ten Cate, J.A. and Shankland, T.J. (1998) Slow dynamics and nonlinear response at low strains in Berea sandstone, in *Proceedings of the 16th International Congress on Acoustics and 135th Meeting of the Acoustical Society of America*, (eds. P.A. Kuhl and L.A. Crum), American Institute of Physics, New York, **3**, pp. 1565–1566.
- [148] Thovert, J.-F., Yousefian, F., Spanne, P., Jacquin, C.G. and Adler, P.M. (2001) Grain reconstruction of porous media: Application to a low-porosity Fontainebleau sandstone. *Phys. Rev. E*, **63**, 061307(17).
- [149] Tittmann, B.R., Clark, V.A., Richardson, J.M. and Spencer, T.W. (1980) Possible mechanism for seismic attenuation in rocks containing small amounts of volatiles. *J. Geophys. Res. B*, **85**, 5199–5208.
- [150] Trebinski, R., Trzcinski, W. and Wladarczyk, E. (1979) On pressurepulse penetration into three-component medium. *J. Technol. Phys.*, **20**, 303–314.
- [151] Truesdell, C. (1984) *Rational thermodynamics*, Springer-Verlag, New York.

- [152] Tseitlin, Ya.I., Gil'manov, R.A. and Nilov, V.G. (1980) On Localization of Action of the Blast Hydro-Shock Wave by Bubble Screen, in *Vzryvnoe delo (Explosives)*, N82/39, (ed. A.V. Korenistov), Nedra Press, Moscow, pp. 264–272 (in Russian).
- [153] Vakhnenko, V.A. (1991) Periodic short-wave perturbations in a relaxing medium, Institute of Geophysics, Ukrainian Acad. Sci., Kiev, Preprint (in Russian).
- [154] Vakhnenko, V.A. (1992) Solitons in a nonlinear model medium. *J. Phys. A: Math.Gen.*, **26**(15), 4181–4187.
- [155] Vakhnenko, V.A. (1999) Increase of nonlinear effect in a medium with microstructure. *Acoustical Physics*, **45**, 151–157.
- [156] Vakhnenko, V.A. (1996) Diagnosis of the properties of a structured medium by long nonlinear waves. *J. Appl. Mech. Techn. Phys.*, **37**(5), 643–649 (in Russian).
- [157] Vakhnenko, V.O. (1997) The existence of loop-like solutions of a model evolution equation. *Ukr. J. Phys.*, **42**(1), 104–110 (in Ukrainian).
- [158] Vakhnenko, V.O. (1999) High frequency soliton-like waves in a relaxing medium. *J. Math. Phys.*, **40**(3), 2011–2020.
- [159] Vakhnenko, V.O. (2010) An analogy of the self-similar flows of a gas and a two-phase medium with noncompressive component. *Rep. Nation. Acad. Sc. Ukraine*, N12, 97–104 (in Ukrainian).
- [160] Vakhnenko, V.O. (2011) Similarity in stationary motions of gas and two-phase medium with incompressible component. *Intern. J. Non-Linear Mech.*, **46**, 1356–1360.
- [161] Vakhnenko, V.O. (2011) Modeling of hysteretic behavior for sandstone under slow cyclic loading. *Ukr. Geophys. J.*, **33**(4), 153–158 (in Ukrainian).
- [162] Vakhnenko, V.O. (2011) Applying the inverse scattering transform method to the Vakhnenko-Parkes equation to describe the interaction of a soliton and a periodic wave. *Rep. NAS Ukr.*, N8, 73–79 (in Ukrainian).
- [163] Vakhnenko, V.O. (2012) Special form of the singularity function for continuous part of the spectral data in inverse scattering method. *Ukr. J. Phys.*, **57**(1), 95–99.
- [164] Vakhnenko, V.O. (2014) Blast waves in multi-component medium with thermal relaxation. *Natural Science*, **6**, 1055–1092.
- [165] Vakhnenko, V.O., Danilenko, V.A., and Kulich, V.V. (1991) Wave processes in periodic relaxing medium. *Dokl. Akad. nauk Ukrain.SSR*, N4, 93–96.
- [166] Vakhnenko, V.A., Danilenko, V.A. and Kulich, V.V. (1996) Asymptotic justification of the Lyakhov model for multicomponent media. *Combustion Explosion and Shock Waves*, **32**(2), 176–180.
- [167] Vakhnenko, V.A. and Danilenko, V.A. (1997) An asymptotic model of non-linear waves in natural multi-component media. *Geophysics J. (Ukraine)*, **16**, 674–685.

- [168] Vakhnenko, V.A., Danilenko, V.A. and Michtchenko, A.V. (1999) An asymptotic averaged model of nonlinear long waves propagation in media with a regular structure. *Inter. J. Non-Linear Mech.*, **34**, 643–654.
- [169] Vakhnenko, V.A., Danilenko, V.A. and Michtchenko, A.V. (2000) Diagnostics of the medium structure by long wave of finite amplitude. *Inter. J. Non-Linear Mech.*, **35**, 1105–1113.
- [170] Vakhnenko, V.A., Danilenko, V.A. and Kulich, V.V. (1993) Averaged description of wave processes in geophysical medium. *Geophysics J. (Ukraine)*, **15**(6) 66–71.
- [171] Vakhnenko, V.A., Danilenko, V.A. and Kulich, V.V. (1994) Averaged description of shock-wave processes in periodic media. *Sov. J. Chem. Phys.*, **12**(3), 534–546.
- [172] Vakhnenko, V.A. and Kulich, V.V. (1992) Long-wave processes in periodic media. *J. Appl. Mech. Techn. Phys.*, **32**, 814–820.
- [173] Vakhnenko, V.A., Kudinov, V.M. and Palamarchuk, B.I. (1982) Effect of thermal relaxation of attenuation of shock waves in two-phase medium. *Soviet Applied Mechanics*, **18**(12), 1126–1133.
- [174] Vakhnenko, V.A., Kudinov, V.M. and Palamarchuk, B.I. (1983) Analogy of motion of the two-phase media containing incompressible and gaseous phases with gas motion. *Doklady Akademii nauk Ukr.SSR A*, N6, 22–24 (in Russian).
- [175] Vakhnenko, V.A., Kudinov, V.M. and Palamarchuk, B.I. (1984) Damping of strong shocks in relaxing media. *Combustion Explosion and Shock Waves*, **20**(1), 97–103.
- [176] Vakhnenko, V.O., Nagornyy, V.P., Denisyuk, I.I., and Mishchenko, A.V. (2003) Estimation of rock failure zone under confined explosion. *Journal of Mining Science*, **39**, N3, 247–254 .
- [177] Vakhnenko, V.A. and Palamarchuk, B.I. (1984) Description of shock-wave processes in a two-phase medium containing an incompressible phase. *Journal of Applied Mechanics and Technical Physics*, **25**(1), 101–107.
- [178] Vakhnenko, V.A. and Palamarchuk, B.I. (1986) Evolution of strong shock waves in a medium with thermal relaxation. *Soviet Applied Mechanics*, **22**(3), 267–272.
- [179] Vakhnenko, V.O. and Parkes, E.J. (1998) The two loop soliton solution of the Vakhnenko equation. *Nonlinearity*, **11**, 1457–1464.
- [180] Vakhnenko, V.O., Parkes, E.J. and Danylenko, V.A. (1999) Exact two-soliton solutions of a model nonlinear equation. *Ukr. J. Phys.*, **44**(6), 782–790 (in Ukrainian).
- [181] Vakhnenko, V.O., Parkes, E.J. and Michtchenko, A.V. (2000) The Vakhnenko equation from the viewpoint of the inverse scattering method for the KdV equation. *Inter. J. Differ. Eq. Appl.*, **1**(4), 429–450.

- [182] Vakhnenko, V.O. and Parkes, E.J. (2001) A novel nonlinear evolution equation and its Backlund transformation. *Rep. NAS Ukr.*, N6, 91–96.
- [183] Vakhnenko, V.O. and Parkes, E.J. (2001) A novel nonlinear evolution equation integrable by the inverse scattering method. *Rep. NAS Ukr.*, N7, 81–86.
- [184] Vakhnenko, V.O. and Parkes, E.J. (2002) The calculation of multi-soliton solutions of the Vakhnenko equation by the inverse scattering method. *Chaos, Solitons and Fractals*, **13/9**, 1819–1826.
- [185] Vakhnenko, V.O. and Parkes, E.J. (2002) A novel nonlinear evolution equation integrable by the inverse scattering method, in *Proceedings of Fourth International Conference 'Symmetry in Nonlinear Mathematical Physics' (9-15 July, 2001, Kyiv)*, (eds. A.G. Nikitin, V.M. Boyko and R.O. Popovych), Institute of Mathematics, Kyiv, **43(2)**, pp. 384–391.
- [186] Vakhnenko, V.O. and Parkes, E.J. (2002) The inverse scattering method for the equation describing the high-frequency waves in a relaxing medium, in *Proceedings of 16 International Symposium on Nonlinear Acoustics (August 19 - 23, 2002, Moscow)*, (eds. O.V. Rudenko and O.A. Sapozhnikov), Moscow State University, Moscow, pp. 121–124.
- [187] Vakhnenko, V.O., Parkes, E.J. and Morrison, A.J. (2002) Integrability of a novel nonlinear evolution equation. *Rep. NAS Ukr.*, N6, 86–92.
- [188] Vakhnenko, V.O., Parkes, E.J. and Morrison, A.J. (2003) A Backlund transformation and the inverse scattering transform method for the generalised Vakhnenko equation. *Chaos, Solitons and Fractals*, **17**, 683–692.
- [189] Vakhnenko, V.O. and Parkes, E.J. (2011) Solutions associated with both the bound state spectrum and the special singularity function for continuous spectrum in inverse scattering method, in *Proceeding of School of Mechanics and Mathematics, Contemporary problems of mathematics, mechanics and computing sciences*, (eds. N.N. Kizilova, G.N. Zholtkevych), Karazin Kharkov National University, Kharkov, pp. 364–376.
- [190] Vakhnenko, V.O. and Parkes, E.J. (2012) The singular solutions of a nonlinear evolution equation taking continuous part of the spectral data into account in inverse scattering method. *Chaos, Solitons and Fractals*, **45**, 846–852.
- [191] Vakhnenko, V.O. and Parkes, E.J. (2012) Solutions associated with discrete and continuous spectrums in the inverse scattering method for the Vakhnenko-Parkes equation. *Progress of Theoretical Physics*, **127(4)**, 593–613.
- [192] Vakhnenko, V.O. and Parkes, E.J. (2012) Special singularity function for continuous part of the spectral data in the associated eigenvalue problem for nonlinear equations. *J. Math. Phys.*, **53(6)**, 063504(11).
- [193] V.O. Vakhnenko, O.O. Vakhnenko and V.A. Danylenko, A relaxation model of the mechanical behaviour of a sandstone under quasistatic loading, *Rep. NAS Ukr.*, N7 (2007) 109–115 (in Ukrainian).

- [194] Vakhnenko, O.O., Vakhnenko, V.O., Shankland, T.J. and TenCate, J.A. (2004) Strain-induced kinetics of intergrain defects as the mechanism of slow dynamics in the nonlinear resonant response of humid sandstone bars. *Phys. Rev. E, Rapid communication*, **70**, 015602(R).
- [195] Vakhnenko, O.O., Vakhnenko, V.O. and Shankland, T.J. (2005) Soft-ratchet modelling of end-point memory in the nonlinear resonant response of sedimentary rocks. *Phys. Rev. B*, **71**, 174103.
- [196] Vakhnenko, O.O., Vakhnenko, V.O., Shankland, T.J. and TenCate, J.A. (2006) Soft-ratchet modeling of slow dynamics in the nonlinear resonant response of sedimentary rocks, in *Innovations in nonlinear acoustics, ISNA17, 17th International Symposium on Nonlinear Acoustics including the International Sonic Boom Forum*, AIP Conference Proceedings, **838**, pp. 120–123.
- [197] Vakhnenko, V.O., Vakhnenko, O.O., Shankland, T.J. and TenCate, J.A. (2006) Dynamical realization of end-point memory in consolidated materials, in *Innovations in nonlinear acoustics, ISNA17, 17th International Symposium on Nonlinear Acoustics including the International Sonic Boom Forum*, AIP Conference Proceedings, **838**, pp. 124–127.
- [198] Vakhnenko, V.O., Vakhnenko, O.O., TenCate, J.A. and Shankland, T.J. (2007) Modeling of stress-strain dependences for Berea sandstone under quasi-static loading. *Phys. Rev. B*, **76**, 184108(8).
- [199] V.O. Vakhnenko, O.O. Vakhnenko, J.A. TenCate and T.J. Shankland, Quasi-static loading of Berea sandstone, Rep. NAS Ukr., N1 (2008) 118–126.
- [200] Vakhnenko, V.O., Vakhnenko, O.O., TenCate, J.A. and Shankland, T.J. (2008) The dynamics of a sandstone bar under resonance loading, in *Proceeding of the XX Session RAS, (27-31 October, 2008, Moscow)*, pp. 206–209.
- [201] Vakhnenko, V., Vakhnenko, O., TenCate, J. and Shankland, T. (2010) Modeling of the nonlinear resonant response in sedimentary rocks. *Ukr. Geophys. J.*, **32**(4), 195–197 (in English).
- [202] Vasylenko, N.V. (1992) *Teoriya Kolebaniy*, Vyshcha shkola, Kyiv.
- [203] Vladimirov, V.S. (1971) *Equations of mathematical physics*, Dekker, New York.
- [204] Vovk, A.A., Zamyshlyaev, B.V., Evterev, L.S., Belinskii, I.V. and Mikhal'yuk, A.V. (1984) *The behaviour of soil under action of impulse loading*, Naukova Dumka, Kiev (in Russian).
- [205] Washimi, H. and Taniuti, T. (1966) Propagation of ion-acoustic solitary waves of small amplitude. *Phys. Rev. Lett.*, **17**, 996–998.
- [206] Wazwaz, A.M. (2009) *Partial differential equations and solitary waves theory*, Higher Education Press and Springer Verlag, Beijing and Berlin.

- [207] Wazwaz, A.M. (2010) N -soliton solutions for the Vakhnenko equation and its generalized forms. *Phys. Scr.*, **82**, 065006(7).
- [208] Whitham, G.B. (1974) *Linear and nonlinear waves*, Wiley-Interscience, New York.
- [209] Yasnikov, G.P. and Belousov, V.S. (1978) Effective thermodynamic functions of a gas with solid particles. *J. Engng. Phys.*, **34**(6), 734–737.
- [210] Yasnikov, G.P. and Belousov, V.S. (1978) Dynamical state equation for mixture of gas and solid particles. *J. Engng. Phys.*, **35**, 872–876 (in Russian).
- [211] Yasnikov, G.P. and Belousov, V.S. (1982) Dynamic equation of state of a gas containing vaporizing droplets. *J. Engng. Phys.*, **43**, 1207–1212.
- [212] Ye, Y., Song, J., Shen, S. and Di, Y. (2012) New coherent structures of the Vakhnenko-Parkes equation. *Results in Physics*, **2**, 170–174.
- [213] Zener, C. (1948) *Elasticity and anelasticity of metals*, The University of Chicago Press, Chicago.
- [214] Zinszner, B., Johnson, P.A. and Rasolofosaon, P.N.J. (1997) Influence of change in physical state on elastic nonlinear response in rock: Effects of confining pressure and saturation. *J. Geophys. Res.*, **101**, 8105–8120.

Index

- approximation of diagnosed medium by layer medium, 97
- bulk viscosity, 28
- Cauchy-Schwarz inequality, 90, 92
- coefficient of nonlinearity, 91
- computer calculation, 76
- condensed phase, 51, 52
 - volume fraction (portion), 51, 52
- coordinates, 3, 8, 11, 13, 36, 49
 - Eulerian \sim , 3, 13, 49
 - independent $(X, T) \sim$, 36
 - Lagrangian \sim , 3, 8, 11
- dispersive relation, 26
- dispersive term, 31
- dissipative term, 31
- earth materials, 4
 - rocks, 4
 - sandstone, 4
 - stress-strain properties, 4
- end-point (discrete) memory, 151
- end-point memory, 4, 114, 121, 124, 150
 - dynamical realization of \sim , 150
- equation, 3, 25, 26, 28, 30–32, 38, 135
 - evolution \sim of longitudinal displacements, 135
 - Klein-Gordon \sim , 28, 31
 - Korteweg-de Vries (KdV) \sim , 3, 25
 - Korteweg-de Vries-Burgers (KdVB) \sim , 28, 30
 - nonlinear, 3
 - high-frequency waves, 3
 - nonlinear evolution \sim , 25, 26
 - nonlinear Schrödinger \sim , 30
 - sine-Gordon \sim , 30
 - Vakhnenko \sim , 3, 25, 32
 - Vakhnenko–Parkes \sim , 3, 25, 38
 - Whitham \sim , 25, 32
- equations, 8, 17, 26, 132
 - hydrodynamics \sim , 8, 26
 - kinetic \sim , 132
 - motion, 8, 17
- equations system, 12, 14, 21
 - averaged \sim , 12, 14, 21
- equilibrium, 67, 75
 - kinematic \sim , 67, 75
 - thermal \sim , 75
- equilibrium state, 7
- experimental measurements, 152
 - for verification of prediction, 152
 - reproduction \sim for verification of prediction, 152
- experimental results, 76, 104, 105, 124
 - for Berea sandstone, 104
 - for Meule sandstone, 105
 - resonant bar \sim , 124
- explosion, 4, 61–63
 - point \sim , 62, 63
 - self-similar theory, 62
 - strong \sim , 4, 61
- foam, 61
- hydrodynamic approach, 8
- hysteresis, 5, 123, 124, 127, 142, 151
 - calculation of \sim resonance curve, 142
 - dynamical realization \sim , 124, 151
 - prediction of \sim with end-point memory, 151
 - resonance curve, 5
- increase of nonlinearity, 89, 93
 - in medium with structure, 89
- interaction, 42
 - two solitons \sim , 42
- invariant, 16
 - Riemann \sim , 16

- loading, 4, 105, 123
 - dynamical \sim , 4, 123
 - quasistatic \sim , 4, 105
- Mach number, 73
- mass concentrations, 93
 - of the individual compone, 93
- mechanism, 103, 106, 112
 - permanent plastic deformation \sim , 103, 112
 - standard solid relaxation \sim , 103, 106
 - sticky-spring \sim , 103
- mechanism of interior processes, 4, 109
 - permanent plastic deformation \sim , 4
 - standard solid relaxation \sim , 4
 - sticky-spring \sim , 4, 109
- medium, 4, 7, 8, 24
 - barotropic \sim , 8
 - geophysical \sim , 7
 - multi-component \sim , 4
 - nonequilibrium \sim , 24
 - two-component \sim , 4
- method, 3, 10, 17, 25, 28, 39, 93
 - analytical-numerical calculation \sim , 17
 - asymptotic averaging, 10
 - diagnostic \sim , 3, 93
 - Hirota \sim , 25, 39
 - inverse scattering \sim , 25
 - multiscale \sim , 10, 28
- model, 2, 4, 5, 7, 9, 21, 24, 48, 63, 103, 106, 112, 128
 - asymptotic averaged \sim , 2, 7, 24, 48, 63
 - Hertz-Mindlin \sim , 103
 - Lyakhov \sim , 21
 - McCall-Guyer \sim , 128
 - phenomenological \sim , 103, 106
 - Zener \sim , 106
 - Preisach-Mayergoyz \sim , 103, 112
 - relaxing medium, 9
 - resonance response, 5
 - vibration resonance, 4
- nonequilibrium state, 3
- nonlinear resonant response, 123
- nonlinearity, 26
 - hydrodynamic \sim , 26
- physical interpretation, 44
- process, 9, 26
 - fast \sim , 9, 26
 - slow \sim , 9, 26
- rate, 135
 - of defect annihilation μ , 135
 - of defect creation ν , 135
- relaxation, 4, 8, 48, 61, 62, 75, 128
 - thermal \sim , 4, 48, 61, 62, 75
- relaxation time, 9, 28, 61
- relaxing medium, 14, 25
 - homogeneous \sim , 14
- resonance frequency, 5, 123, 128
 - linear decrease \sim , 123
 - logarithmic recovery \sim , 5, 123, 128
 - softening \sim , 5
- resonance peak, 127
 - independent of, 127
 - conditioned state, 127
 - direction of sweep frequency, 127
 - unconditioned state, 127
 - shift, 127
- self-similar motion, 56
- shock front parameters, 59
- shock wave, 4, 16, 47, 61
 - action, 47
 - attenuation \sim , 4, 47
 - localizing \sim , 61
- shock waves, 61
 - attenuation \sim , 61
 - damping \sim , 61
- similarity, 53, 55
 - planar flows, 55
 - stationary flows, 53, 55
- similarity in motion, 4, 51
 - gas and two-phase medium, 4, 51
- slow dynamics, 126, 128, 149
 - simulation of \sim , 149
- soft-ratchet kinetics, 137
- soliton, 35, 40
- solution, 3, 25, 33, 35, 41, 42, 44
 - N -soliton \sim , 25
 - ambiguous (multi-valued) \sim , 3, 35, 44
 - loop-like \sim , 25, 35
 - one loop soliton \sim , 41

- traveling wave \sim , 33
- two solitons \sim , 42
- specific volume, 12
 - averaged \sim , 12
- state equations, 9, 17, 50, 103
 - dynamic \sim , 9, 50
- Stokes internal friction, 135
- stress-strain curves, 105, 109, 112, 114
 - conditioned \sim , 105, 112
 - for Meule sandstone, 109
 - hysteresis \sim , 105
 - loops \sim , 105
 - small loops \sim , 114
 - unconditioned \sim , 105, 112
- stress-strain properties, 103, 113
 - rock, 103
 - simulation \sim , 113
- stress-strain trajectories, 4
- subsystem, 131
 - fast \sim longitudinal displacements, 131
 - slow \sim ruptured intergrain cohesive bonds, 131
- Sutherland temperature extrapolation, 134
- water saturation, 5, 148
- wave, 8, 14, 15, 24, 25, 28, 30, 31, 35, 61, 72, 76
 - acoustic \sim , 14
 - blast \sim , 61, 72
 - high-frequency \sim , 25, 28, 30, 31
 - loop solitary \sim , 35
 - low-frequency \sim , 25, 28, 30
 - nonlinear \sim , 8, 15, 24
 - shock \sim , 76
 - solitary \sim , 35
- wavelength, 34
- Young modulus, 5, 131, 134, 141
 - logarithmic recovery \sim , 141

**More
Books!** 



yes
i want morebooks!

Buy your books fast and straightforward online - at one of the world's fastest growing online book stores! Environmentally sound due to Print-on-Demand technologies.

Buy your books online at

www.get-morebooks.com

Kaufen Sie Ihre Bücher schnell und unkompliziert online – auf einer der am schnellsten wachsenden Buchhandelsplattformen weltweit!
Dank Print-On-Demand umwelt- und ressourcenschonend produziert.

Bücher schneller online kaufen

www.morebooks.de

OmniScriptum Marketing DEU GmbH
Heinrich-Böcking-Str. 6-8
D - 66121 Saarbrücken
Telefax: +49 681 93 81 567-9

info@omniscrptum.de
www.omniscrptum.de

OMNI Scriptum 

